Project No. 12-113

Proposed Modifications to AASHTO Cross-Frame Analysis and Design

APPENDIX E
PHASE II SUMMARY

Table of Contents

Table of Contents i
Table of Figures iii
Table of Tables viii
E1 Introduction 1
E2 Bridge Information 2
E2.1 Bridge 1 2
E2.2 Bridge 2 5
E2.3 Bridge 3 9
E3 Instrumentation Plan 13
E3.1 Schedule 13
E3.2 Preliminary Finite Element Analysis 15
E3.2.1 Preliminary FEA of Bridge 1 16
E3.2.2 Preliminary FEA of Bridge 2 17
E3.2.3 Preliminary FEA of Bridge 3 17
E3.3 Stage I - Installation of Sensors and Data Acquisition System 18
E3.3.1 Description of Data Acquisition System 19
E3.3.2 Instrumentation of Bridge 1 23
E3.3.3 Instrumentation of Bridge 2 26
E3.3.4 Instrumentation of Bridge 3 31
E3.4 Stage II – Controlled Live Load Testing 35
E3.4.1 Desired Data 35
E3.4.2 Outline of Procedure 36
E3.4.3 Load Cases 40
E3.5 Stage III – In-Service Monitoring 50
E3.5.1 Procedure for Data Collection 50
E3.6 Stage IV – Demobilization of Sensors and DAQ System 50
E4 Field Experiment Results 52
E4.1 Controlled Live Load Test Data 52
E4.1.1 Overview of Collected Data 52
E4.1.2 Significance of Collected Data 53
E4.1.3 Bridge 1 Results 55
E4.1.4 Bridge 2 Results 83
E4.1.5 Bridge 3 Results 110

E4.1.6 Comparison of Results 134
E4.2 In-Service Rainflow Data 136
E4.2.1 Overview of Collected Data 136
E4.2.2 General Rainflow Counting Parameters 141
E4.2.3 Significance of Collected Data 145
E4.2.4 Bridge 1 Results 146
E4.2.5 Bridge 2 Results 165
E4.2.6 Bridge 3 Results 174
E4.2.7 Comparison of Results 183
E5 Part 1 of Analytical Program 187
E5.1 Modeling Parameters and Assumptions 187
E5.1.1 Boundary Conditions 188
E5.1.2 Contribution of Concrete Rails 192
E5.1.3 Elastic Concrete Stiffness 193
E5.1.4 Important Dimensions 195
E5.1.5 Loading Conditions 196
E5.1.6 Constraints and Meshing 196
E5.1.7 Summary of Modeling Parameters 197
E5.2 Bridge 1 Validation 198
E5.2.1 Preliminary Model Results 199
E5.2.2 Validated Model Results 202
E5.3 Bridge 2 Validation 207
E5.3.1 Preliminary Model Results 208
E5.3.2 Validated Model Results 211
E5.4 Bridge 3 Validation 215
E5.4.1 Preliminary Model Results 216
E5.4.2 Validated Model Results 218
References 223
E6 Model Validation Results 224

Table of Figures

Figure E2-1: Bridge 1 from parallel service road below bridge ... 3
Figure E2-2: Cross-section of Bridge 1 (adapted from contract plans provided by TxDOT)... 3
Figure E2-3: Girder elevation of Bridge 1 (adapted from contract plans provided by TxDOT) ... 3
Figure E2-4: Typical intermediate cross-frame configuration of Bridge 1 (from contract plans provided by TxDOT) ... 4
Figure E2-5: Bridge 2 from parallel frontage road below bridge ... 5
Figure E2-6: SB Span 1 of Bridge 2 highlighting lean-on braces (adapted from contract plans provided by TxDOT) ... 6
Figure E2-7: Cross-section A of Bridge 2 (adapted from contract plans provided by TxDOT)... 7
Figure E2-8: Cross-section B of Bridge 2 showing lean-on braces near interior support (adapted from contract plans provided by TxDOT) ... 7
Figure E2-9: Girder elevation of Bridge 2 (adapted from contract plans provided by TxDOT) ... 7
Figure E2-10: Typical intermediate cross-frame configuration on Bridge 2 (from contract plans provided by TxDOT)... 8
Figure E2-11: Typical lean-on cross-frame on Bridge 2 (from contract plans provided by TxDOT) ... 8
Figure E2-12: Bridge 3 from NB SH 146 (Image from Google Maps) ... 10
Figure E2-13: Cross-section of Bridge 3 (adapted from contract plans provided by TxDOT)... 10
Figure E2-14: Girder elevation of Bridge 3 (adapted from contract plans provided by TxDOT) ... 10
Figure E2-15: Typical intermediate cross-frame configuration on Bridge 3 (from contract plans provided by TxDOT)... 11
Figure E3-1: Screenshot of 3D FEA model for Bridge 1... 16
Figure E3-2: Screenshot of 3D FEA model for Bridge 2... 17
Figure E3-3: Screenshot of 3D FEA model for Bridge 3... 18
Figure E3-4: Location of gateway and wireless modem during field monitoring of Bridge 1 ... 19
Figure E3-5: Strain gage layout for single angles... 20
Figure E3-6: Laboratory study conducted to validate the linear regression programming... 20
Figure E3-7: Typical position of installed strain gages on the bottom flange of girders... 21
Figure E3-8: Typical position of wireless nodes during field instrumentation... 22
Figure E3-9: Typical welded strain gage used for instrumentation (wax and silicon for environmental protection are not shown)... 23
Figure E3-10: Boom lift and working platform stations utilized during instrumentation of Bridge 1 ... 24
Figure E3-11: Framing plan of Span 11... 24
Figure E3-12: Plan view of instrumented cross-frame locations ... 25
Figure E3-13: Cross-section view of strain gage locations at cross-frame line 4 in Span 11 ... 25
Figure E3-14: Cross-section view of strain gage locations at cross-frame line 7 in Span 11 ... 26
Figure E3-15: View of cross-frame line 4 after instrumentation ... 26
Figure E3-16: TMA blocking off traffic to the turnaround lane under Span 1 (Bridge 2) ... 27
Figure E3-17: RT instrumenting Bridge 2 on platforms and boom lift ... 28
Figure E3-18: Framing plan of Span 1... 28
Figure E3-19: Plan view of instrumented cross-frame locations ... 29
Figure E3-20: Cross-section view of strain gage locations at cross-frame line 8 in Span 1 ... 29
Figure E3-21: Partial cross-section view of strain gage locations at cross-frame line 5 in Span 1 ... 30
Figure E3-22: Cross-section view of strain gage locations at cross-frame line 2 in Span 1 ... 30
Figure E3-23: View of the cross-frame between girders 21 and 22 in line 2 after instrumentation ... 31
Figure E3-24: Position of boom lift relative to Bridge 3 ... 32
Figure E3-25: Researchers instrumenting Bridge 3 on platforms and boom lift ... 32

Figure E3-26: Framing plan of Span 11 33
Figure E3-27: Plan view of instrumented cross-frame locations 33
Figure E3-28: Cross-section view of strain gage locations at cross-frame line 10 in Span 11 34
Figure E3-29: Cross-section view of strain gage locations at cross-frame line 4 in Span 11 34
Figure E3-30: View of the cross-frame between girders 2 and 3 in line 10 after instrumentation 35
Figure E3-31: Setting a level surface for the laser distance meters prior to the Bridge 1 load test 36
Figure E3-32: Setting a level surface for the laser distance meters prior to the Bridge 2 load test 37
Figure E3-33: The RT preparing the bridge deck for a load test 37
Figure E3-34: TxDOT lane closure during Bridge 3 load test 38
Figure E3-35: Typical TxDOT dump truck used for the controlled live load test 39
Figure E3-36: Load case performed during the Bridge 1 load test 40
Figure E3-37: Load case performed during the Bridge 2 load test 41
Figure E3-38: Load case performed during the Bridge 3 load test 42
Figure E3-39: Previously instrumented cross-frame at Bridge 1 after equipment removed 51
Figure E4-1: Example showing the axial stress component of a cross-frame angle section versus the individual strain gage responses 53
Figure E4-2: Longitudinal and lateral bending stresses in girder flanges according to sign convention 55
Figure E4-3: Typical TxDOT truck wheel base dimensions for Bridge 1 load test 56
Figure E4-4: Instrumented cross-frame identification numbers at cross-frame line 4 57
Figure E4-5: Instrumented cross-frame identification numbers at cross-frame line 7 57
Figure E4-6: Typical plot used to align Load Case 0 time stamp with longitudinal position on bridge 58
Figure E4-7: Qualitative influence line for girder bending moment at cross-frame line 4 in Span 11 58
Figure E4-8: Influence line plots for bottom flange stresses at cross-frame line 4 (Load Case 0A through 0D) 61
Figure E4-9: Influence line plots for bottom flange stresses at cross-frame line 7 (Load Case 0A through 0D) 62
Figure E4-10: Influence line plots for bottom flange lateral stresses at cross-frame line 4 (Load Case 0A through 0D) 63
Figure E4-11: Influence line plots for bottom flange lateral stresses at cross-frame line 7 (Load Case 0A through 0D) 64
Figure E4-12: Influence line plots for cross-frame axial stresses at cross-frame line 4 (Load Case 0A through 0D) 65
Figure E4-13: Influence line plots for cross-frame axial stresses at cross-frame line 4 (Load Case 0A through 0D) 66
Figure E4-14: Influence line plots for cross-frame axial stresses at cross-frame line 4 (Load Case 0A through 0D) 67
Figure E4-15: Influence line plots for cross-frame axial stresses at cross-frame line 4 (Load Case 0A through 0D) 68
Figure E4-16: Influence line plots for cross-frame axial stresses at cross-frame line 7 (Load Case 0A through 0D) 69
Figure E4-17: Measured Load Case 1 bottom flange stress in girder 1 at cross-frame line 4 70
Figure E4-18: Cross-frame stress states at line 4 during Load Case 3 (Units: ksi) 72
Figure E4-19: Distribution of girder bending stresses along cross-frame line 4 for Load Cases 2, 3, 4, and 5 78
Figure E4-20: Girder deflection progression at cross-frame line 4 for Load Cases 1, 3, and 4 81
Figure E4-21: Girder deflection progression at cross-frame line 4 for Load Cases 5 through 7 82
Figure E4-22: Typical TxDOT truck wheel base dimensions for Bridge 2 load test 83
Figure E4-23: Instrumented cross-frame identification numbers at cross-frame line 8 84
Figure E4-24: Instrumented cross-frame identification numbers at cross-frame line 5 84

Figure E4-25: Instrumented cross-frame identification numbers at cross-frame line 2 84
Figure E4-26: Influence line plots for bottom flange stresses at cross-frame line 5 (Load Case 0A though 0C) 87
Figure E4-27: Influence line plots for bottom flange stresses at cross-frame line 8 (Load Case 0A through 0C) 88
Figure E4-28: Influence line plots for bottom flange lateral stresses at cross-frame line 5 (Load Case 0A through 0C) 89
Figure E4-29: Influence line plots for bottom flange lateral stresses at cross-frame line 8 (Load Case 0A through 0C) 90
Figure E4-30: Influence line plots for cross-frame axial stresses at cross-frame line 2 between girders 20 and 22 (Load Cases 0A through 0C) 91
Figure E4-31: Influence line plots for cross-frame axial stresses at cross-frame line 5 between girders 20 and 22 (Load Case 0A through 0C) 92
Figure E4-32: Influence line plots for cross-frame axial stresses at cross-frame line 8 between girders 18 and 20 (Load Case 0A through 0C) 93
Figure E4-33: Cross-frame stress states at cross-frame line 5 during Load Case 4 (Units: ksi) 95
Figure E4-34: Distribution of girder lateral and longitudinal bending stresses on instrumented girders along cross-frame line 5 for Load Cases 1 through 5 101
Figure E4-35: Distribution of girder lateral and longitudinal bending stresses on instrumented girders along cross-frame line 8 for Load Cases 2 through 6 102
Figure E4-36: Instrumented girders for bottom flange deflection measurements 103
Figure E4-37: Girder deflection progression at normal cross-section along cross-frame line 6 for Load Cases 1-4 106
Figure E4-38: Girder deflection progression at normal cross-section along cross-frame line 6 for Load Cases 5-7 107
Figure E4-39: Girder deflection progression at skewed midspan cross-section for Load Cases 1-4........ 108
Figure E4-40: Girder deflection progression at skewed midspan cross-section for Load Cases 5-7........ 109
Figure E4-41: Typical TxDOT truck wheel base dimensions for Bridge 3 load test. Dimensions between parenthesis correspond to Truck 2 only. 110
Figure E4-42: Instrumented cross-frame identification numbers at cross-frame line 4........................... 111
Figure E4-43: Instrumented cross-frame identification numbers at cross-frame line 10.......................... 111
Figure E4-44: Influence line plots for bottom flange stresses at cross-frame line 10 (Load Case 0A through 0D) 114
Figure E4-45: Influence line plots for bottom flange stresses at cross-frame line 4 (Load Case 0A through 0D) 115
Figure E4-46: Influence line plots for bottom flange lateral stresses at cross-frame line 10 (Load Case 0A through 0D)... 116
Figure E4-47: Influence line plots for bottom flange lateral stresses at cross-frame line 4 (Load Case 0A through 0D)... 117
Figure E4-48: Influence line plots for cross-frame axial stresses at cross-frame line 4 between girders 1 and 3 (Load Cases 0A through 0D) 118
Figure E4-49: Influence line plots for cross-frame axial stresses at cross-frame line 10 between girders 2 and 4 (Load Cases 0A through 0D) 119
Figure E4-50: Influence line plots for cross-frame axial stresses at cross-frame line 10 between girders 1 and 2 (Load Cases 0A through 0D) 120
Figure E4-51: Cross-frame stress states at cross-frame line 10 during Load Case 3 (Units: ksi)............. 122
Figure E4-52: Distribution of girder bending stresses on instrumented girders along cross-frame line 10 for Load Cases 1, 2, 3, 4 and 7. 128

Figure E4-53: Distribution of girder bending stresses on instrumented girders along cross-frame line 4 for Load Cases 1, 3, 4, 5 and 6. 129
Figure E4-54: Girder deflection progression at cross-frame line 11 for Load Cases 1-4 132
Figure E4-55: Girder deflection progression at cross-frame line 11 for Load Cases 5-7 133
Figure E4-56: Graphical depiction of converting variable stress range spectrum to single effective stress range........ 138
Figure E4-57: Sample cumulative density function depicting absolute maximum stress range and 99.99th percentile stress range 139
Figure E4-58: Sample of effective stress ranges and number of cycle counts using different truncation stress values 142
Figure E4-59: Sample plot demonstrating the effect of different levels of truncation on a data set........ 144
Figure E4-60: Sample rainflow histogram for cross-frame member 07 at Bridge 1........ 147
Figure E4-61: Sample calculation showing how AASHTO design metrics were determined 150
Figure E4-62: Sample rainflow histogram for cross-frame member 07 at Bridge 1 showing key Fatigue II design metrics 158
Figure E4-63: Daily stress range trends cross-frame member 09 at Bridge 1 159
Figure E4-64: Hourly stress range trends cross-frame member 09 at Bridge 1 159
Figure E4-65: Sample rainflow histogram for the critical flange tips at girder 3 (near cross-frame line 4) at Bridge 1........ 161
Figure E4-66: Sample rainflow histogram for cross-frame member 08 at Bridge 2........ 166
Figure E4-67: Sample rainflow histogram for cross-frame member 08 at Bridge 2 showing key Fatigue II design metrics 169
Figure E4-68: Daily stress range trends cross-frame member 08 at Bridge 2 170
Figure E4-69: Hourly stress range trends cross-frame member 08 at Bridge 2 170
Figure E4-70: Sample rainflow histogram for the critical flange tips at Girder 19 (near cross-frame line 8) at Bridge 2........ 171
Figure E4-71: Sample rainflow histogram for cross-frame member 10 at Bridge 3........ 175
Figure E4-72: Sample rainflow histogram for cross-frame member 10 at Bridge 3 showing key Fatigue II design metrics 178
Figure E4-73: Daily stress range trends cross-frame member 10 at Bridge 3 179
Figure E4-74: Hourly stress range trends cross-frame member 10 at Bridge 3 179
Figure E4-75: Sample rainflow histogram for the critical flange tips at Girder 1 (near cross-frame line 10) at Bridge 3........ 180
Figure E5-1: Front elevation of standard elastomeric bearing detail for E- and F-type bearings (from TxDOT standard drawing SGEB) 189
Figure E5-2: Close-up of standard elastomeric bearing detail for ES-type bearing (from TxDOT standard drawing SGEB)........ 189
Figure E5-3: Expansion bearing photographed at Bridge 2........ 190
Figure E5-4: Screenshot of Bridge 3 model demonstrating boundary conditions assignments........ 192
Figure E5-5: SSTR-type concrete rail used at Bridge 3 (adapted from Google Maps) 193
Figure E5-6: Representative concrete rail element in the validated FEA models 193
Figure E5-7: Cross-section of validated Bridge 3 model showing deck and haunch thickness........ 195
Figure E5-8: Partitioned deck shells for the application of truck loads........ 196
Figure E5-9: Cross-frame detail showing tie constraints between connection plates and gusset plates... 197
Figure E5-10: Isometric view of the Bridge 1 FEA model (steel framing only) 198
Figure E5-11: Comparing measured data, preliminary model results, and validated model results for load case 1 and 4 girder deflections........ 205
Figure E5-12: Comparing measured data, preliminary model results, and validated model results for load case 2 and 4 girder flange stresses 206

Figure E5-13: Comparing measured data, preliminary model results, and validated model results for load case 3 cross-frame forces at line 4 (Units: kips) 207
Figure E5-14: Isometric view of the Bridge 2 FEA model (steel framing only) 208
Figure E5-15: Transverse section of Bridge 2 (from contract plans provided by TxDOT) 209
Figure E5-16: Connection detail for the interior concrete rail at Bridge 2 (from contract plans provided by TxDOT) 210
Figure E5-17: Comparing measured data, preliminary model results, and validated model results for load case 2 girder deflections 213
Figure E5-18: Comparing measured data, preliminary model results, and validated model results for load case 2 girder flange stresses of line 5 214
Figure E5-19: Comparing measured data, preliminary model results, and validated model results for load case 5 cross-frame forces at line 5 (Units: kips) 215
Figure E5-20: Isometric view of the Bridge 3 FEA model (steel framing only) 216
Figure E5-21: Comparing measured data, preliminary model results, and validated model results for load case 4 girder deflections 220
Figure E5-22: Comparing measured data, preliminary model results, and validated model results for load case 4 girder flange stresses 221
Figure E5-23: Comparing measured data, preliminary model results, and validated model results for load case 4 cross-frame forces at line 10 (Units: kips) 222

Table of Tables

Table E2-1: Pertinent information of three instrumented bridges ... 2
Table E3-1: Instrumentation schedule for three instrumented bridges ... 14
Table E3-2: Procedural outline for controlled live load testing ... 39
Table E3-3: Critical Stage II (controlled live load test) load cases for Bridge 1 ... 43
Table E3-4: Critical Stage II (controlled live load test) load cases for Bridge 2 ... 45
Table E3-5: Critical Stage II (controlled live load test) load cases for Bridge 3 ... 48
Table E4-1: TxDOT truck axle weights for Bridge 1 load test ... 56
Table E4-2: Summary of static stress states from Figure E4-17 ... 71
Table E4-3: Bottom flange longitudinal stresses in instrumented girders for Load Cases 1-7 ... 73
Table E4-4: Bottom flange lateral bending stresses in instrumented girders for Load Cases 1-7. ... 74
Table E4-5: Axial stresses in instrumented cross-frame members for Load Cases 1-7 ... 75
Table E4-6: Girder deflection measurements at cross-frame line 4 for Load Cases 1-7 ... 79
Table E4-7: TxDOT truck axle weights for Bridge 2 load test ... 83
Table E4-8: Bottom flange longitudinal stresses in instrumented girders for Load Cases 1-7 ... 96
Table E4-9: Bottom flange lateral bending stresses in instrumented girders for Load Cases 1-7. ... 97
Table E4-10: Axial stresses in instrumented cross-frame members for Load Cases 1-7 ... 98
Table E4-11: Girder deflection measurements for load cases 1-7 ... 104
Table E4-12: TxDOT truck axle weights for Bridge 2 load test ... 110
Table E4-13: Bottom flange longitudinal stresses in instrumented girders for Load Cases 1-7 ... 123
Table E4-14: Bottom flange lateral bending stresses in instrumented girders for Load Cases 1-7 ... 124
Table E4-15: Axial stresses in instrumented cross-frame members for Load Cases 1-7 ... 125
Table E4-16: Girder deflection measurements for Load Cases 1-7 at cross-frame line 11 ... 130
Table E4-17: Comparison of live load test results ... 134
Table E4-18: Summary of truncation stresses assigned at each subject bridge ... 145
Table E4-19: Comparison between measured rainflow cross-frame response and key AASHTO design metrics (Bridge 1) ... 149
Table E4-20: Comparison between measured rainflow girder response and key AASHTO design metrics (Bridge 1) ... 163
Table E4-21: Comparison between measured rainflow cross-frame response and key AASHTO design metrics (Bridge 2) ... 167
Table E4-22: Comparison between measured rainflow girder response and key AASHTO design metrics (Bridge 2) ... 173
Table E4-23: Comparison between measured rainflow cross-frame response and key AASHTO design metrics (Bridge 3) ... 176
Table E4-24: Comparison between measured rainflow girder response and key AASHTO design metrics (Bridge 3) ... 182
Table E4-25: Ranges of all equivalent cycles, effective stress ranges, and maximum stress ranges measured for cross-frames at each subject bridge ... 185
Table E4-26: Ranges of all equivalent cycles, effective stress ranges, and maximum stress ranges measured for girders at each subject bridge ... 185
Table E5-1: Assumed lateral stiffness of expansion bearings in FEA models ... 191
Table E5-2: Summary of the key modeling parameters modified ... 198
Table E5-3: Preliminary analytical versus measured girder deflections at cross-frame line 4 for Load Cases 1-7 (Bridge 1) ... 200
Table E5-4: Preliminary analytical versus measured girder deflections at cross-frame line 4 for pertinent load cases (Bridge 1) ... 201

Table E5-5: Preliminary analytical versus measured girder bottom flange stresses for pertinent load cases (Bridge 1) 201
Table E5-6: Preliminary analytical versus measured cross-frame axial forces for pertinent load cases (Bridge 1) 202
Table E5-7: Validated analytical versus measured girder deflections at cross-frame line 4 for pertinent load cases (Bridge 1) 203
Table E5-8: Validated analytical versus measured girder bottom flange stresses for pertinent load cases (Bridge 1) 203
Table E5-9: Validated analytical versus measured cross-frame axial forces for pertinent load cases (Bridge 1) 204
Table E5-10: Preliminary analytical versus measured girder deflections for pertinent load cases (Bridge 2) 209
Table E5-11: Preliminary analytical versus measured girder bottom flange stresses for pertinent load cases (Bridge 2) 210
Table E5-12: Preliminary analytical versus measured cross-frame axial forces for pertinent load cases (Bridge 2) 211
Table E5-13: Validated analytical versus measured girder deflections for pertinent load cases (Bridge 2) 212
Table E5-14: Validated analytical versus measured girder bottom flange stresses for pertinent load cases (Bridge 2) 212
Table E5-15: Validated analytical versus measured cross-frame axial forces for pertinent load cases (Bridge 2) 213
Table E5-16: Preliminary analytical versus measured girder deflections at cross-frame line 11 for pertinent load cases (Bridge 3) 217
Table E5-17: Preliminary analytical versus measured girder bottom flange stresses at cross-frame line 10 for pertinent load cases (Bridge 3) 217
Table E5-18: Preliminary analytical versus measured cross-frame axial forces at cross-frame line 10 for pertinent load cases (Bridge 3) 218
Table E5-19: Validated analytical versus measured girder deflections at cross-frame line 11 for pertinent load cases (Bridge 3) 219
Table E5-20: Validated analytical versus measured girder bottom flange stresses at cross-frame line 10 for pertinent load cases (Bridge 3) 219
Table E5-21: Validated analytical versus measured cross-frame axial forces at cross-frame line 10 for pertinent load cases (Bridge 3) 220

CHAPTER E1

Introduction

The final report of NCHRP Project 12-113 succinctly summarizes the key outcomes of the research for practicing engineers. As such, many of the detailed results were not included in the body of the main document for clarity. The intent of this appendix is to provide a more comprehensive overview of the work completed in Phase II of the project. Similarly, Appendix D and F expand on Phase I and III of the project, respectively. For reference, Phase II is comprised of the following tasks, which were previously identified in main body of the final report as well as the project Request for Proposals (RFP):

- Task 7: Execute the Part 1 of analytical program that is related to field experiment only (i.e., three bridges) to finalize the field experiment work plan including a matrix of testing parameters and design details. Submit a task report for panel review and approval before conducting a field experiment.
- Task 8: Execute the field experiment according to the approved Task 7 report.
- Task 9: Validate the analytical program based on the results of the field experiment.
- Task 10: Prepare Interim Report No. 2 that documents the results of Tasks 7 through 9 and provides an updated work plan for the remainder of the project. This report is due no later than 12 months after approval of Phase I. The updated plan must describe the work proposed for Phases III through IV.

This appendix outlines the procedures used to accomplish Tasks 7 through 9, as well as presents pertinent results. It is organized in a traditional report format and is divided into seven distinct chapters. Following this introductory chapter, Chapter E2 provides a detailed description for the three instrumented bridges, including location, geometry, and unique cross-frame details. Chapter E3 outlines the instrumentation plan executed by the research team (RT) to obtain field measurements. Four different stages of field activity are outlined in this chapter: installation of sensors and data acquisition system, controlled live load testing, in-service monitoring, and demobilization of sensors and data acquisition system. Chapter E4 presents the results of the field monitoring studies for both the controlled live load test and the in-service rainflow data. The field measurements summarized in Chapter E4 were used to validate the finite element models. The development and validation of the finite element models based on the field measurements is discussed in Chapter E5. Finally, two supplementary chapters are included at the end to provide the reader with the additional reference material. In Chapter E6, the full results of the model validation are provided for reference.

CHAPTER E2

Bridge Information

This chapter summarizes the basic information of the three bridges that were instrumented and monitored as part of the study. The information that is provided includes geometry and cross-frame details. References to the general location have been intentionally excluded from this appendix. In accordance with the project RFP, the instrumented bridges include (i) a straight bridge with normal supports, (ii) a straight bridge with skewed supports, and (iii) a horizontally curved bridge. Pertinent information for the three bridges is summarized in Table E2-1. The bridge number corresponds to the order in which the bridges were instrumented, monitored, and tested.

Table E2-1: Pertinent information of three instrumented bridges

Bridge No.	Type	Highway System
1	Straight; normal supports	Northbound (NB) Interstate Highway (IH) 45 Frontage Road
2	Straight; skewed supports	Southbound (SB) IH 45
3	Horizontally-curved	Southbound (SB) SH 146

E2.1 Bridge 1

Constructed in 2007, Bridge 1 serves as an off-ramp for traffic traveling northbound on IH 45. The bridge contains 13 spans with a total length of 1724 feet. The girders in Spans 1 through 8 and 12 through 13 are prestressed concrete and are not considered in this investigation. Spans 9 through 11 consist of continuous, built-up steel plate girders acting compositely with an 8-inch thick concrete deck. Bridge 1 is straight with supports oriented normal to the girder lines. The respective lengths of Spans 9, 10, and 11 are 194 feet, 240 feet, and 194 feet. The total width of the bridge is 41-5″. The bridge supports three 12-foot northbound lanes of traffic. There are five girder lines spaced at 8′-6″ on center and deck overhangs of approximately 4 feet on each side of the bridge. Girder webs are 6-feet deep except at the dapped ends, which results in a span-to-girder depth ratio of 32 at the end spans. There are several flange thickness transitions along the length of the girders. According to the 2007 construction drawings, the estimated average daily traffic (ADT) for this bridge is 3,300.

Figure E2-1 shows an image of the bridge taken from ground level next to the residential service road parallel to the subject bridge. Spans 10 and 11 are identified in this figure. Note that only Span 11 was instrumented, as is discussed later in the appendix. Figure E2-2 shows the typical cross-section of Spans 9 through 11, and Figure E2-3 shows an elevation view to demonstrate the basic span lengths and the nonprismatic girder sections.

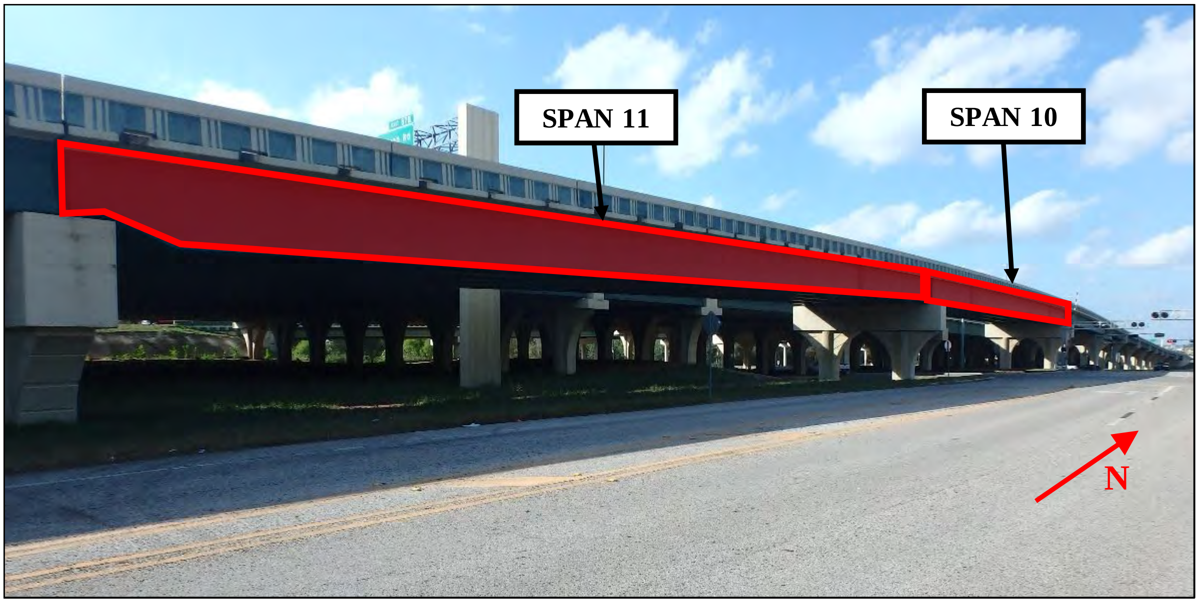

Figure E2-1: Bridge 1 from parallel service road below bridge

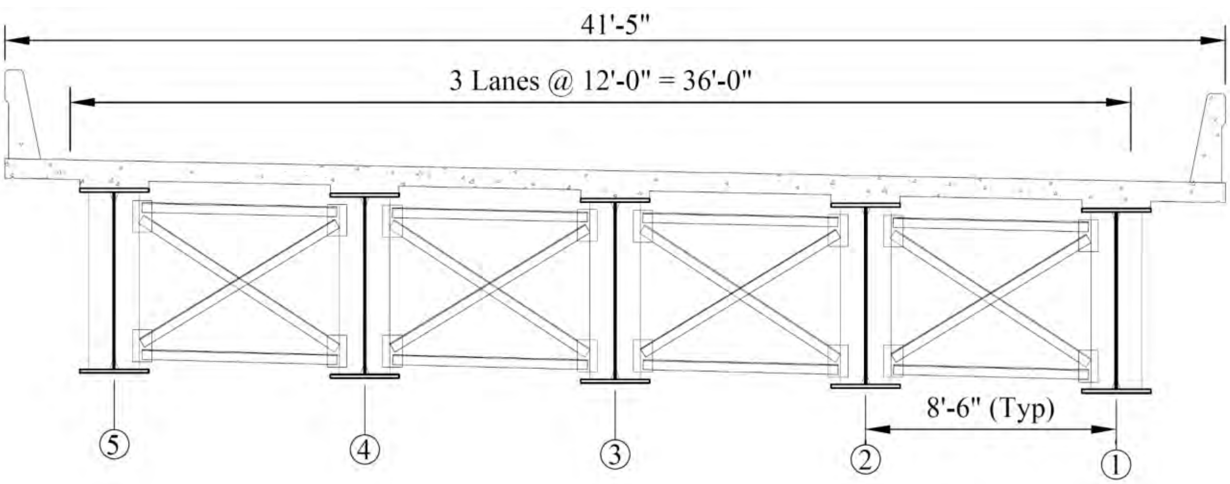

Figure E2-2: Cross-section of Bridge 1 (adapted from contract plans provided by TxDOT)

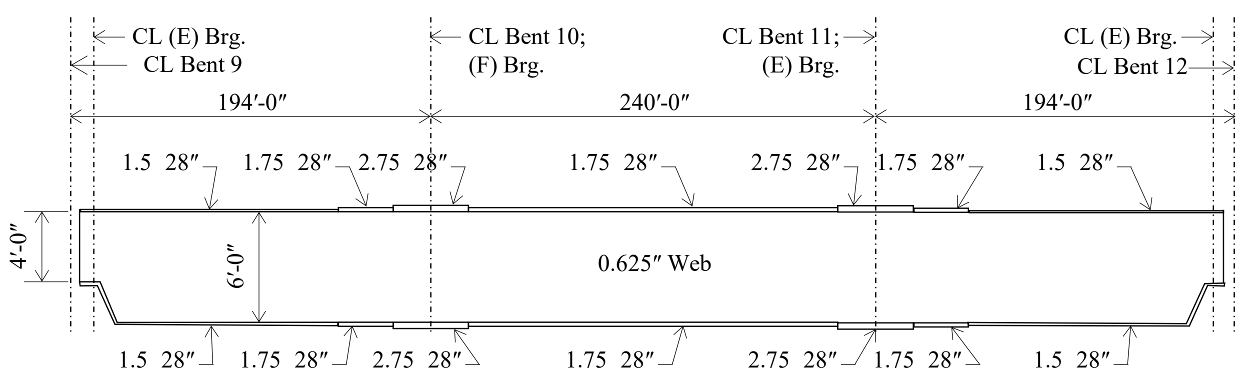

Figure E2-3: Girder elevation of Bridge 1 (adapted from contract plans provided by TxDOT)

There are three types of cross-frame configurations used on this bridge. End cross-frames are K-type frames that consist of a WT top strut compositely connected to the deck and single angle L4x4x1/2 bottom strut and diagonal sections. Cross-frames at interior pier locations are X-type frames with single angle L4x4x1/2 sections for the top struts, bottom struts, and diagonal members.

Of particular interest for this investigation are the intermediate cross-frames (between supports). The intermediate cross-frames are X-type frames with single angle L4x4x3/8 sections for the top struts, bottom struts, and diagonal members. All member-to-gusset and gusset-to-connection plate connections are welded, as illustrated by Figure E2-4. The detailing of this cross-frame is identical to the standard TxDOT intermediate cross-frame. Based upon the results of the Phase I industry survey, aside from the welded connections, the layout of the cross frame is also consistent with one of the most popular cross-frame geometries used by bridge owners throughout the US. Note that the connection plates are welded along three sides (i.e., along the girder web and both girder flanges), which mitigates distortion-induced fatigue issues that plagued many bridges built prior to the 1980s.

Cross-frames are typically spaced at approximately 19 feet on center. The framing plan provided in Figure E3-11 schematically shows the layout of cross-frames on Bridge 1.

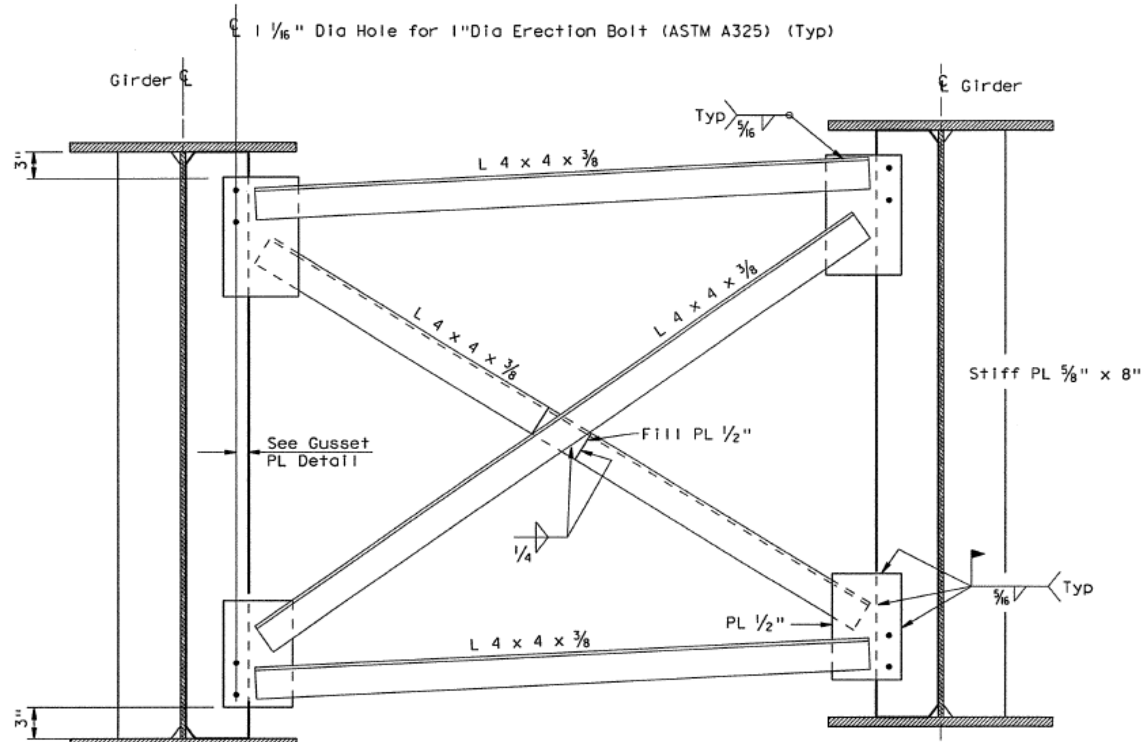

Figure E2-4: Typical intermediate cross-frame configuration of Bridge 1 (from contract plans provided by TxDOT)

In selecting the bridges for instrumentation during Phase I of the project, Bridge 1 offered several advantages including the following:

- The spans are long and relatively narrow but still support three striped lanes. The system is not overly redundant, and three lanes offer a variety of potential load positions for the controlled live load tests;
- Access for instrumentation on Span 11 is ideal and requires no traffic control;

- Traffic control for the frontage road off-ramp should be simple for controlled live load testing since the bridge can essentially be closed with little impact to the travelling public;
- The IH 45 corridor has a high traffic volume with large ADTT.

In contrast, the only difficulties identified and observed by the RT are the following:

- The speed of traffic on the off-ramp may be lower than typical highway bridges thereby affecting dynamic load effects;
- A railroad line and roadway beneath eliminated two of the three steel girder spans for potential instrumentation.

In the opinion of the RT, the above-referenced difficulties presented little impact on the suitability of this bridge for instrumentation in the study.

E2.2 Bridge 2

Constructed in 2007, Bridge 2 is a three-span continuous, steel I-girder bridge with a total length of 465 feet. It serves the IH 45 corridor. Each span is constructed with steel plate girders acting compositely with an 8-inch thick concrete deck. The bridge supports are skewed relative to the centerline of the bridge to accommodate the roadway below. The skew angle is approximately 42 degrees. The respective lengths of Spans 1, 2, and 3 are 125 feet, 215 feet, and 125 feet. The total width of the bridge is approximately 96 feet. The bridge supports five 12-foot southbound lanes of traffic and shoulders on each side of the deck. There are twelve girder lines spaced at 8.11 feet on-center and deck overhangs of approximately 3 feet on each side of the bridge. All twelve girders are identical in design. Similar to Bridge 1, there are several flange thickness transitions along the length of the girders. The girder webs are 60 inches deep, which results in a span-to-girder depth ratio of 25 at the end spans.

According to 2016 TxDOT traffic maps, the ADT for this bridge is 120,510, which provides excellent rainflow data for gaining a measure of the stress history of the structural components.

Figure E2-5 shows an image of the bridge taken from the frontage road parallel to the subject bridge. Spans 1 and 2 are identified in this figure. Note that only Span 1 over the north turnaround lane was instrumented, as is discussed later in the appendix.

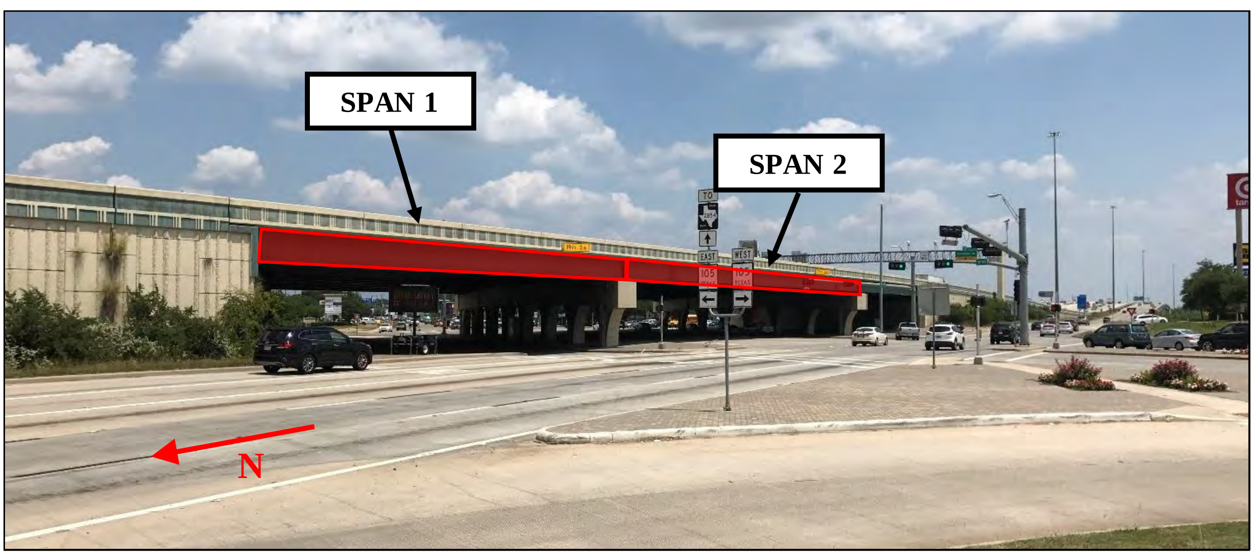

Figure E2-5: Bridge 2 from parallel frontage road below bridge

There are four types of cross-frame configurations used in this bridge. End cross-frames are X-type frames that consist of a WT top strut compositely connected to the deck and single angle L5x5x1/2 bottom strut and diagonal sections. Cross-frames at interior pier locations are X-type frames with single angle L5x5x1/2 sections for the top struts, bottom struts, and diagonal members.

Similar to Bridge 1, the intermediate cross-frames (between supports) are the major focus of the research. Typical intermediate cross-frames are X-type frames with single angle L5x5x1/2 sections for the top struts, bottom struts, and diagonal members. Contiguous lines of cross-frames are utilized, despite the severe support skews, in accordance with current guidance in American Association of State Highway and Transportation Officials LRFD Bridge Design Specifications (henceforth referred to as AASHTO LRFD). Unique to Bridge 2, the designer employed lean-on bracing near the interior skewed support lines. Lean-on braces utilize only top and bottom struts, thereby eliminating the diagonal members. Lean-on braces are double angle (2L5x5x1/2) sections for top and bottom struts only with one intermediate spacer plate. The first line of cross-frames are offset at least 3 feet from the girder support, and the typical spacing for intermediate cross-frame lines is 17 feet for the instrumented span.

Figure E2-6 illustrates the location of lean-on braces in Span 1. Figure E2-7 shows the typical cross-section without lean-on braces, labeled as Section A in Figure E2-6 . For referencing purposes, the intermediate (i.e., between supports) cross frame lines were numbered sequentially from north to south. Section A corresponds to intermediate cross-frame line 5. Figure E2-8 shows the typical cross-section with lean-on braces, labeled as Section B in Figure E2-6. Section B corresponds to intermediate cross-frame line 7. Figure E2-9 shows an elevation view to demonstrate the basic span lengths and the nonprismatic girder sections.

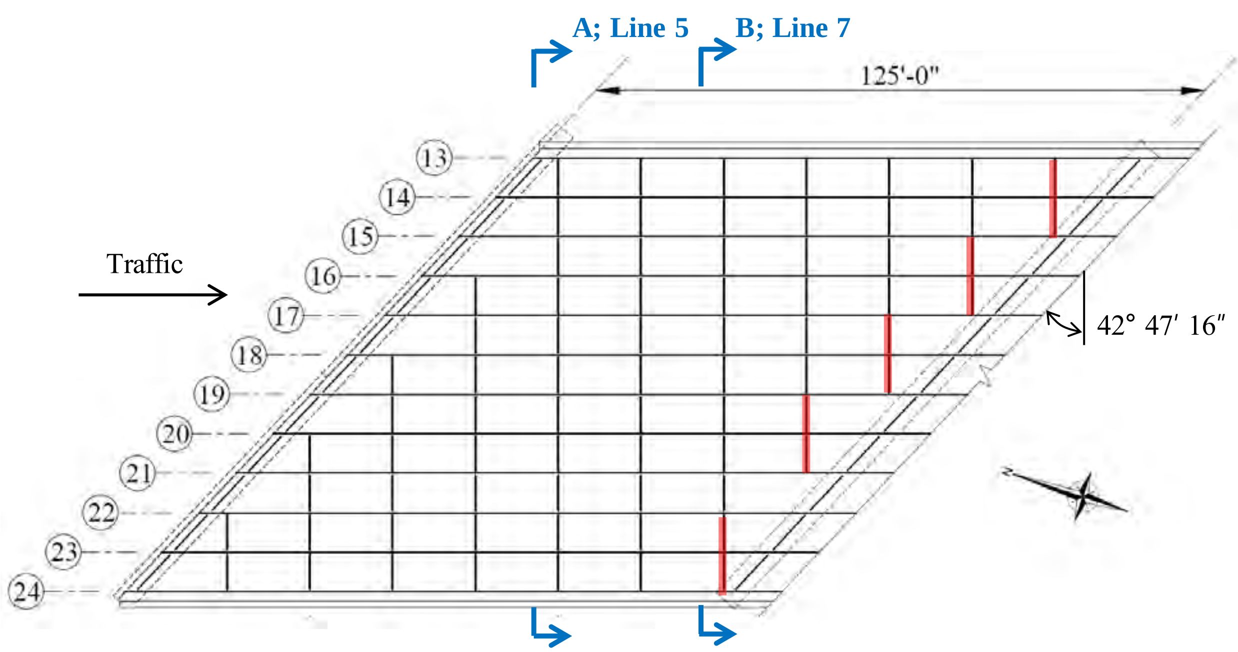

Figure E2-6: SB Span 1 of Bridge 2 highlighting lean-on braces (adapted from contract plans provided by TxDOT)

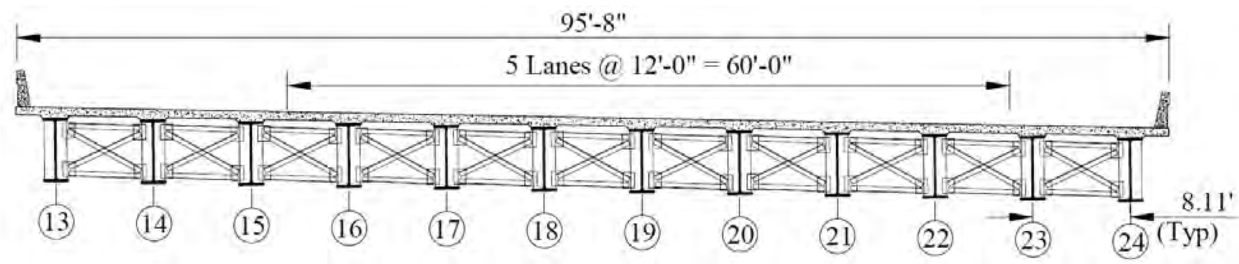

Figure E2-7: Cross-section A of Bridge 2 (adapted from contract plans provided by TxDOT)

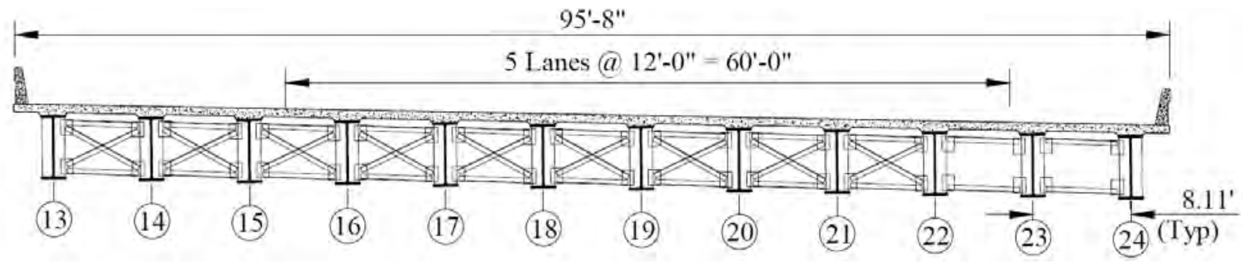

Figure E2-8: Cross-section B of Bridge 2 showing lean-on braces near interior support (adapted from contract plans provided by TxDOT)

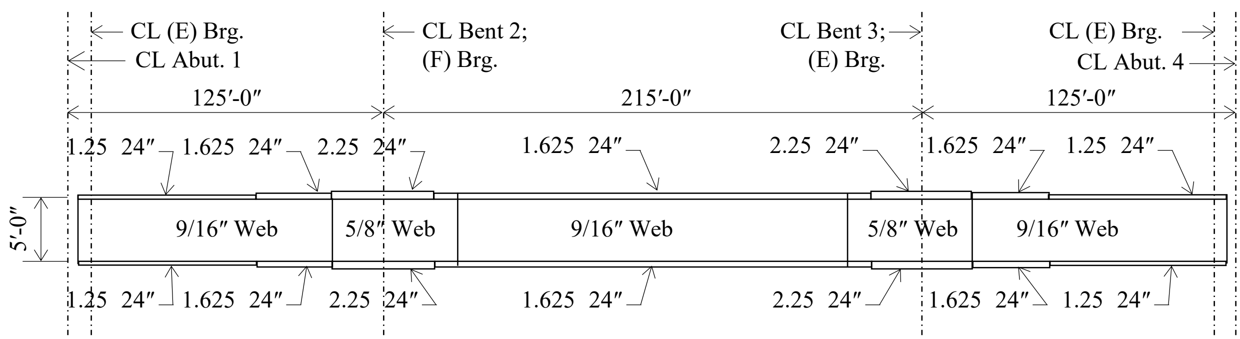

Figure E2-9: Girder elevation of Bridge 2 (adapted from contract plans provided by TxDOT)

In bridges with skewed supports and cross-frames oriented perpendicular to the girder lines, cross-frames connect to the girders at different locations along the individual girder lengths. As a result, there can be relatively large forces induced in the cross-frames due to differential girder deflections under truck traffic. This is of particular concern for cross-frames that frame into or near skewed supports where the differential deflection between adjacent girders can be large since deflection of one girder is relatively small or negligible. By removing the diagonal members in these select cross-frames, the bracing line is softened, and the live-load-induced forces are reduced. Despite the fact that lean-on bracing schemes can be used throughout an entire framing system, the designer in this case opted to only apply the concepts in the regions around interior supports. All member-to-gusset and gusset-to-connection plate connections are welded, as illustrated by Figure E2-10 and Figure E2-11. The detailing of this cross-frame is identical to the standard TxDOT intermediate cross-frame. Note that the connection plates are welded along three sides to the girder web and flanges.

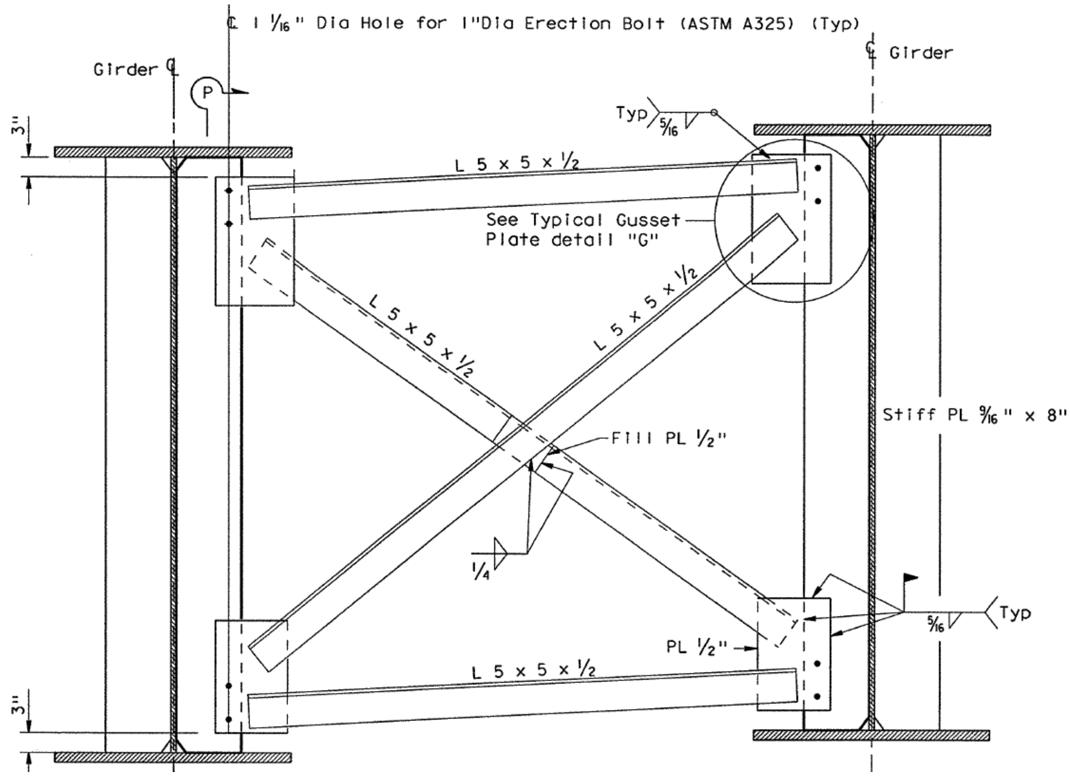

Figure E2-10: Typical intermediate cross-frame configuration on Bridge 2 (from contract plans provided by TxDOT)

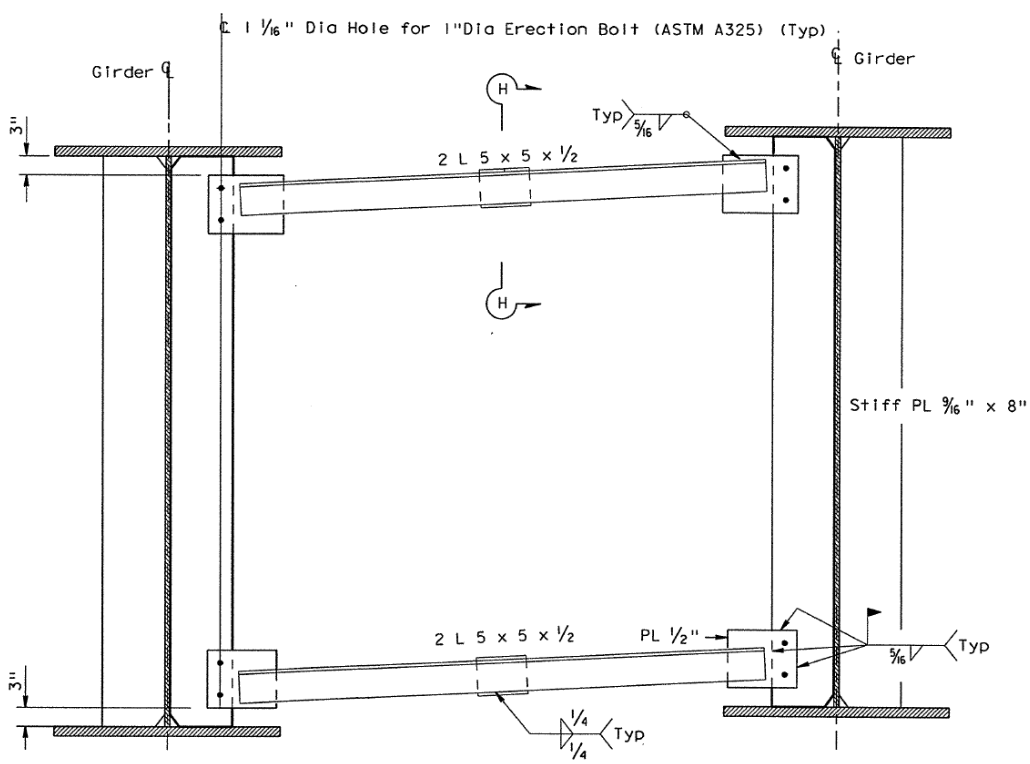

Figure E2-11: Typical lean-on cross-frame on Bridge 2 (from contract plans provided by TxDOT)

In selecting the bridges for instrumentation during Phase I of the project, Bridge 2 offered several advantages including the following:

- The span lengths are reasonably representative of steel bridge systems;
- The girders support five striped lanes, which offers a variety of potential load positions for the controlled live load tests;
- Access for instrumentation on Span 1 is ideal and requires relatively limited traffic control;
- The IH 45 corridor is high volume with large ADTT.

In contrast, the only difficulties identified and observed by the RT are the following:

- The bridge is a highly redundant system given the number of girders;
- Traffic control of SB IH 45 for controlled live load testing is complex.

In the opinion of the RT, the above-referenced difficulties had little impact on the suitability of this bridge for instrumentation in the study.

E2.3 Bridge 3

Bridge 3 was constructed in 2009 and is a direct connector along the SH 146 corridor that primarily serves large trucks traveling to nearby shipping ports. According to the 2009 construction drawings, the ADT is 40,000.

The bridge contains 14 spans with a total length of 2268 feet. The girders in Spans 1 through 7 and 12 through 14 are prestressed concrete and are not considered in this investigation. Spans 8 through 11 are constructed with continuous, built-up steel plate girders acting compositely with an 8-inch thick concrete deck. Bridge 3 is horizontally curved with an 800-foot radius of curvature. The supports are normal to the centerline of the bridge. The respective lengths of Spans 8, 9, 10, and 11 are 255 feet, 310 feet, 238 feet, and 216 feet. The total width of the bridge is 28′-5″. The bridge is striped for one 14-foot lane of traffic and two shoulders (4 and 8 feet wide, respectively). Based on the width of the bridge, this bridge could have two design lanes. There are four parallel girder lines spaced approximately 7.5 feet on center and deck overhangs of 3 feet on each side of the bridge. Similar to the other two subject bridges, there are several flange thickness transitions along the length of the girders. The design of all four girders is identical, except for small variations in flange transition locations as well as the radius and corresponding girder span. Girder webs are 8-feet deep except at the dapped ends, which results in a span-to-girder depth ratio of 27 at Span 11.

Figure E2-12 shows an image of the bridge taken from the northbound lanes of SH 146 below the curved steel spans. Spans 10 and 11 are identified in this figure. Note that only Span 11 was instrumented. Figure E2-13 shows the typical cross-section and intermediate cross-frame of the bridge, and Figure E2-14 shows an elevation view to demonstrate the basic span lengths and the nonprismatic girder sections. Note the girder lengths vary across the width; thus, the centerline span dimension is presented in the elevation sketch.

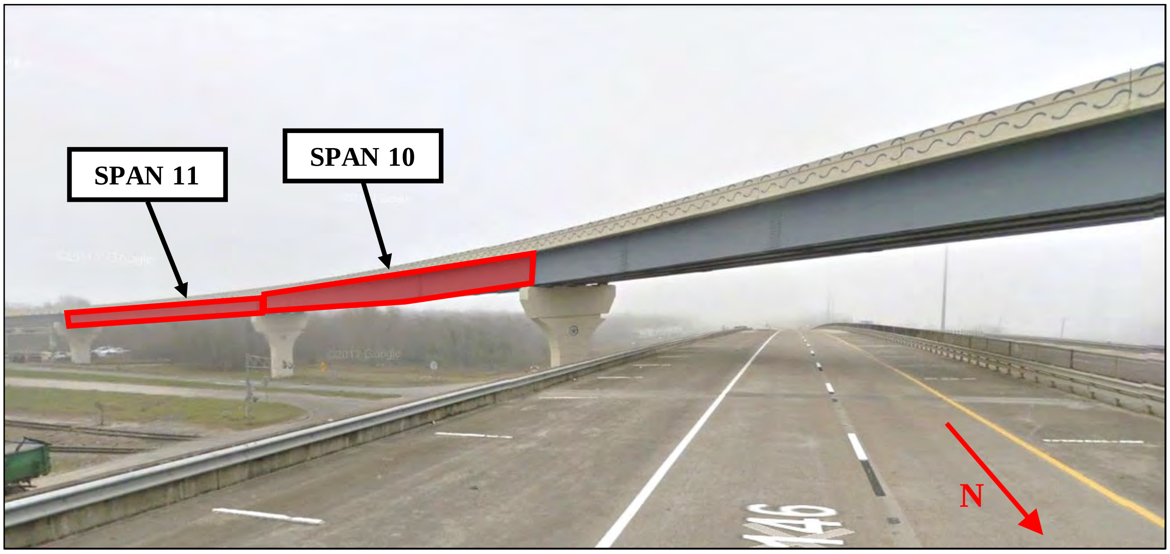

Figure E2-12: Bridge 3 from NB SH 146 (Image from Google Maps)

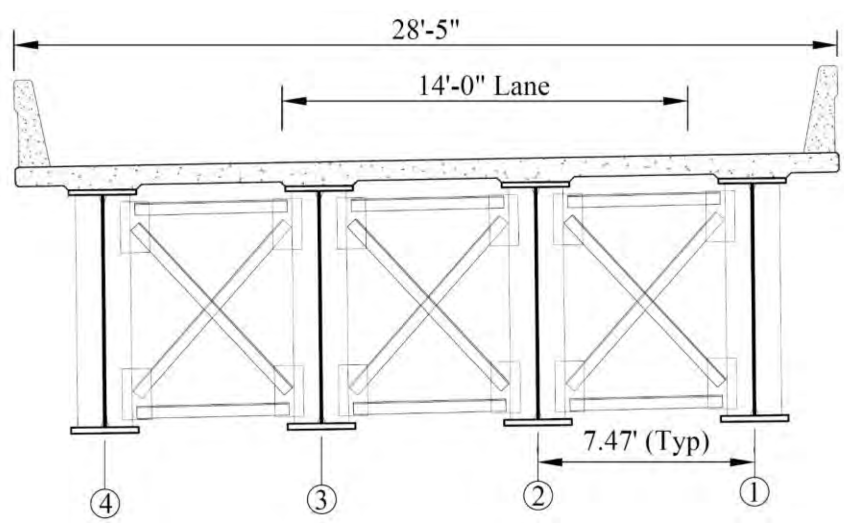

Figure E2-13: Cross-section of Bridge 3 (adapted from contract plans provided by TxDOT)

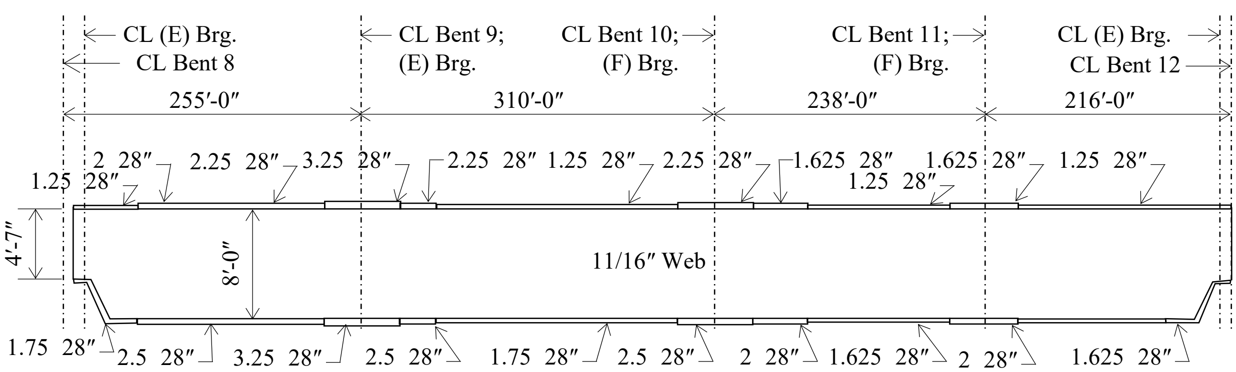

Figure E2-14: Girder elevation of Bridge 3 (adapted from contract plans provided by TxDOT)

There are three types of cross-frame configurations used on this bridge. End cross-frames are K-type frames that consist of a WT top strut compositely connected to the deck and single angle L5x5x1/2 bottom strut and diagonal sections. Cross-frames at interior support locations are X-type frames with single angle L5x5x1/2 sections for the top struts, bottom struts, and diagonal members.

The intermediate cross-frames are X-type frames with single angle L5x5x1/2 sections for the top struts, bottom struts, and diagonal members. Like the other two subject bridges, all member-to-gusset and gusset-to-connection plate connections are welded, as illustrated by Figure E2-15. The design plans provided an alternate bolted connection detail for gusset-to-connection plate connections; however, the connections the RT observed were all welded connections. Also note that the connection plates are welded along three sides to the girder web and flanges.

Cross-frames are typically spaced radially at approximately 12′-3″ feet on center. The cross-frames are normally oriented with respect to the curved girders. The framing plan provided in Figure E3-26 schematically shows the layout of cross-frames on Bridge 3.

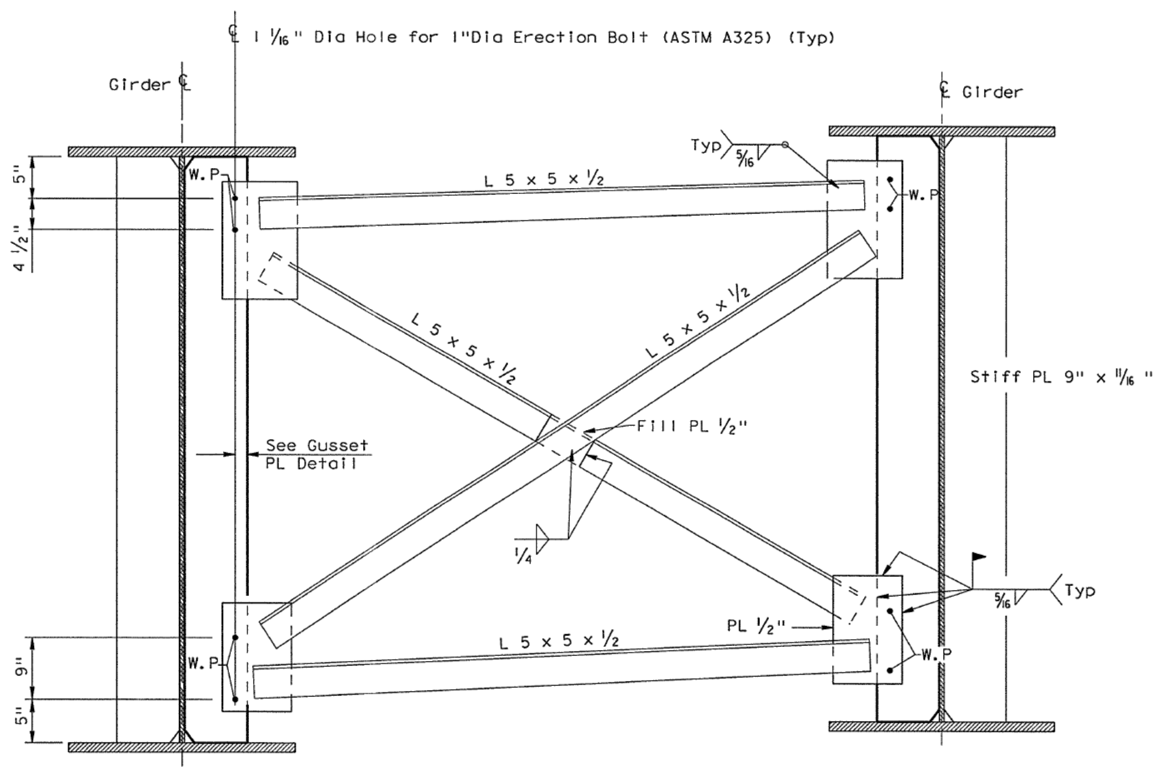

Figure E2-15: Typical intermediate cross-frame configuration on Bridge 3 (from contract plans provided by TxDOT)

In selecting the bridges for instrumentation during Phase I of the project, Bridge 3 offered several advantages including the following:

- The spans are long and the bridge has significant curvature (radius of curvature is 800 feet);
- Since the bridge has only four girders, every cross-frame should be engaged for all loading conditions;
- Access for instrumentation requires limited traffic control given the low volume of traffic on the roadway beneath the bridge;

- The direct connector services large volumes of heavy trucks.
- The bridge has a single striped lane, but two design lanes. Data can be obtained considering both the striped lanes as well as likely design lane positions during the controlled live load tests.

In contrast, the difficulties of this bridge identified and observed by the RT are as follows:

- The relatively narrow deck width limits the number of load cases that can be considered during the controlled live load tests.

In the opinion of the RT, the above-referenced difficulty had little impact on the suitability of this bridge for instrumentation in the study.

CHAPTER E3

Instrumentation Plan

This chapter outlines preliminary finite element analysis (FEA) work of Task 7 that preceded the field instrumentation work of Task 8 and outlines the instrumentation plan and schedule executed for all three bridges. Four different stages of field activity are discussed for each bridge: installation of sensors and data acquisition system, controlled live load testing, in-service monitoring, and demobilization of sensors and data acquisition system.

E3.1 Schedule

The RT divided the instrumentation of each bridge into the following four stages:

- Stage I – Installation of Sensors and Data Acquisition (DAQ) System
- Stage II – Controlled Live Load Testing
- Stage III – In-Service Monitoring
- Stage IV – Removal of Sensors and DAQ System

The tasks and procedures for each of these stages is outlined in detail in the following sections. Table E3-1 presents the final executed schedule for each stage of field activities. Note that there was no need for Stages II and III to occur in sequential order. Stage II (controlled live load testing) could occur at any time while the instrumentation was deployed on the bridge, and could occur prior to, during, or after Stage III. The timing of Stage II depended on the schedule constraints of TxDOT and of the RT. Traffic control was a major consideration for when Stage II could occur.

Table E3-1: Instrumentation schedule for three instrumented bridges

Bridge	Phase	Task Description	Week Starting																									
			March				April					May				June				July					August			
			4	11	18	25	1	8	15	22	29	6	13	20	27	3	10	17	24	1	8	15	22	29	5	12	19	26
1	I	Installation of DAQ System	9																									
	II	Controlled Live Load Testing					4																					
	III	Continuous Data Collection	March 10 – June 6																									
	IV	Removal of DAQ System														6												
2	I	Installation of DAQ System															10 - 12											
	II	Controlled Live Load Testing																		7								
	III	Continuous Data Collection															June 12 – July 8											
	IV	Removal of DAQ System																			8							
3	I	Installation of DAQ System																			11 - 12							
	II	Controlled Live Load Testing																						28				
	III	Continuous Data Collection																			July 14 – August 10							
	IV	Removal of DAQ System																							10			

Contingency time was built into the schedule to allow for troubleshooting of the DAQ system, particularly during the monitoring period of Bridge 1. Hence, the continuous in-service monitoring time (Stage III) of Bridge 1 lasted over two months longer than the instrumentation period for Bridges 2 and 3. This extra time was largely used to modify programming on the DAQ system. The initial programming of the DAQ system captured rainflow data on individual strain gages, which consisted of storing measured strains and stresses of individual gages into specific bins so that a histogram of specific stress cycles could be obtained over the allotted measuring period. Upon initial review of the collected data, the RT recognized that the collected data was not consistent with a conventional fatigue evaluation of cross-frame members.

In computer models that are used during design, cross-frames are typically idealized as trusses with the members primarily subjected to axial forces/stresses. However, since these members often consist of single angle sections with eccentric connections, the actual members experience combined bending and axial stress. As a result, each angle is instrumented with four strain gages. In a static loading case, the individual strain gage readings can be used to eliminate the bending component and determine the equivalent axial stress that is consistent with how a designer evaluates fatigue in these members. Since the initial rainflow algorithms that were used on the DAQ system collected individual strain gage readings over time, it was not possible to associate readings from the respective gages on a given angle, and therefore the equivalent axial stress could not be determined. A significant effort was dedicated to processing the data on the nodes so that the axial stress component in each member was determined in real-time and the strains/stresses that were then stored in the rainflow bins consisted of the equivalent axial stresses in the individual members. The DAQ program stores rainflow data on both the individual strain gage readings as well as the equivalent axial strain/stress reading. Additional discussion on the rainflow counting techniques employed is presented in Section E3.3.1. The modification of the DAQ program to accomplish this feature required extensive work, leading to the longer instrumentation period for Bridge 1. Despite the longer time of field studies for Bridge 1, contingency time built into the schedule allowed the RT to remain on schedule.

E3.2 Preliminary Finite Element Analysis

Before outlining each stage of the instrumentation plan, the preliminary finite element analysis (FEA) work performed by the RT for each of the three bridges is discussed. Phase II of the NCHRP 12-113 project includes Part 1 of the analytical program, and Part 1 can be broken into two separate tasks (Tasks 7 and 9). The first task is performing preliminary FEA studies to aid in the development of the experimental plan (Task 7 of the project). This is the focus of this subsection. The second task involves validating the finite element model based on the results of the field studies (Task 9 of the project).

To maintain cohesiveness in the appendix, the preliminary FEA work performed before the experimental field studies is discussed in this section. The remainder of the Phase II analytical program work is outlined in Chapter E5 of this appendix. Chapter E5 includes a detailed discussion on the development and assumptions of the Abaqus model.

Two different versions of the FEA model were developed in Abaqus for purposes of this preliminary analytical study: A) cross-frames fully modeled with shell elements, and B) cross-frames modeled as truss elements (consistent with most common FEA models for bridges) and modified with the stiffness reduction factor (R-factor) to account for connection eccentricity (Wang 2013, Battistini, et. al. 2016).

There are two primary purposes for the preliminary analysis: (i) identification of key truck positions to be used in the controlled live load tests (Stage II of the field work) and (ii) identification of the critical cross-frame and girder locations for instrumentation (Stages II and III of the field work). By performing these preliminary analyses, the RT was able to identify the cross-frame members and girder cross-sections that were good candidates for instrumentation. This helped to ensure that meaningful data was collected from the field instrumentation.

The following items were of particular interest for the preliminary analyses:

- Identification of cross-frames that are likely to experience the largest stress ranges due to truck traffic.
- Identification of girder flanges to be instrumented to determine flange stress and vertical displacements.
- Truck positions and orientation likely to provide the most meaningful data for validating the FEA models.
- Confirmation that the load test trucks would likely create significant cross-frame forces and provide meaningful data.

Specific information on the strain gage locations and loading positions for Stage II are addressed in later sections of this chapter. It should be noted that the RT was limited to a total of approximately 70 strain gages per bridge, based on the capacity of the wireless DAQ system. As a result, care was taken in selecting specific gage locations and the most meaningful members and locations to instrument.

The following subsections address specific FEA techniques and results that are unique to each subject bridge.

E3.2.1 Preliminary FEA of Bridge 1

In addition to developing the two Abaqus models as discussed previously, the bridge was also modeled in a commercial bridge software program to compare results with Abaqus and obtain initial influence surface data. As noted in the main report and Appendix D, the names of the commercial software programs are not provided as to avoid promoting a specific name brand. As such, the 3D software package used throughout this appendix is referred to as Software A similarly, the 2D software package referenced is identified as Software B. Figure E3-1 shows the model developed in Abaqus. The instrumentation of this bridge was limited to Span 11, given the railroad and roadway obstructions underneath the other two steel I-girder spans.

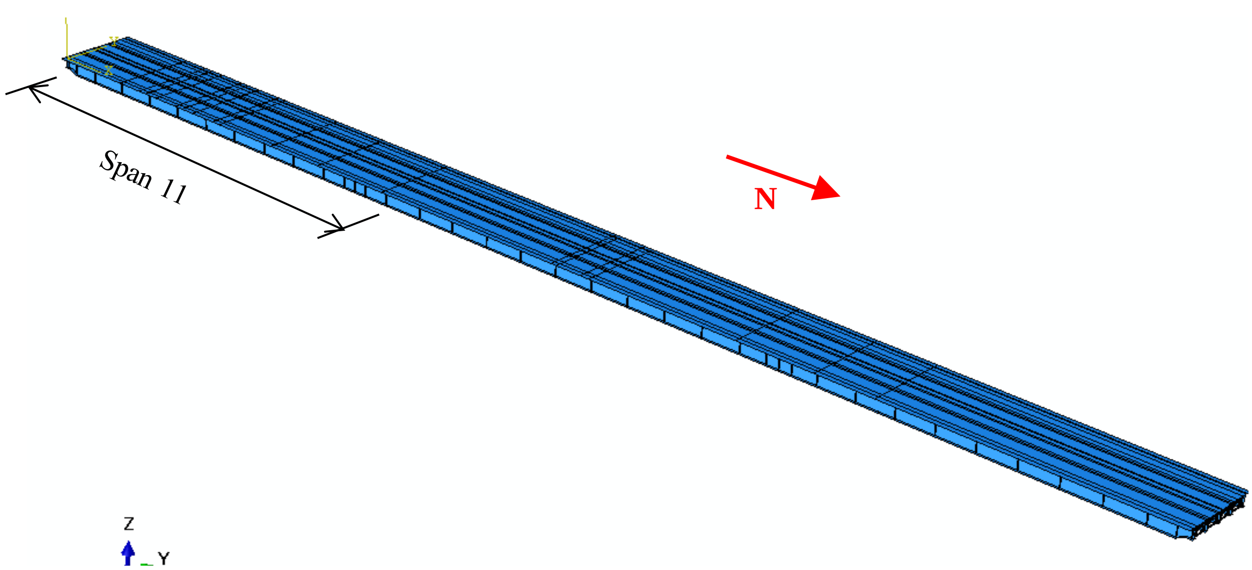

Figure E3-1: Screenshot of 3D FEA model for Bridge 1

Based on the Abaqus and commercial bridge software analyses, it was determined that instrumenting a full cross-frame line for the normal support bridge provided the most meaningful data. Maximum girder displacements and stresses were found near intermediate cross-frame line 4 in Span 11. Subsequently, maximum cross-frame stresses were also found in the same line of cross braces. Because there is no skew or curvature to this bridge, the expected cross-frame stresses were relatively small, but significant enough to validate the FEA model with four loaded dump trucks during Stage II of the field work.

E3.2.2 Preliminary FEA of Bridge 2

Similar to Bridge 1, two different Abaqus models and one model from a commercial bridge software program (Software A) were developed for the preliminary analysis stage. Figure E3-2 presents a screenshot of the skewed bridge model, with the deck shell elements hidden for clarity. Recall that instrumentation of this bridge was limited to Span 1 due to heavy traffic volume on the roadway passing beneath Span 2.

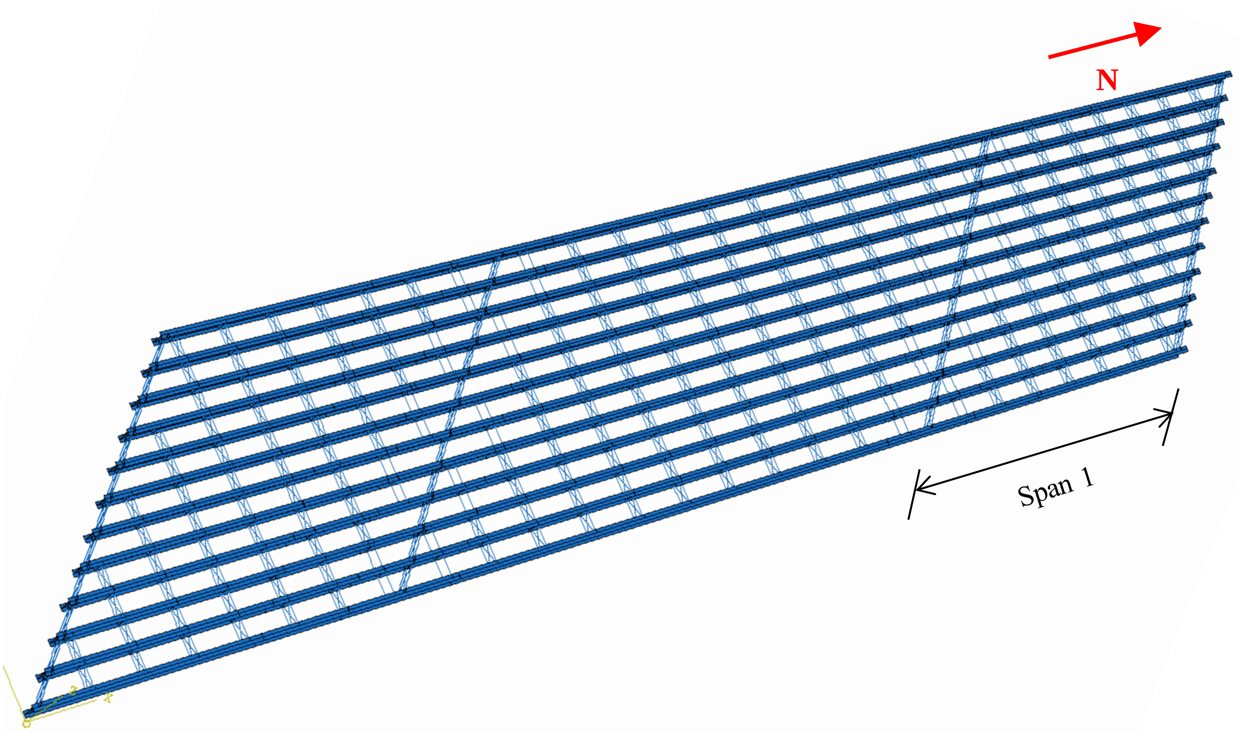

Figure E3-2: Screenshot of 3D FEA model for Bridge 2

Based on the preliminary FEA results, there were several cross-frames of interest. In particular, cross-frames and girder flanges near regions of maximum positive bending moments were expected to provide meaningful data. Given the anticipated differential deflection of girders near interior and end supports, cross-frames at these areas were also expected to produce larger load-induced stresses and thus provide meaningful data. Lean-on braces are typically designed and utilized to lessen the force effects in those bracing lines near skewed supports. The RT was interested in verifying this design assumption. The locations of strain gages were distributed to capture all of these different effects, within the limits of the DAQ system.

E3.2.3 Preliminary FEA of Bridge 3

Similar to Bridges 1 and 2, two different Abaqus models and one model from a commercial bridge software program (Software A) were developed for the preliminary analysis stage. Figure E3-3 shows the model developed in Abaqus with deck shell elements hidden for clarity. As previously mentioned, Span 11 was the most accessible span from the ground and required no traffic control. As such, this span was the primary focus of the initial FEA studies.

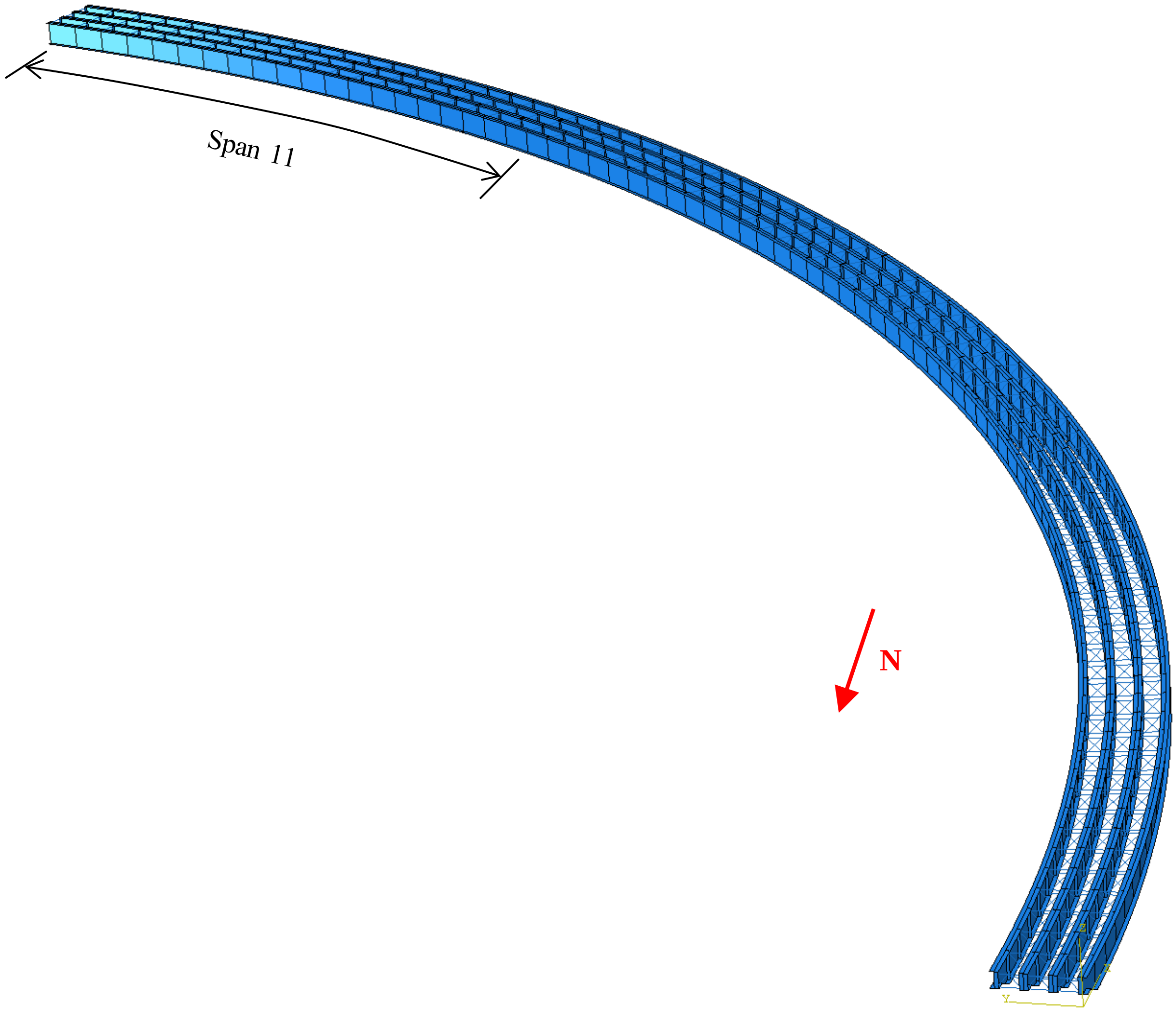

Figure E3-3: Screenshot of 3D FEA model for Bridge 3

The preliminary FEA studies concluded that instrumenting full cross-frame lines provided the most meaningful data. The models indicated the maximum girder deflections occurred near cross-frame line 12. Similarly, the highest predicted cross-frame stresses were in line 12. Under normal circumstances, the RT would instrument cross-frame line 12; however, due to the risk of fouling the nearby railroad track, the RT opted to instrument cross-frame line 10 instead. The preliminary analysis indicated cross-frame line 10 would still provide significant stresses.

E3.3 Stage I - Installation of Sensors and Data Acquisition System

The subsequent sections outline the data acquisition system and the detailed instrumentation plan that were employed at all three subject bridges. The detailed plan includes a discussion on sensor locations and other pertinent measurements. Obtaining the absolute maximum possible stresses in the cross-frame members or girder flanges was not necessary during these tests; instead, the goal was to obtain stresses and deflections under known load conditions so that the FEA models could be validated. Provided that good correlation between measured and modeled stresses is obtained, the behavior of variable geometries and load positions can be accurately predicted in the parametric studies carried out in Phase III of the investigation.

E3.3.1 Description of Data Acquisition System

This section outlines all components of the monitoring system that were consistent across all three subject bridges. For specific features of each bridge, refer to subsequent Sections E3.3.2, E3.3.3, and E3.3.4.

The National Instruments (NI) Wireless Sensor Network (WSN) was used for data collection for both the controlled live load tests (Stage II) and in-service monitoring (Stage III). This monitoring setup was ideal for the purposes of instrumenting the bridges for the study, since the WSN minimizes setup time when compared to traditional wired systems (i.e., there is no need to run wires along the length of the bridge). Using the WSN system allows the RT to utilize approximately 70 strain gages per bridge.

The WSN system is comprised of a wireless gateway, wireless nodes, and a cellular modem. The gateway acts a central hub that communicates with and collects data from the network of wireless nodes. The gateway was attached securely to a nearby pier in a weather-protected enclosure. Figure E3-4 shows the typical position of the gateway and modem enclosed in a box on the pier cap during a four-week monitoring period. The series of 12-volt batteries powering the hardware is also depicted in Figure E3-4. A similar gateway and battery configuration were utilized for the instrumentation of Bridges 2 and 3.

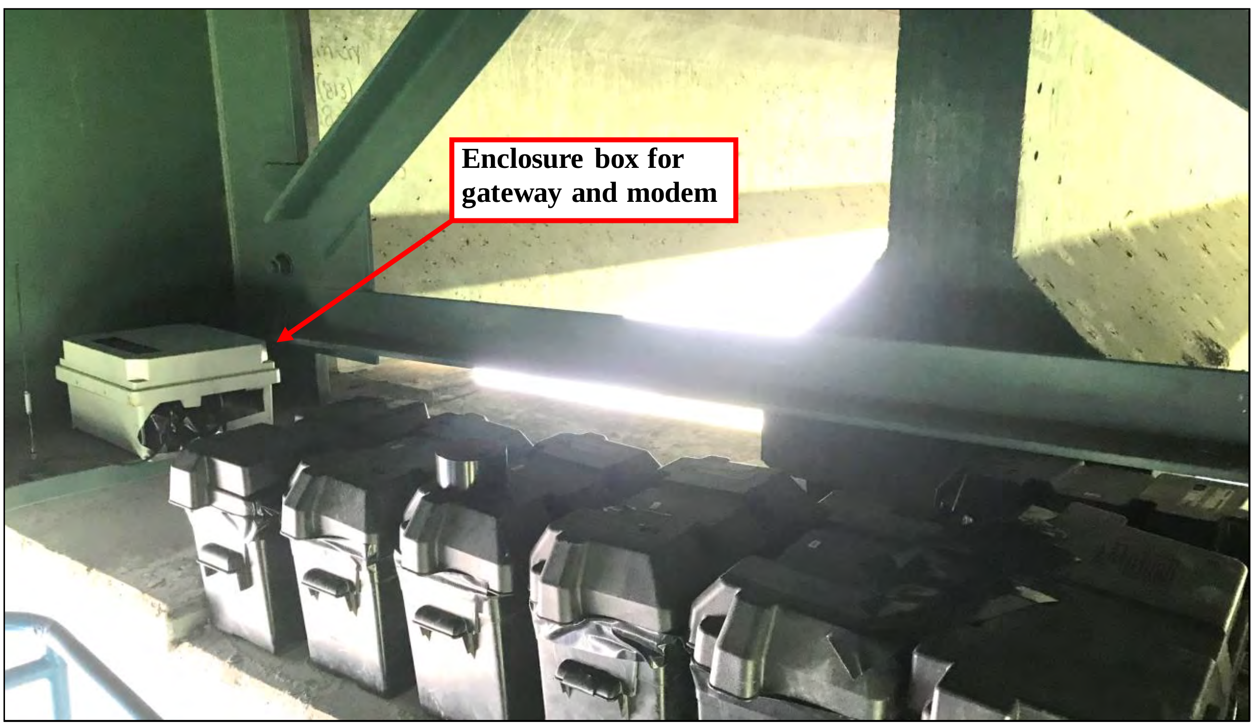

Figure E3-4: Location of gateway and wireless modem during field monitoring of Bridge 1

The programmable wireless nodes each contain four channels, and each channel can support a quarter-bridge strain gage. As noted earlier, DAQ programming was developed to perform a real-time linear regression and rainflow counting, as outlined by Fasl (2013). The regression method outlined in Helwig and Fan (2000) was implemented to isolate the axial force component from bending in the cross-frame members. To perform linear regression on an angle section, four strain gages were installed at a given cross-section on the angle member. Figure E3-5 schematically demonstrates a typical strain gage layout used for the instrumentation of angle members. Prior to implementing in the field, the programming was validated on a laboratory test specimen in a 220-kip MTS machine under known, controlled stress cycles.

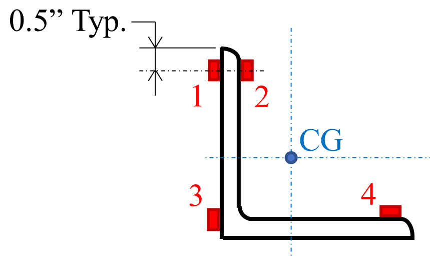

Figure E3-5: Strain gage layout for single angles

Figure E3-6: Laboratory study conducted to validate the linear regression programming

Gage sensors measured changes in strain on the instrumented steel surface. Because stress is typically a more useful measurement, changes in strain were converted to changes in stress using Hooke's Law and multiplying the strain response with Young's modulus for steel (E = 29000 ksi). This procedure implicitly assumes that the structure remains elastic during all field monitoring tests. Given the low strain levels recorded during the controlled live load test and in-service monitoring, this assumption was valid. The terms *"measured strain"* and *"measured stress"* are used interchangeably throughout this appendix.

All strain gages on cross-frame members were attached near the quarter-point of the member length in the cross-sectional layout depicted in Figure E3-5. The quarter point was selected to position the gages as far away as possible from the ends of the angles and the intersection of the cross-frame diagonals as to avoid stress concentrations. Since the bending moments in the cross-frame elements can be significant at the quarter-point given the end restraints of the members, the regression techniques on the corresponding strain gage readings allow the corresponding bending and axial force terms to be isolated in the angle members. Measuring the axial force in each cross-frame member was a critical aspect to the field instrumentation program.

Also note that no strain gages were installed at or near the gusset plate connections. Although substantial stress concentrations can occur in the localized regions near welds and weld terminations, these effects were beyond the scope of the project. As such, the axial stresses in the cross-frame members were the primary focus, as these stress components relate to the load-induced fatigue behavior of the member.

Gages were also installed on bottom girder flanges near the locations of instrumented cross-frames. Two strain gages, each at 2 inches from the edge of the flange, were used to measure the longitudinal bending stresses in the girders, as well as the warping or lateral bending stresses due to torsional deformations. The average longitudinal girder bending component can be determined from the average of the two readings, while the torsional warping component can be obtained from the difference of the two readings. Figure E3-7 schematically shows the typical position of strain gages installed on the bottom flange of the girders. Note that no gages were attached to the top flange of the girders since the neutral axis of the composite girder is close to this position in the positive moment region. Strain gages at the neutral axis would not yield meaningful data.

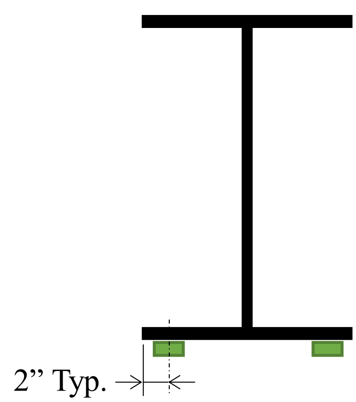

Figure E3-7: Typical position of installed strain gages on the bottom flange of girders

Wireless nodes were securely clamped to the nearby bottom flanges of the girders in a weather-protected enclosure. Data was collected remotely from the wireless gateway via a wireless modem and cellular internet connection. Figure E3-8 shows the typical position of a wireless node fastened to the bottom flange of a girder in close proximity to its instrumented member; a small 12-volt battery powering the nodes is also depicted in Figure E3-8.

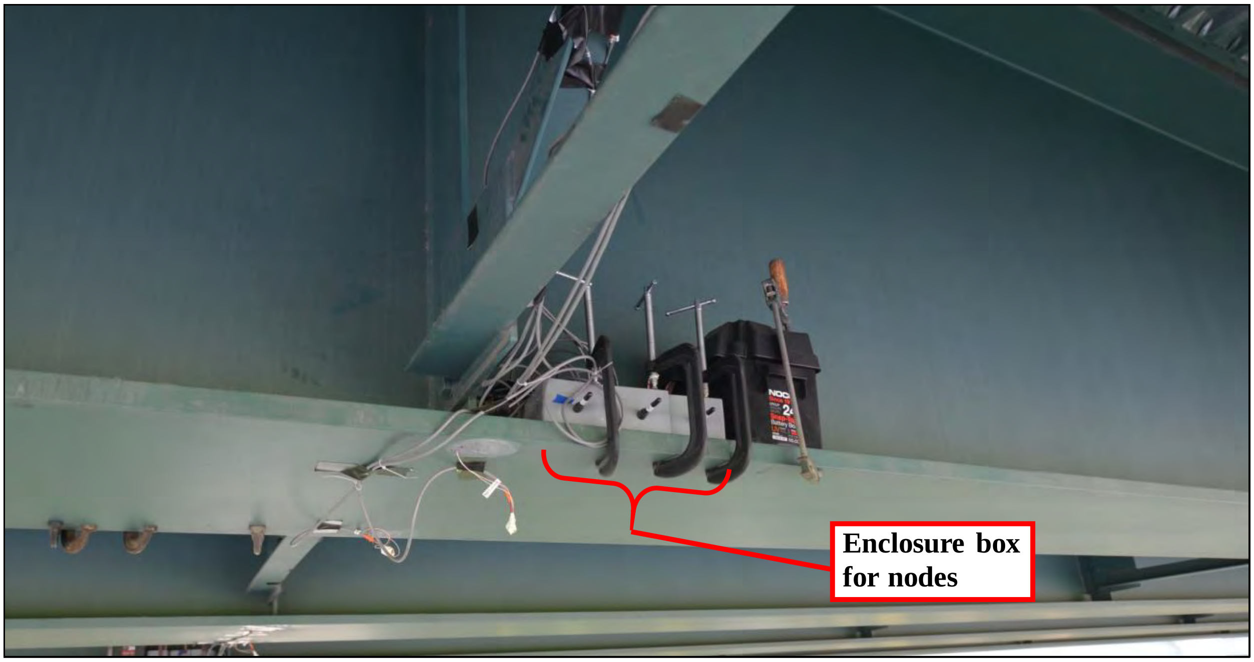

Figure E3-8: Typical position of wireless nodes during field instrumentation

The RT used Micro-Measurements LWK-Series weldable strain gages on both the cross-frame members and girder flanges. The use of the weldable gages simplified the surface preparation in the field and expedited the instrumentation process. Weldable gages require very little energy and have shown to have no discernible fatigue effects on the bridge components during or after instrumentation (Micro-Measurements 2018). Figure E3-9 shows a typical strain gage after the steel surface has been prepped and the gage welded. The final stage of the instrumentation consists of protecting the gage from the environment with wax and silicone, which is not shown in the picture.

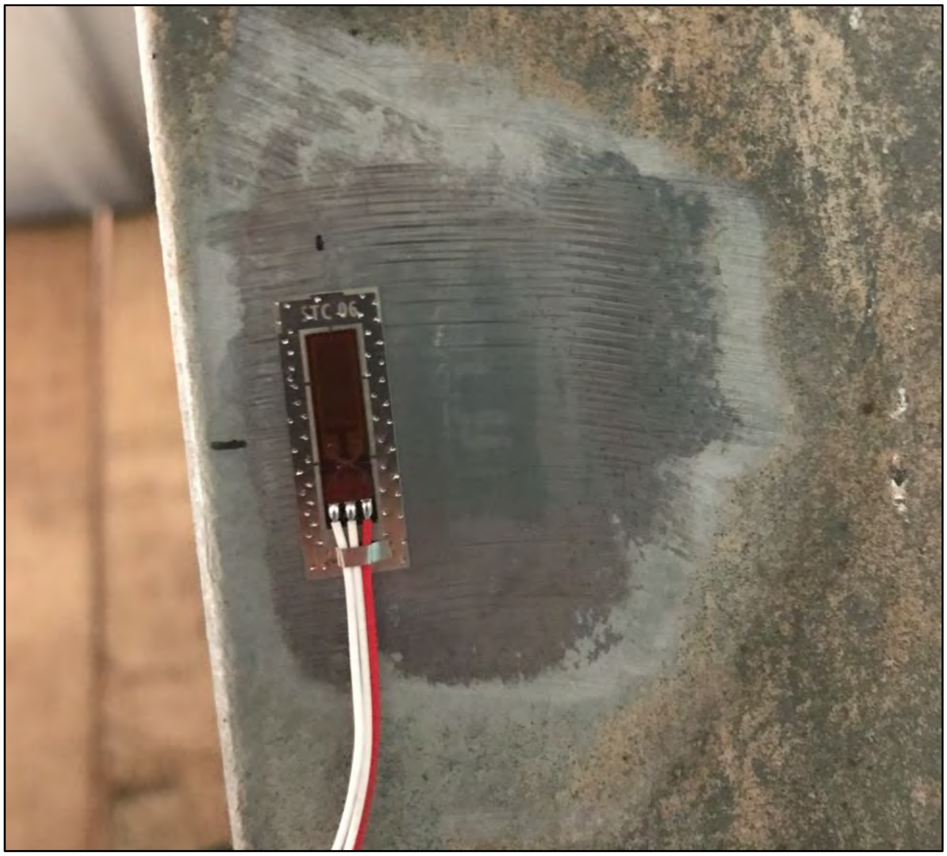

Figure E3-9: Typical welded strain gage used for instrumentation (wax and silicon for environmental protection are not shown)

The power demands of each component of the wireless monitoring system were considered by the RT, and the power supply was designed such that the system could run for the minimum four-week monitoring period. There were no major battery issues encountered during the three individual instrumentations.

Specific features of the data acquisition system for Stages II and III are further addressed in Sections E3.4 and E3.5, respectively. The gages described in the following subsections were used for both Stage II and Stage III for each subject bridge.

E3.3.2 Instrumentation of Bridge 1

As presented in Table E3-1, Bridge 1 was instrumented on March 9, 2018 by the RT. The RT, which included six researchers, set up working platforms, installed strain gages, and positioned all hardware and batteries on March 9, 2018, and the monitoring system was configured and began collecting data on the following day. The RT were prepared for various issues that could have occurred during the instrumentation such as limited access to top strut members due to large girder depths, faulty gage installation, and issues with the wireless system. Fortunately, none of these issues were encountered by the team.

Span 11 is located directly above a median; therefore, no traffic control was required during the installation of the strain gages and DAQ system. A boom lift and working platform stations were utilized to access the various elements of the bridge superstructure. The boom lift and all equipment were safely placed in the grassy area below Span 11 without causing any disruption to traffic on or below the bridge during instrumentation. The residential road running parallel to the frontage road has a low traffic volume and was unaffected by the work. However, the RT still placed signage along the oncoming service road to alert traffic of the ongoing work underneath the bridge. Figure E3-10 shows the RT instrumenting Bridge 1 with the use of a boom lift and working platform stations. Figure E3-11 shows the framing plan of Span 11. Members of the RT wore appropriate fall protection harnesses when working at elevated positions on the bridge.

Figure E3-10: Boom lift and working platform stations utilized during instrumentation of Bridge 1

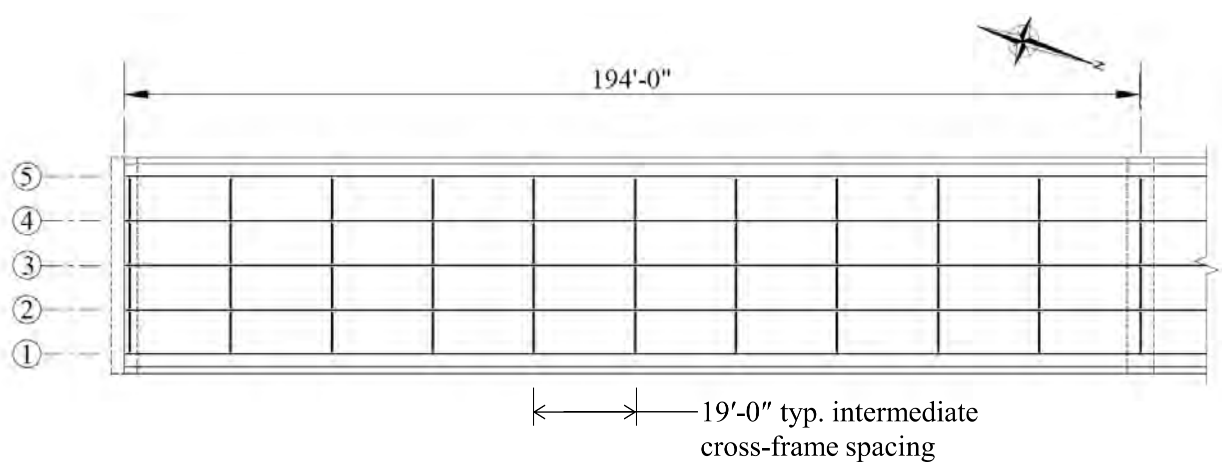

Figure E3-11: Framing plan of Span 11

As mentioned in Section E3.2.1 of the appendix, the full intermediate cross-frame line 4 was selected for instrumentation since the preliminary FEA studies predicted that these braces were likely to experience the most significant live load-induced stresses. With the exception of several top and bottom strut members that experience little stress, all cross-frame members were instrumented with four quarter-bridge strain gages. Previous laboratory tests performed on cross-frames at the University of Texas at Austin have shown that top and bottom struts are essentially zero-force members. As such, only one top strut and two bottom strut members were instrumented to verify this assumption. To improve the longitudinal distribution of sensors and broaden the measured response of the bridge, select cross-frame diagonals in cross-frame line 7 were also instrumented.

Figure E3-12 shows the locations of the cross-frames instrumented in plan. Figure E3-13 and Figure E3-14 present the strain gage locations in a cross-sectional view for clarity. Note that the red dot represents four strain gages per cross-section (Figure E3-5), and the green rectangle represents two strain gages installed at each tip of the girder flange (Figure E3-7). This notation is consistent throughout the remaining figures. Additionally, the gateway was secured on top of the pier cap of Bent 12 for the period of the in-service monitoring.

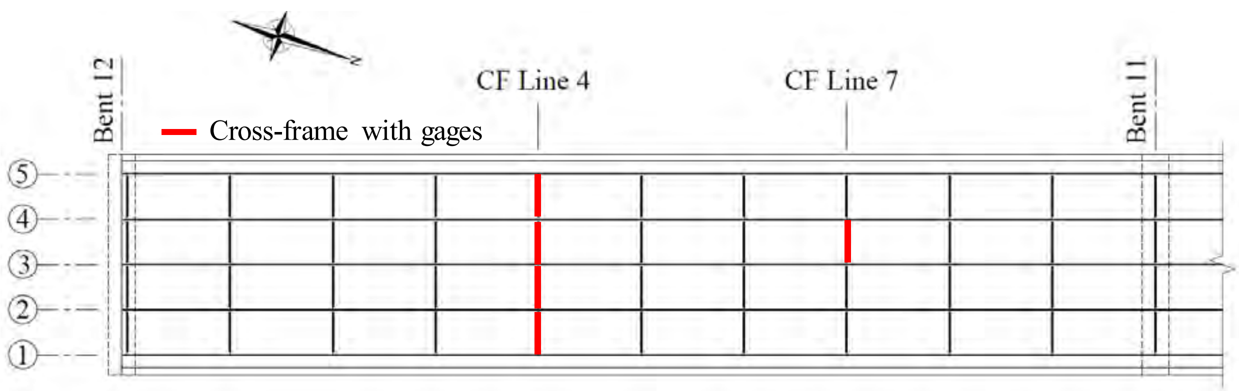

Figure E3-12: Plan view of instrumented cross-frame locations

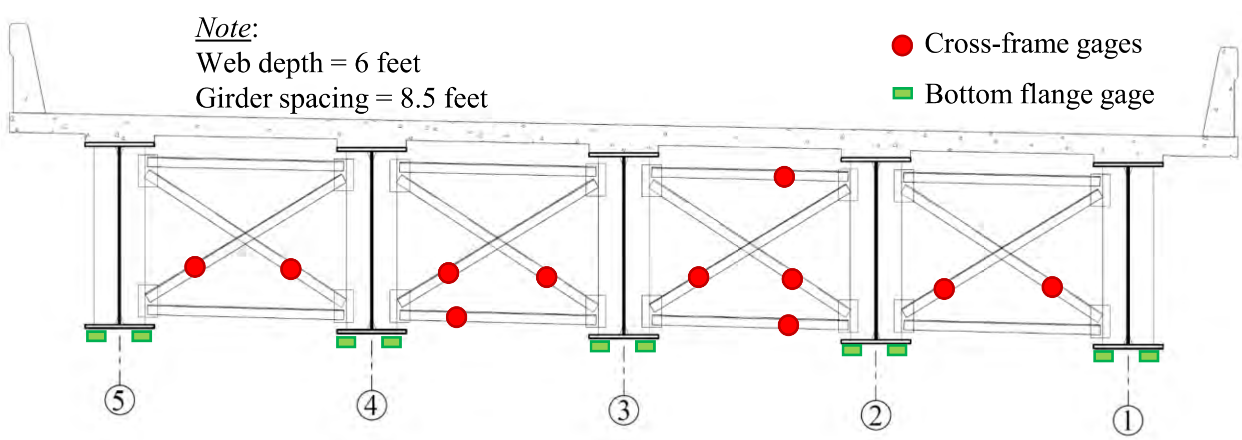

Figure E3-13: Cross-section view of strain gage locations at cross-frame line 4 in Span 11

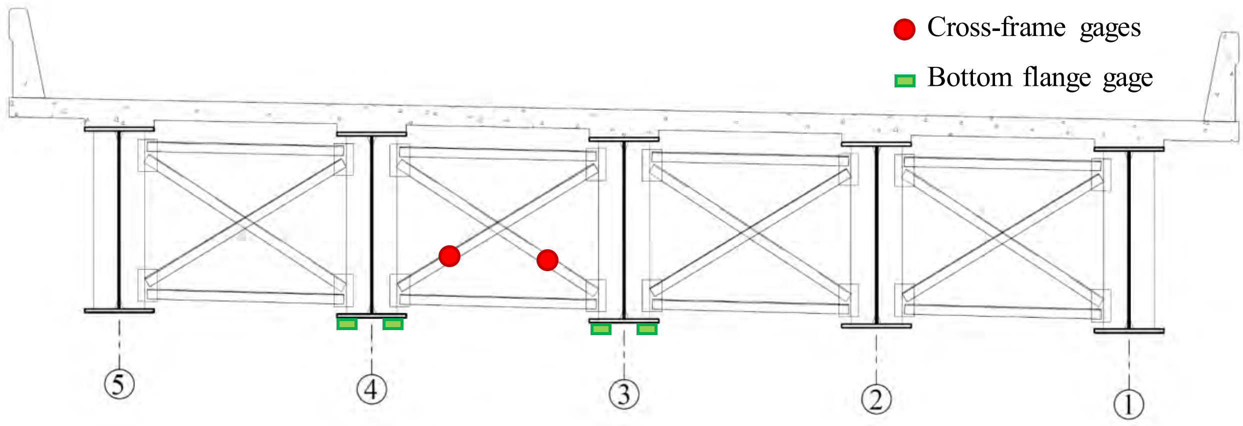

Figure E3-14: Cross-section view of strain gage locations at cross-frame line 7 in Span 11

Figure E3-15 shows the cross-frame members at line 4 near the completion of the instrumentation. The majority of the monitoring equipment was mostly hidden from pedestrians walking along the residential road parallel to the bridge.

Figure E3-15: View of cross-frame line 4 after instrumentation

E3.3.3 Instrumentation of Bridge 2

Bridge 2 was instrumented by the RT in the period from June 10 through June 12, 2018, as is outlined in Table E3-1. Instrumentation of Bridge 2 took longer than that of Bridge 1 since traffic control was required. The RT did not otherwise encounter any setbacks during the instrumentation. Span 1 of the southbound bridge is located above the north turnaround lane for IH 45 frontage road traffic. TxDOT assisted the RT by providing a full turnaround lane closure and a truck mounted attenuator (TMA) between 9 am and 3 pm each day. TxDOT set up traffic cones approximately 200 feet before the entry of the turnaround. The RT performed all instrumentation work directly above the turnaround lane during the six-hour lane closure windows provided by TxDOT. Figure E3-16 shows the TMA positioned at the entry of the turnaround lane, which afforded the RT full access beneath the span.

Figure E3-16: TMA blocking off traffic to the turnaround lane under Span 1 (Bridge 2)

Similar to Bridge 1 instrumentation, a boom lift and working platform stations were utilized to access the various elements of the bridge superstructure. The boom lift and all equipment were safely placed in the paver area and turnaround lane during the designated lane closure times. Figure E3-17 shows the RT stationed on the working platform stations with safety harnesses connected to cross-frames during the instrumentation of Bridge 2. Figure E3-18 shows the framing plan of Span 1.

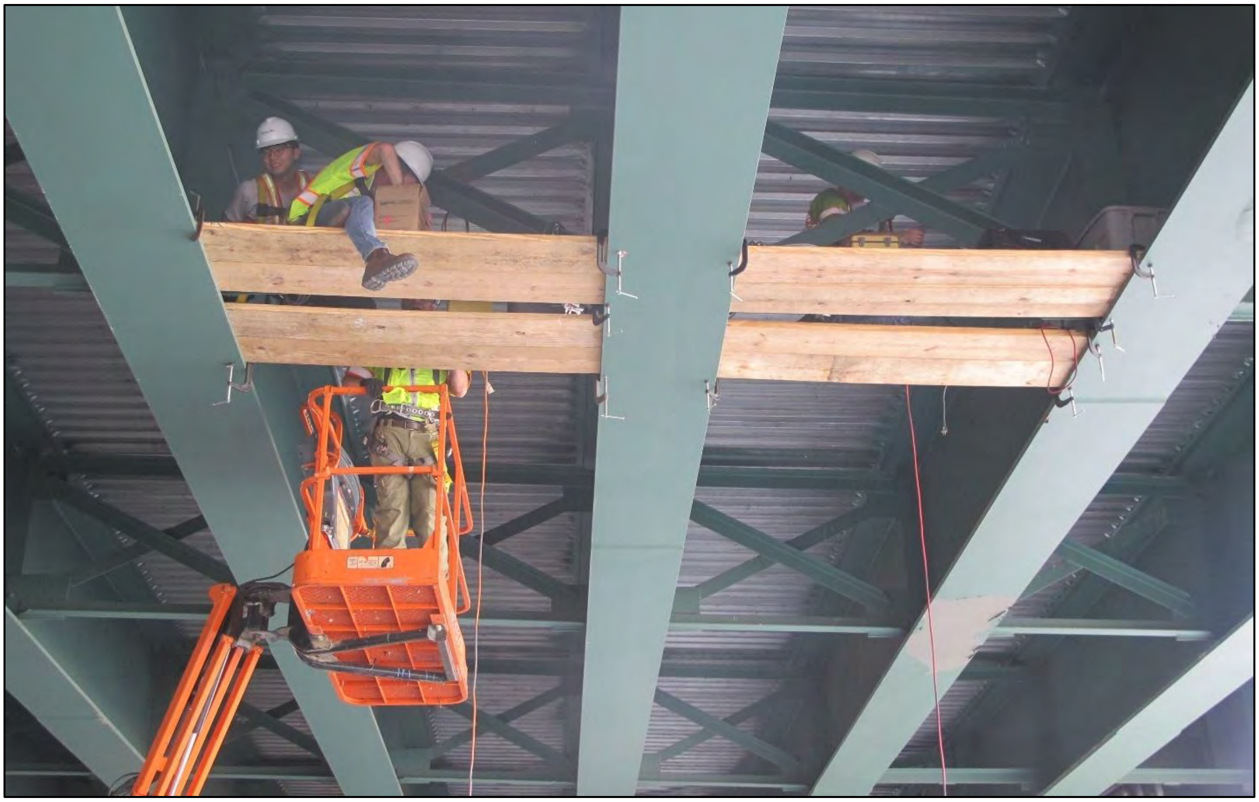

Figure E3-17: RT instrumenting Bridge 2 on platforms and boom lift

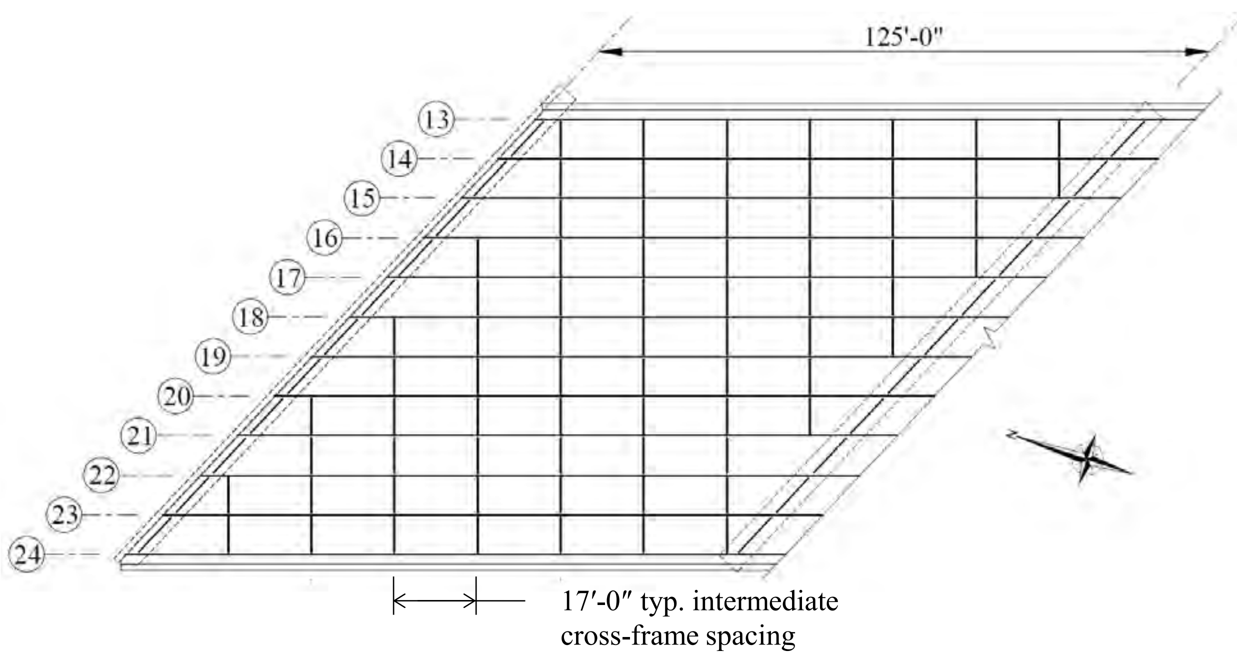

Figure E3-18: Framing plan of Span 1

There were a variety of instrumentation locations of interest for this skewed bridge, as mentioned in Section

E3.2.2. These locations selected for monitoring included cross-frames at acute angles where differential deflections are significant, cross-frames at midspan, and lean-on braces. The instrumented cross-frame locations, illustrated in Figure E3-19, cover each of the critical areas. Due to the large width of the bridge, only the west half of the southbound bridge was monitored during Stages II and III. Figure E3-20, Figure E3-21, and Figure E3-22 show the gage locations at each instrumented cross-frame location. Note that no top strut members are included in the instrumentation (refer to Section E3.3.2 for a discussion on top strut members).

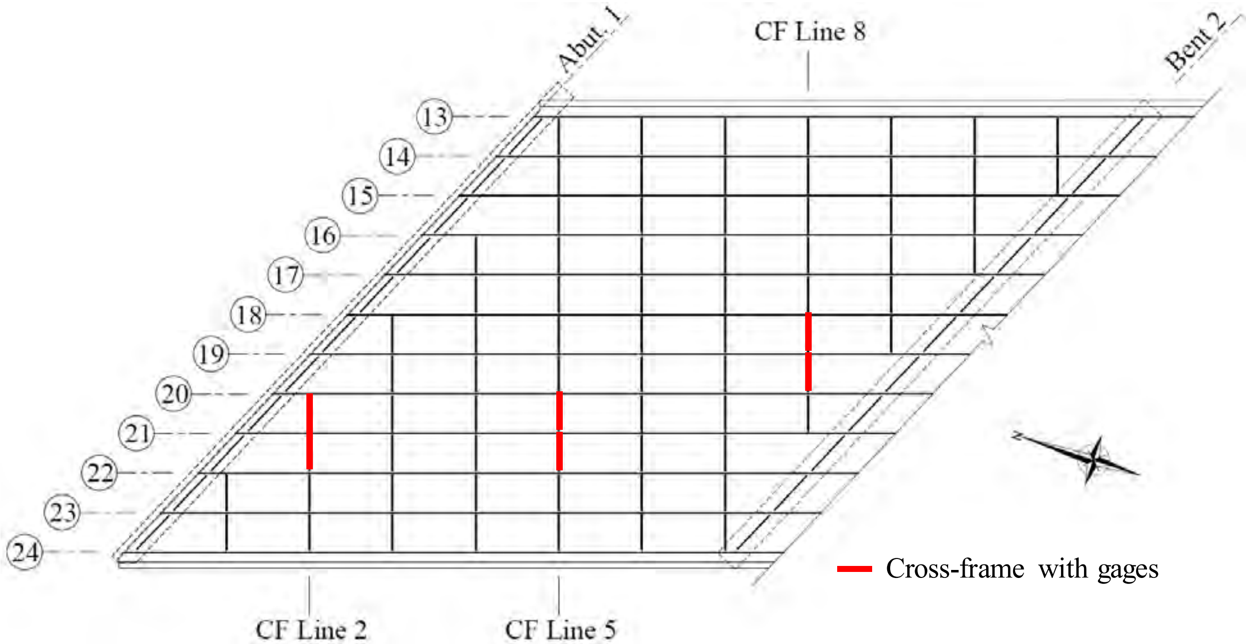

Figure E3-19: Plan view of instrumented cross-frame locations

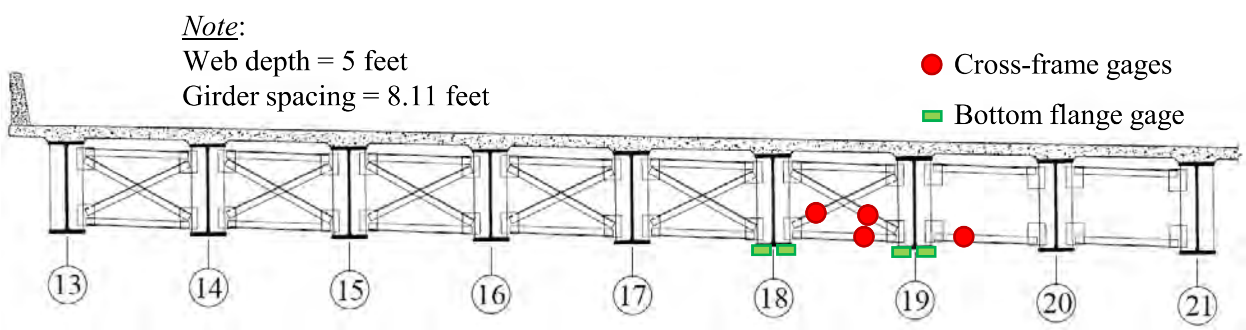

Figure E3-20: Cross-section view of strain gage locations at cross-frame line 8 in Span 1

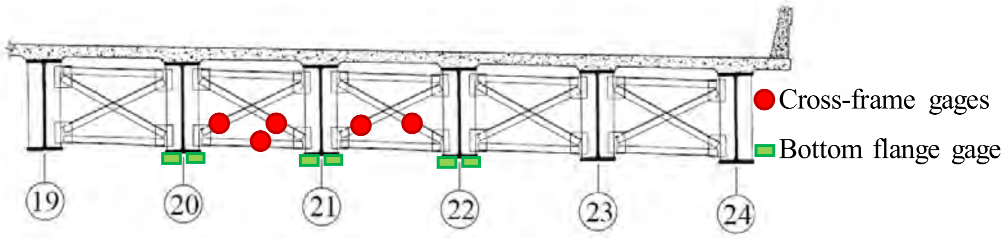

Figure E3-21: Partial cross-section view of strain gage locations at cross-frame line 5 in Span 1

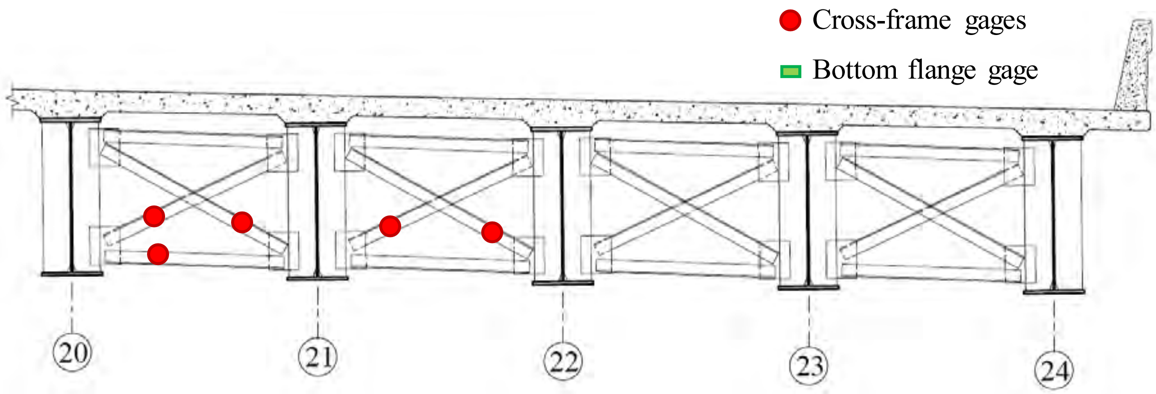

Figure E3-22: Cross-section view of strain gage locations at cross-frame line 2 in Span 1

Figure E3-23 shows the cross-frame members at line 2 between girders 21 and 22 after completion of the instrumentation. The wireless nodes for these strain gages are positioned on the girder bottom flange on the back side of the gusset plate shown. Note that the bolts through the gusset plate are erection bolts and the cross-frame-to-gusset and gusset-to-connection plate connections are fully welded, as demonstrated by the detail shown in Figure E2-10.

Figure E3-23: View of the cross-frame between girders 21 and 22 in line 2 after instrumentation

E3.3.4 Instrumentation of Bridge 3

Bridge 3 was instrumented by the RT in the period from July 11 through July 12, 2018, as outlined in Table E3-1. No major setbacks were encountered during this two-day instrumentation. Span 11 runs parallel with eastbound roadway below the bridge. There is a grassy area under Span 11 that is partially protected by a guardrail and curb. Consequently, a lane closure of eastbound roadway below was not necessary. The RT was able to perform all instrumentation activities without the assistance of TxDOT. Figure E3-24 shows the position of the boom lift in the grassy area below Span 11 relative to the roadway below the bridge.

Figure E3-24: Position of boom lift relative to Bridge 3

Similar to the Bridge 1 and 2 instrumentations, working platform stations were utilized to access the various elements of the bridge superstructure. Figure E3-25 shows the RT stationed on the working platform stations with safety harnesses tied off to the cross-frames during the instrumentation of Bridge 3. Figure E3-26 shows the framing plan of Span 11.

Figure E3-25: Researchers instrumenting Bridge 3 on platforms and boom lift

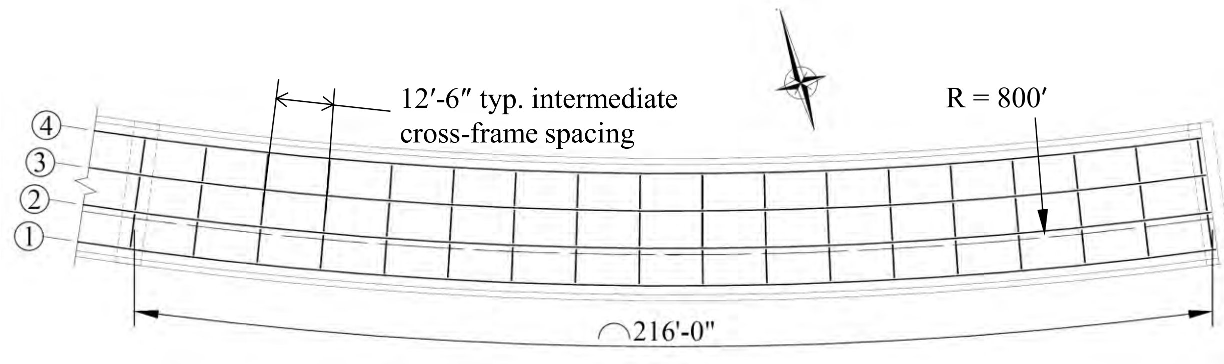

Figure E3-26: Framing plan of Span 11

As mentioned in Section E3.2.3 of the appendix, the full intermediate cross-frame line 10 was selected for instrumentation to maximize cross-frame forces and still maintain a safe working distance during instrumentation. With the exception of top strut members and one bottom strut member, the full cross-frame line was instrumented.

To improve the longitudinal distribution of sensors and broaden the measured response of the bridge, select cross-frame diagonals in cross-frame line 4 were also instrumented. Figure E3-27, Figure E3-28, and Figure E3-29 schematically show the selected strain gage locations for Bridge 3.

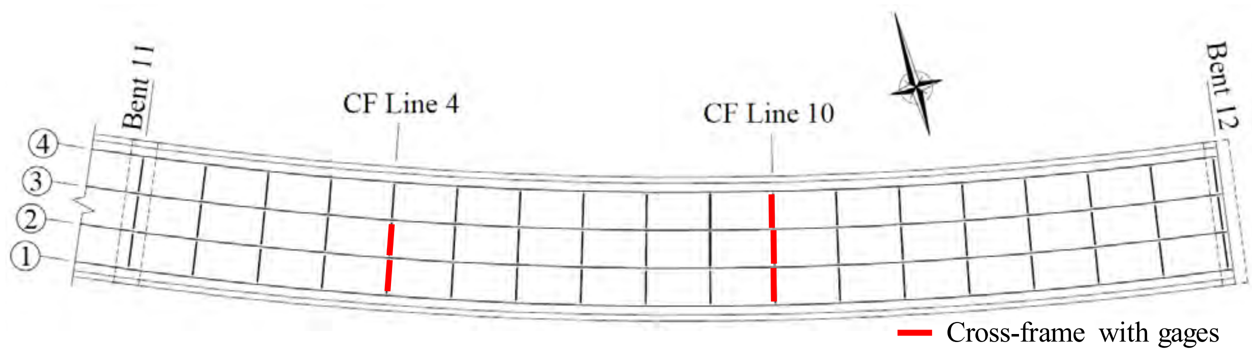

Figure E3-27: Plan view of instrumented cross-frame locations

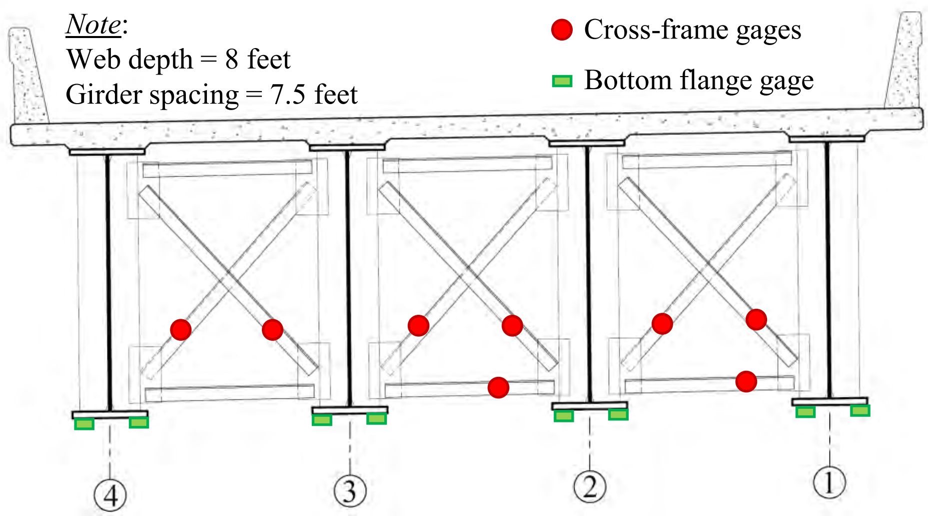

Figure E3-28: Cross-section view of strain gage locations at cross-frame line 10 in Span 11

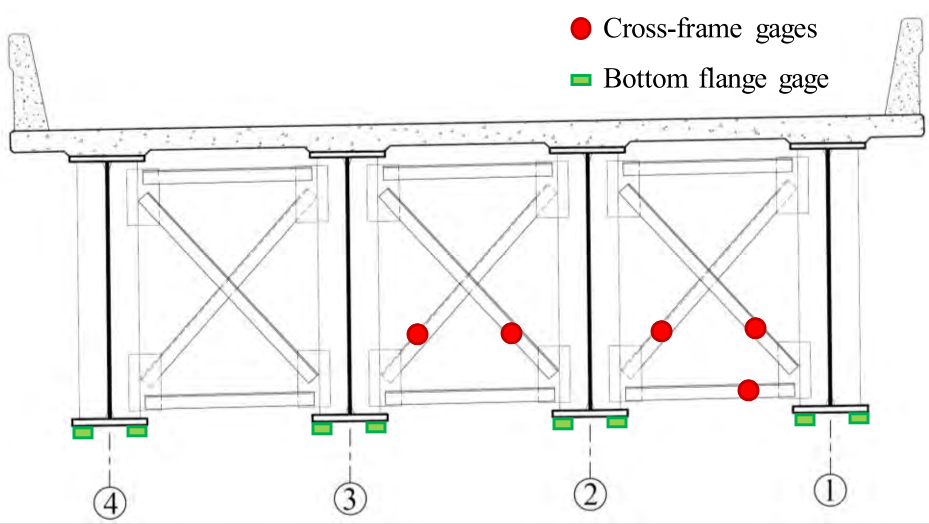

Figure E3-29: Cross-section view of strain gage locations at cross-frame line 4 in Span 11

Figure E3-30 shows the cross-frame members at line 10 between girders 2 and 3 after the completion of the instrumentation. The wireless nodes for these strain gages were clamped to the bottom flange of girder 2. As was discussed in the previous section, the bolts shown in this photograph are erection bolts and the cross-frame connections are fully-welded details.

Figure E3-30: View of the cross-frame between girders 2 and 3 in line 10 after instrumentation

E3.4 Stage II – Controlled Live Load Testing

The subsequent sections in this chapter outline the means and methods executed to perform the controlled live load tests. Many of the general procedures were consistent across all three subject bridges; therefore, the procedures are generally discussed without reference to a specific bridge. Discussion of specific load cases for each subject bridge is provided in Section E3.4.3.

It was in the interest of the RT to work with TxDOT to minimize traffic interruptions and pose as little inconvenience as possible. The RT coordinated with TxDOT representatives about receiving assistance for these tests. For improved safety, TxDOT preferred full closures instead of the rolling road block option that was presented in the Interim Report No. 1. As such, TxDOT provided full bridge closures for each subject bridge as well as four loaded, three-axle dump trucks for use during testing. The trucks were weighed before the test, and the gross weight was typically around 50 kips. Based on previous experience, multiple 50-kip trucks are generally heavy enough to provide reliable data from strain gages.

The load tests for Bridges 1 and 2 were performed during a nighttime closure, whereas the load test for Bridge 3 was performed during a morning closure. Load tests for Bridges 2 and 3 were conducted on a Saturday. Dates and times were selected to accommodate TxDOT and alleviate potential traffic congestion problems.

E3.4.1 Desired Data

The data collected during the controlled live load tests include strain data for cross-frames and girder bottom flanges and girder vertical deflection measurements at predetermined points along the bridge. In total, eight different load cases were performed for each bridge: one moving case and seven static cases.

Strain data was measured by the strain gages outlined in Section E3.3.1. The data was measured continuously as trucks were moved onto the bridge to their final predetermined locations for all eight cases. This enabled the RT to understand the influence line effects on the full spectrum of data collected.

Deflection data was measured for the seven static load cases only. A Hilti PD-E (+/- 1/25 inch accuracy) laser distance meter was employed to measure deflections at selected cross-frame lines. For example, on Bridge 1, deflections of all five girders along cross-frame line 4 were measured for each truck position. The laser distance meter was positioned on the ground directly below the girder bottom flanges at the desired reading locations. Three independent readings were recorded at each location and averaged for improved reliability in the measurements; note that the variability in the three independent readings was typically very small. Distance readings were recorded in the ″unloaded″ state prior to testing and ″loaded″ state for all seven static load cases, and the corresponding displacement was the net change in the readings.

E3.4.2 Outline of Procedure

Prior to performing the load test, the RT arrived at the site early to prepare. Preparation included setting a level base for laser distance meter readings with quick-setting gypsum cement (Hydrostone), measuring haunch thicknesses and metal stay-in-place form dimensions at predetermined points along the span, configuring the data acquisition system, and marking truck positions on the deck surface with colored tape and traffic cones. Figure E3-31 and Figure E3-32 depict the RT setting a level base with Hydrostone on which the laser distance meters measured deflections below the bridge. This ensured the measured deflections were consistently read and aligned vertically. At Bridges 1 and 3, a hole was dug into the earth after dropping a plumb bob from the girder of interest. The hole was then filled with Hydrostone, which hardened within a few minutes. At Bridge 2, the RT constructed small boxes to set the Hydrostone since there are pavers below the span. Figure E3-33 depicts the RT applying colored tape to the bridge deck in preparation for the various static load cases performed during the load test; note that this work occurred after the lanes were fully closed.

Figure E3-31: Setting a level surface for the laser distance meters prior to the Bridge 1 load test

Figure E3-32: Setting a level surface for the laser distance meters prior to the Bridge 2 load test

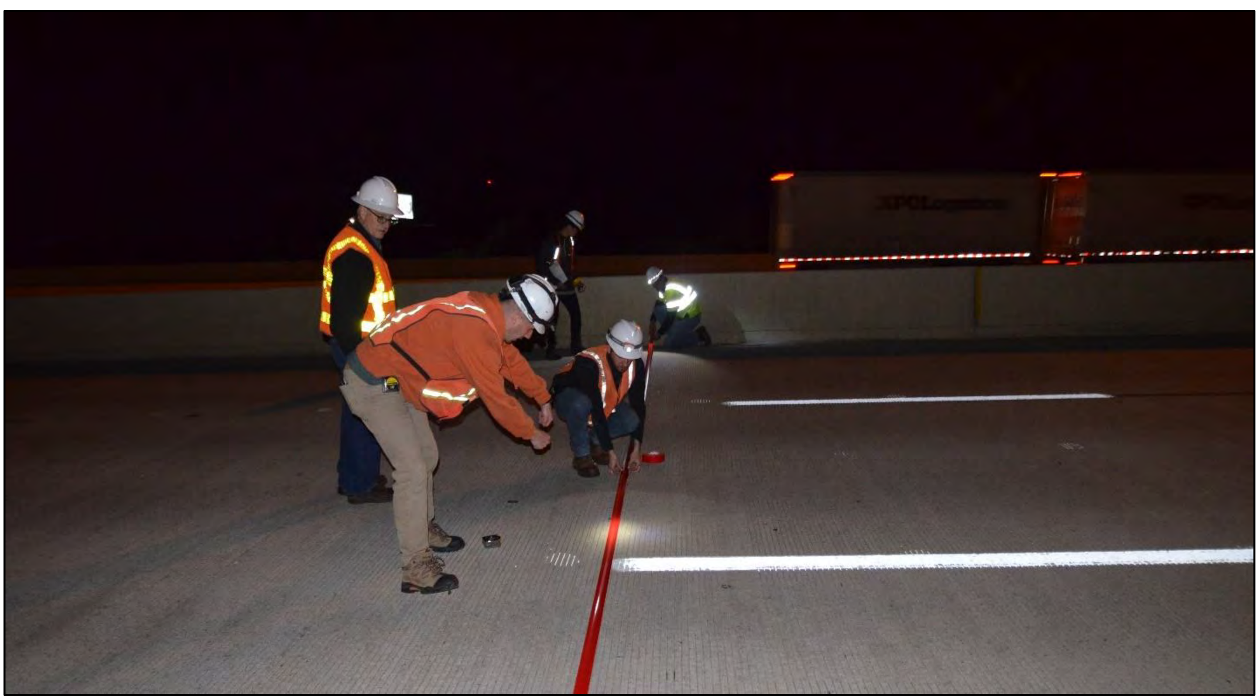

Figure E3-33: The RT preparing the bridge deck for a load test

The controlled live load testing and data collection was carried out systematically for each load case and for each bridge according to the steps shown in Table E3-2. Step 0, the closure of the bridge and other necessary traffic control procedures, occurred only one time and was handled by TxDOT. The complexity and magnitude of the lane closures differed between the bridges. Traffic control for Bridge 2, which serves five lanes of IH 45 traffic, was far more challenging than the other two bridges. As such, the time associated with Step 0 varied for the three bridges. Figure E3-34 shows the lane closure methods used during the Bridge 3 load test.

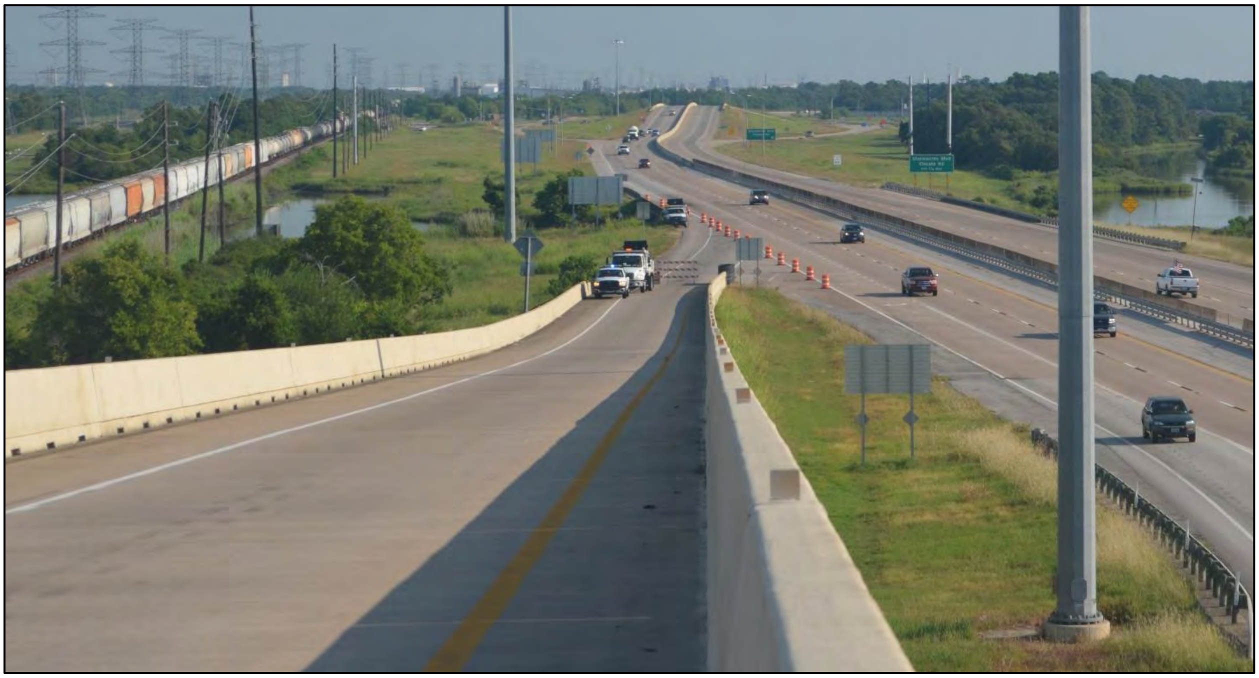

Figure E3-34: TxDOT lane closure during Bridge 3 load test

Prior to conducting the load test, the RT spent approximately one hour preparing for the different load cases. The preparation efforts included work below the bridge as well as on the bridge deck. As demonstrated in Figure E3-33, work on the deck included applying tape to mark truck stopping positions on the deck, positioning traffic cones to improve guidance for the drivers, and measuring the wheel base of each truck. Work below the deck included obtaining baseline strain and deflection readings of the unloaded bridge. These tasks are identified as Steps 1 and 2 in Table E3-2.

Steps 3 through 5 were repeated for each load case performed during the test. For Step 3, the RT positioned the lead truck as close as possible to the predetermined position as marked with the colored tape and traffic cones. The other three trucks were then directed to follow the lead truck. Each truck entered onto the bridge and reached its final position one at a time. Incrementally introducing the trucks afforded the opportunity to obtain additional intermediate load cases and yielded cleaner data. For Step 4, vertical deflection measurements were taken after all four of the trucks was positioned, and the position of the truck wheels were documented. For Step 5, all four trucks were removed from the bridge simultaneously.

A single load case (Steps 3 through 5) generally took 25-30 minutes to complete. In total, eight iterations of Steps 3 through 5 took approximately 4 hours to complete once traffic control (Step 0) was in place and prep work (Steps 1 and 2) was finished. At the completion of the live load test, TxDOT crews reopened the bridge to traffic (Step 6). Figure E3-35 show the typical three-axle dump truck provided by TxDOT and loaded with sand. The truck consists of one front steer axle and two rear drive axles.

Table E3-2: Procedural outline for controlled live load testing

Step #	Name	Description	Estimated Time
0	Road Closure	Traffic is stopped and all vehicles are removed from bridge. The bridge is shut down for the entire duration of testing.	N/A
1	Prep work	The bridge deck is prepped with colored tape and traffic cones. The wheel bases of the truck are measured and documented.	~30 mins
2	Baseline measurements (Unloaded Condition)	Baseline strain readings of the unloaded bridge are recorded; baseline laser distance readings of the unloaded bridge are recorded. Five locations minimum were used for deflection readings.	~ 30 mins
3	Truck positioning	The trucks are moved onto the bridge one at a time to the predetermined locations.	~ 12 mins
4	Loaded measurements (Loaded Condition)	Strain measurements are recorded continuously, laser distance measurements are taken for the loaded condition of the bridge, and the exact position of the trucks on the deck is measured and documented.	~ 12 mins
5	Removal of trucks	All vehicles are removed from the bridge.	~ 3 mins
6	Road reopened	Traffic control is removed, and the bridge is opened back up to traffic	N/A

Figure E3-35: Typical TxDOT dump truck used for the controlled live load test

E3.4.3 Load Cases

Based on the results of the preliminary FEA investigation, the RT prepared a list of static and moving loading cases for each bridge to conduct during the bridge closures. The primary purpose of the static load cases was the validation of the Abaqus models for each bridge. Moving load cases effectively captured influence lines/surfaces and lateral distribution effects for various design and striped lanes by measuring girder and cross-frame stresses as trucks slowly traversed the bridge.

The four dump trucks were positioned in various longitudinal and transverse positions to maximize stresses in different cross-frame components. The measured data from these load cases facilitated the validation of the FEA models. The eight loading cases were prioritized in order of importance to maximize the data obtained under limited time constraints. The prioritization was necessary in case problems were encountered and the RT was not able to complete all eight load cases. There were no problems with the schedule on any of the bridges and all desired load cases were completed. Seven critical static and one moving load cases are presented schematically for each bridge in following subsections.

E3.4.3.1 Load Cases for Bridge 1

As shown in Table E3-1, the controlled live load test for Bridge 1 was conducted on the night of April 4, 2018 and into the morning of April 5. The general procedure outlined in Section E3.4.2 was followed. TxDOT initiated its road closure at approximately 9 pm, and the RT began the prep work on the deck around 10 pm. The test itself was conducted between 11 pm and 3 am. No major issues were encountered by the RT nor TxDOT crews. As stated previously, one moving load case (Case 0) and seven static load cases (Cases 1 through 7) were performed. Table E3-3 outlines each of these load cases schematically. Although not displayed on the figures, precise measurements were taken for the position of each truck on the deck.

Figure E3-36 shows a load case performed during the Bridge 1 load test. All four trucks are positioned along the right barrier in this photo.

Figure E3-36: Load case performed during the Bridge 1 load test

E3.4.3.2 Load Cases for Bridge 2

The controlled live load test for Bridge 2 was conducted on the night of July 7, 2018 and into the morning of July 8. As previously stated, the traffic control for this bridge was more challenging than for the other two bridges. TxDOT began prep for total closure of SB IH 45 at approximately 8 pm. All five lanes of IH 45 traffic were shut down by 10 pm. The RT conducted the load test between 11 pm and 3:30 am. The general procedure outlined in Section E3.4.2 was followed, and no major issues were encountered. Similar to Bridge 1, one moving load case (Case 0) and seven static load cases (Cases 1 through 7) were performed. Table E3-4 outlines each of these load cases schematically.

Figure E3-37 shows a load case performed during the Bridge 2 load test. All four trucks are positioned; trucks 1 and 2 are in the center of the right lane, and trucks 3 and 4 are along the right (west) barrier.

Figure E3-37: Load case performed during the Bridge 2 load test

E3.4.3.3 Load Cases for Bridge 3

The controlled live load test for Bridge 3 was conducted on the morning of July 28, 2018. Traffic control was relatively straightforward for this test. TxDOT was able to close the bridge within 30 minutes. The RT was given access to the bridge at 7:30 am, and the test was conducted between 8 am and 12:30 pm. The general procedure outlined in Section E3.4.2 was followed, and no major issues were encountered. Similar to Bridge 1, one moving load case (Case 0) and seven static load cases (Cases 1 through 7) were performed. Table E3-5 outlines each of these load cases schematically.

Figure E3-38 shows a load case performed during the Bridge 3 load test. In this photo, only three of the four trucks are visible along the left barrier, with the fourth truck still further back around the curve. Trucks were typically placed within two feet of each other, measured from the back bumper of the front truck to the front bumper of the back truck. As stated in Section E3.4.2, data was also obtained during these intermediate stages of the load cases.

Figure E3-38: Load case performed during the Bridge 3 load test

Table E3-3: Critical Stage II (controlled live load test) load cases for Bridge 1

Load Case No.	Description	Illustration (Span 11 shown)
0 (Moving)	Individual dump trucks driving slowly (5 mph) in various design and striped lanes: 2 feet from left barrier (shown), center of left striped lane, center of middle striped lane, and center of striped right lane	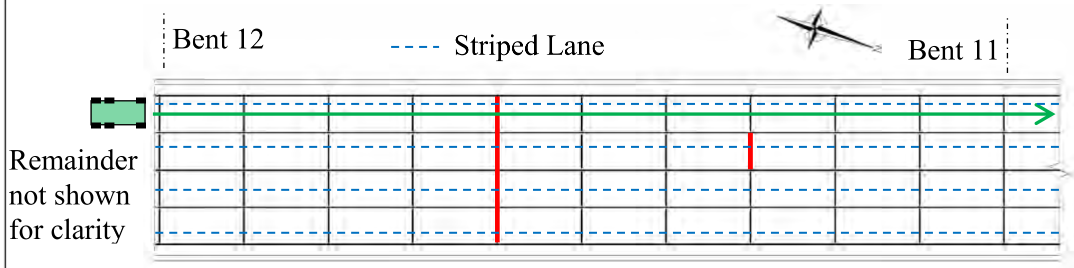
1 (Static)	Four dump trucks front-to-rear 2 feet from right barrier; centered about cross-frame line 4	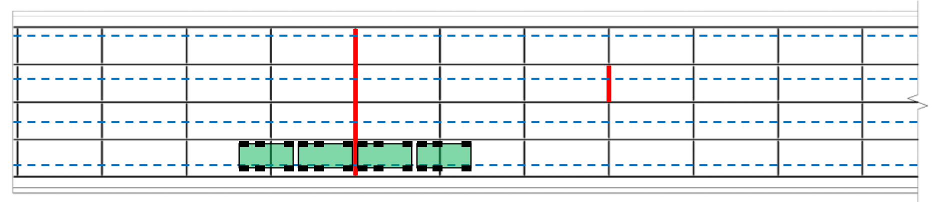
2 (Static)	Four dump trucks front-to-rear in center of right lane; centered about cross-frame line 4	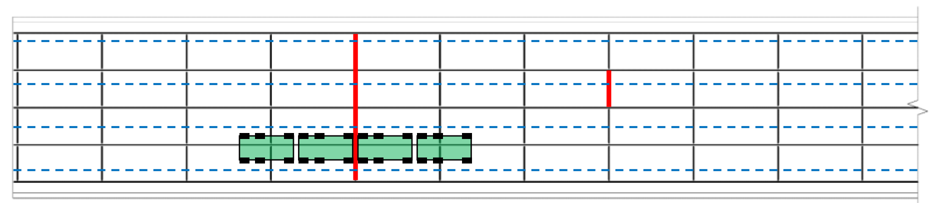
3 (Static)	Four dump trucks front-to-rear in center of middle lane; centered about cross-frame line 4	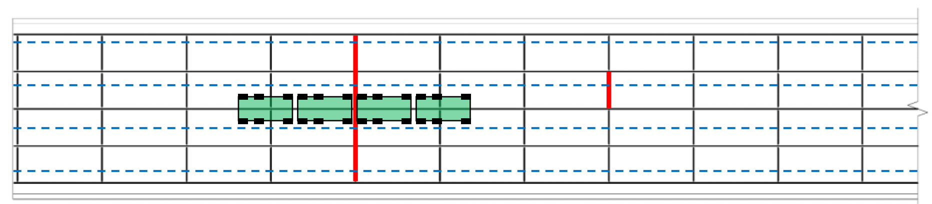

(Con't) Table E3-3: Critical Stage II (controlled live load test) load cases for Bridge 1

Load Case No.	Description	Illustration (Span 11 shown)
4 (Static)	Four dump trucks front-to-rear in center of left lane; centered about cross-frame line 4	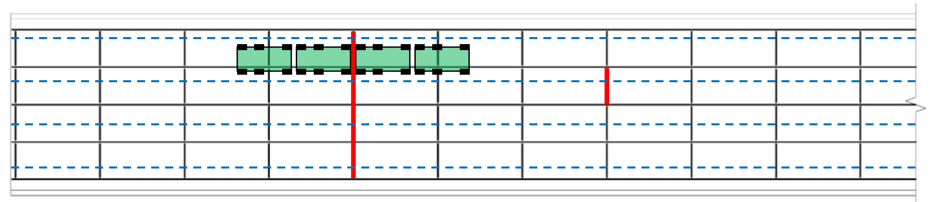
5 (Static)	Two dump trucks in center of left lane, two in center of right lane; centered about cross-frame line 7	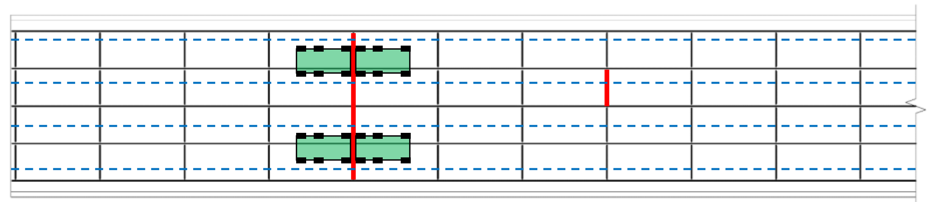
6 (Static)	Four dump trucks front-to-rear to left of girder 4; centered about cross-frame line 4	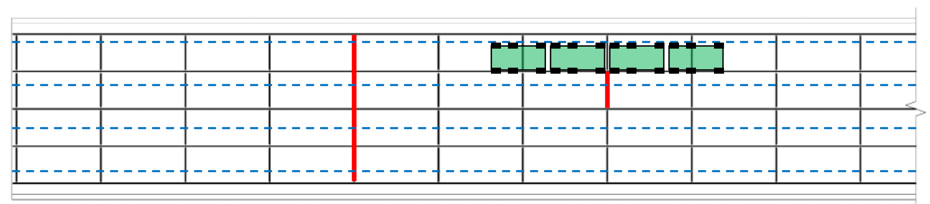
7 (Static)	Four dump trucks front-to-rear to right of girder 3; centered about cross-frame line 7	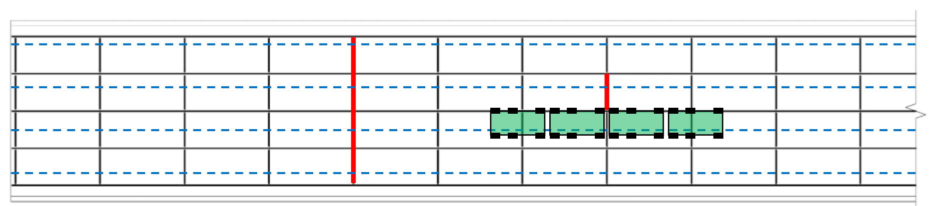

Table E3-4: Critical Stage II (controlled live load test) load cases for Bridge 2

Load Case No.	Description	Illustration (Span 11 shown)
0 (Moving)	Individual dump trucks driving slowly (5 mph) in various design and striped lanes: center of middle lane (shown), center of second lane from right, center of right lane, and 2 feet from right barrier	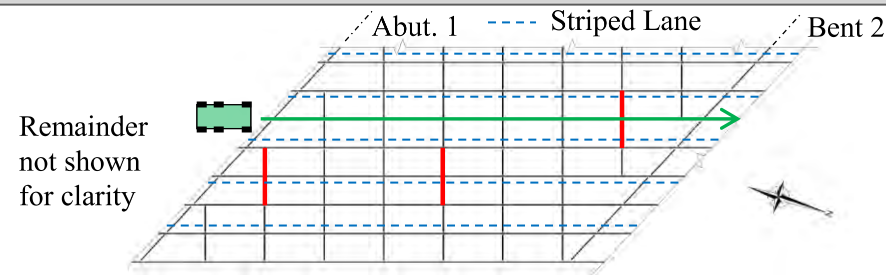
1 (Static)	Two dump trucks front-to-rear in center of second lane from right, centered about cross-frame line 3; two dump trucks front-to-rear 2 feet from right barrier, centered about cross-frame line 3	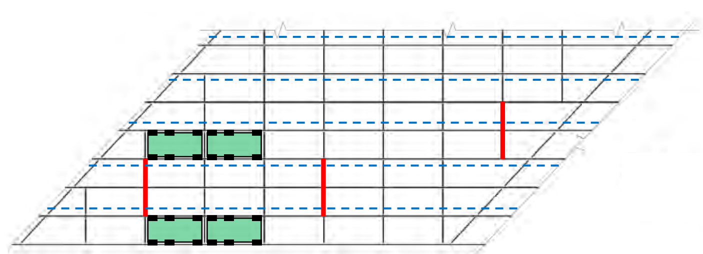
2 (Static)	Two dump trucks front-to-rear in center of right lane, centered about cross-frame line 3; two dump trucks front-to-rear 2 feet from right barrier, centered about cross-frame line 3	
3 (Static)	Four dump trucks front-to-rear in center of middle lane; centered about cross-frame line 5	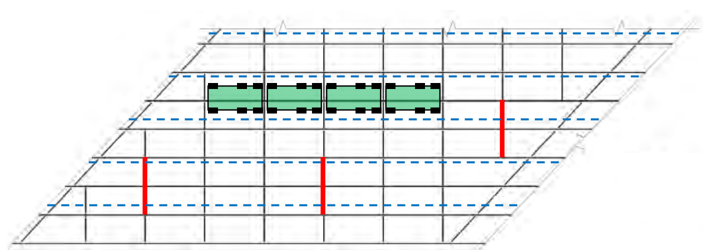

(Con't) Table E3-4: Critical Stage II (controlled live load test) load cases for Bridge 2

Load Case No.	Description	Illustration (West Half of Span 1 shown, except for LC 6 & 7)
4 (Static)	Four dump trucks front-to-rear in center of right lane; centered about cross-frame line 5	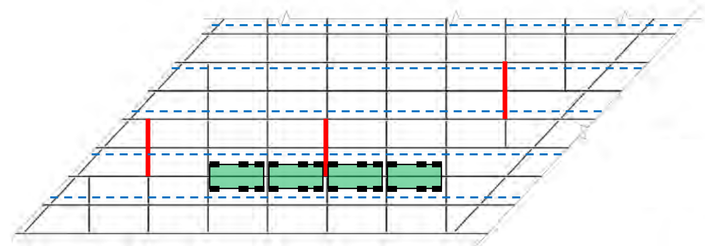
5 (Static)	Two dump trucks front-to-rear in center of second lane from right, centered about cross-frame line 7; two dump trucks front-to-rear in center of right lane, centered about cross-frame line 7	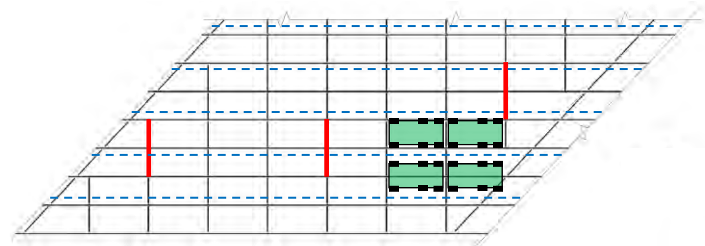
6 (Static)	Two dump trucks front-to-rear in center of left lane, centered about cross-frame line 7; two dump trucks front-to-rear in second lane from left, centered about cross-frame line 7	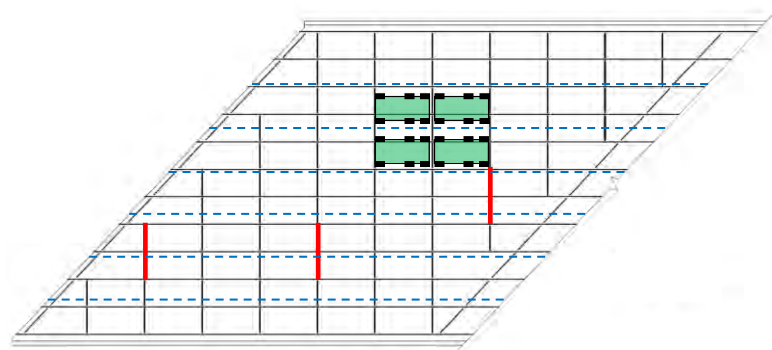

(Con't) Table E3-4: Critical Stage II (controlled live load test) load cases for Bridge 2

Load Case No.	Description	Illustration (West Half of Span 3 shown, except for LC 6 & 7)
7 (Static)	Four dump trucks front-to-rear 2 ft from left barrier; centered about cross-frame line 8	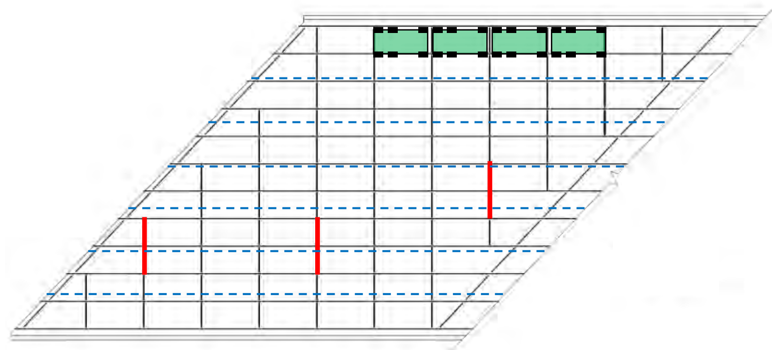

Table E3-5: Critical Stage II (controlled live load test) load cases for Bridge 3

Load Case No.	Description	Illustration (Span 11 shown)
0 (Moving)	Individual dump trucks driving slowly (5 mph) in various design and striped lanes: 2 feet from left barrier (shown), center of lane, 6 feet from right barrier, and 2 feet from right barrier	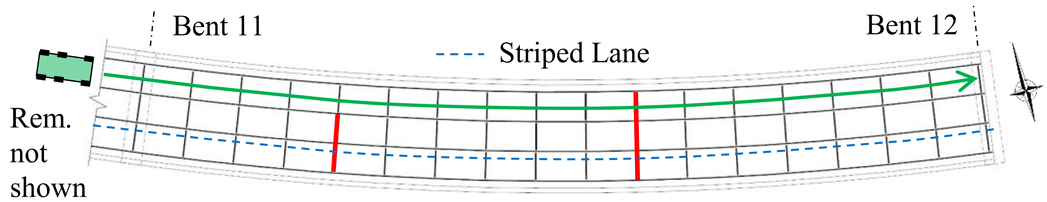
1 (Static)	Four dump trucks front-to-rear 2 feet from left barrier; centered about cross-frame line 10	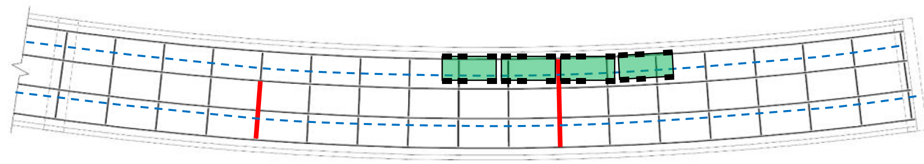
2 (Static)	Four dump trucks front-to-rear in center of lane; centered about cross-frame line 10	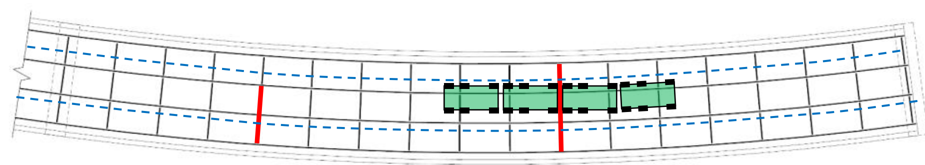
3 (Static)	Four dump trucks front-to-rear 6 feet from right barrier; centered about cross-frame line 10	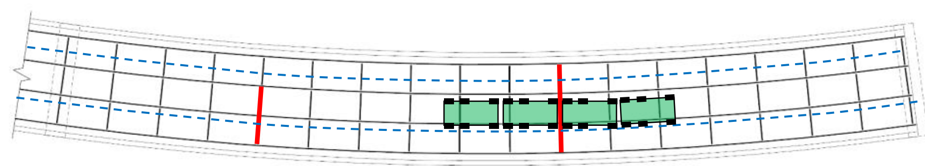

(Con't) Table E3-5: Critical Stage II (controlled live load test) load cases for Bridge 3

Load Case No.	Description	Illustration (Span 11 shown)
4 (Static)	Four dump trucks front-to-rear 2 feet from right barrier; centered about cross-frame line 10	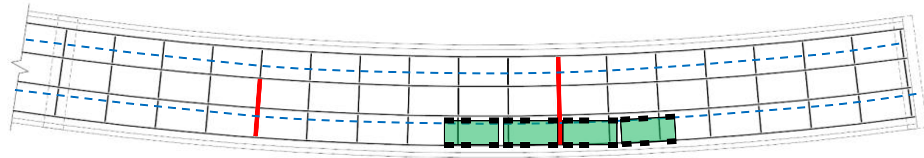
5 (Static)	Four dump trucks front-to-rear 2 feet from left barrier; centered about cross-frame line 4	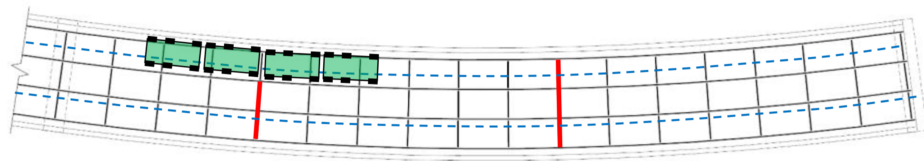
6 (Static)	Four dump trucks front-to-rear 2 feet from right barrier; centered about cross-frame line 4	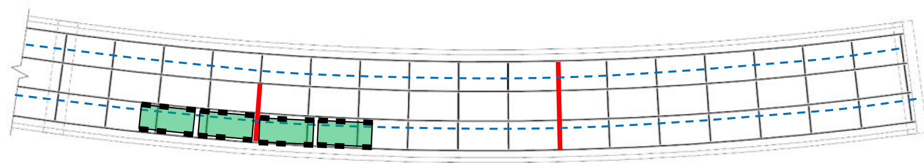
7 (Static)	Two dump trucks front-to-rear 2 feet from left barrier, centered about cross-frame line 10; two dump trucks front-to-rear 2 feet from right barrier, centered about cross-frame line 10	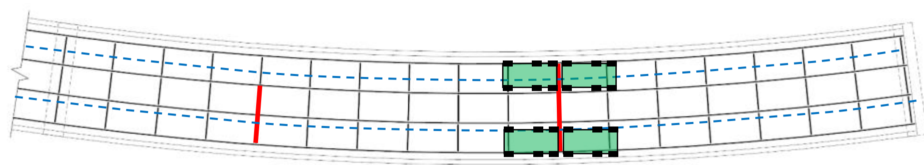

E3.5 Stage III – In-Service Monitoring

This section outlines the means and methods used to accomplish the in-service monitoring task. Note that identical procedures were applied with all three subject bridges and are therefore not presented on a bridge-by-bridge basis.

In-service monitoring of the bridge typically began immediately after the DAQ system was installed and troubleshooting was complete. The system ran for approximately four weeks to ensure sufficient data was obtained to characterize daily fatigue cycles on the bridge. Past work (Fasl 2013, Connor and Fisher 2006) has shown that between one week and four weeks are usually adequate to obtain representative fatigue data for in-service bridges. In the absence of special circumstances, 1-2 weeks is generally more than adequate to obtain a good measure of daily and weekly traffic that typically occurs on the bridge. Factors that can affect that data are holidays, weekends, and other severe conditions such as extreme weather. There were no special circumstances observed in the bridge monitoring that significantly changed the traffic over the monitoring periods.

Refer to Table E3-1 for the monitoring dates for each bridge. The monitoring period for Bridge 1 was much longer than the monitoring period of the other two bridges, since the system was shut down for a period of weeks while modifications were developed in the DAQ monitoring program so that the effective axial stress in the cross-frame members could be determined. Despite the delay, four weeks of monitoring time was satisfied.

E3.5.1 Procedure for Data Collection

The main source of data collected during the in-service monitoring is a spectrum of stress range measurements in the instrumented elements. With some post-processing, effective and maximum stress ranges can be computed from this data. The strain data is measured by the same gages in the same manner as the controlled live load test procedure previously outlined, with two differences. The first differences between the two stages is the sampling rate. The RT recorded in-service data at 50 Hz, such that dynamic effects could be accurately captured.

The second difference is how the data was processed. Unlike the continuous sampling used during the Stage II controlled live loads tests, in the Stage III monitoring, the wireless nodes were programmed to sort strain data into bins based on the rainflow counting technique developed by Downing and Socie (1982). The RT set bridge-specific rainflow input values (bin size, threshold strain, time window size, etc.) based on data measured during the troubleshooting phase of Stage I.

Temperature effects were also considered by the RT. Not only are temperature-compensated gages used, but additional considerations for temperature compensation were included in the rainflow algorithms run by the wireless nodes. The main method that is necessary in rainflow counting is “closing out” the data over short time intervals to avoid large temperature-induced stress cycles from affecting the truck data. Rainflow data was processed in 30-minute increments to avoid counting large temperature-induced cycles.

E3.6 Stage IV – Demobilization of Sensors and DAQ System

For all three bridges, the removal of the field monitoring system occurred after the in-service rainflow data was collected for a period of approximately four weeks. Demobilization included removing all strain gages from the bridge, using “touch-up” paint to match the original color in the areas in which paint was removed for gage installation, and taking down all monitoring equipment and batteries. Figure E3-39 shows Bridge 1 after the equipment was removed and spot painting was completed.

Traffic control during Stage IV was similar to that used in Stage I for all three bridges. For example, an

TMA and a full closure of the turnaround lane was provided for demobilization of the second bridge instrumentation.

Figure E3-39: Previously instrumented cross-frame at Bridge 1 after equipment removed

CHAPTER E4

Field Experiment Results

A summary of the procedures and plan executed to obtain field measurements at all three bridges was provided in the previous chapter. This chapter presents the pertinent results of those field experiments. Two different sets of results are presented for each bridge, which include the controlled live load test and the in-service rainflow data. Hence, this chapter is divided into two major sections: controlled live load test data and in-service rainflow data.

For the controlled live load test data, strain measurements for instrumented girder flanges and cross-frame members, deflection readings of select girders, and truck properties are presented. For the in-service data, histogram plots of stress range bin counts are presented. Commentary on the results is also offered at the end of each section.

E4.1 Controlled Live Load Test Data

E4.1.1 Overview of Collected Data

For each controlled live load test, the following measurements were obtained by the RT:

- Continuous strain history of select girder flanges and cross-frame members.
- Vertical deflection at select locations on the bridge.
- Truck properties including gross vehicle weight and wheel base dimensions.
- Specific load case information including final truck position dimensions and time elapsed.
- Haunch dimensions at predetermined points along the length of the bridge.

Strain data, vertical deflection data, and truck properties are presented for the various load cases. Continuous strain data was measured and evaluated for both the moving load case (Load Case 0) and the seven static load cases (Cases 1 through 7). Vertical deflections at select locations along the bridge were measured and evaluated for the static load cases only. Recall that girder flange stresses are presented in terms of the average response of the flange edges (equivalent to longitudinal bending stresses) and differential response of the edges (equivalent to lateral bending stresses); cross-frame stresses are presented in terms of the axial component only via the linear regression algorithm outlined in Section E3.3.1.

An example of the linear regression technique used to determine the axial stress component in a loaded cross-frame angle is shown in Figure E4-1. Figure E4-1 represents a stress history of a cross-frame diagonal member measured during a static load case of the live load test on Bridge 1. As outlined in Section E3.3.1, each cross-frame angle was instrumented with four strain gages. Since the gusset plate is connected to a single leg of the angle, two strain gages were placed on the loaded leg and two gages were placed on the unloaded leg (free, unattached leg). The applied load to the angle is tensile in nature; however due to the eccentricity, combined bending and axial stresses are introduced in the angle. Figure E4-1 shows that there is a significant difference in the stress response between the gages on the loaded leg and the unloaded leg. The stress differential is due to the bending induced from the eccentric end connection of the angle member.

The axial component of the stress, derived by the linear regression algorithm, always falls within the bounds set by the extreme stress states measured from free edge to free edge of an angle legs. Given that AASHTO LRFD idealizes these angles as axial-only members and inherently considers bending effects in the Category E′ fatigue designation, the RT only addresses cross-frame stresses in terms of the axial component. This is analogous to average *P*/*A* stresses over a cross-section.

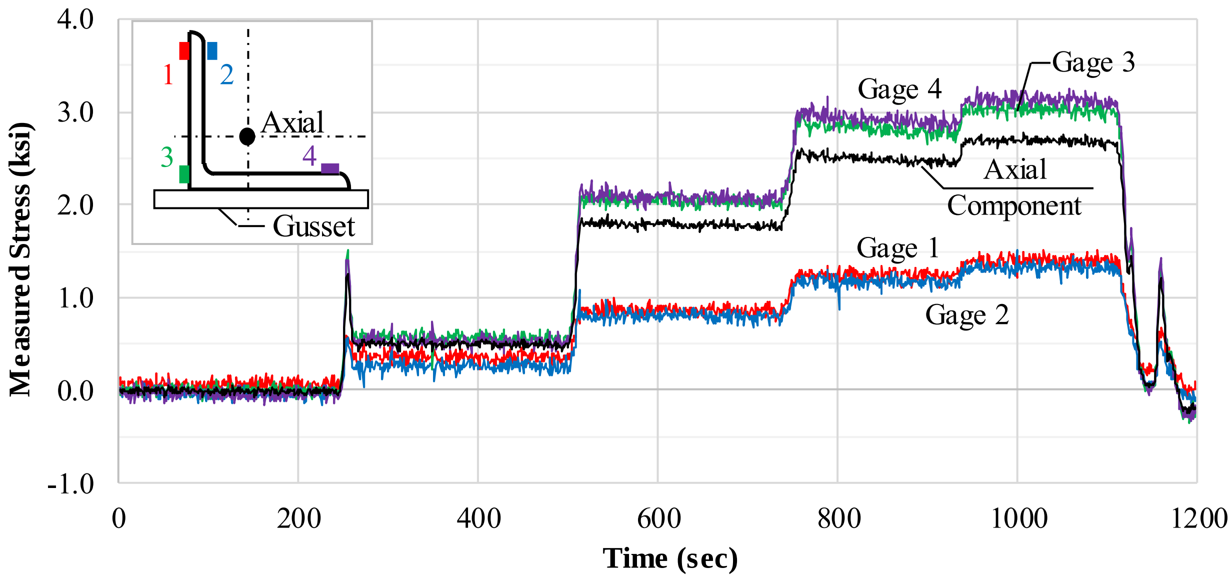

Figure E4-1: Example showing the axial stress component of a cross-frame angle section versus the individual strain gage responses

For this appendix, the strain data is presented in terms of stress, so that consistent comparisons can be made between different members and different bridges. Elastic behavior is assumed as discussed in Section E3.3.1. This is an important distinction for cross-frames since the cross-sectional area of these members varies from bridge-to-bridge, and stiffer cross-frame members generally attract more load-induced force. Lastly, final truck positions and haunch dimensions are not explicitly provided, but these data were implicitly used during the model validation phase outlined in Chapter E5.

E4.1.2 Significance of Collected Data

The results of the controlled live load test served as a vital component towards the validation of the FEA models and the assessment of commercial software in predicting girder and cross-frame stresses. For the former, the FEA models were compared with the measured strain and vertical deflection readings from the load test. Appropriate modifications were applied based on the comparison. The truck properties and loading position were simulated in the FEA models to match the loading conditions of the load test. Lastly, the FEA models were adjusted to match the as-built conditions to obtain good agreement with the composite stiffness of the deck and I-girders. Chapter E5 addresses the validation of the FEA models with respect to the data collected during the field experiments. The validated models are then used in the parametric studies conducted in Phase III of the NCHRP project (Appendix F).

Aside from the benefits to model validation, the live load test data also provides useful insight on how certain bridge components respond to live loads. The benefits of obtaining strain and deflection measurements during a controlled live load test are threefold:

1. The RT can evaluate the unique load distribution and load influence characteristics on the cross-frame members and girders of each subject bridge through strain and deflection measurements.
2. The RT can assess the measured stress and deflection magnitudes with established design metrics as a reference.
3. The RT can make observations about the complexity of load paths for each subject bridge based on differences in basic geometry.

Note that these three topics are repeatedly addressed in the subsequent sections. The commentary provided on all results and figures relate back to these three major concepts.

In addition, the following sign convention has been used for all measurements presented in this section:

- For girder longitudinal bending stresses and cross-frame axial stresses:
  - Positive strain and stress correspond to tension;
  - Negative strain and stress correspond to compression.
- For lateral bending stresses of girder flanges (refer to Figure E4-2):
  - A positive stress value indicates that the left edge of the girder flange experiences more tensile stress than the right edge due to lateral bending;
  - A negative value indicates that the right edge of the girder flange experiences more tensile stress than the average. A negative value indicates that the right edge of the girder flange experiences more tensile stress than the left edge.

The left and right directions are relative to cross-section views provided in this appendix, which always look in the direction of traffic. Also recall that the longitudinal bending stresses and lateral warping stresses in the girder flanges are computed based on the commentary associated with Figure E3-7.

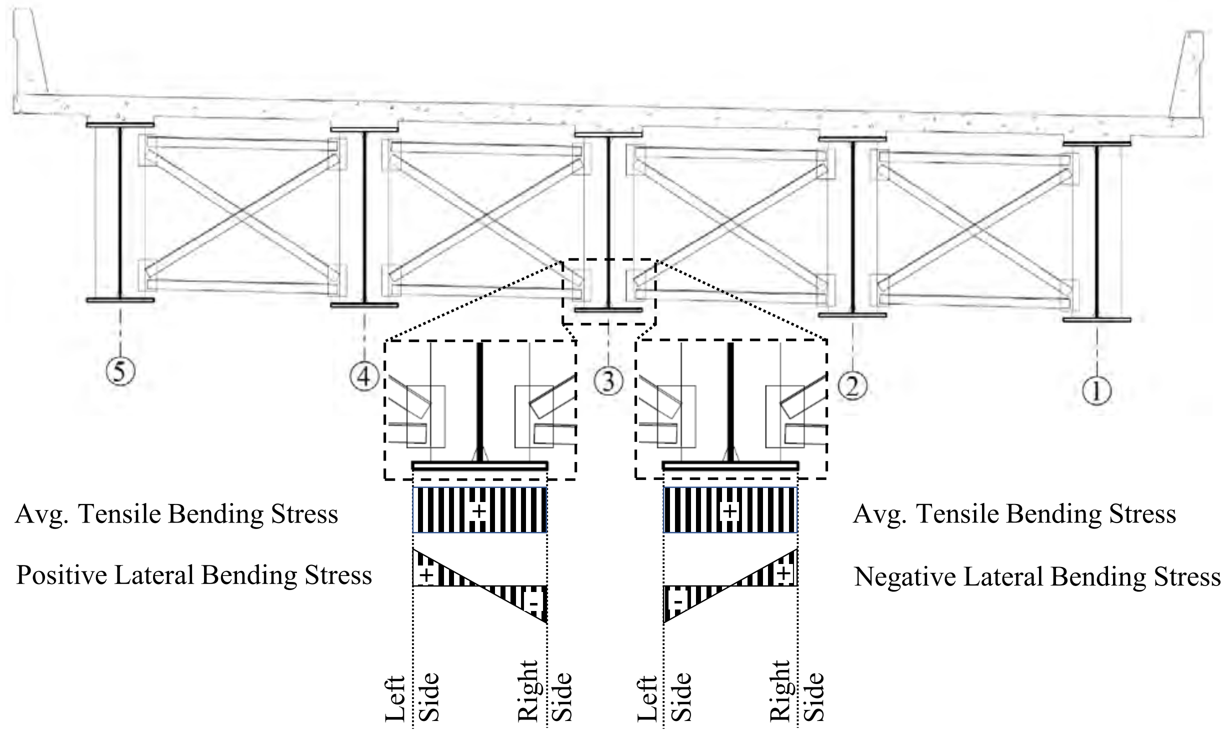

Figure E4-2: Longitudinal and lateral bending stresses in girder flanges according to sign convention

E4.1.3 Bridge 1 Results

The following subsections pertain to the controlled live load test data for Bridge 1. Individual subsections focus on truck properties, influence-line strain data for the moving load case (Case 0), strain data for the static load cases (Cases 1 through 7), and deflection data for the static load cases (Cases 1 through 7). The format for each subsequent bridge follows a similar format.

E4.1.3.1 Truck Properties for Bridge 1

As discussed in Section E3.4, TxDOT provided four dump trucks loaded with sand for the controlled live load test. TxDOT crews weighed the trucks, and the RT measured the wheel bases prior to the load test. The results are summarized in Table E4-1 and Figure E4-3.

Trucks 2, 3, and 4 were identical in geometry while Truck 1 had a slightly smaller wheel base. The smaller wheel base did not significantly impact the weight of the truck as Trucks 1, 2, and 3 were relatively close in total weight. Variations in the geometry and weights of the individual trucks do not impact the usefulness of the data since the measured weights and wheel positions can be closely simulated in the FEA models during validation studies.

Table E4-1: TxDOT truck axle weights for Bridge 1 load test

Truck #	Steer Axle Weight (lb)	Combined Drive Axle Weight (lb)	Gross Vehicle Weight (lb)
1	12620	37900	50520
2	11580	38800	50380
3	11840	40140	51980
4	12180	42640	54820

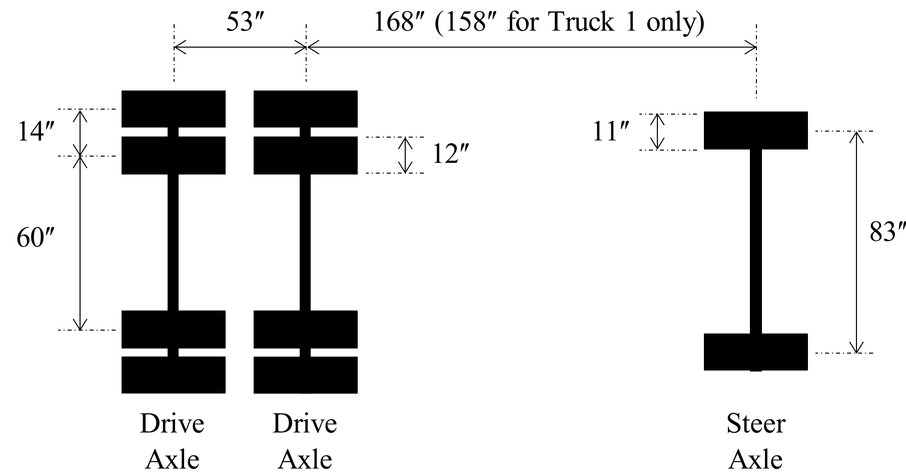

Figure E4-3: Typical TxDOT truck wheel base dimensions for Bridge 1 load test

E4.1.3.2 Load Case 0 Strain Data for Bridge 1

As discussed previously, strain data was continuously recorded during the controlled live load test. As such, the RT obtained strain data at all instrumented elements for Load Case 0. Figure E3-12 through Figure E3-14 graphically presented all girder and cross-frame elements instrumented on Bridge 1, but did not identify each with a name or number, especially cross-frame members. The cross-frame member numbers in subsequent plots are presented in Figure E4-4 and Figure E4-5, which are adapted versions of Figure E3-13 and Figure E3-14.

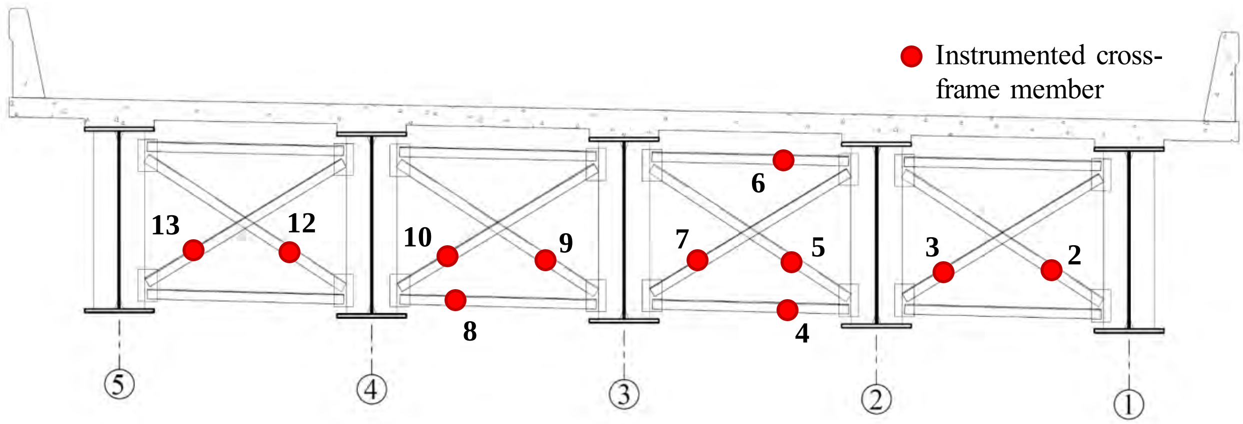

Figure E4-4: Instrumented cross-frame identification numbers at cross-frame line 4

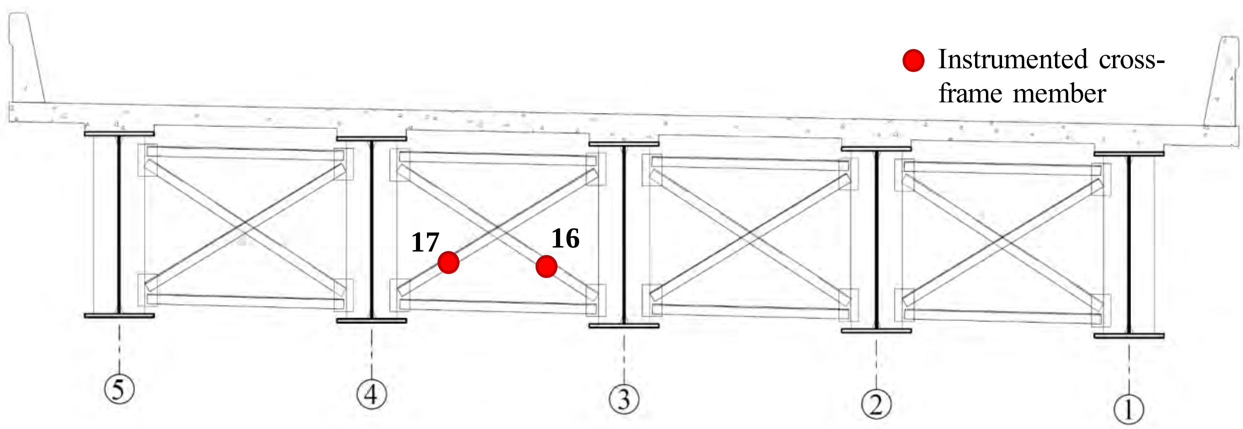

Figure E4-5: Instrumented cross-frame identification numbers at cross-frame line 7

Strain data for the influence line plots were collected as a time-history (i.e., as a function of time). However, to obtain a more meaningful understanding of the behavior, a graph of the influence lines as a function of load position on the bridge is necessary. To create influence lines as a function of longitudinal position on the bridge, the girder bottom flange stress data was manipulated. As noted earlier, the longitudinal bending stress was derived as the average of the strain readings at the two bottom flange gages (Section E3.3.1), whereas the difference of the bottom gages is the lateral bending stress in the flange.

The longitudinal bending stresses for the seven instrumented girder locations were averaged and plotted against the time elapsed during the four individual truck passages of Load Case 0, which will be referred to as Load Case 0A through 0D. Refer to Table E3-3 for precise locations of the test trucks for each case. It can be assumed that when the longitudinal bending stress in girders is equal to zero, the center of gravity of a truck passed over a bearing line at a bent or abutment. Using this information, the points of zero stress were used to align the time data with the longitudinal position of the trucks on the bridge. The plot for Load Case 0A is shown in Figure E4-6 as an example. In this example, times of 64 seconds, 132 seconds, and 185 seconds correspond to longitudinal positions of 194 feet, 434 feet, and 628 feet along the bridge, respectively. Longitudinal positions of 194 feet, 434 feet, and 628 feet correspond to the locations of bearing lines and pier supports, where 0 to 194 feet represents Span 11.

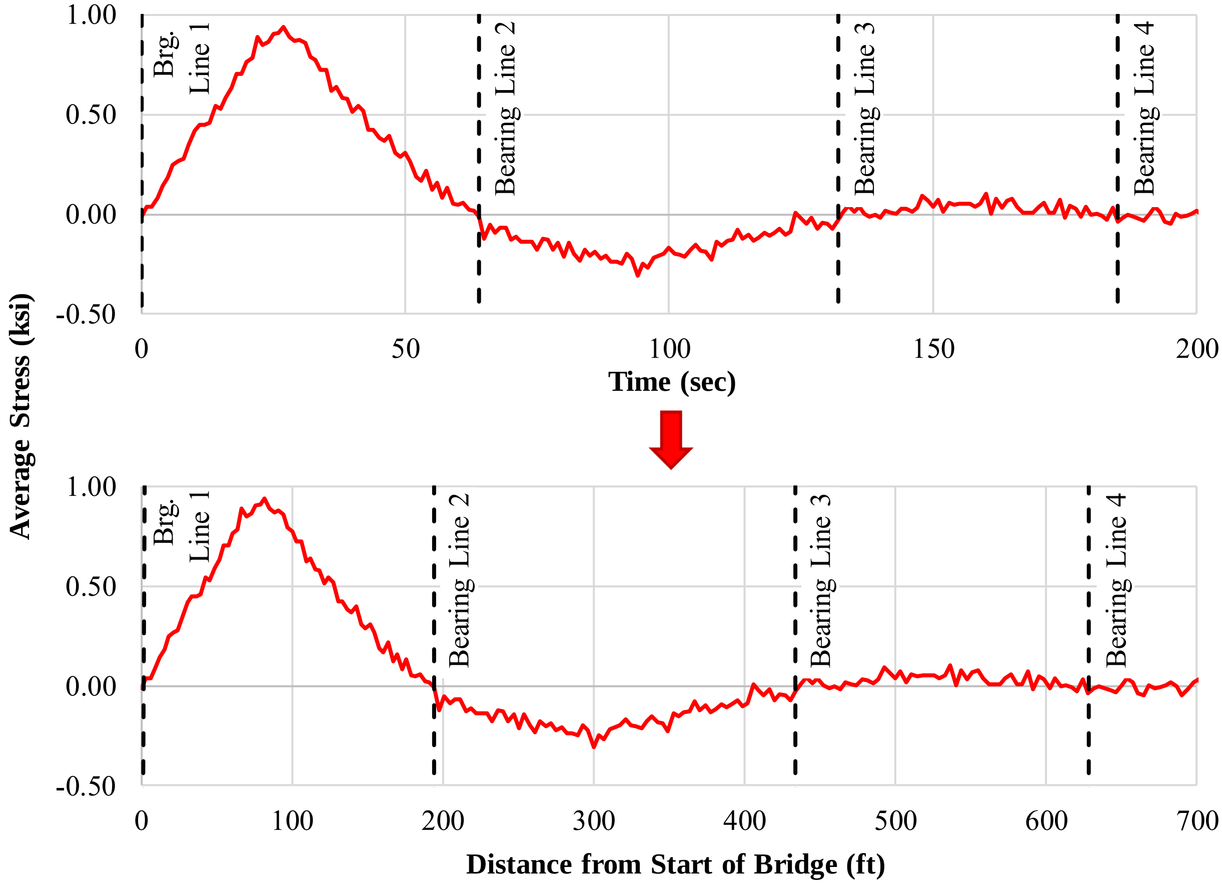

Figure E4-6: Typical plot used to align Load Case 0 time stamp with longitudinal position on bridge

Once the time component was converted to distance, influence lines were developed for all instrumented girder flanges and cross-frame members. Figure E4-7 presents the qualitative influence line for the bending moment of a three-span continuous beam with span lengths proportional to Bridge 1 using the Muller-Breslau Principle. This qualitative figure provides a good reference when evaluating the measured influence line data at the bottom flange of the girders.

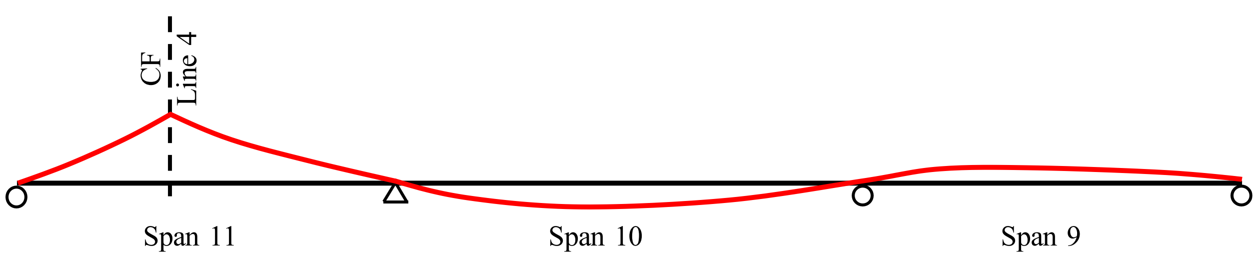

Figure E4-7: Qualitative influence line for girder bending moment at cross-frame line 4 in Span 11

Figure E4-8 through Figure E4-16 illustrate different examples of the measured influence line plots. Figure E4-8 and Figure E4-9 display the influence line for longitudinal stresses in the girder bottom flanges at cross-frame lines 4 and 7, respectively. Figure E4-10 and Figure E4-11 display the influence line for lateral bending stresses in the instrumented bottom flanges at lines 4 and 7, respectively. Lastly, Figure E4-12 through Figure E4-16 show influence line plots for axial stresses in all instrumented cross-frame members.

Note that only the first two spans (Spans 11 and 10) are plotted on the x-axis for girder-related plots and only the instrumented span (Span 11) for cross-frame-related plots. The influence of load application on Span 9 is negligible to the instrumented girder flanges, whereas the influence of load application on Spans 9 and 10 is negligible to the instrumented cross-frame members. For clarity, these portions of the respective influence line plots are not presented. The results for Load Cases 0A through 0D are presented sequentially for all influence line graphs on the same figure such that trends can be more easily recognized.

As outlined in Section E4.1.2, the commentary provided for live load test results is focused on three major topics: (i) evaluating load distribution and load influence characteristics on girders and cross-frame members through strain and deflection measurements, (ii) evaluating measured stress and deflection magnitudes with established design metrics, and (iii) understanding complex load paths based on the unique geometry of the bridge.

It is also important to note that the measured stress readings outlined below are based on the full stress cycle (tension minus compression component, if both exist). The data obtained from the strain gages simply provide the change in strain/stress during the applied loading. The data does not indicate the state of stress prior the gage being installed. As such, the strain gage response only indicates whether the change in stress is compressive or tensile but does not provide information on the dead load or residual stresses. This concept is consistent across all Load Case 0 results presented for Bridges 1, 2, and 3.

These concepts, with respect to the moving Load Case 0, are addressed by the observations from Figure E4-8 through Figure E4-11 for the girders and Figure E4-12 through Figure E4-16 for the cross-frame members. The discussion of the results for each bridge follow the same general format. The basic observations have been categorized within specific goals that are provided in bold text. The categories are the same for each of the specific bridges. Within each of the following bolded categories are specific observations that were made from the data for each bridge type.

- **Evaluate load distribution (transverse) and load influence (longitudinal) characteristics on girders.**
    - The distribution of girder stresses indicates that the transverse stiffness of the bridge, as a result of the combined deck and cross-frame system, is relatively significant. Load Case 0C, which represents the case in which the truck traveled in the center of the middle lane, shows a nearly even distribution of girder stresses, likely due to substantial transverse bridge stiffness.
    - In fact, the measured distribution factor for middle girder 3 is 0.25, which is close to the value of 0.20 which would indicate a uniform distribution among the five girders. The design-based single lane distribution factor for this bridge is 0.34 per AASHTO LRFD Table 4.6.2.2.2b-1. As such, the design-based distribution factors are approximately 35% conservative compared to the measured response. A similar observation was made for the exterior girders, which showed 31% conservatism compared to the AASHTO design criteria.
    - The relative contribution of the concrete deck versus the cross-frames with regards to transverse load distribution cannot be fully understood based on the live load test results only. This type of relationship was further evaluated during Phase III.
    - The shapes of the measured influence lines generally match the simple 1-D qualitative influence line presented in Figure E4-7. Load influence is only significant on the span instrumented and the closest adjacent span. Also, bottom flange stresses are most significant when the centroid of the truck axles are centered over the longitudinal point of

interest. For instance, bottom flange stresses at cross-frame line 4 are maximum when the centroid of the truck axles is centered over cross-frame line 4, and bottom flange stresses at cross-frame line 7 are maximum when the centroid of the truck axles is centered over cross-frame line 7.

- **Compare and evaluate measured girder stress (longitudinal and lateral) and deflections with established design metrics.**
  - Longitudinal girder stresses at cross-frame line 4 are generally higher than longitudinal girder stresses at cross-frame line 7. This is consistent with the preliminary FEA results that estimated cross-frame line 4 to be near the maximum positive moment region of the girders, and cross-frame line 7 to be near the assumed dead load inflection point.
  - The lateral stress plots presented show no discernible trends. Refer to the static load case results for more information regarding patterns in lateral flange stresses.
- **Evaluate load distribution (transverse) and load influence (longitudinal) characteristics on cross-frames.**
  - Cross-frame stress ranges are highly sensitive to the transverse position of the truck. Cross-frame members, especially diagonals, are prone to stress reversal as evidenced by the varied response to Load Cases 0A through 0D.
  - The shapes of the influence lines suggest that cross-frame stresses are sensitive to loading only in close proximity to the cross-frame of interest. Cross-frame stresses typically dissipated to zero when the truck traveled approximately 80 feet longitudinally beyond the specific cross-frame. Only one stress cycle per truck passage was observed.
- **Compare and evaluate measured cross-frame stress with established design metrics.**
  - In all cases, measured cross-frame stress ranges are significantly less than the constant-amplitude fatigue limit (CAFL) of 2.6 ksi for the Category E′ welded angle-to-gusset detail. Although different wheel bases, the gross weight of the individual test trucks (approximately 50 kips) is less than the unfactored AASHTO fatigue truck (72 kips total), but comparable to the Fatigue II factored truck (57.6 kips).
  - Axial stresses in cross-frame members are generally less than longitudinal stresses in girder bottom flanges. This trend suggests that the cross-frames in this normal, straight bridge are lightly loaded relative to the stresses that are typically experienced by the girders to which the cross-frames are attached.
  - Stresses in the instrumented top strut member are generally insignificant, regardless of truck position. The RT instrumented the cross frames assuming that the top strut stresses would be small, and this assumption was verified by the test data. This is likely because the top strut nearly coincides with the neutral axis of the composite girder section. The top struts are also close to a stiff diaphragm element in the concrete deck, which is capable of transferring those lateral forces generated in cross-frames due to relative moment of the girders. With this in mind, no top strut members were instrumented at Bridge 2 and 3, given that obtaining useful data at these locations was unlikely. However, it is important to note that top struts are important to stability bracing of girders, particularly in the non-composite stage, and should not be eliminated; stability problems have been documented when the top strut is not provided.
- **Understanding complex load paths based on unique characteristics of the measured data.**
  - During Load Case 0 no unusual behavior was observed from the instrumented girders or cross-frames on the straight bridge, which is expected for a simple geometry.

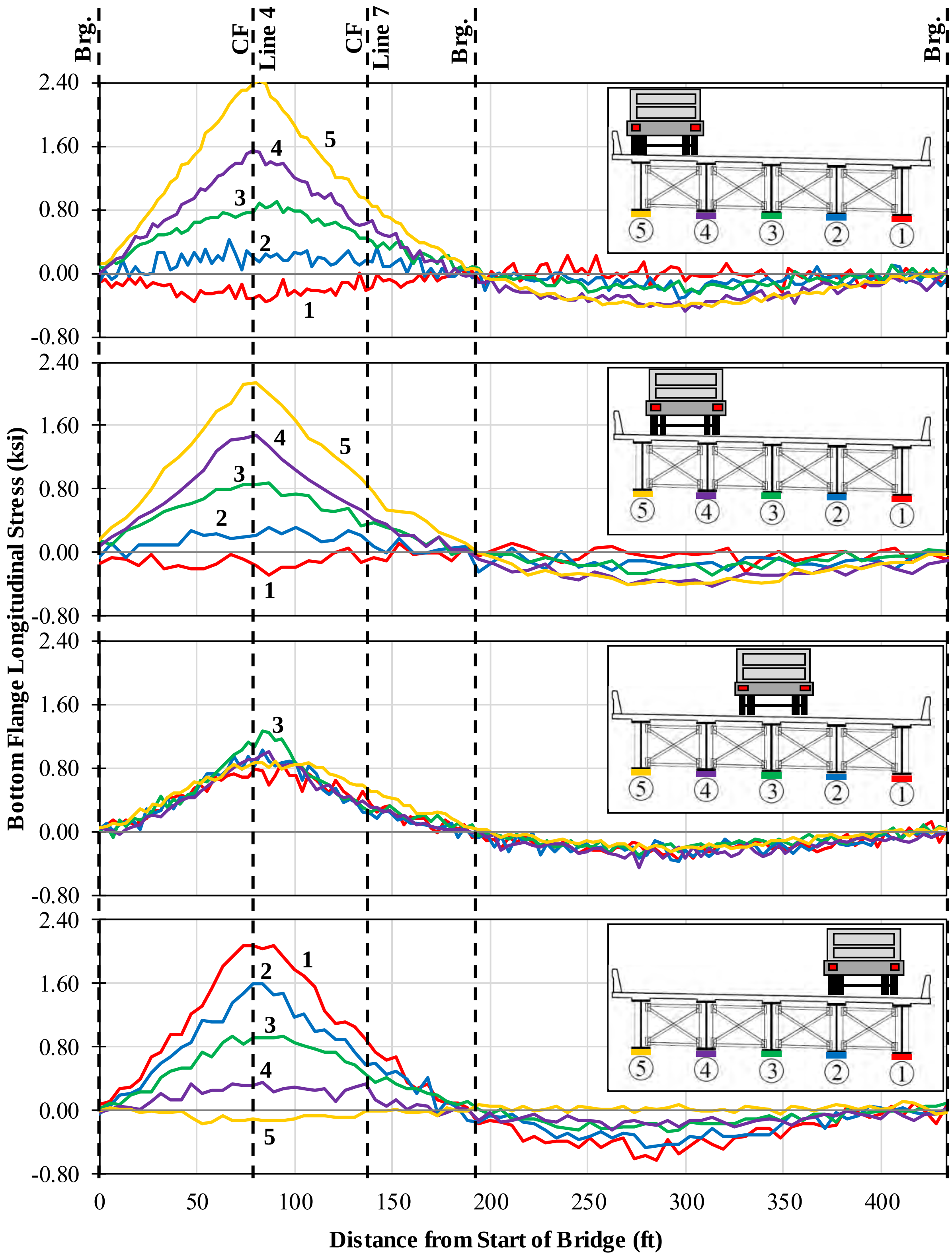

Figure E4-8: Influence line plots for bottom flange stresses at cross-frame line 4 (Load Case 0A through 0D)

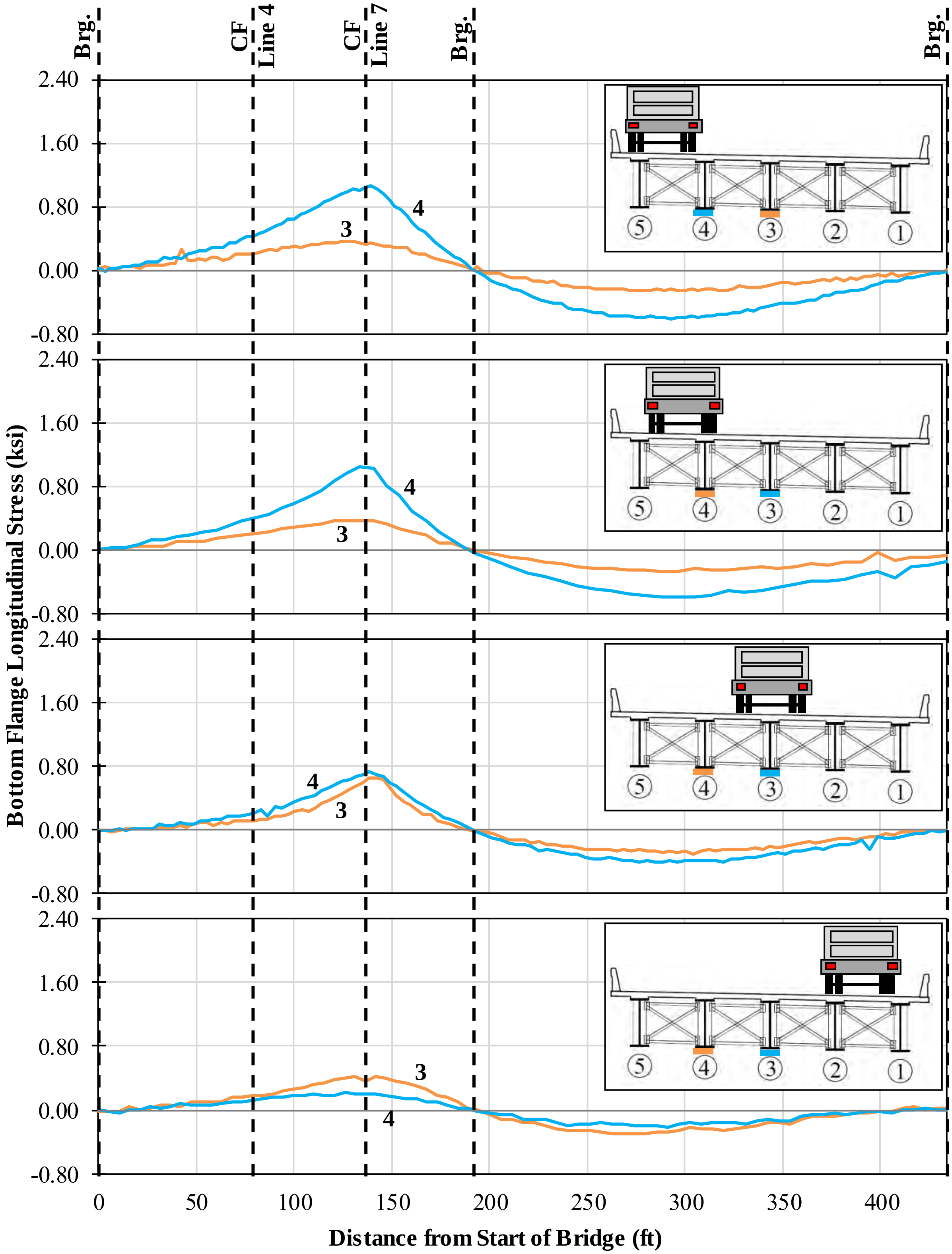

Figure E4-9: Influence line plots for bottom flange stresses at cross-frame line 7 (Load Case 0A through 0D)

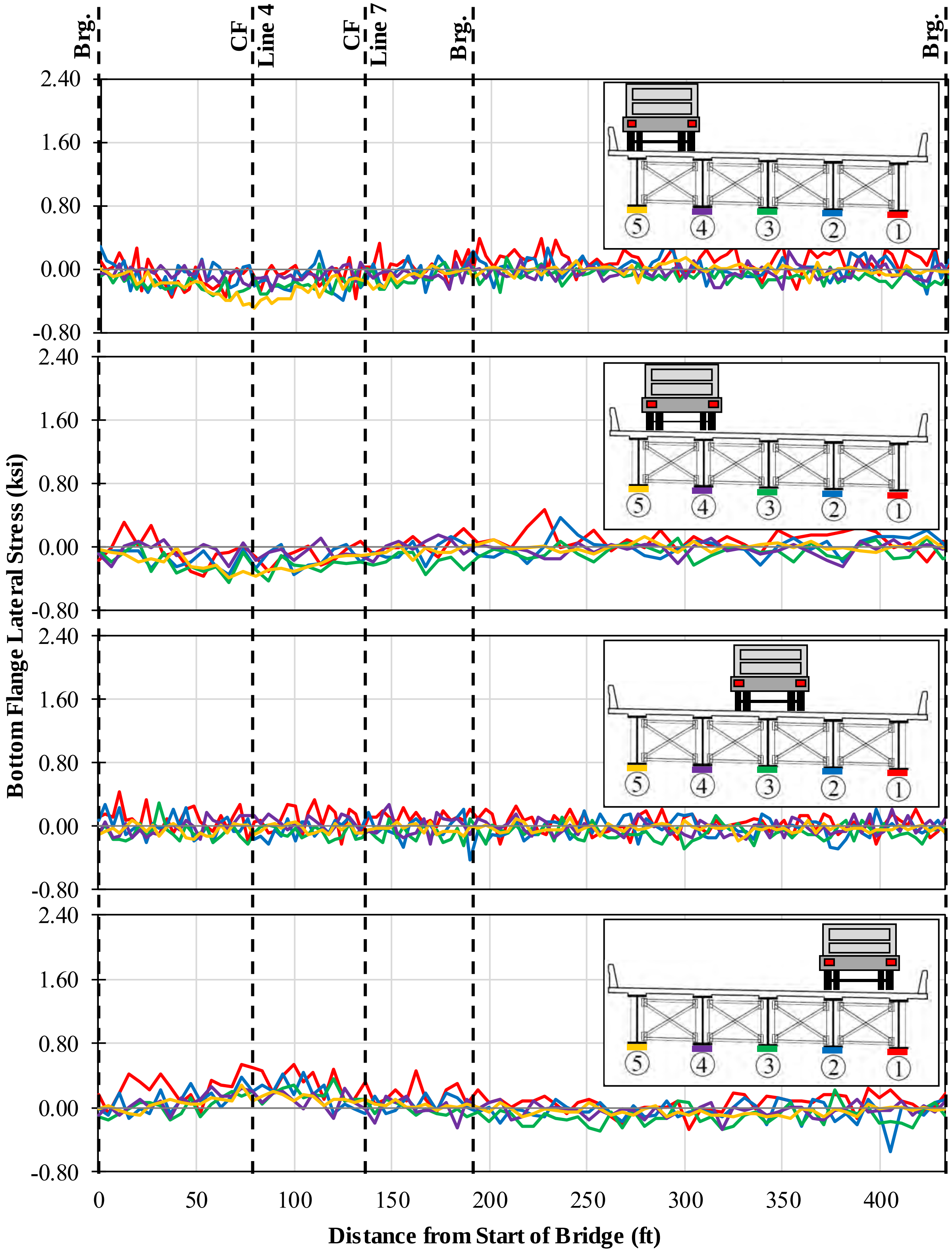

Figure E4-10: Influence line plots for bottom flange lateral stresses at cross-frame line 4 (Load Case 0A through 0D)

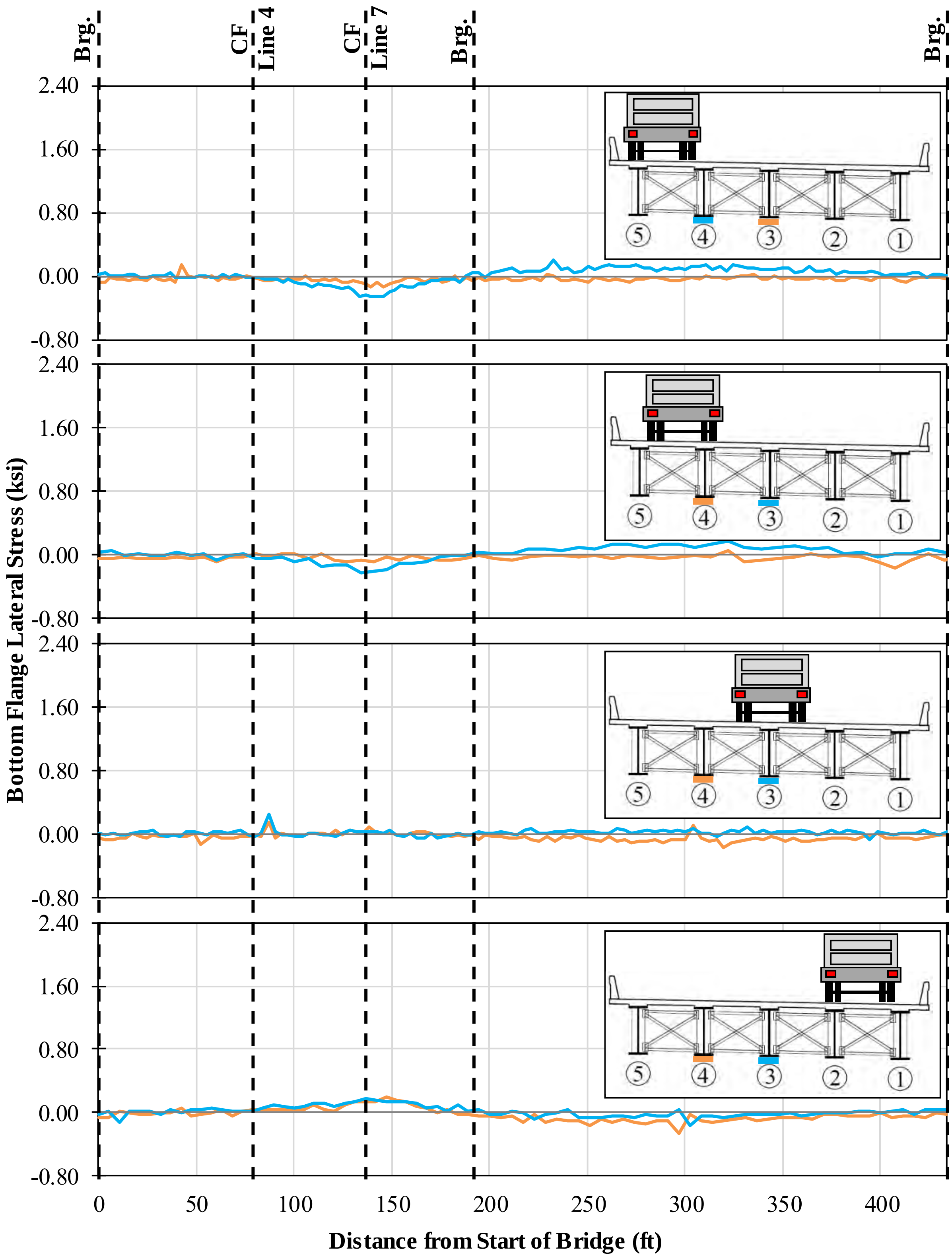

Figure E4-11: Influence line plots for bottom flange lateral stresses at cross-frame line 7 (Load Case 0A through 0D)

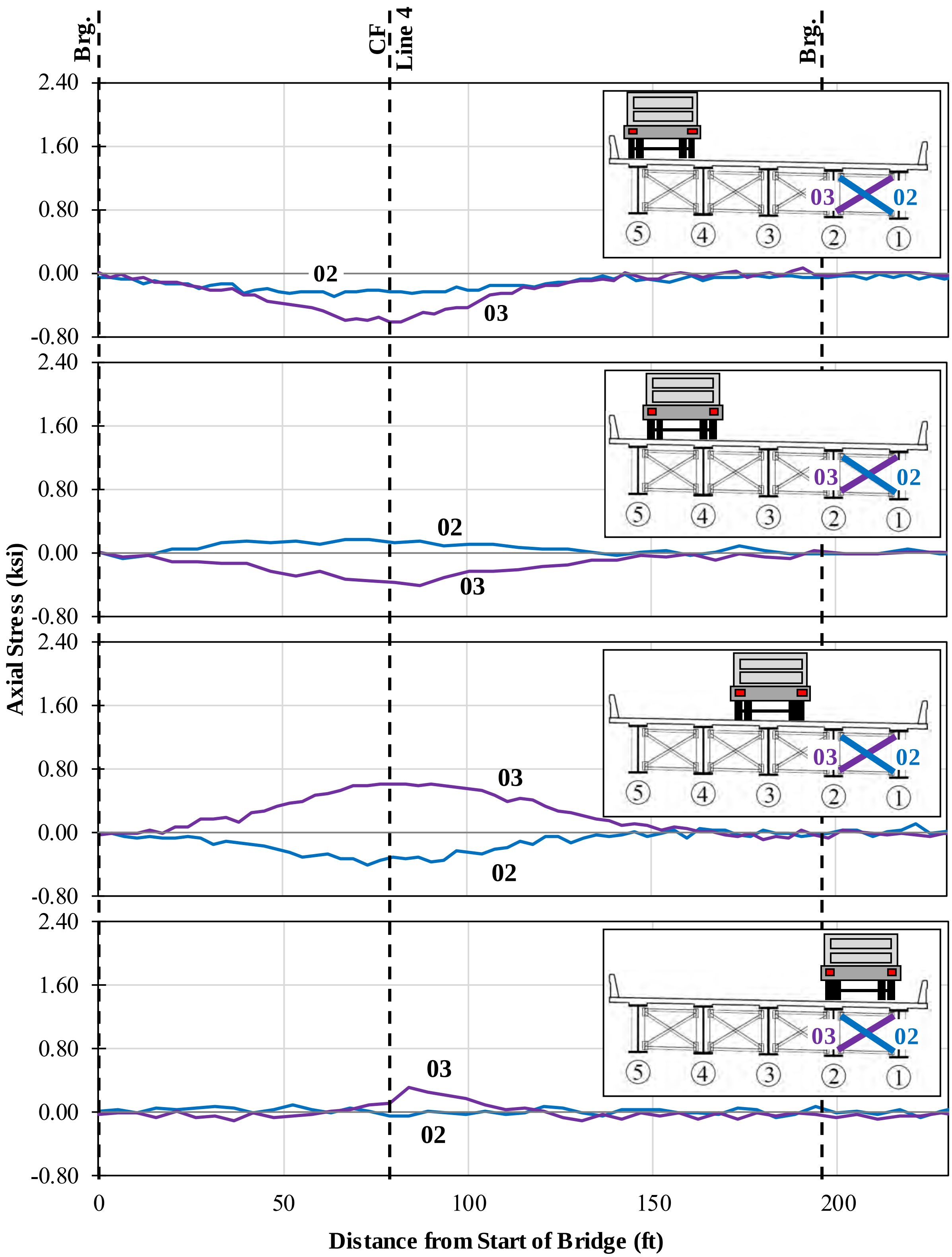

Figure E4-12: Influence line plots for cross-frame axial stresses at cross-frame line 4 (Load Case 0A through 0D)

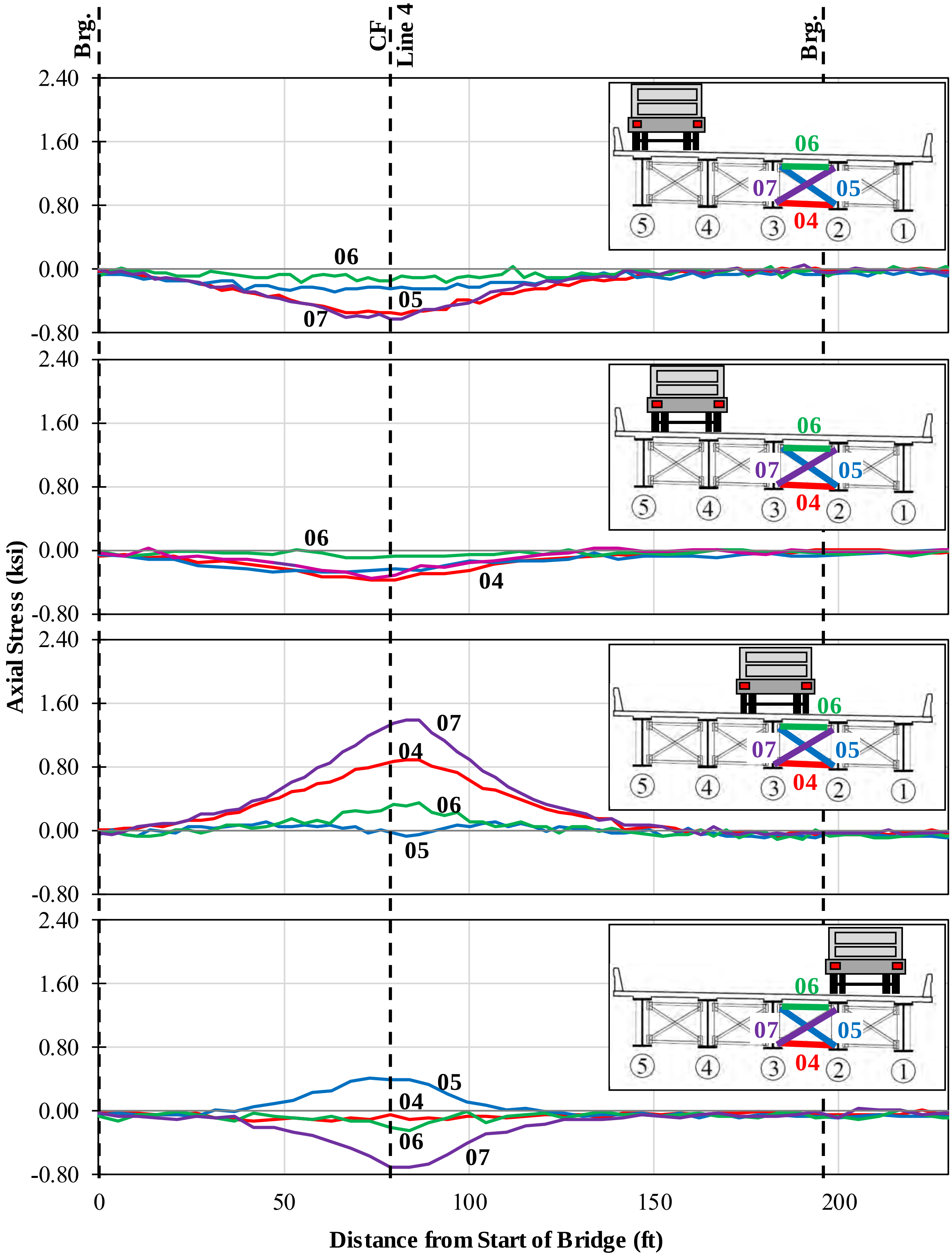

Figure E4-13: Influence line plots for cross-frame axial stresses at cross-frame line 4 (Load Case 0A through 0D)

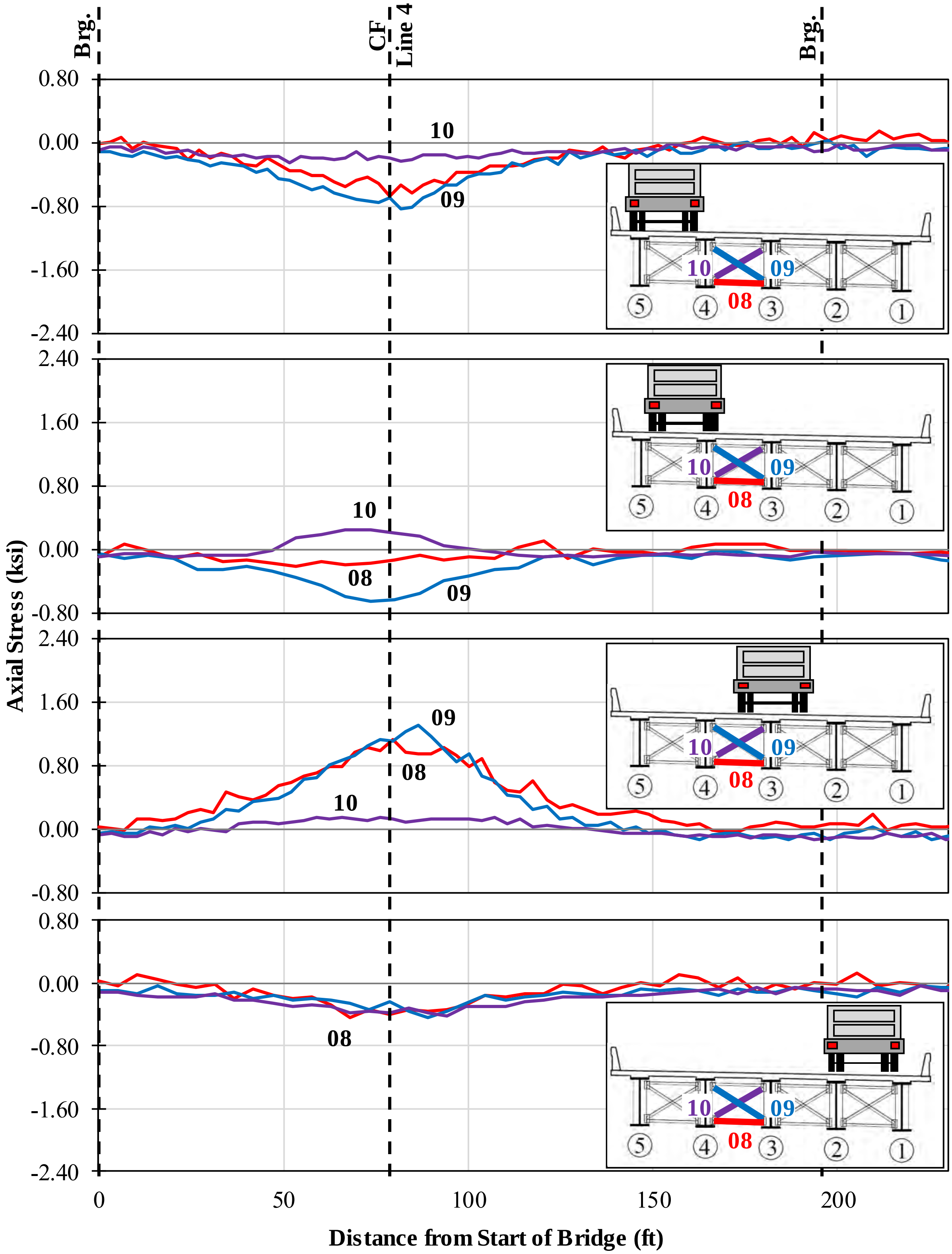

Figure E4-14: Influence line plots for cross-frame axial stresses at cross-frame line 4 (Load Case 0A through 0D)

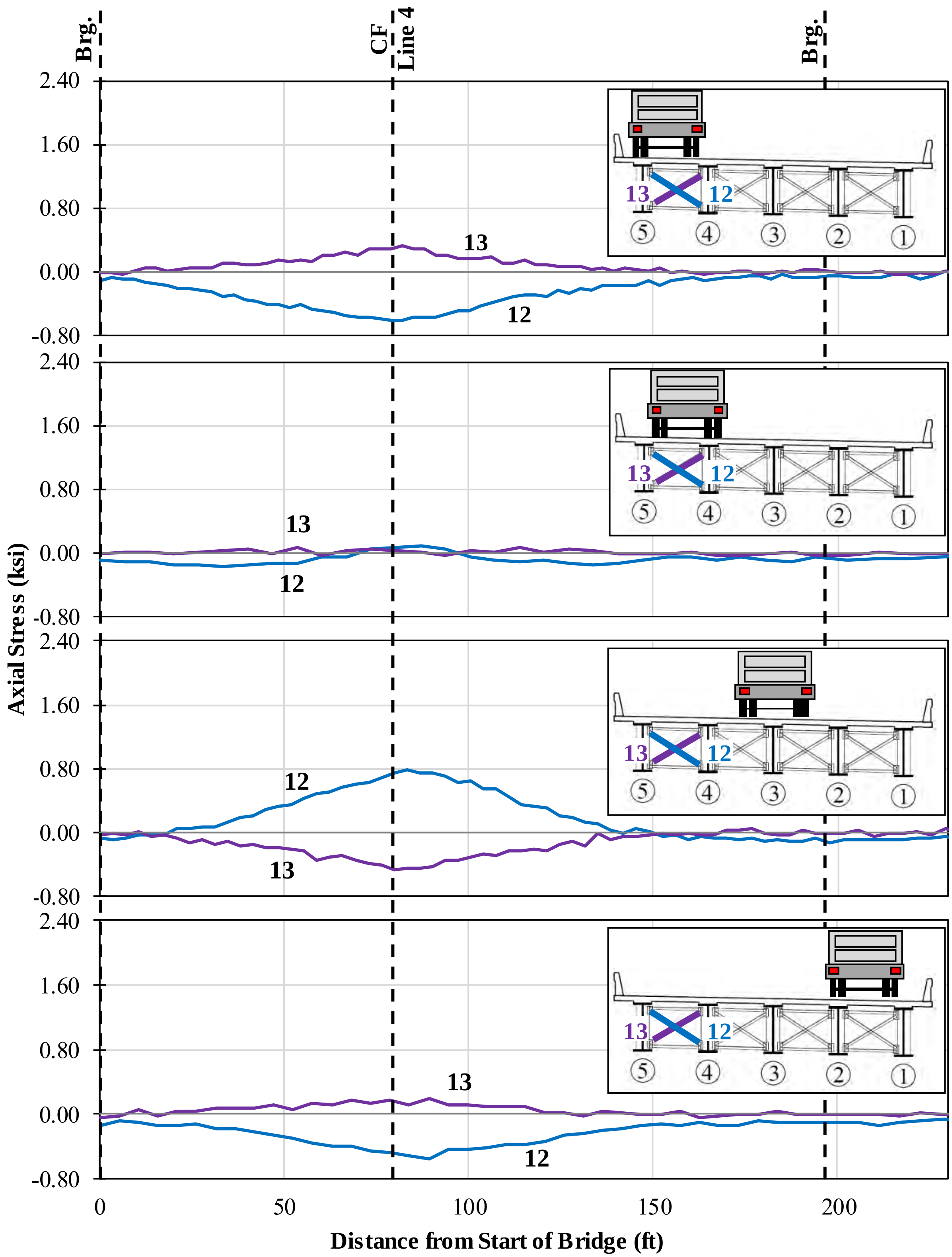

Figure E4-15: Influence line plots for cross-frame axial stresses at cross-frame line 4 (Load Case 0A through 0D)

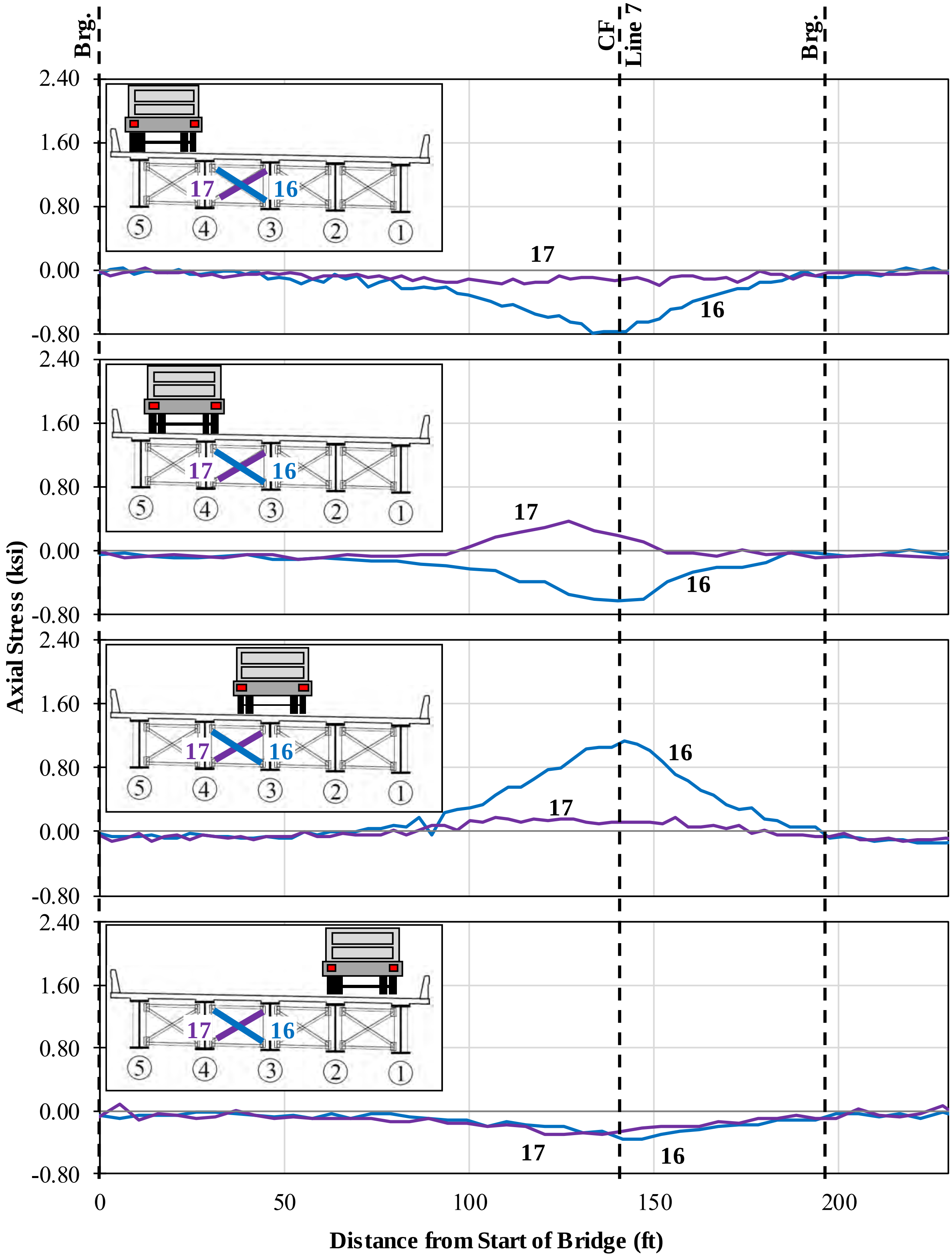

Figure E4-16: Influence line plots for cross-frame axial stresses at cross-frame line 7 (Load Case 0A through 0D)

E4.1.3.3 Load Case 1-7 Strain Data for Bridge 1

Load Cases 1 through 7 provided the RT the opportunity to measure strains in the instrumented members under pseudo-static loading conditions. These load cases allowed the measurement of stresses and deflections induced for specific loading conditions. Similar to Load Case 0, the data for these load cases were collected continuously. Except for Load Case 2, each test truck in Load Cases 1 and 3 through 7 was placed one at a time to the designated position. As a result, the DAQ system captured the stress state after each new truck entered the bridge. The result is a stepped time-history response of increasing stress. An example of this is presented in Figure E4-17, where measured bottom flange stresses in girder 1 are graphed over time during the entirety of Load Case 1 (four trucks in a line one-after-another near the right barrier, centered about cross-frame line 4). Refer to Table E3-3 for a schematic of Load Case 1.

There are 6 distinct steps that can be seen in this time-history plot:

A. No trucks positioned on bridge; no live load induced stress

B. Truck 1 (lead truck) positioned on the bridge; live load induced stress increases

C. Truck 2 positioned on the bridge behind Truck 1; live load induced stress increases

D. Truck 3 positioned on the bridge behind Trucks 1 and 2; live load induced stress increases

E. Truck 4 positioned on the bridge behind Trucks 1, 2, and 3; live load induced stress increases

F. All four trucks are removed from bridge simultaneously; live load induced stress returns to zero

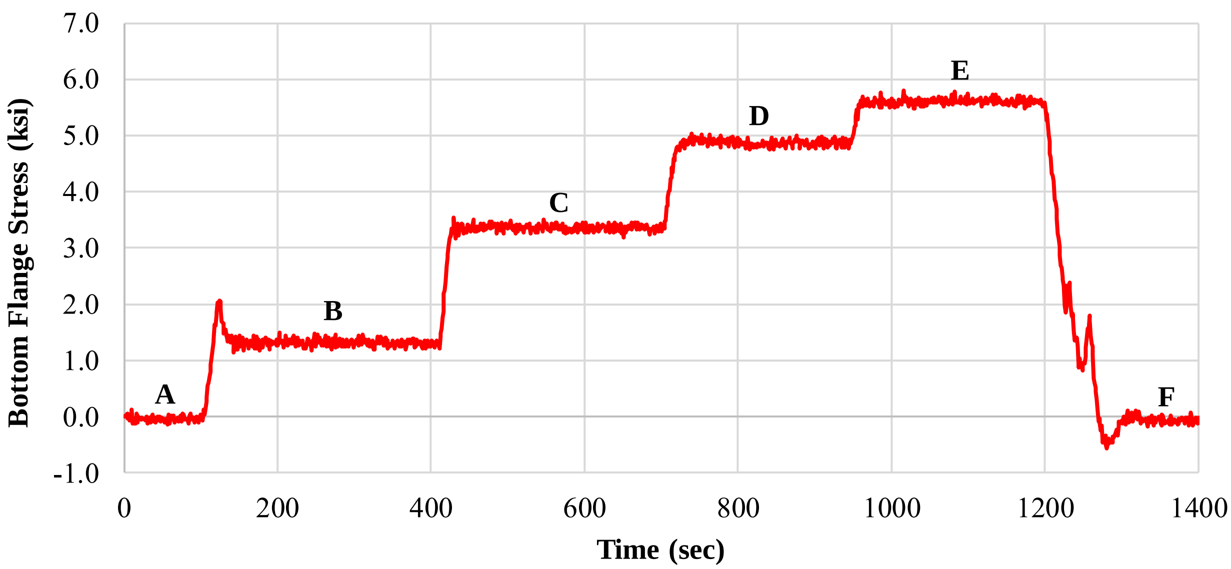

Figure E4-17: Measured Load Case 1 bottom flange stress in girder 1 at cross-frame line 4

Due to the relatively static nature of this test, the stress response for each instrumented element essentially follows a step function. Small spikes were periodically recorded because the load was not purely static. For example, a small spike was recorded at the beginning of plateau B in Figure E4-17. This spike occurs as the truck passes over the maximum point on the influence line for the girder bottom flange, which happens to not coincide with the final static position of Truck 1 in Load Case 1. Had the final position of Truck 1 coincided with the maximum point on the influence line plot, the spike would not have been measured. There are also a few spikes as the trucks are moved off the bridge, which can be explained the same way as the spike in plateau B. Given that these load cases were performed at very low speeds, the RT does not believe these spikes are related to a dynamic impact effect of the truck entering the bridge.

These small spikes are not important to understanding the behavior of the bridge under static loading and are also not important to validating the FEA models. Instead, the magnitudes of the plateaus are the major focus. These values indicate the stress imposed on the instrumented elements under static loading conditions. In order to cancel out potential effects of electromechanical noise, an average stress value was taken from each of these load-step plateaus. Time-history plots were effectively converted into a series of average, static stresses which can be displayed in tabular form. An example of this data is shown in Table E4-2.

Table E4-2: Summary of static stress states from Figure E4-17

Loading Condition	No. of Trucks	Longitudinal Stress (ksi)
A	0	0.00
B	1	1.32
C	2	3.36
D	3	4.87
E	4	5.59
F	0	0.00

A total of 140 plots similar to Figure E4-17 were distilled, and the average stresses at the plateaus were recorded for all instrumented elements, including girder flanges and cross-frame members. Table E4-3, Table E4-4, and Table E4-5 summarize these results for bottom flange longitudinal stresses, bottom flange lateral stresses, and axial stresses in cross-frame members, respectively. These static stress tables, along with deflection measurements discussed in the subsequent section, serve as the metric by which the FEA model is validated. In Table E4-3 and Table E4-4, the columns are identified by G#, where # indicates the girder number, and CFL##, where ## indicates the cross-frame line (either 4 or 7). Recall that the cross-frame numbers in Table E4-5 were previously established in Figure E4-4 and Figure E4-5. An example of cross-frame stresses for Load Case 3 is illustrated in Figure E4-18. This figure visually presents the Load Case 3 row of Table E4-5.

Again, note that only data for the final condition for Load Case 2 with all trucks in position were recorded; hence, data for intermediate stress states are left blank for this load case.

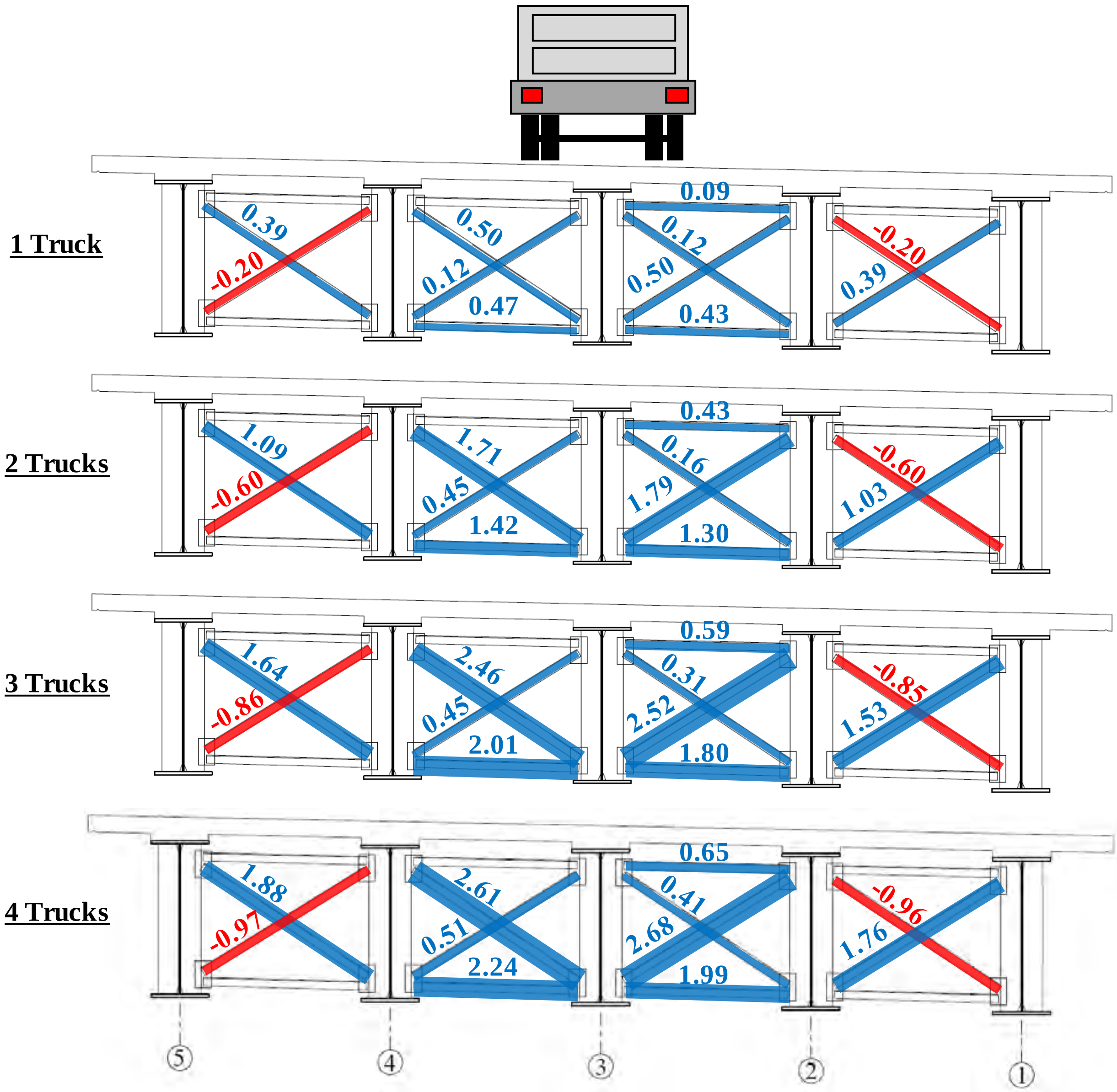

Figure E4-18: Cross-frame stress states at line 4 during Load Case 3 (Units: ksi)

Table E4-3: Bottom flange longitudinal stresses in instrumented girders for Load Cases 1-7

Load Case	No. of Trucks	Average Bottom Flange Longitudinal Stress (ksi)						
		G1-CFL4	G2-CFL4	G3-CFL4	G4-CFL4	G5-CFL4	G3-CFL7	G4-CFL7
1	1	1.32	0.96	0.66	0.18	-0.13	0.35	0.17
	2	3.36	2.51	1.48	0.48	-0.30	0.56	0.31
	3	4.87	3.62	2.15	0.75	-0.45	0.68	0.40
	4	5.59	4.14	2.50	0.89	-0.51	0.74	0.45
2	1	--	--	--	--	--	--	--
	2	--	--	--	--	--	--	--
	3	--	--	--	--	--	--	--
	4	5.32	3.96	2.62	1.14	-0.19	0.75	0.53
3	1	0.56	0.55	0.59	0.56	0.66	0.32	0.43
	2	1.26	1.49	1.79	1.49	1.43	0.47	0.69
	3	1.87	2.16	2.48	2.21	2.12	0.55	0.85
	4	2.27	2.49	2.77	2.53	2.48	0.59	0.91
4	1	-0.09	0.24	0.65	0.87	1.37	0.35	0.70
	2	-0.24	0.54	1.45	2.41	3.44	0.57	1.15
	3	-0.41	0.81	2.14	3.48	4.98	0.68	1.42
	4	-0.46	0.98	2.49	4.00	5.67	0.75	1.54
5	1	1.72	1.33	0.89	0.32	-0.03	0.24	0.17
	2	3.16	2.44	1.62	0.66	-0.05	0.36	0.27
	3	3.07	2.79	2.47	2.12	1.90	0.59	0.73
	4	2.99	3.13	3.22	3.32	3.57	0.72	1.01
6	1	-0.05	0.04	0.12	0.16	0.28	0.18	0.35
	2	-0.08	0.23	0.47	0.67	1.01	0.55	1.38
	3	-0.16	0.53	1.11	1.59	2.36	0.89	2.12
	4	-0.24	0.91	2.00	3.21	4.42	1.11	2.58
7	1	0.16	0.12	0.17	0.06	0.11	0.17	0.22
	2	0.62	0.50	0.45	0.35	0.42	0.77	0.72
	3	1.43	1.16	1.04	0.92	0.91	1.11	1.16
	4	2.42	2.40	2.28	1.77	1.54	1.28	1.42

Table E4-4: Bottom flange lateral bending stresses in instrumented girders for Load Cases 1-7.

Load Case	No. of Trucks	Bottom Flange Lateral Stress (ksi)						
		G1-CFL4	G2-CFL4	G3-CFL4	G4-CFL4	G5-CFL4	G3-CFL7	G4-CFL7
1	1	0.18	0.12	0.12	0.08	0.12	0.09	0.11
	2	0.48	0.31	0.38	0.30	0.33	0.13	0.17
	3	0.68	0.52	0.54	0.49	0.48	0.16	0.19
	4	0.73	0.65	0.60	0.60	0.59	0.18	0.20
2	1	-	-	-	-	-	-	-
	2	-	-	-	-	-	-	-
	3	-	-	-	-	-	-	-
	4	0.83	0.62	0.62	0.79	0.50	0.15	0.15
3	1	0.05	0.03	-0.06	0.10	-0.03	0.01	-0.07
	2	-0.01	-0.04	-0.06	0.22	0.02	0.04	-0.08
	3	0.06	-0.04	-0.05	0.25	-0.04	0.05	-0.08
	4	0.07	0.03	-0.03	0.26	-0.07	0.06	-0.08
4	1	-0.10	-0.15	-0.04	-0.02	-0.19	-0.01	-0.10
	2	-0.30	-0.36	-0.23	-0.17	-0.52	0.00	-0.14
	3	-0.45	-0.51	-0.33	-0.24	-0.76	0.01	-0.15
	4	-0.53	-0.57	-0.36	-0.23	-0.89	0.03	-0.15
5	1	0.23	0.15	0.10	0.22	0.18	0.02	0.06
	2	0.42	0.31	0.27	0.38	0.31	0.04	0.08
	3	0.27	0.12	0.12	0.26	0.04	0.06	0.04
	4	0.12	-0.02	-0.02	0.18	-0.22	0.08	0.03
6	1	0.08	0.06	-0.01	0.02	-0.06	-0.02	-0.08
	2	0.02	0.00	-0.03	-0.01	-0.14	-0.06	-0.26
	3	-0.09	-0.13	-0.16	-0.06	-0.31	-0.04	-0.35
	4	-0.30	-0.33	-0.31	-0.15	-0.62	-0.02	-0.39
7	1	0.09	0.00	0.06	0.06	0.03	0.00	0.01
	2	0.17	0.02	0.07	0.12	0.01	0.11	0.08
	3	0.24	0.08	0.08	0.16	0.01	0.17	0.09
	4	0.23	0.04	0.13	0.34	0.09	0.19	0.10

* Positive values indicate that the left side of the bottom flange sees more tension whereas negative values indicate that the right side of the flange sees more tension.

Table E4-5: Axial stresses in instrumented cross-frame members for Load Cases 1-7

Load Case	No. of Trucks	Average Axial Stress (ksi)												
		CF-2	CF-3	CF-4	CF-5	CF-6	CF-7	CF-8	CF-9	CF-10	CF-12	CF-13	CF-15	CF-17
1	1	0.06	-0.13	-0.13	0.00	0.00	-0.26	-0.13	-0.21	-0.21	-0.29	0.07	-0.28	-0.21
	2	0.09	0.04	-0.22	0.35	-0.19	-0.91	-0.51	-0.51	-0.45	-0.69	0.22	-0.35	-0.22
	3	0.17	-0.07	-0.37	0.44	-0.22	-1.26	-0.82	-0.72	-0.66	-1.01	0.34	-0.37	-0.23
	4	0.24	-0.21	-0.48	0.41	-0.24	-1.36	-0.94	-0.78	-0.74	-1.16	0.39	-0.37	0.00
2	1	-	-	-	-	-	-	-	-	-	-	-	-	-
	2	-	-	-	-	-	-	-	-	-	-	-	-	-
	3	-	-	-	-	-	-	-	-	-	-	-	-	-
	4	-0.26	0.88	0.32	1.12	-0.02	-0.83	-0.36	-0.06	-0.64	-0.69	0.21	-0.05	-0.15
3	1	-0.20	0.39	0.43	0.12	0.09	0.50	0.47	0.50	0.12	0.39	-0.20	0.64	0.15
	2	-0.60	1.03	1.30	0.16	0.43	1.79	1.42	1.71	0.23	1.09	-0.60	0.83	0.20
	3	-0.85	1.53	1.80	0.31	0.59	2.52	2.01	2.46	0.45	1.64	-0.86	0.79	0.20
	4	-0.96	1.76	1.99	0.41	0.65	2.68	2.24	2.61	0.51	1.88	-0.97	0.79	0.20
4	1	0.05	-0.17	-0.46	-0.17	-0.02	-0.07	-0.07	-0.14	0.04	-0.04	-0.01	-0.25	0.15
	2	0.23	-0.52	-0.68	-0.38	-0.09	-0.38	-0.20	-0.75	0.34	0.10	0.04	-0.34	0.10
	3	0.34	-0.78	-0.75	-0.57	-0.12	-0.54	-0.33	-1.02	0.43	0.05	0.05	-0.39	0.05
	4	0.37	-0.86	-0.01	-0.63	-0.12	-0.59	-0.40	-1.09	0.39	-0.04	0.08	-0.41	0.03
5	1	-0.17	0.52	0.17	0.56	0.02	-0.37	-0.09	-0.05	-0.28	-0.31	0.06	-0.01	-0.04
	2	-0.30	0.85	0.33	0.96	0.04	-0.53	-0.24	0.06	-0.46	-0.49	0.12	-0.02	-0.03
	3	-0.15	0.52	0.08	0.68	0.01	-0.63	-0.09	-0.47	0.02	-0.06	0.02	-0.09	-0.03
	4	-0.04	0.24	-0.14	0.45	-0.03	-0.69	-0.20	-0.73	0.24	0.05	-0.03	-0.12	-0.06
6	1	-0.01	-0.05	-0.02	-0.05	-0.03	-0.03	-0.04	-0.08	-0.01	-0.06	0.01	-0.12	0.11
	2	0.00	-0.08	-0.05	-0.08	-0.04	-0.05	-0.07	-0.09	-0.02	-0.10	0.02	-0.65	0.64
	3	0.07	-0.21	-0.17	-0.20	-0.06	-0.08	-0.10	-0.20	0.07	-0.09	0.02	-0.90	0.83
	4	0.21	-0.51	-0.42	-0.45	-0.09	-0.18	-0.02	-0.74	0.62	0.40	-0.10	-0.94	0.79
7	1	-0.01	-0.03	0.01	-0.04	-0.05	0.00	0.02	-0.04	-0.01	-0.02	-0.01	0.37	0.00
	2	-0.08	0.07	0.10	0.01	-0.03	0.09	0.12	0.06	0.01	0.06	-0.07	1.47	-0.24
	3	-0.29	0.51	0.53	0.23	0.10	0.51	0.51	0.53	0.07	0.36	-0.23	2.16	-0.20
	4	-0.87	1.49	1.53	0.73	0.51	1.60	1.31	1.78	-0.10	0.83	-0.49	2.36	-0.14

Many of the same trends observed in the Load Case 0 data were also observed in the static Load Cases 1 through 7. Also note that the discussion of these moving load case results follows the same general format of the static load case results. Within each bolded category are specific observations that were made from the data for each bridge type.

- **Evaluate load distribution (transverse) and load influence (longitudinal) characteristics on girders.**
  - The transverse distribution of girder stresses results in a nearly-linear distribution. Figure E4-19 better demonstrates this phenomenon, which depicts the longitudinal bending stresses in all five girders at cross-frame line 4 during Load Cases 2, 3, 4, and 5. This figure shows how live loads are distributed transversely through the deck and cross-frames into the girders. Load Cases 2, 3, and 4 represent a loading condition where all four trucks are located front-to-back in a line in the right lane, middle lane, and left lane, respectively. Load Case 5 represents a condition where there is a row of two trucks in the left and right lanes. Refer to Table E3-3 for a visual depiction of these load cases.

    It can be seen from Figure E4-19 that Load Cases 2 and 4 (trucks in the left lane and right lane, respectively) produce results that nearly mirror one another, which shows the inverse response of the girder system as the truck is moved transversely. A linear girder stress distribution is observed for these two load cases. In fact, the girder on the opposite side of the load application experiences slight negative bending, which can be attributed to transverse stiffness of the deck and cross-frames.

    For Load Case 3, the girders have approximately the same bottom flange bending stresses when the four trucks are located in the middle lane of the bridge. For Load Case 5, the trucks are again placed symmetrically along the width of the bridge; however, the trucks are positioned in such a way where they will have a higher influence on the girder bending stresses at cross-frame line 4. As expected, the bending stresses in the girders for Load Case 5 are approximately equal but have a consistently higher magnitude than Load Case 3.
  - Due to only a single placement of the group of trucks, load influence effects are not applicable to Load Cases 1 through 7. Refer to Section E4.1.3.2 for more information regarding longitudinal load influence.
- **Compare and evaluate measured girder stress (longitudinal and lateral) and deflections with established design metrics.**
  - Similar to the Load Case 0 results, maximum girder stresses at cross-frame line 4 were generally higher than maximum girder stresses at cross-frame line 7, even during Load Cases 6 and 7 in which the trucks were centered about cross-frame line 7.
  - When the centroid of the load is positioned near the center of the deck (Load Case 3 and 5), lateral stresses measured were consistently small. However, when the load was positioned in either the left or right lanes (Load Case 4 and 2), a noticeable trend was observed. When the load is in the left lane, the bottom flanges across the width of the instrumented cross-frame line consistently measured negative lateral stresses (right flange edge experiences tension); the opposite is true for a load in the right lane. This trend demonstrates that an eccentric load relative to the center of rotation results in a torsional response, even on a straight bridge. This torsional response is reflected in the lateral warping stresses developed in the bottom flanges.
- **Evaluate load distribution (transverse) and load influence (longitudinal) characteristics on cross-frames.**

  - Similar to Load Case 0 results, cross-frame stresses are highly sensitive to transverse position of the truck, as is demonstrated by the stress reversal in members from one load case to another.
  - Load influence effects were not measured in Load Cases 1 through 7 due to the group of trucks located at a single position. Refer to Section E4.1.3.2 for more information regarding longitudinal load influence.
- **Compare and evaluate measured cross-frame stress with established design metrics.**
  - In all but two cross-frame members for Load Case 3, maximum measured axial stresses are less than the CAFL of 2.6 ksi. Cross-frame diagonals 7 and 9 exceeded 2.6 ksi once all four trucks were positioned during Load Case 3 (trucks in center of middle lane). Although the wheel bases and truck spacing varies, the total combined load during these test cases (over 200 kips) far exceeds the unfactored AASHTO fatigue truck.
  - Similar to the Load Case 0 results, the maximum girder stresses measured are generally higher than the maximum axial stresses measured in cross-frame members for equivalent load cases.
- **Understanding complex load paths based on unique characteristics of the measured data.**
  - The Load Case 1 through 7 data demonstrates no unusual behavior from the instrumented girders or cross-frames on this straight bridge, which is expected for a simple geometry.

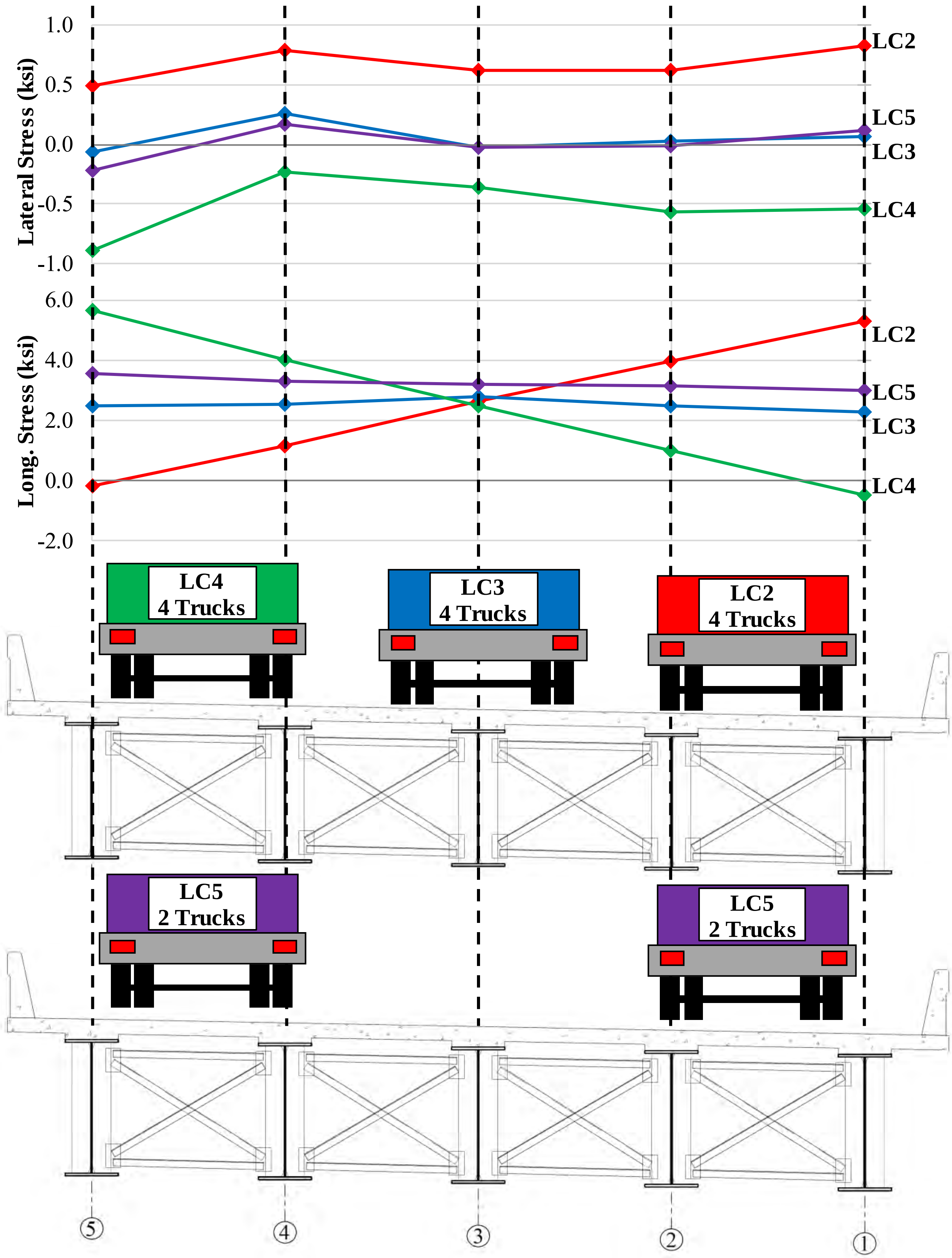

Figure E4-19: Distribution of girder bending stresses along cross-frame line 4 for Load Cases 2, 3, 4, and 5

E4.1.3.4 Deflection Data for Bridge 1

Laser distance meter readings at all five girders at cross-frame line 4 were taken after every truck was introduced to the bridge for all seven static load cases. Vertical deflections were computed by subtracting the baseline distance reading on the unloaded bridge from the distance reading on the loaded bridge. Table E4-6 summarizes the deflection measurements for Load Cases 1 through 7. Since the four trucks were introduced simultaneously for Load Case 2, only the deflections associated with four loaded trucks were measured for this case. The deflection reading shown is the average of three readings. Downward deflections are recorded as negative values.

Table E4-6: Girder deflection measurements at cross-frame line 4 for Load Cases 1-7

Load Case	No. of Trucks	Vertical Deflections (in)				
		Girder 1	Girder 2	Girder 3	Girder 4	Girder 5
1	1	-0.41	-0.30	-0.17	-0.16	0.03
	2	-0.92	-0.67	-0.39	-0.26	0.07
	3	-1.30	-0.91	-0.56	-0.30	0.10
	4	-1.48	-1.12	-0.71	-0.38	0.09
2	1	-	-	-	-	-
	2	-	-	-	-	-
	3	-	-	-	-	-
	4	-1.44	-1.05	-0.70	-0.43	0.04
3	1	-0.24	-0.18	-0.20	-0.28	-0.21
	2	-0.42	-0.38	-0.39	-0.59	-0.39
	3	-0.56	-0.56	-0.63	-0.70	-0.59
	4	-0.68	-0.67	-0.70	-0.79	-0.70
4	1	-0.01	-0.12	-0.18	-0.41	-0.38
	2	0.05	-0.13	-0.38	-0.76	-0.85
	3	0.09	-0.24	-0.52	-1.01	-1.27
	4	0.07	-0.29	-0.64	-1.17	-1.44
5	1	-0.41	-0.30	-0.18	-0.34	0.01
	2	-0.83	-0.54	-0.38	-0.28	0.00
	3	-0.81	-0.68	-0.59	-0.59	-0.45
	4	-0.77	-0.77	-0.77	-0.93	-0.88
6	1	-0.01	-0.04	-0.04	-0.20	-0.12
	2	-0.01	-0.08	-0.16	-0.54	-0.39
	3	0.00	-0.21	-0.34	-0.66	-0.80
	4	-0.01	-0.30	-0.58	-1.05	-1.29
7	1	-0.10	-0.07	-0.05	-0.30	-0.07
	2	-0.34	-0.22	-0.14	-0.46	-0.16
	3	-0.52	-0.45	-0.33	-0.47	-0.31
	4	-0.81	-0.71	-0.62	-0.66	-0.46

Figure E4-20 graphically shows deflection measurements for Load Cases 1, 3, and 4 as trucks are individually placed on the bridge. Four different measurements are plotted for each location, as each measurement corresponds to a new dump truck placed on the bridge. Load Cases 1, 3, and 4 represent a loading condition where all four trucks are located in a line, front-to-back along the right barrier, in the middle lane, and in the left lane, respectively. Similarly, Figure E4-21 depicts deflection measurements for Load Cases 5 through 7 as trucks are individually place on the bridge. Load Case 5 represents a condition where two lines of two trucks are located on the left and right lanes, centered above cross-frame line 4. Load Cases 6 and 7 represent a loading condition where all four trucks are located in a line, 2 feet from the left barrier and to right of girder 3, respectively.

Again, the same general format of the observations is followed. The bolded text represents the general categories investigated by the RT, and the commentary within that category are specific observations made for this data set.

- **Evaluate load distribution (transverse) and load influence (longitudinal) characteristics on girders.**
    - There are three major observations with regards to transverse distribution of the five-girder system. First, the girders closer to the applied load deflect the most, as one would expect. Second, the change in deflection across the deck is nearly linear, which is a similar response to the measured girder stresses presented in the preceding section. Third, deflections are nearly uniform and symmetric for Load Case 3, where the trucks were positioned in the center of the middle lane. Again, this response is similar to the stress measurements. Differential deflections between adjacent girders are not significant, and thus cross-frame forces are relatively small.
    - Load influence effects are not applicable to deflection measurements. Refer to Section E4.1.3.2 for more information regarding longitudinal load influence.
- **Compare and evaluate measured girder stress (longitudinal and lateral) and deflections with established design metrics.**
    - The maximum deflections measured during this study correspond to a deflection-to-span ratio of L/1580, which would indicate that the bridge is relatively stiff. Note that this ratio is only intended for relative comparison between bridges, given that the AASHTO LRFD deflection criteria (Article 2.5.2.6.2) are based on heavier loading conditions than the experimental tests.
- **Understanding complex load paths based on unique characteristics of the measured data.**
    - The Load Case 1 through 7 deflection data demonstrates no unusual behavior from the instrumented girders or cross-frames on this straight bridge, which is expected for a simple geometry.

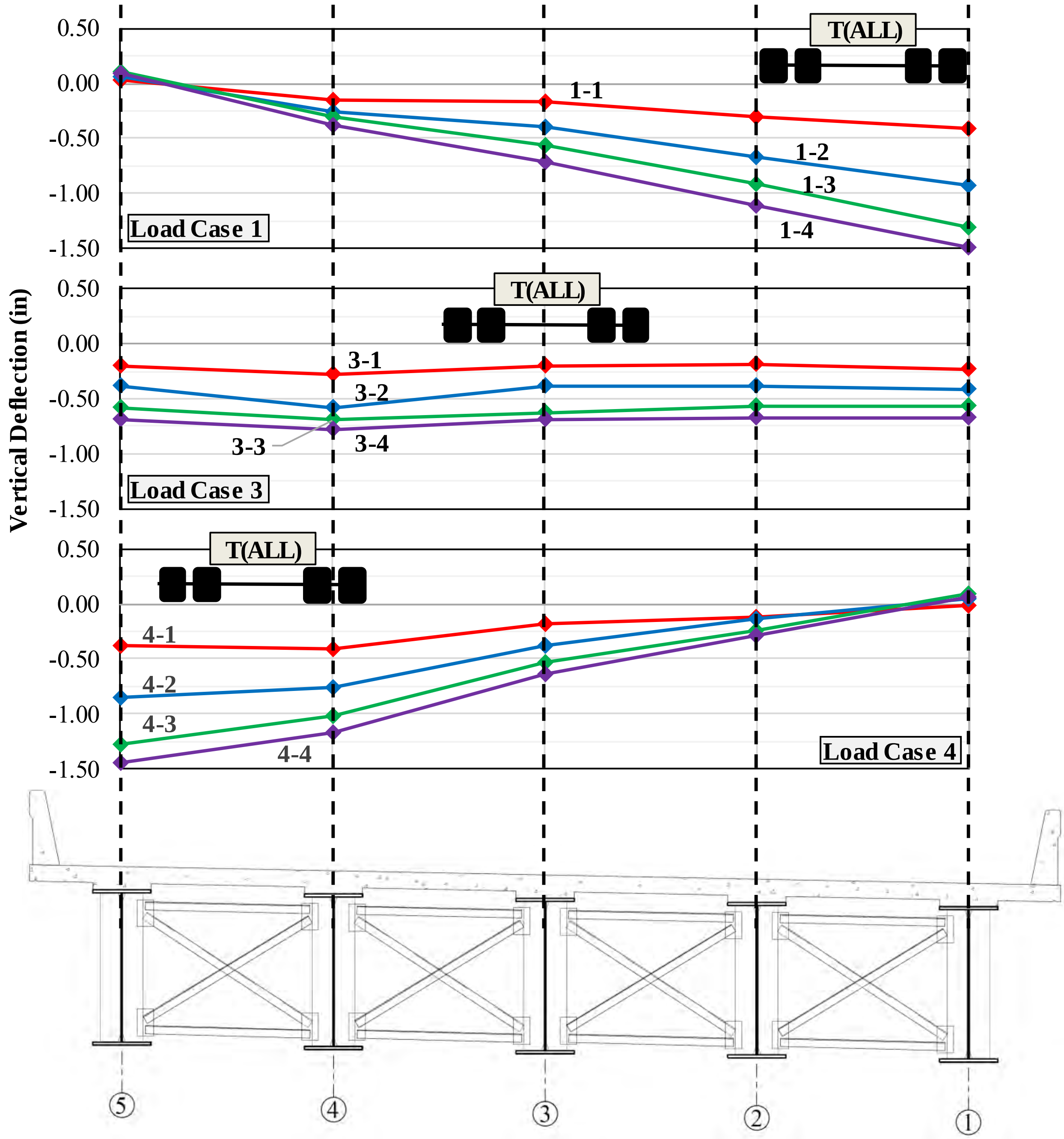

Figure E4-20: Girder deflection progression at cross-frame line 4 for Load Cases 1, 3, and 4

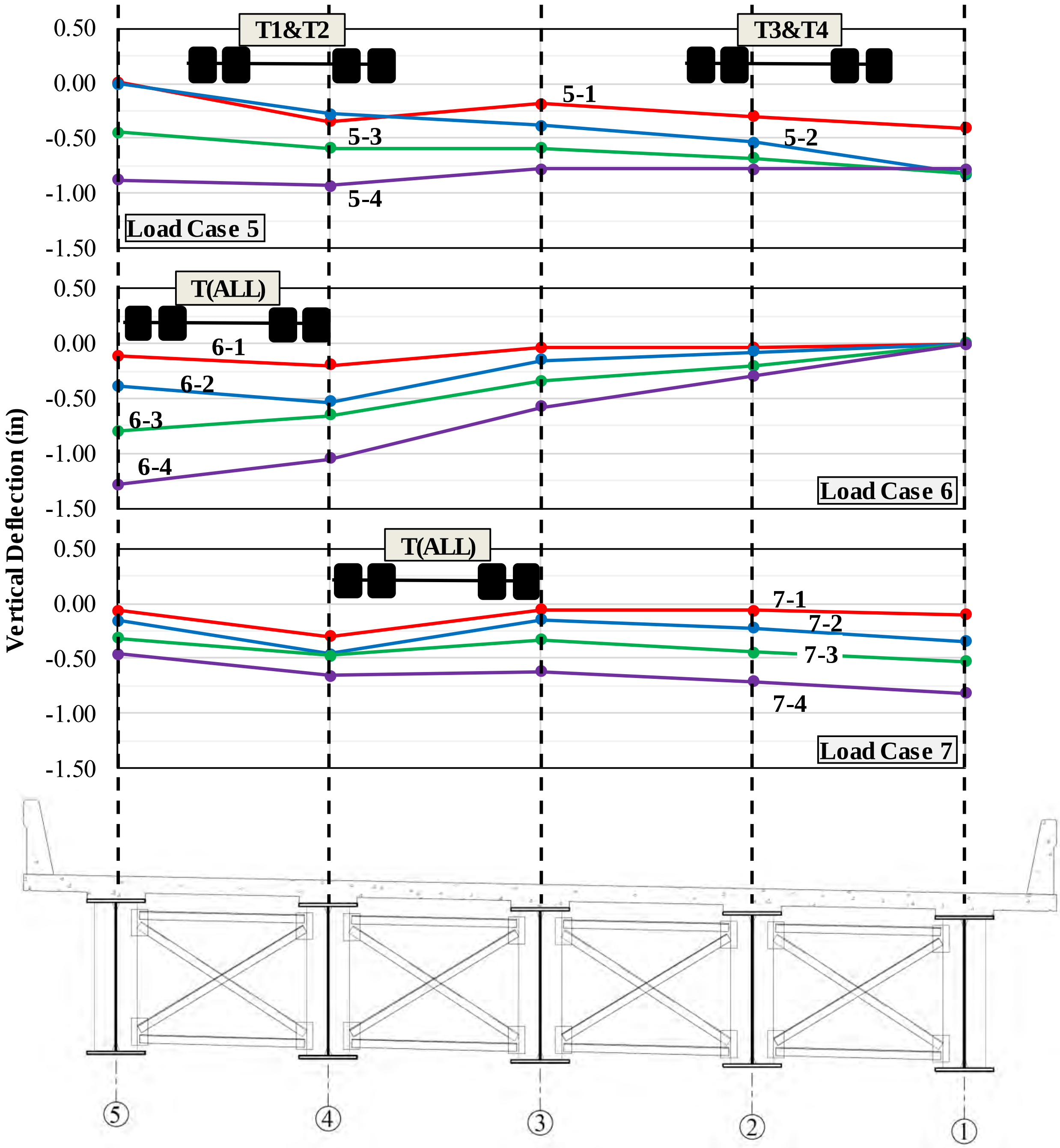

Figure E4-21: Girder deflection progression at cross-frame line 4 for Load Cases 5 through 7

Note that the deflection measurements, along with the maximum stress tables presented in the previous section, serve as the metric by which the FEA model was validated. The FEA model was adjusted until reasonable agreement was achieved between the predicted stresses and deflections and measured data. The model validation process is covered in Chapter E5.

E4.1.4 Bridge 2 Results

The following subsections provide an outline of the controlled live load test data for Bridge 2. Subsections include truck properties, influence-line strain data for the moving load case (Case 0), strain data for the static load cases (Cases 1 through 7), and deflection data for the static load cases (Cases 1 through 7).

E4.1.4.1 Truck Properties for Bridge 2

Similar to the Bridge 1 load test, TxDOT crews provided four dump trucks loaded with sand for the controlled live load test of Bridge 2. Note that three of the four trucks used in the Bridge 1 load test were again used for the Bridge 2 load test; one new truck was introduced. TxDOT crews weighed all four trucks, and the RT measured the wheel base of only the new truck prior to the load test. The results of the gross weights are summarized in Table E4-7, and the wheel base dimensions of the trucks are presented in Figure E4-22. It is important to note that despite using three of the same trucks, the gross vehicle weights used during the Bridge 2 load test (approximately 44 kips) were consistently less than what was used during the Bridge 1 test (approximately 50 kips). The reason for the difference was most likely the moisture condition of the sand used for each test.

Table E4-7: TxDOT truck axle weights for Bridge 2 load test

Truck #	Steer Axle Weight (lb)	Combined Drive Axle Weight (lb)	Gross Vehicle Weight (lb)
1	10280	34400	44680
2	9950	33330	43280
3	10010	33530	43540
4	10440	34940	45380

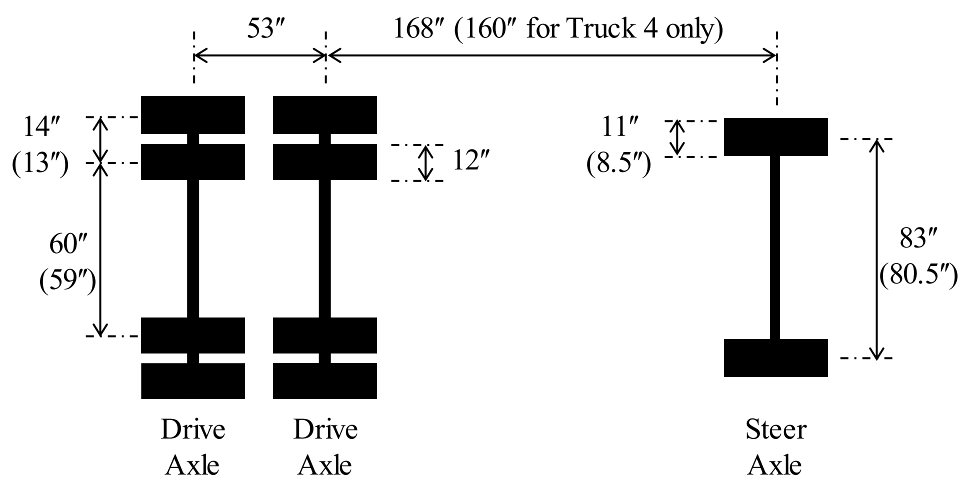

Figure E4-22: Typical TxDOT truck wheel base dimensions for Bridge 2 load test.

E4.1.4.2 Load Case 0 Strain Data for Bridge 2

As discussed previously, strain data were continuously recorded during the controlled live load test for all instrumented girder flanges and cross-frame members. Strain data for moving Load Case 0 were collected as a time-history. The time-history data was then converted into an influence line using the same procedure outlined in Section E4.1.3.2. Figure E3-19 through Figure E3-22, shown earlier, graphically presented all girder and cross-frame elements instrumented on Bridge 2 but did not identify each with a name or number. The cross-frame member numbers in subsequent plots are presented in Figure E4-23, Figure E4-24, and Figure E4-25, which are adapted versions of Figure E3-20 through Figure E3-22.

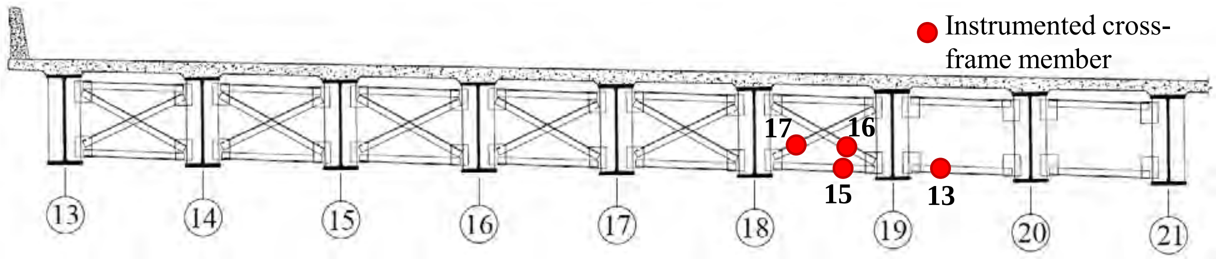

Figure E4-23: Instrumented cross-frame identification numbers at cross-frame line 8

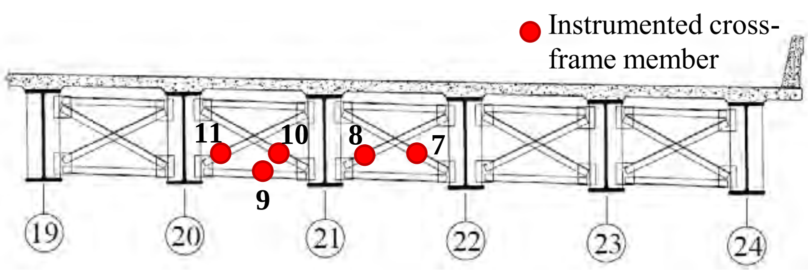

Figure E4-24: Instrumented cross-frame identification numbers at cross-frame line 5

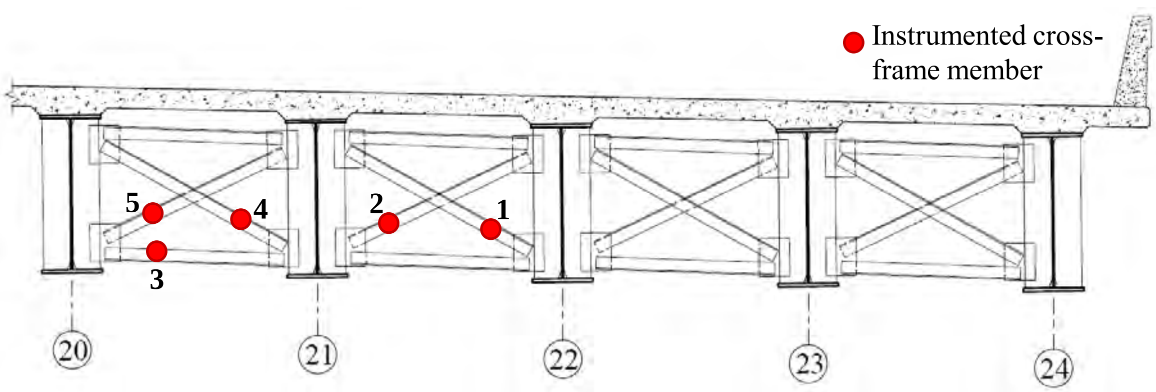

Figure E4-25: Instrumented cross-frame identification numbers at cross-frame line 2

Figure E4-26 through Figure E4-32 illustrate various measured influence line plots. Figure E4-26 and Figure E4-27 display the influence lines for longitudinal stresses in the instrumented girder bottom flanges at cross-frame line 5 and 8 respectively. Figure E4-28 and Figure E4-29 display influence lines for lateral stresses in the instrumented bottom flanges at cross-frame lines 5 and 8 respectively. The sign convention for positive lateral bending stress was previously established in Section E4.1.3.2. Figure E4-31 and Figure E4-32 show the influence line plots for axial stresses in instrumented cross-frame members at cross-frame lines 2, 5 and 8, respectively.

Only the first two spans are graphed on the x-axis in these figures, as the influence of loading the third span is negligible to the girder flanges and cross-frame members instrumented. Therefore, that portion of the influence line is not presented. For all graphs, the results for Load Cases 0A through 0C are presented sequentially. By plotting each load case on the same figure, trends can be more easily recognized. Lastly, note that only three truck positions are presented for Load Case 0 of Bridge 2, unlike the four trucks presented for Load Case 0 of Bridge 1. The results from the fourth truck passage were neglected from this study due to a data acquisition error that failed to record data for many of the strain gages during this case.

Similar to Section E4.1.3.2 that contained the Bridge 1 results, commentary on the Bridge 2 results follows the same format introduced in Section E4.1.2. The three major concepts, with respect to the moving Load Case 0, are addressed by the observations from Figure E4-26 through Figure E4-29 for girders and Figure E4-30 through Figure E4-32 for cross-frame members. The bolded text represents the general categories investigated by the RT, and the commentary within that category are specific observations made for this data set.

- **Evaluate load distribution (transverse) and load influence (longitudinal) characteristics on girders.**
    - Compared to the Bridge 1 data, a trend for the transverse distribution of live load to adjacent girders is less obvious for the skewed Bridge 2; this is mainly because a full line of girders across the width was not instrumented, as it was at the other two bridges. In general terms, the longitudinal stress in a particular girder is largely dependent on the truck position relative to midspan of that girder.
    - Because only a few girders were instrumented across the width of the bridge, a comprehensive comparison to the simplified AASHTO distribution factors, as was done for Bridge 1 results, cannot be made for Bridge 2.
    - Similar to the Bridge 1 results, the shape of the measured influence lines matches the simple 1-D qualitative influence line presented in Figure E4-7. The bottom flange stresses are generally most significant when the truck axles are centered over the longitudinal point of interest. However, it is observed in several influence line plots that the skewed geometry of Bridge 2 induces offsets between the location of the girder flange strain gages and the load position producing a peak response from the girders.

      Negative live load bending moments are more prominent in the instrumented girders along cross-frame line 8 than girders at line 5. Note that girders at line 8 are near a dead load inflection point; thus, stresses at this location are more prone to negative live load bending, especially for a skewed system.
- **Compare and evaluate measured girder stress (longitudinal and lateral) and deflections with established design metrics.**
    - Girder stresses at cross-frame line 5 are generally higher than girder stresses at cross-frame line 8. Per the preliminary FEA results, cross-frame line 5 is near the maximum positive moment region of the girders, and cross-frame line 8 is near the assumed dead load inflection point. The trend in the data therefore agrees with the predicted trends from the FEA results.

      Additionally, the girder stresses measured on Bridge 2 are relatively small when compared to those measured on Bridge 1. This can be attributed to two major factors: first, Bridge 2 is a very wide and redundant system that distributes live loads evenly due to its high transverse stiffness; second, the small span-to-depth ratio of the instrumented end span leads to high longitudinal stiffness and low girder stresses under applied live loads.

- o Lateral bending stress plots failed to demonstrate a clear trend. Much of the data appears random and noisy. The stress readings in each flange tip were relatively small such that the algebraic difference in the reading is typically within the electromechanical noise band. An extended discussion on lateral bending stresses in girder flanges is provided for the static load cases, where the applied loads were more substantial than the single truck load of Load Case 0.
- o Lastly, the influence-line plots for the Bridge 2 data appear to have a noisier signal than for Bridge 1 data, but that observation is largely a product of the overall scale of the plots. Bridge 2 stresses are generally smaller, so the noise is simply accentuated.

- **Evaluate load distribution (transverse) and load influence (longitudinal) characteristics on cross-frames.**
  - o Similar to the Bridge 1 results, the cross-frame stresse ranges were highly sensitive to the transverse position of the truck. The cross-frame members, especially diagonals, were prone to stress reversal as evidenced by the varied response to Load Cases 0A through 0C.
  - o The shape of the influence lines suggests that cross-frame stresses are generally only sensitive to loading near the specific cross-frame. The only instrumented cross-frame element that experienced significant influence from loading on the adjacent middle span was member 13 (the bottom strut of the lean-on brace on line 8). In general, only one stress cycle per truck passage was observed.
- **Compare and evaluate measured cross-frame stress with established design metrics.**
  - o The highest axial stress ranges on the instrumented cross-frame members at cross-frame line 2 occurred when the truck was located closer to the right barrier (Load Case 0C). In that position, the truck induced maximum differential deflections on girders 23 and 24 given the proximity to the support. Therefore, the cross-frame members were subjected to higher forces.
  - o Cross-frames at line 5 exhibited the largest stresses when the load was closer to midspan. This simply implies that differential deflections and rotations at midspan of the girders are maximized when the load is applied near midspan.
  - o At line 8, cross-frame stresse ranges were small due to the proximity of the intermediate support. Only member 13 (bottom strut of a lean-on brace) for Load Case 0A developed significant stresses.
  - o In all cases, the measured cross-frame stresses were significantly less than the constant-amplitude fatigue limit (CAFL) for the Category E′ welded angle-to-gusset detail of 2.6 ksi
  - o Axial stresses in the instrumented cross-frame members were generally comparable to the longitudinal stresses in the girder bottom flanges. This behavior is observed largely due to the skewed geometry and high longitudinal and transverse stiffness of the instrumented span. This was not observed at Bridge 1, where girder stresses were notably higher than cross-frame stresses.
- **Understanding complex load paths based on unique characteristics of the measured data.**
  - o The Load Case 0 data demonstrates that the skewed geometry affects the distribution of live loads to the girders and cross-frames. Particularly for the girder response, load position relative to the support and midspan of a particular girder can greatly impact the stress ranges experienced.

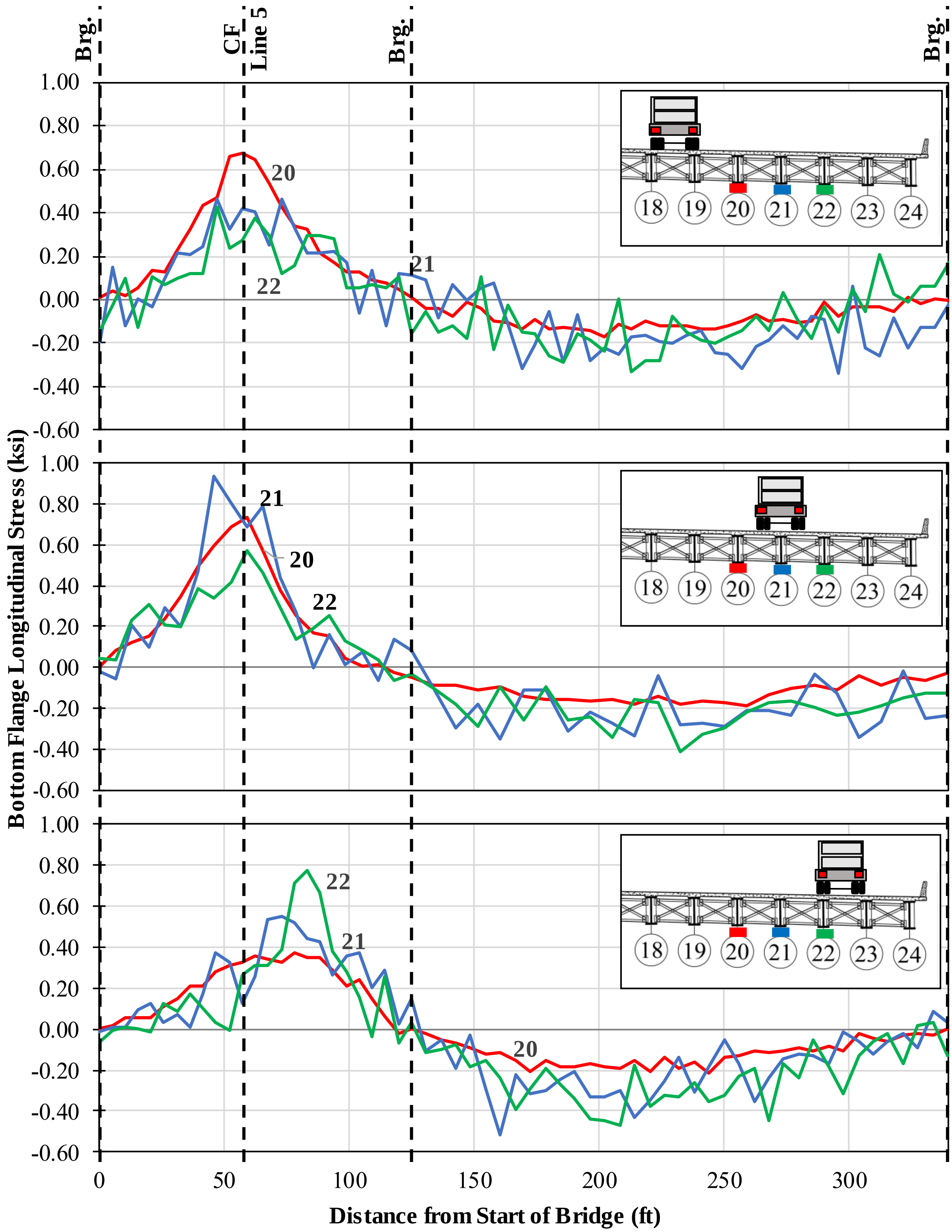

Figure E4-26: Influence line plots for bottom flange stresses at cross-frame line 5 (Load Case 0A though 0C)

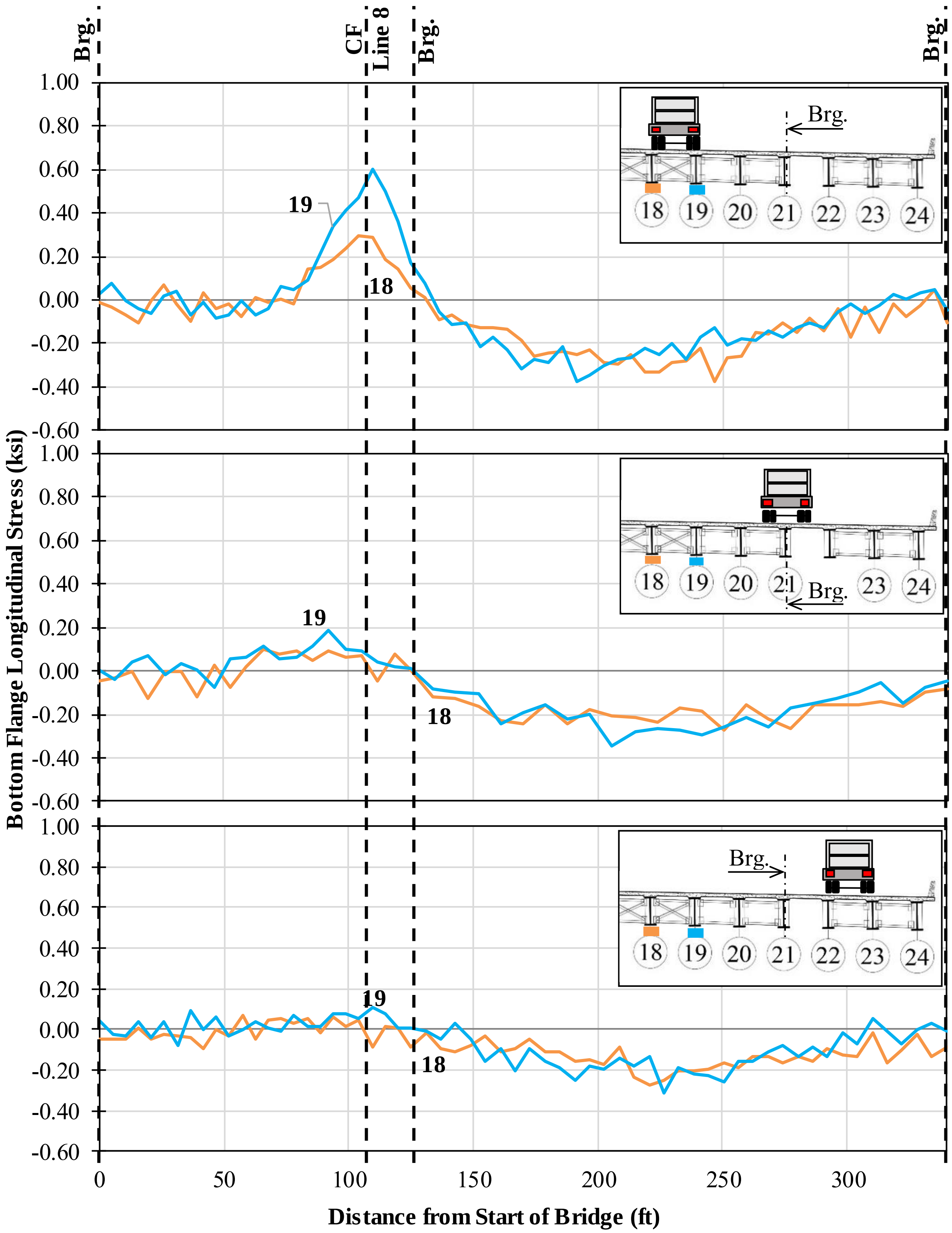

Figure E4-27: Influence line plots for bottom flange stresses at cross-frame line 8 (Load Case 0A through 0C)

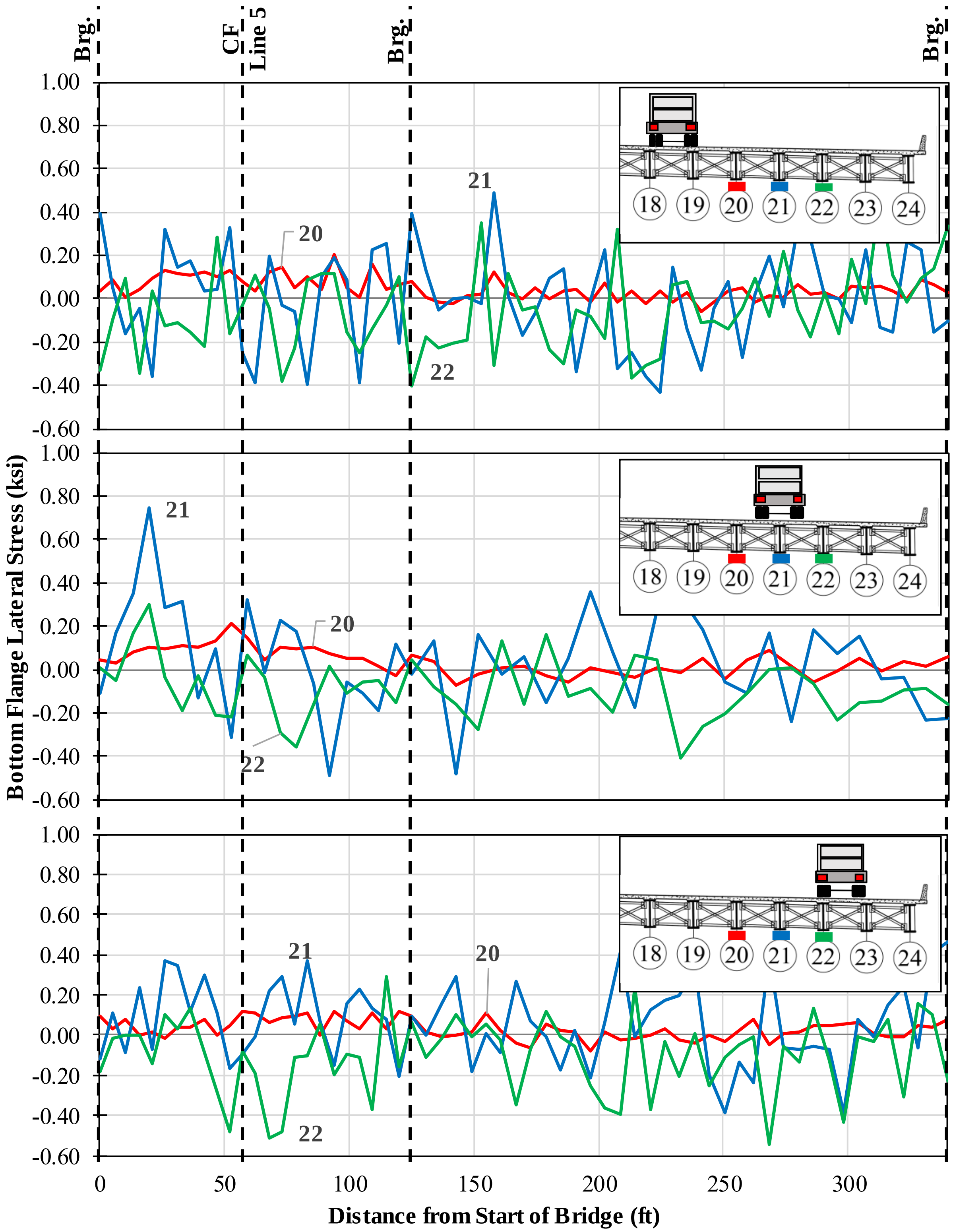

Figure E4-28: Influence line plots for bottom flange lateral stresses at cross-frame line 5 (Load Case 0A through 0C)

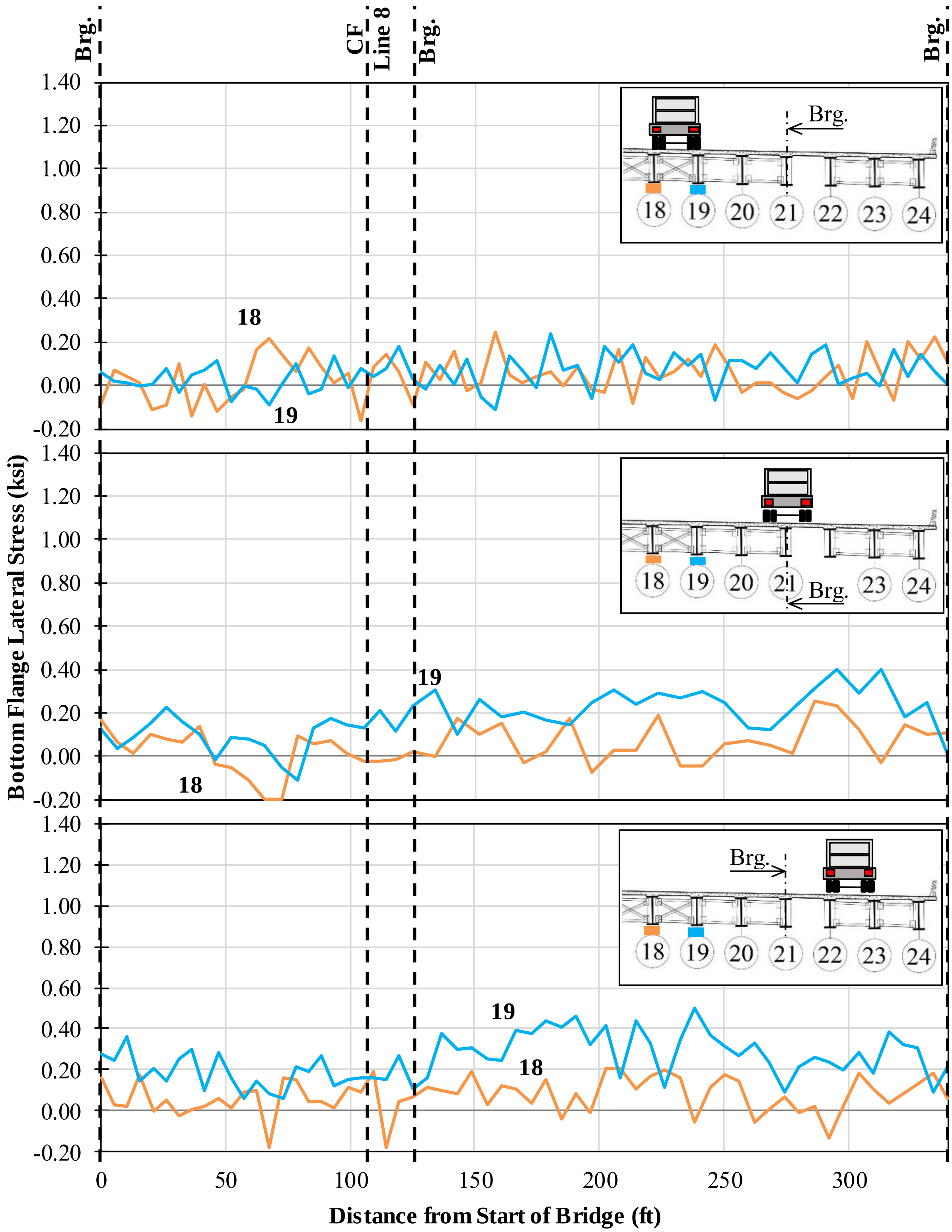

Figure E4-29: Influence line plots for bottom flange lateral stresses at cross-frame line 8 (Load Case 0A through 0C)

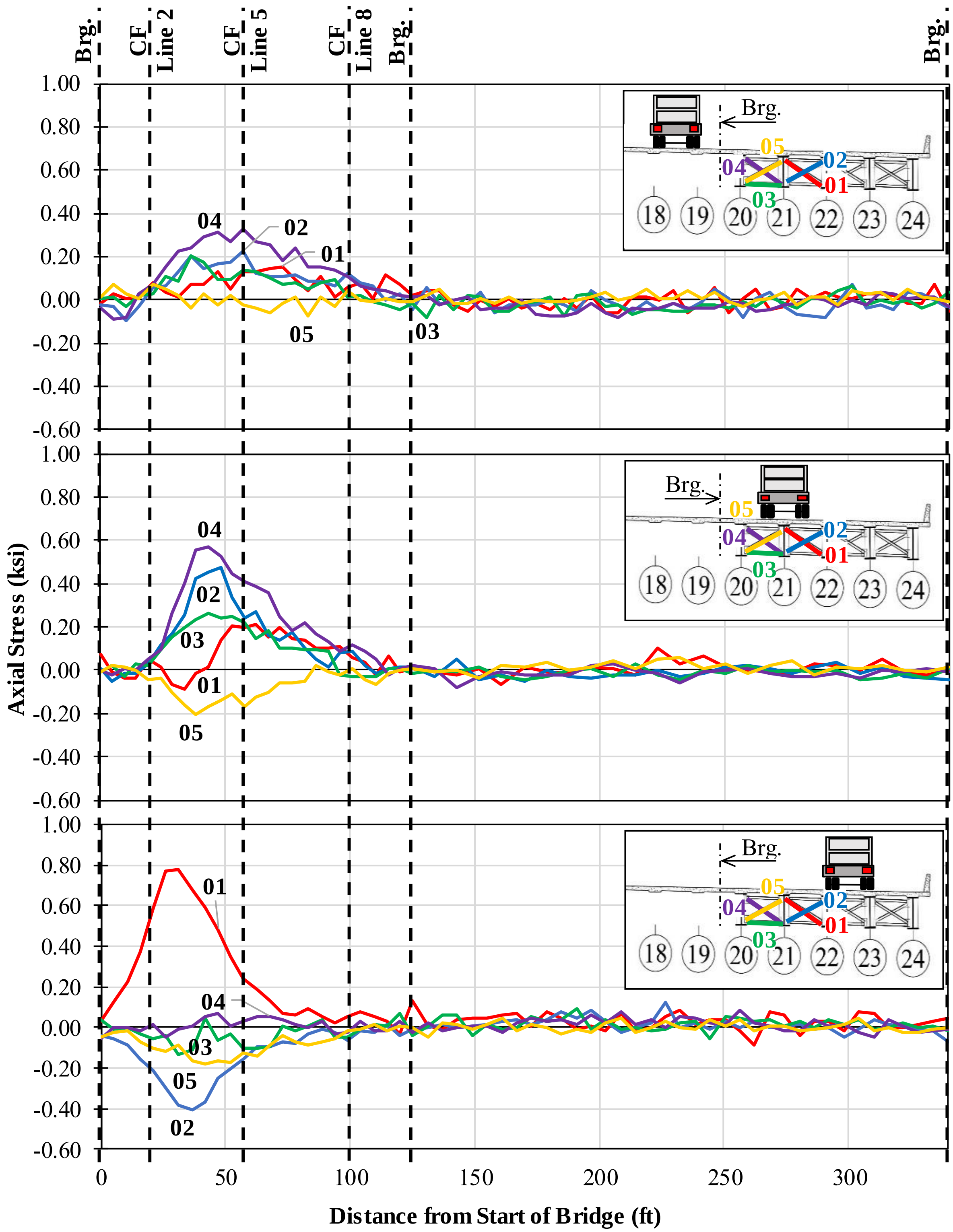

Figure E4-30: Influence line plots for cross-frame axial stresses at cross-frame line 2 between girders 20 and 22 (Load Cases 0A through 0C)

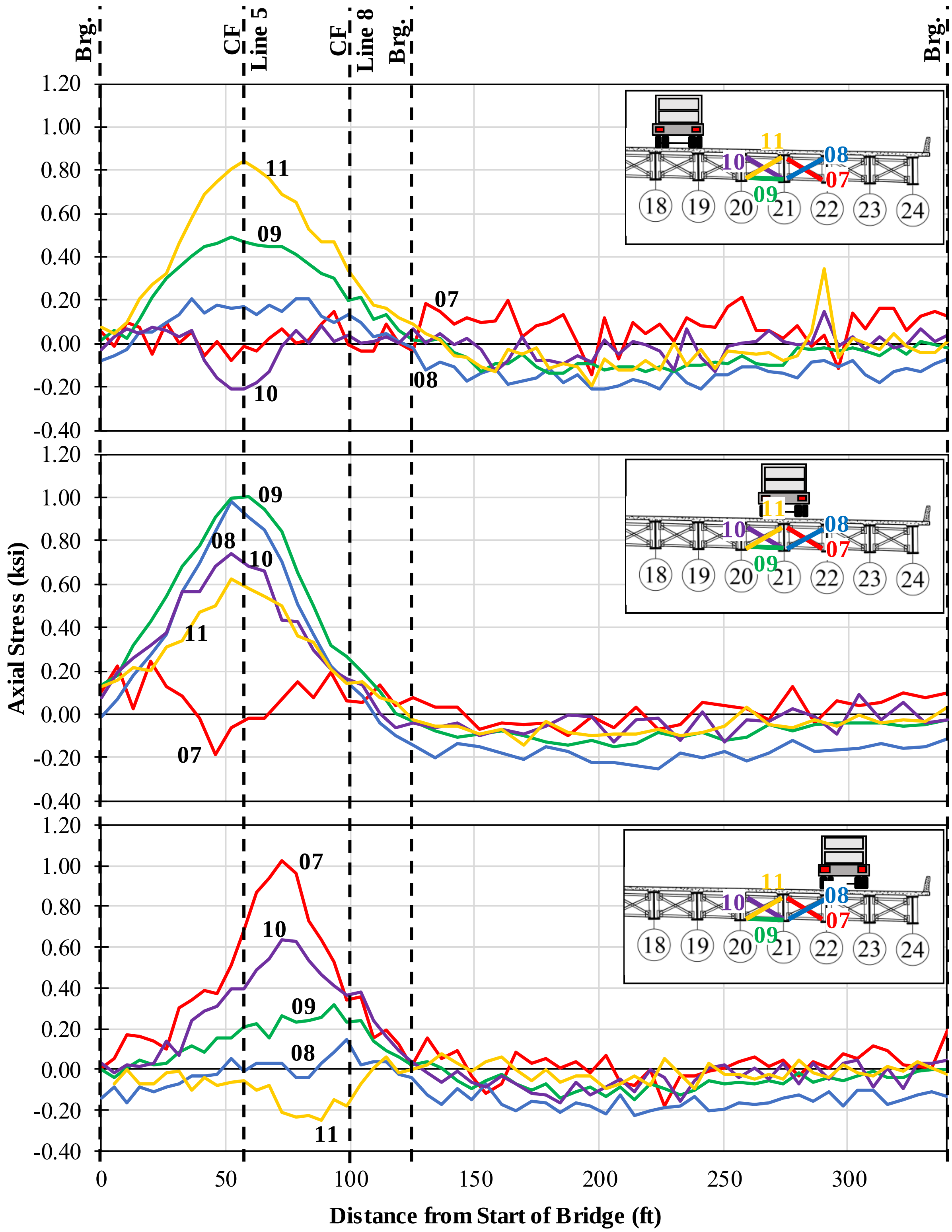

Figure E4-31: Influence line plots for cross-frame axial stresses at cross-frame line 5 between girders 20 and 22 (Load Case 0A through 0C)

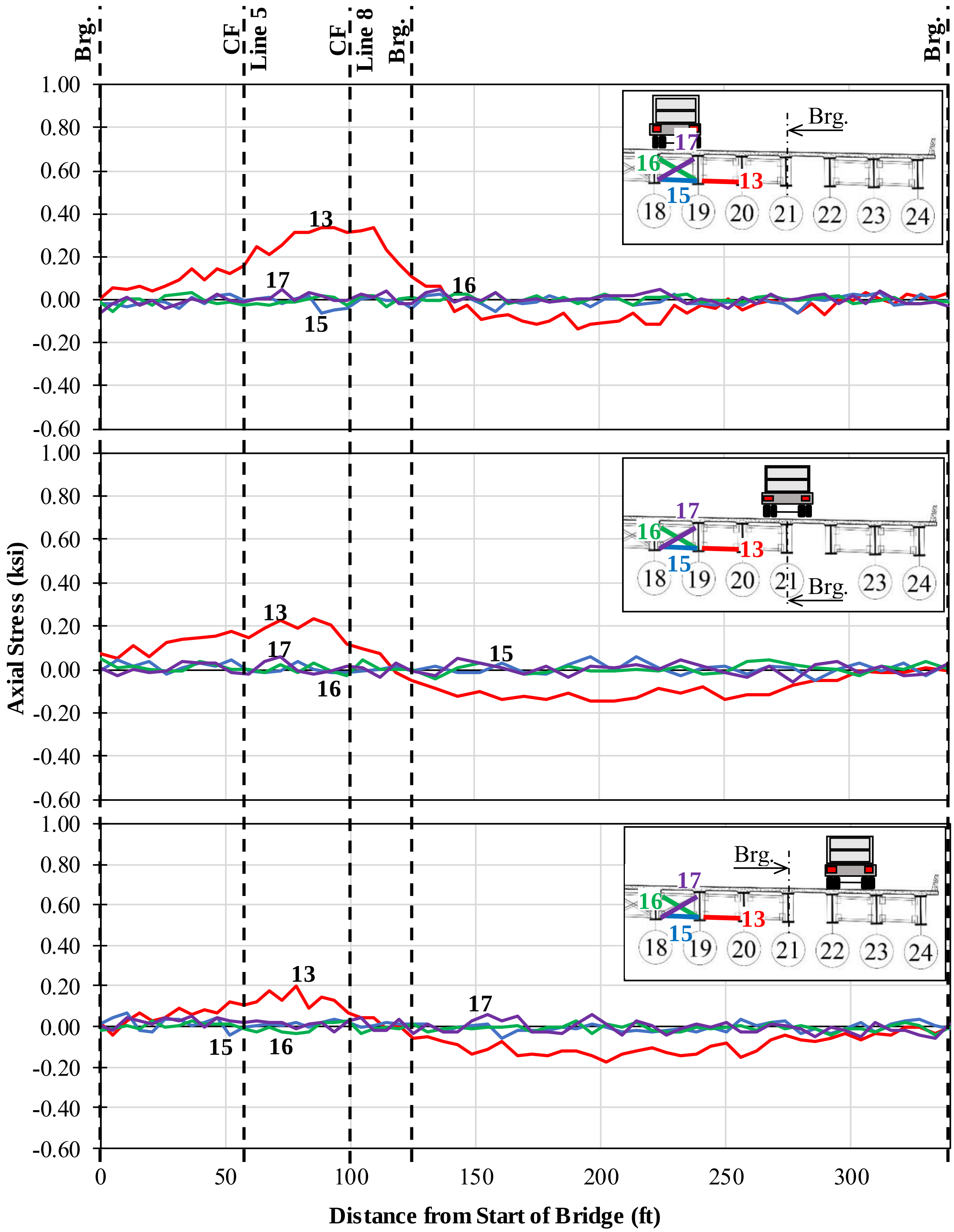

Figure E4-32: Influence line plots for cross-frame axial stresses at cross-frame line 8 between girders 18 and 20 (Load Case 0A through 0C)

E4.1.4.3 Load Case 1-7 Strain Data for Bridge 2

Similar to the Bridge 1 live load tests, the purpose of Load Cases 1 through 7 is to measure strains in the instrumented members under static loading conditions. Each test truck in Load Cases 1 through 7 was moved one at a time to the designated position, as the DAQ system recorded continuously and captured the stress state after each new truck loaded the bridge. The result is a stepped time-history response of increasing stress, as it was shown in subsection E4.1.3.3 for Bridge 1. The same procedure applied for Bridge 1 data was applied to Bridge 2 data in order to convert time-history plots into a series of average, static stresses displayed in tabular form.

Table E4-8, Table E4-9, and Table E4-10 summarize the respective results for the bottom flange longitudinal stresses in the instrumented girders, the lateral bending stresses in the instrumented girders, and the axial stresses in instrumented cross-frame members. These static stress tables, along with deflection measurements discussed in the subsequent section, serve as the metric by which the FEA model was validated. In Table E4-8 and Table E4-9, the columns are identified by G#, where # indicates the girder number, and CFL## where ## indicates the cross-frame line (either 5 or 8). Recall that the cross-frame member numbers in Table E4-10 were previously presented in Figure E4-23, Figure E4-24 and Figure E4-25. An example of cross-frame stresses for Load Case 4 is illustrated in Figure E4-33. This figure visually presents the Load Case 4 row of Table E4-10.

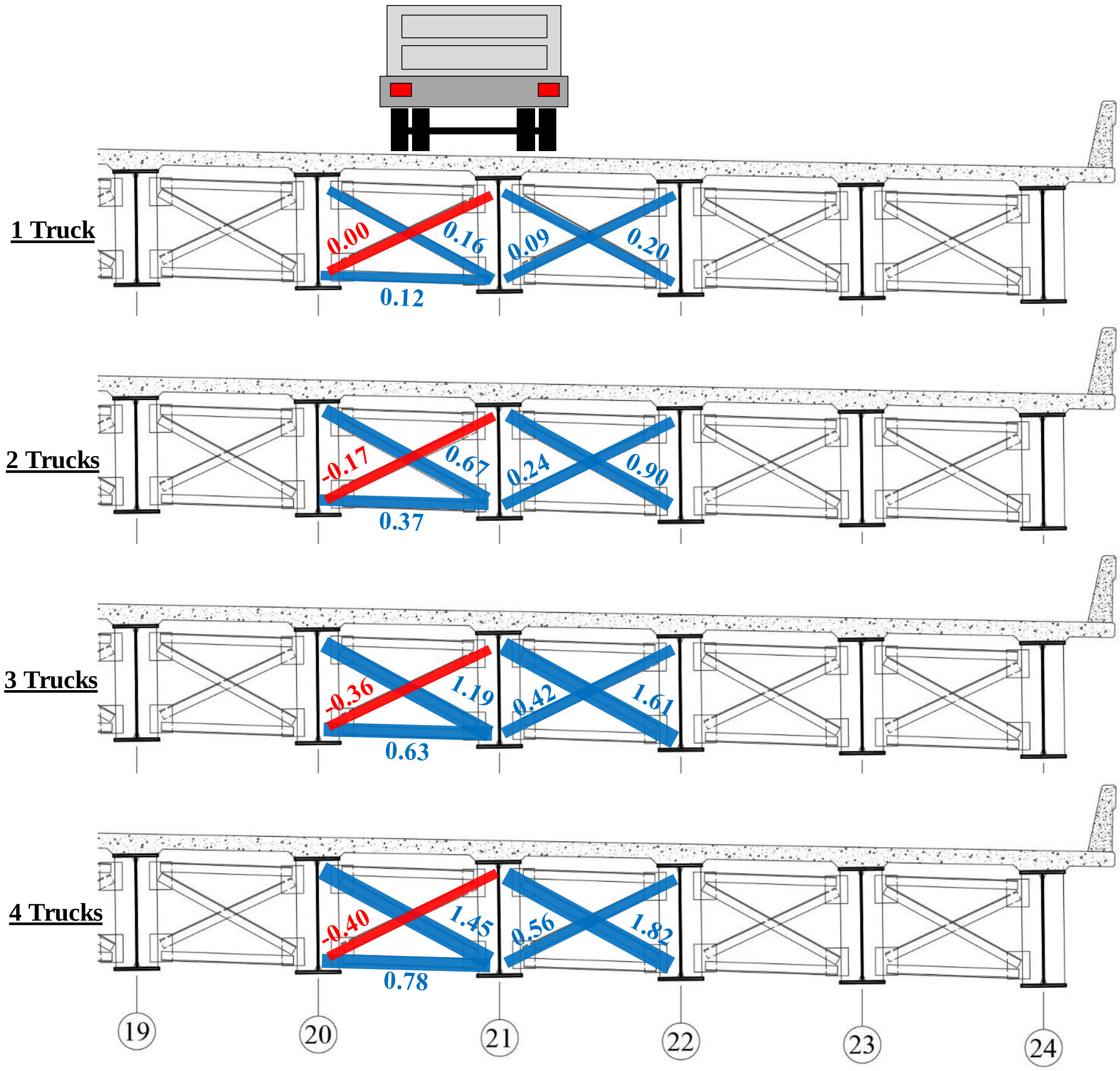

Figure E4-33: Cross-frame stress states at cross-frame line 5 during Load Case 4 (Units: ksi)

Table E4-8: Bottom flange longitudinal stresses in instrumented girders for Load Cases 1-7

Load Case	No. of Trucks	Average Bottom Flange Longitudinal Stress (ksi)				
		G22-CFL5	G21-CFL5	G20-CFL5	G19-CFL8	G18-CFL8
1	1	0.34	0.32	0.33	-0.03	0.01
	2	0.41	0.35	0.39	-0.04	0.02
	3	0.83	0.70	0.65	0.01	0.06
	4	1.07	0.95	0.84	0.04	0.09
2	1	0.32	0.41	0.36	0.02	0.04
	2	0.40	0.54	0.52	0.03	0.06
	3	0.85	0.84	0.76	0.08	0.10
	4	1.08	1.11	0.96	0.12	0.14
3	1	0.19	0.23	0.21	0.32	0.22
	2	0.45	0.62	0.71	0.27	0.24
	3	0.69	0.97	1.19	0.20	0.22
	4	0.79	1.07	1.29	0.17	0.20
4	1	0.11	0.13	0.10	0.02	0.02
	2	0.65	0.58	0.43	0.04	0.06
	3	1.17	1.07	0.82	0.06	0.10
	4	1.32	1.27	1.05	0.07	0.14
5	1	-0.12	0.20	0.08	0.10	0.05
	2	0.33	0.40	0.46	0.13	0.12
	3	0.43	0.46	0.53	0.14	0.13
	4	0.90	1.09	0.85	0.18	0.18
6	1	0.10	0.13	0.15	0.12	0.28
	2	0.17	0.24	0.31	0.22	0.41
	3	0.26	0.40	0.50	0.49	0.80
	4	0.42	0.65	0.81	0.60	0.83
7	1	0.00	0.00	0.02	0.01	0.03
	2	0.01	0.02	0.05	0.02	0.09
	3	0.01	0.06	0.08	0.03	0.15
	4	0.01	0.08	0.10	0.03	0.18

Table E4-9: Bottom flange lateral bending stresses in instrumented girders for Load Cases 1-7.

Load Case	No of Trucks	Bottom Flange Lateral Bending Stresses (ksi)				
		G22 - CFL5	G21 - CFL5	G20 - CFL5	G19 - CFL8	G18 - CFL8
1	1	0.05	0.01	0.09	-0.06	0.01
	2	0.05	0.02	0.11	-0.08	0.01
	3	0.03	0.08	0.12	-0.12	0.00
	4	0.00	0.12	0.14	-0.19	-0.02
2	1	0.00	0.02	0.06	-0.09	-0.05
	2	0.00	0.02	0.07	-0.10	-0.07
	3	0.00	0.05	0.08	-0.14	-0.05
	4	-0.04	0.06	0.08	-0.17	-0.05
3	1	0.00	0.04	0.07	0.03	0.02
	2	-0.08	0.06	0.15	0.02	0.02
	3	-0.10	0.02	0.23	-0.01	0.00
	4	-0.10	0.07	0.26	-0.01	0.00
4	1	0.07	0.01	0.01	-0.03	0.03
	2	0.07	0.09	0.07	-0.08	0.01
	3	0.07	0.11	0.13	-0.14	0.00
	4	0.11	0.09	0.16	-0.17	-0.02
5	1	-0.51	0.02	0.02	-0.03	0.01
	2	-0.41	0.65	0.12	-0.12	-0.01
	3	-0.27	0.67	0.13	-0.14	-0.02
	4	-0.15	0.42	0.17	-0.21	-0.03
6	1	0.04	0.03	0.01	-0.06	-0.09
	2	0.02	-0.01	0.02	-0.06	-0.13
	3	-0.04	-0.02	0.05	-0.13	-0.22
	4	-0.05	0.01	0.08	-0.13	-0.27
7	1	-0.01	0.00	0.01	0.03	0.05
	2	-0.02	0.01	0.00	0.10	0.10
	3	-0.03	-0.01	0.00	0.19	0.11
	4	-0.04	0.01	-0.02	0.21	0.12

* Positive values indicate that the left side of the bottom flange sees more tension whereas negative values indicate that the right side of the flange sees more tension.

Table E4-10: Axial stresses in instrumented cross-frame members for Load Cases 1-7

Load Case	No. of Trucks	Average Axial Stress (ksi)													
		CF-1	CF-2	CF-3	CF-4	CF-5	CF-7	CF-8	CF-9	CF-10	CF-11	CF-13	CF-15	CF-16	CF-17
1	1	0.19	0.30	0.24	0.49	-0.14	0.09	0.68	0.70	0.52	0.39	0.13	0.12	0.05	0.04
	2	0.08	0.77	0.49	1.02	-0.29	0.16	0.83	0.88	0.66	0.48	0.16	0.16	0.06	0.09
	3	-0.29	0.33	0.10	0.37	-0.23	0.14	0.50	0.50	0.47	0.18	0.22	0.20	0.09	0.13
	4	-0.82	-0.15	-0.37	-0.44	-0.13	0.12	0.31	0.26	0.37	-0.02	0.27	0.23	0.12	0.16
2	1	0.32	-0.12	-0.02	0.09	-0.14	0.52	0.19	0.24	0.47	-0.11	0.11	0.09	0.04	0.01
	2	1.06	-0.41	-0.05	0.21	-0.35	0.65	0.27	0.33	0.61	-0.14	0.17	0.13	0.06	0.02
	3	0.65	-0.83	-0.44	-0.47	-0.30	0.60	-0.05	-0.06	0.41	-0.43	0.24	0.18	0.10	0.02
	4	0.07	-1.29	-0.90	-1.28	-0.22	0.59	-0.23	-0.29	0.31	-0.63	0.29	0.22	0.13	0.01
3	1	0.07	0.07	0.06	0.22	-0.01	-0.06	0.19	0.26	-0.01	0.34	0.34	0.33	0.19	0.22
	2	0.18	0.23	0.19	0.43	-0.05	-0.18	0.46	0.71	-0.14	1.04	0.56	0.59	0.28	0.42
	3	0.27	0.42	0.36	0.68	-0.06	-0.27	0.71	1.15	-0.25	1.71	0.67	0.73	0.33	0.52
	4	0.30	0.47	0.41	0.71	-0.02	-0.30	0.85	1.35	-0.23	1.93	0.71	0.75	0.34	0.51
4	1	0.01	-0.01	0.00	0.00	0.00	0.20	0.09	0.12	0.16	0.00	0.01	0.01	0.01	-0.02
	2	0.04	-0.03	-0.01	0.02	-0.04	0.90	0.24	0.37	0.67	-0.17	0.11	0.09	0.06	0.04
	3	0.23	-0.09	-0.02	0.09	-0.16	1.61	0.42	0.63	1.19	-0.36	0.23	0.18	0.11	0.12
	4	0.92	-0.36	-0.06	0.20	-0.36	1.82	0.56	0.78	1.45	-0.40	0.31	0.25	0.15	0.17
5	1	0.03	0.02	0.03	0.06	-0.02	-0.04	0.22	0.24	0.15	0.17	0.16	0.11	0.08	0.04
	2	0.14	0.11	0.11	0.22	-0.06	-0.09	0.93	0.97	0.62	0.62	0.38	0.29	0.18	0.18
	3	0.14	0.11	0.10	0.22	-0.06	0.08	1.00	1.05	0.74	0.61	0.37	0.28	0.18	0.18
	4	0.18	0.11	0.09	0.24	-0.09	0.68	1.20	1.32	1.23	0.50	0.48	0.37	0.23	0.23
6	1	0.03	0.06	0.04	0.09	0.00	-0.05	-0.05	-0.03	-0.07	0.02	-0.19	-0.11	-0.13	-0.04
	2	0.07	0.14	0.10	0.18	0.01	-0.12	-0.14	-0.12	-0.16	0.01	-0.29	-0.11	-0.23	0.01
	3	0.11	0.20	0.16	0.29	0.00	-0.17	-0.10	-0.06	-0.23	0.17	-0.33	0.21	-0.38	0.36
	4	0.18	0.32	0.26	0.45	0.00	-0.28	-0.11	-0.04	-0.35	0.34	-0.30	0.45	-0.43	0.60
7	1	0.00	0.00	0.00	0.01	0.00	-0.01	-0.02	-0.03	-0.02	-0.01	-0.07	-0.09	-0.01	-0.09
	2	0.01	0.02	0.02	0.03	0.00	-0.03	-0.05	-0.07	-0.05	-0.04	-0.21	-0.29	-0.03	-0.25
	3	0.01	0.03	0.04	0.05	0.01	-0.03	-0.11	-0.13	-0.08	-0.08	-0.34	-0.48	-0.05	-0.41
	4	0.02	0.04	0.04	0.07	0.01	-0.05	-0.14	-0.16	-0.10	-0.11	-0.41	-0.56	-0.07	-0.48

Many of the same trends observed in the Load Case 0 data were also apparent in the static Load Cases 1 through 7. Again, the same general format of the observations is followed. The bolded text represents the general categories investigated by the RT, and the commentary within that category are specific observations made for this data set.

- **Evaluate load distribution (transverse) and load influence (longitudinal) characteristics on girders.**
  - The transverse distribution of girder stresses seems to follow a nearly-linear distribution for the three girders instrumented. Figure E4-34 demonstrates this phenomenon, which depicts the longitudinal bending stresses in girders 20, 21 and 22 at cross-frame line 5 during Load Cases 1 through 5. This figure shows how live loads were distributed transversely through part of the deck and cross-frames into the girders. A visual depiction of the load cases is included in Figure E4-34. For a highly redundant, skewed system, the trends are less obvious than what was observed at the other two bridges, especially since instrumenting all twelve girders across the width was not feasible.

    Similar to Figure E4-34, Figure E4-35 displays the longitudinal stress response of the instrumented girders at line 8 for Load Cases 2 through 6. Girder stresses were insignificant for Load Cases 2, 4, and 5, since the girders at this cross-frame line are near a dead load inflection point. The stresses for Load Case 6 are much higher than for Load Case 5, despite the truck positions in Case 5 being closer to the instrumented girders. This is likely because the trucks in Load Case 6 were positioned closer to midspan relative to that transverse location of the span, whereas the trucks in Case 5 are positioned closer to the support. This trend further highlights the complexity of the skewed system.
  - Load influence effects are not applicable to Load Cases 1 through 7. Refer to Section E4.1.4.2 for more information regarding longitudinal load influence.
- **Compare and evaluate measured girder stress (longitudinal and lateral) and deflections with established design metrics.**
  - The maximum longitudinal girder stresses at cross-frame line 5 were significantly higher than the maximum longitudinal girder stresses at line 8 for Load Cases 1 through 5 when the trucks were positioned closer to the instrumented portions of the superstructure. On the other hand, the longitudinal girder stresses at these two locations were similar for Load Cases 6 and 7 when the trucks were positioned further away from the instrumented portions.
  - For the bottom flange lateral bending stresses, it was observed that these values are generally 30% or lower of the corresponding longitudinal stresses at line 5. Load Case 5 is the only exception to this rule, exhibiting much higher lateral bending stresses than longitudinal bending stresses, as clearly shown in Table E4-8 and Table E4-9. The RT is unable to infer any trends on lateral bending and warping stresses in the girder flanges at this stage given the limited data and redundancy of the wide system.

- **Evaluate load distribution (transverse) and load influence (longitudinal) characteristics on cross-frames.**
  - Similar to the Load Case 0 results, cross-frame stresses were highly sensitive to transverse position of the truck, as is demonstrated by the stress reversal in members from one load case to another, particularly at cross-frame lines 2 and 5 for Load Case 1.
  - Load influence effects are not applicable to Load Cases 1 through 7. Refer to Section E4.1.4.2 for more information regarding longitudinal load influence.

- **Compare and evaluate measured cross-frame stress with established design metrics.**
  - In all cross-frame members, the measured axial stresses are less than the CAFL of 2.6 ksi
  - Similar to the Load Case 0 results, the maximum girder stresses are generally lower than or equal to maximum axial stresses in cross-frame members for equivalent load cases. This is due to the low span-to-depth ratio and skewed geometry of the instrumented end span.
- **Understanding complex load paths based on unique characteristics of the measured data.**
  - As previously stated, inferring clear trends was far more challenging for the skewed Bridge 2 data than the other two subject bridges. The instrumented span of Bridge 2 has a large skew and is nearly as wide as it is long. For these reasons, rationalizing load paths and responses from localized instrumentation proved to be difficult. The RT intends to broaden its understanding of this skewed bridge better during the parametric study phase of the project.

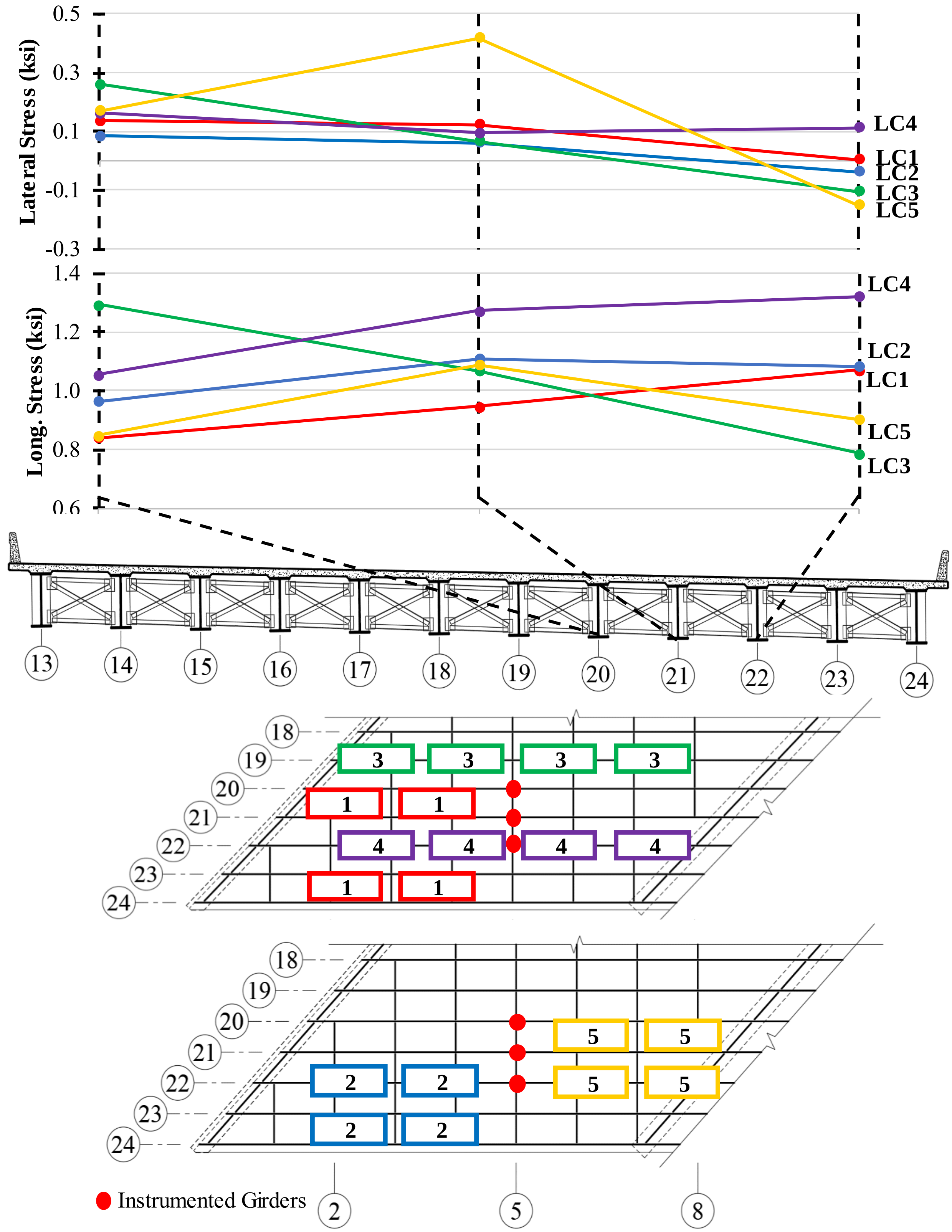

Figure E4-34: Distribution of girder lateral and longitudinal bending stresses on instrumented girders along cross-frame line 5 for Load Cases 1 through 5

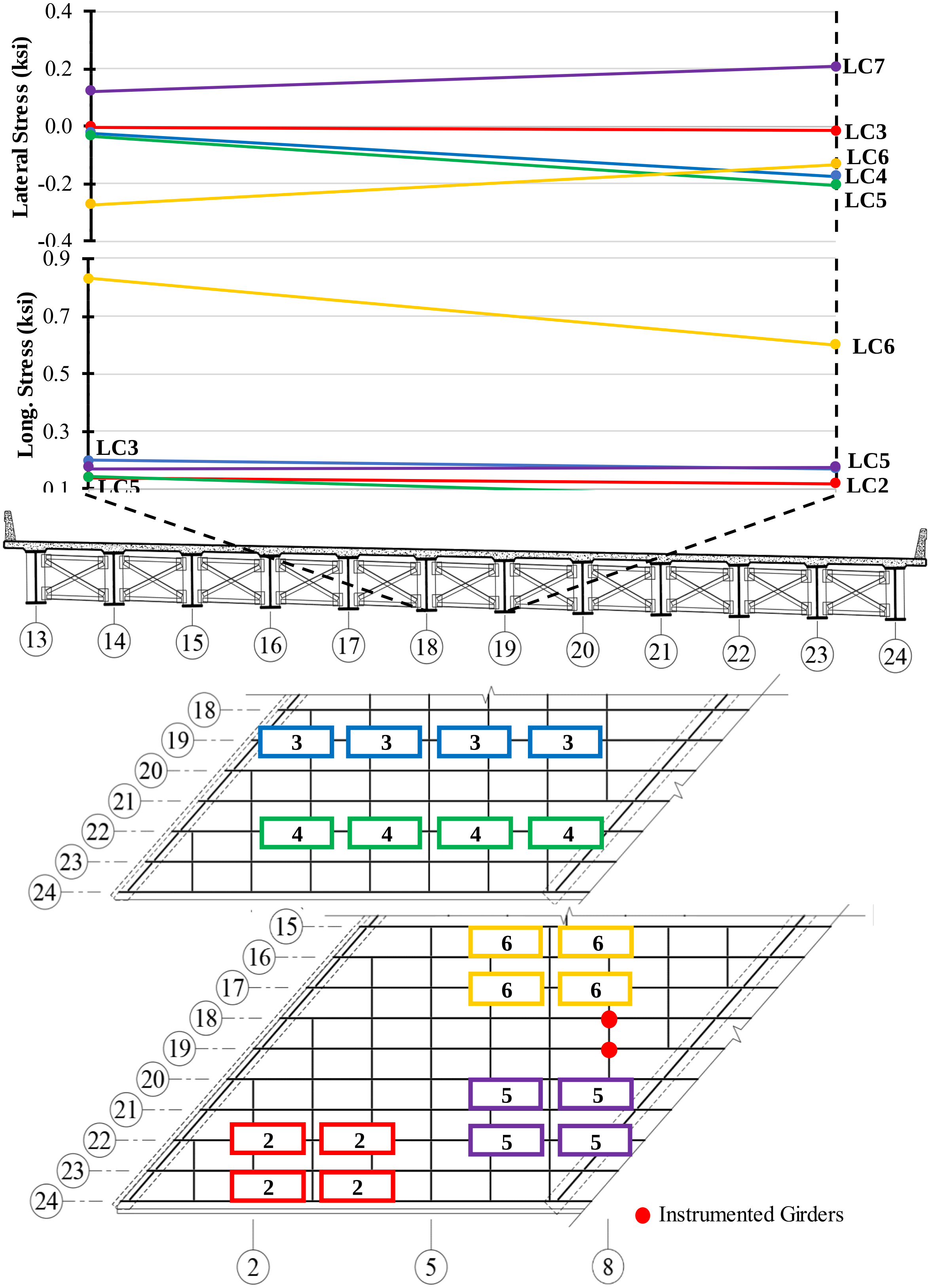

Figure E4-35: Distribution of girder lateral and longitudinal bending stresses on instrumented girders along cross-frame line 8 for Load Cases 2 through 6

E4.1.4.4 Deflection Data for Bridge 2

Similar to Bridge 1, laser distance meter readings were taken after every truck was introduced to the bridge for all seven static load cases. Measurements were taken at the center of the bottom flange at the following six girder locations (refer to Figure E4-36 for a plan view of the instrumented points):

1. Girder 23 at cross-frame line 4
2. Girder 24 at cross-frame line 6
3. Girder 21 at cross-frame line 6
4. Girder 18 at cross-frame line 6
5. Girder 15 at cross-frame line 6
6. Girder 14 at cross-frame line 8

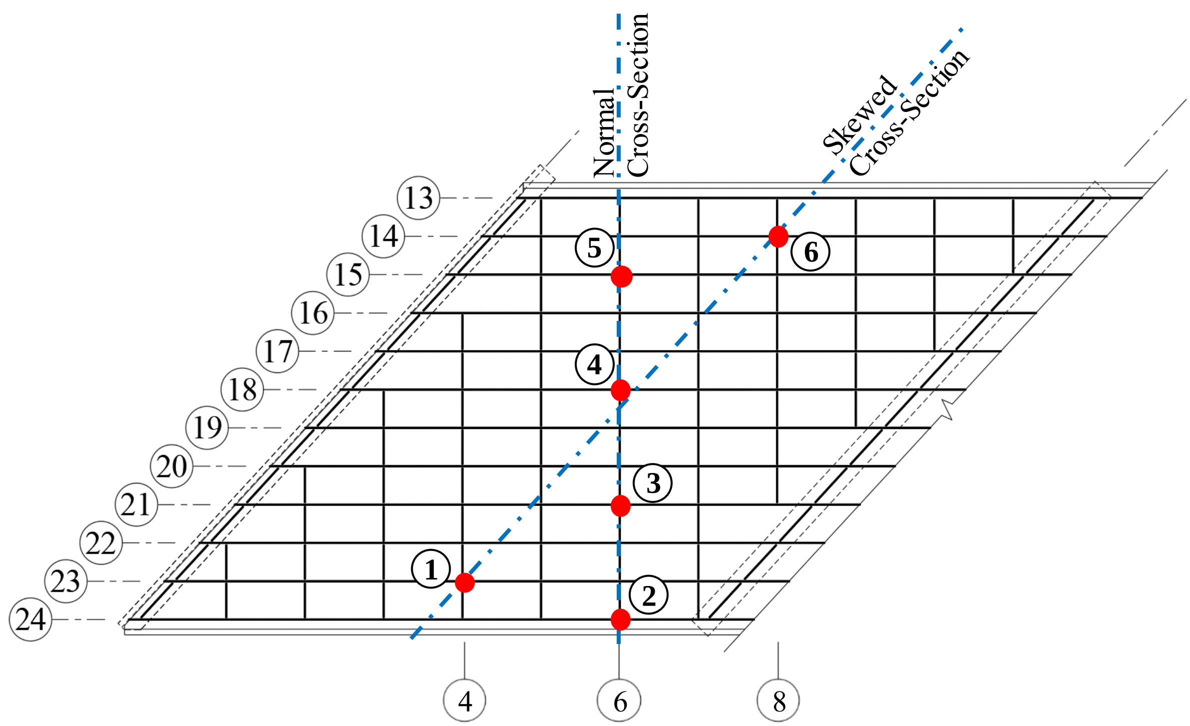

Figure E4-36: Instrumented girders for bottom flange deflection measurements

These points were chosen to create a cross-section perpendicular to the bridge axis along cross-frame line 6 (points 2 through 5) and a cross-section parallel to the skew near midspan of each girder (points 1, 4 and 6). For the sake of brevity, these arrangements will be referred as the normal cross-section and the skewed cross-section respectively in the subsequent paragraphs.

Similar to the procedure used for Bridge 1, the vertical deflections were computed by subtracting the baseline distance reading on the unloaded bridge from the distance reading on the loaded bridge. Table E4-11 summarizes the deflection measurements for Load Cases 1 through 7. In this table each reading point is labelled as “G# @ CF##” where G# indicates the girder number and CF## refers to the cross-frame line location.

Table E4-11: Girder deflection measurements for load cases 1-7

Load Case	No. of Trucks	Vertical Deflections (in)					
		G23@CF4	G24@CF6	G21@CF6	G18@CF6	G15@CF6	G14@CF8
1	1	-0.01	0.03	-0.01	-0.01	0.01	0.01
	2	-0.01	0.01	-0.03	-0.04	0.01	0.01
	3	-0.17	-0.08	-0.07	-0.03	0.00	-0.01
	4	-0.26	-0.12	-0.10	-0.04	0.04	0.00
2	1	-0.09	0.00	-0.04	0.00	0.03	-0.04
	2	-0.09	-0.04	-0.07	-0.03	0.00	0.00
	3	-0.20	-0.12	-0.10	-0.04	0.03	-0.03
	4	-0.29	-0.13	-0.12	-0.01	0.01	-0.04
3	1	0.04	0.03	-0.03	-0.01	0.01	-0.03
	2	-0.01	0.05	-0.07	-0.10	-0.01	-0.04
	3	-0.05	0.00	-0.09	-0.14	-0.03	-0.05
	4	-0.04	0.01	-0.12	-0.16	-0.04	-0.04
4	1	-0.01	0.01	0.00	0.03	0.00	-0.05
	2	-0.05	-0.03	-0.08	-0.03	0.03	-0.01
	3	-0.16	-0.04	-0.10	-0.03	0.00	-0.04
	4	-0.21	-0.08	-0.16	-0.05	0.01	-0.04
5	1	0.00	0.03	-0.03	-0.01	0.00	-0.05
	2	-0.05	0.00	-0.09	-0.01	0.00	-0.07
	3	-0.07	0.00	-0.09	-0.07	-0.01	-0.04
	4	-0.09	-0.04	-0.16	-0.04	0.00	-0.03
6	1	0.01	0.04	-0.01	0.00	-0.04	-0.08
	2	0.01	0.04	-0.01	-0.07	-0.09	-0.12
	3	-0.03	0.04	-0.07	-0.13	-0.10	-0.13
	4	0.00	0.01	-0.07	-0.18	-0.14	-0.16
7	1	0.01	0.04	0.01	0.01	0.00	-0.04
	2	0.01	0.04	0.00	0.03	-0.04	-0.13
	3	0.01	0.04	0.01	-0.01	-0.07	-0.21
	4	0.01	0.05	-0.03	-0.01	-0.09	-0.24

Figure E4-37 and Figure E4-38 show deflection measurements for Load Cases 1 through 7 as trucks were individually placed on the bridge for the normal cross-section. The same graphical representation is presented in Figure E4-39 and Figure E4-40 for the skewed cross-section.

Four different measurements are plotted for each location, as each measurement corresponds to a new dump truck placed on the bridge. These are labeled on each plot as "#-##" where "#" indicates the load case and "##" refers to the number of trucks positioned on the deck during that load case.

From the results of the displacement study, several observations with regards to the skewed bridge can be made. Again, the same general format of the observations is followed. The bolded text represents the general categories investigated by the RT, and the commentary within that category are specific observations made for this data set.

- **Evaluate load distribution (transverse) and load influence (longitudinal) characteristics on girders.**
    - As expected, the girders closer to the applied load deflected the most. Unlike the Bridge 1 results, there was no load case in which all girder defections across the width were nearly uniform, which is largely due to the width and redundancy of Bridge 2.

      When looking at the normal cross-section for Load Cases 1, 2, 6, and 7 it is observed that the girders farthest from where the load was applied exhibited an upwards displacement as much as 80% of the maximum downward displacement (Load Case 1). Considering the same load case, deflections of the fascia girders were higher when considering the skewed cross-section versus the normal cross-section. This trend illustrates the redundancy and relative stiffness of the system.
    - Load influence effects are not applicable to deflection measurements. Refer to Section E4.1.3.2 for more information regarding longitudinal load influence.
- **Compare and evaluate measured girder stress (longitudinal and lateral) and deflections with established design metrics.**
    - Deflections for Bridge 2 were notably smaller than those measured for Bridge 1. As was mentioned for the girder stresses measurements, this behavior is related to the relative transverse and longitudinal stiffness of the instrumented span. The instrumented span length and span-to-depth ratio at Bridge 2 were significantly less than at Bridge 1, which leads to a much stiffer unit and subsequently smaller live load deflections.
    - In fact, the maximum deflections measured during this study correspond to a deflection-to-span ratio of nearly L/5200, which is comparatively much stiffer than Bridge 1.
    - As mentioned previously in Section E3.4.1, the resolution of the laser distance meter is +/- 1/25 inches (0.04 inches). In many cases, the measured deflection is within that resolution band. Even for the maximum deflection recorded of 0.29 inches, the nominal resolution of the device makes up 15% of that value.
- **Understanding complex load paths based on unique characteristics of the measured data.**
    - In general, measurement points along the skewed cross-section exhibit larger displacements than those along the normal cross-section. This is can be explained with two hypotheses: (i) measurements along the skewed cross-section are always near midspan of the respective girder, whereas measurements along the normal cross-section have varying distances to the nearest support; (ii) the normal cross-section includes a contiguous line of cross-frames, which further stiffens that axis of the bridge. It would be expected that differential displacements between adjacent girders along a normal cross-section line would be less given that each girder are tied together by cross-frames. This behavior is particularly obvious for Load Case 2.

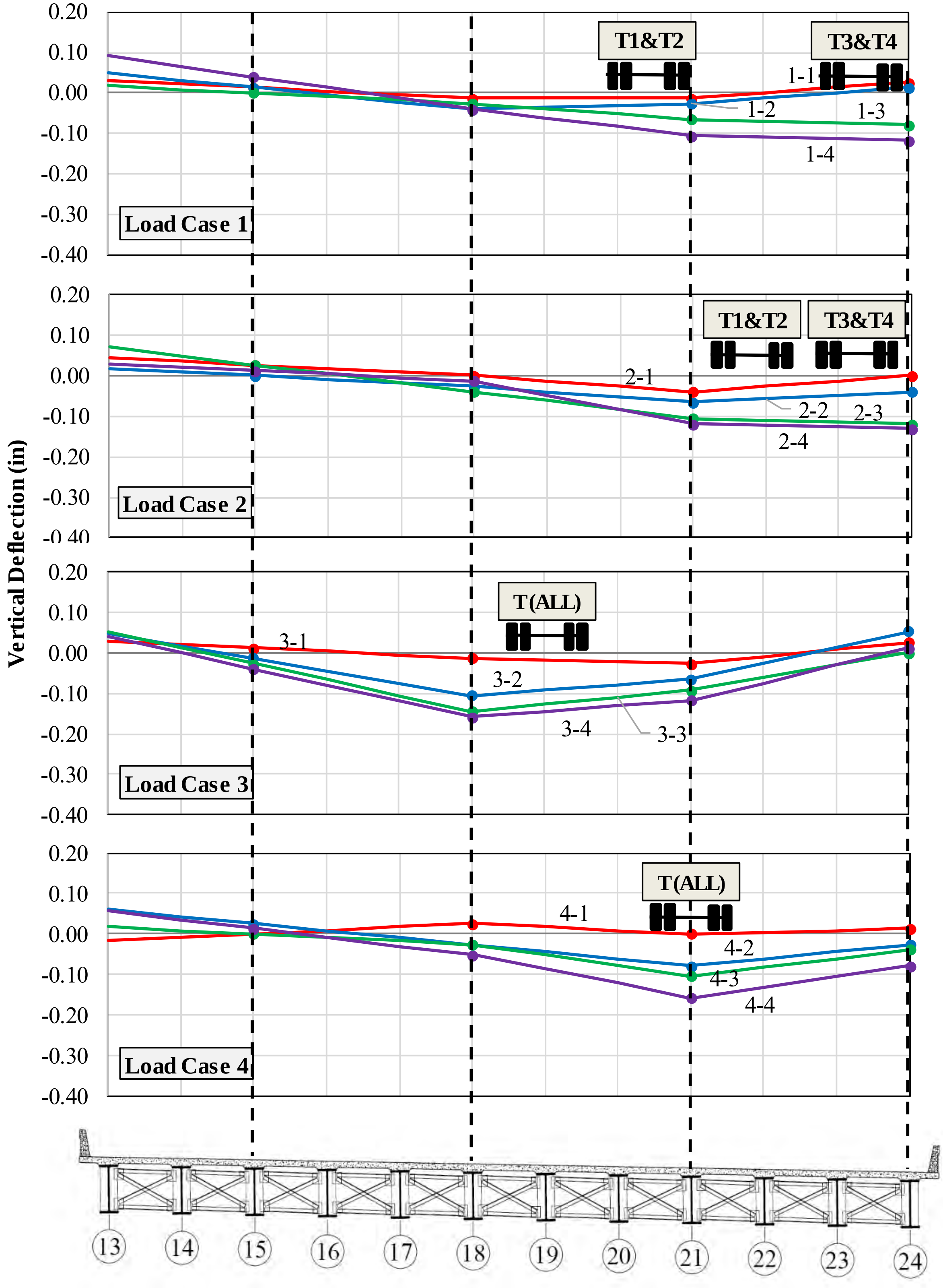

Figure E4-37: Girder deflection progression at normal cross-section along cross-frame line 6 for Load Cases 1-4

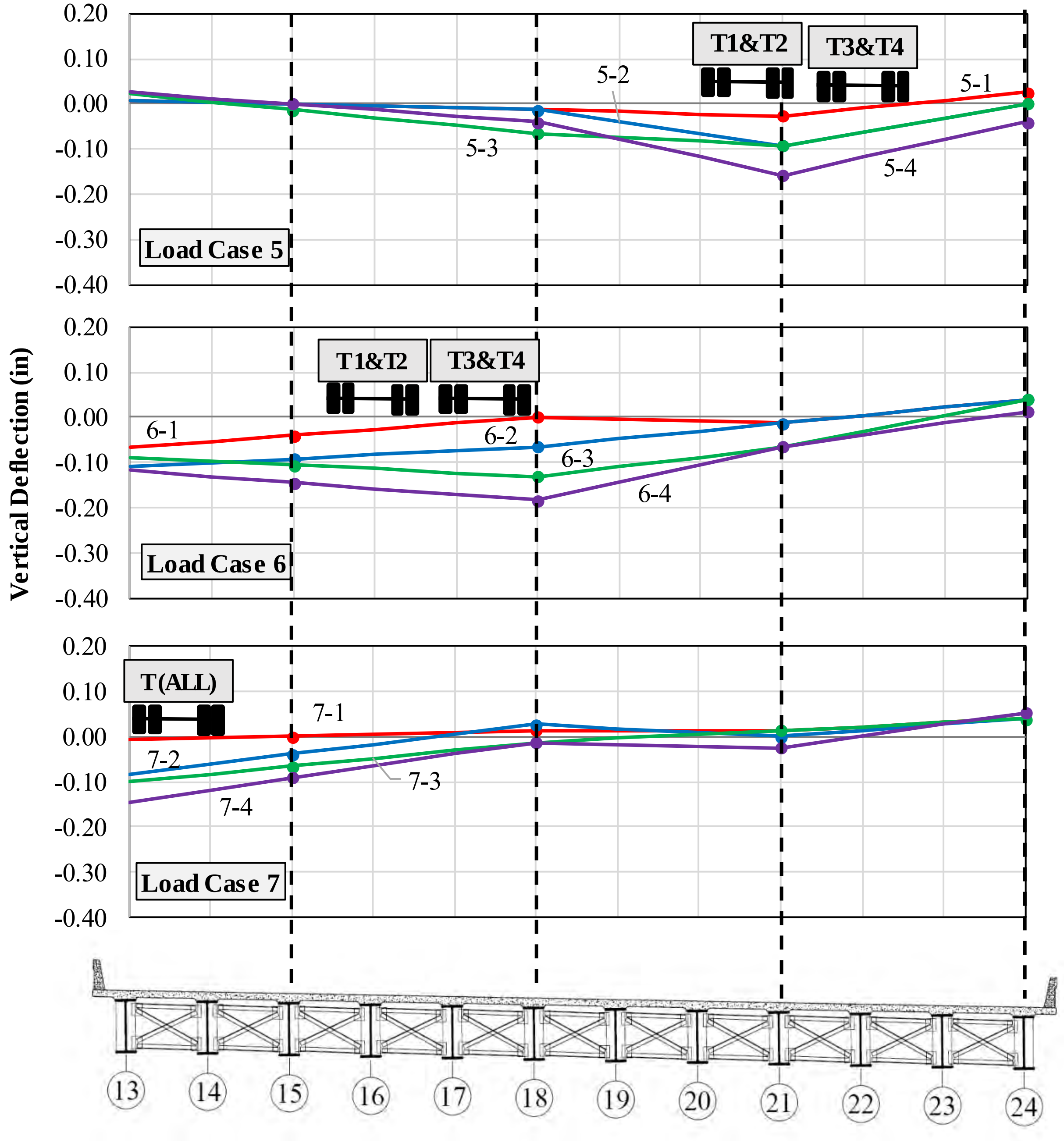

Figure E4-38: Girder deflection progression at normal cross-section along cross-frame line 6 for Load Cases 5-7

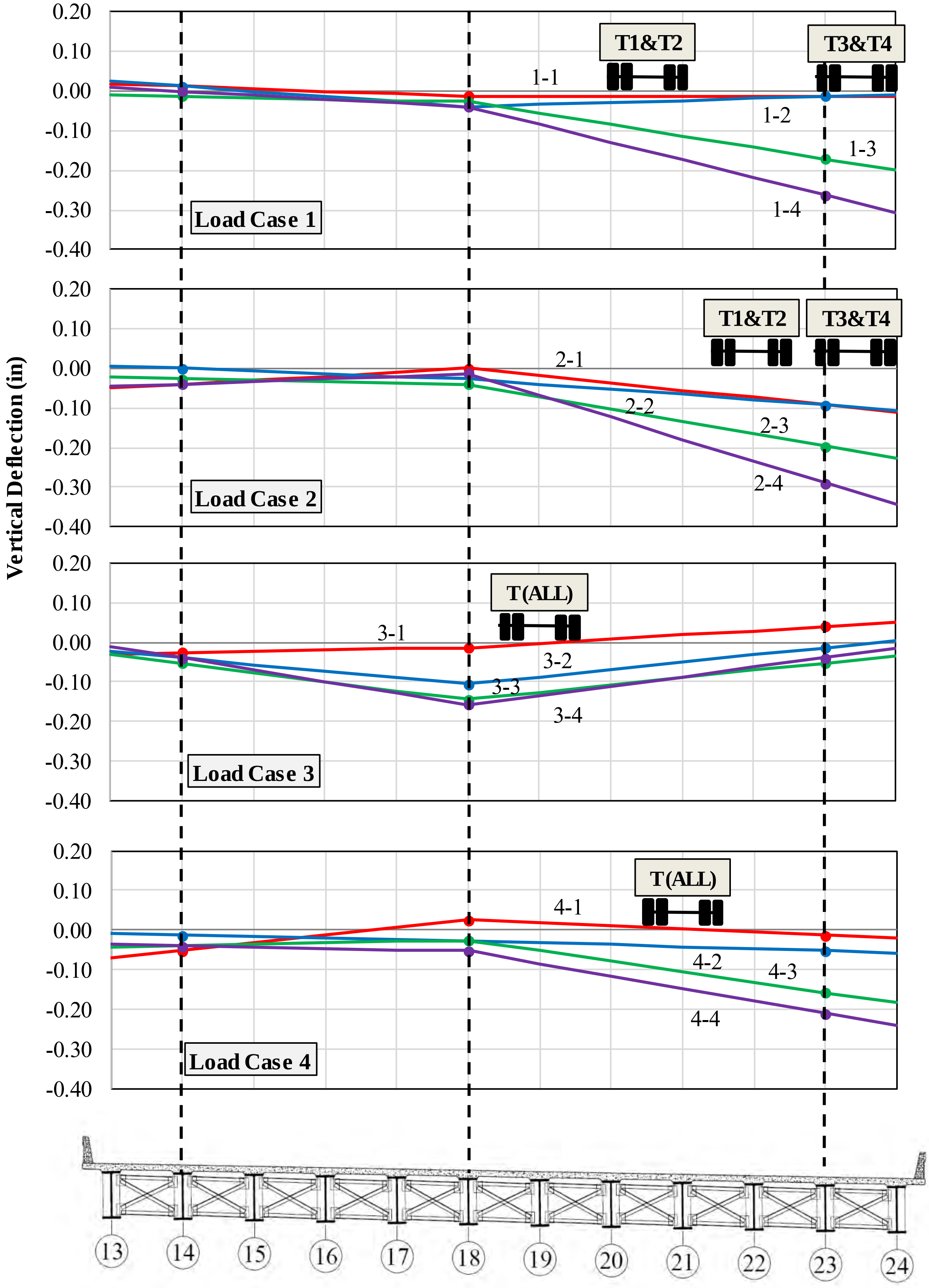

Figure E4-39: Girder deflection progression at skewed midspan cross-section for Load Cases 1-4

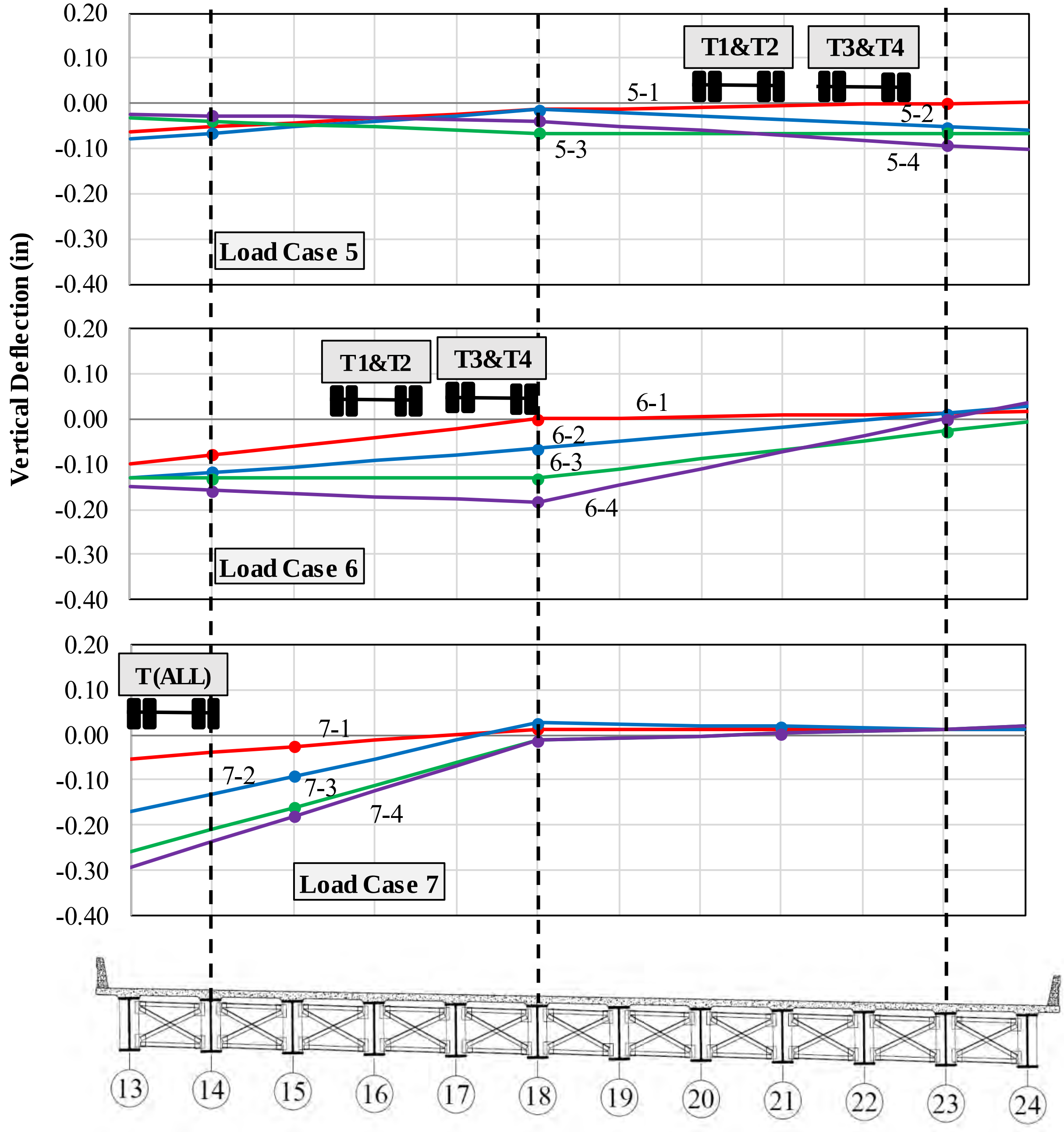

Figure E4-40: Girder deflection progression at skewed midspan cross-section for Load Cases 5-7

The deflection measurements, along with the maximum stress tables presented in the previous section, serve as the metric by which the FEA model was validated. Based upon comparisons of predicted and measured response, the model was adjusted until reasonable agreement was achieved between the predicted stresses and deflections and measured data. The model validation process is covered in Chapter E5.

E4.1.5 Bridge 3 Results

The following subsections summarize the controlled live load test data for Bridge 3. Subsections include truck properties, influence-line strain data for the moving load case (Case 0), strain data for the static load cases (Cases 1 through 7), and deflection data for the static load cases (Cases 1 through 7).

E4.1.5.1 Truck Properties for Bridge 3

Similar to the Bridge 1 and 2 load tests, TxDOT provided four dump trucks loaded with sand for the controlled live load test of Bridge 3. The four trucks provided were different from those used during the Bridge 1 and 2 load tests. TxDOT crews weighed these trucks, and the RT measured the wheel bases prior to the load test. The results are summarized in Table E4-12 and Figure E4-41.

Trucks 1, 3, and 4 were identical in geometry while Truck 2 was slightly different, as it is shown in Figure E4-41. Nevertheless, these discrepancies did not have a significant impact the gross weight of the truck. The weights the trucks are within approximately 5% of each other. Variations in the geometry and weights of the individual trucks do not impact the usefulness of the data since the measured weights and wheel positions were closely simulated in the FEA models during validation studies.

Table E4-12: TxDOT truck axle weights for Bridge 2 load test

Truck #	Steer Axle Weight (lb)	Combined Drive Axle Weight (lb)	Gross Vehicle Weight (lb)
1	10500	38680	49180
2	10480	39020	49500
3	10620	41040	51660
4	11460	39620	51080

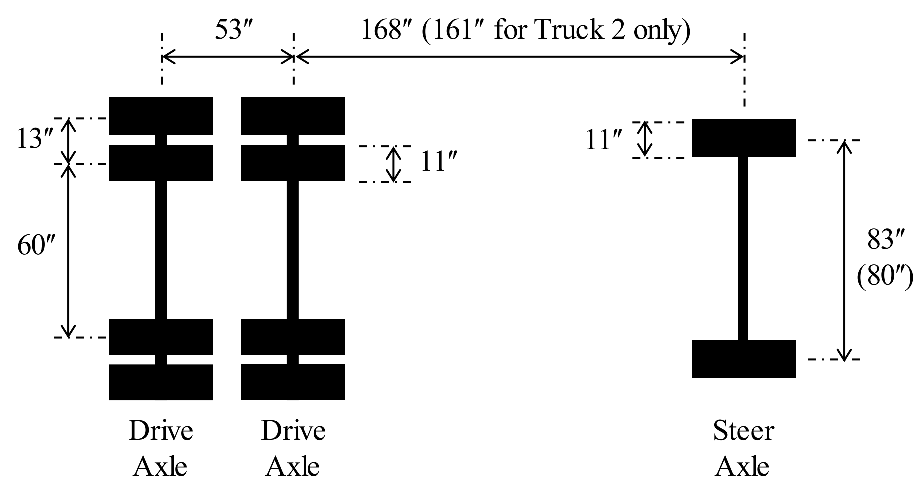

Figure E4-41: Typical TxDOT truck wheel base dimensions for Bridge 3 load test. Dimensions between parenthesis correspond to Truck 2 only.

E4.1.5.2 Load Case 0 Strain Data for Bridge 3

As was done for Bridge 1 and Bridge 2, strain data was continuously recorded during the Bridge 3 controlled live load test. As such, the RT obtained strain data at all instrumented elements for Load Case 0. Recall that Figure E3-27, Figure E3-28 and Figure E3-29 schematically presented all instrumented girder and cross-frame elements on Bridge 3 but did not identify each with a specific name or number, especially for cross-frame members. The cross-frame member numbers used in subsequent plots are presented in Figure E4-42 and Figure E4-43, which are adapted versions of Figure E3-28 and Figure E3-29.

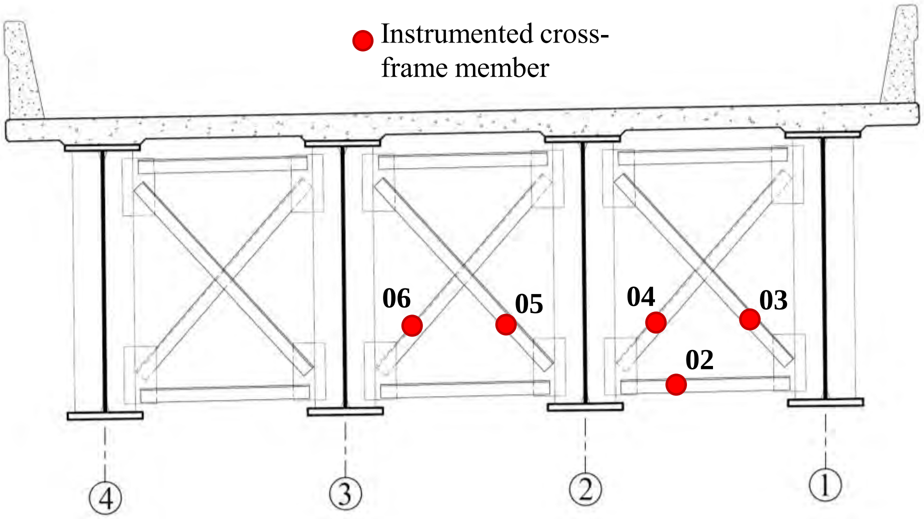

Figure E4-42: Instrumented cross-frame identification numbers at cross-frame line 4

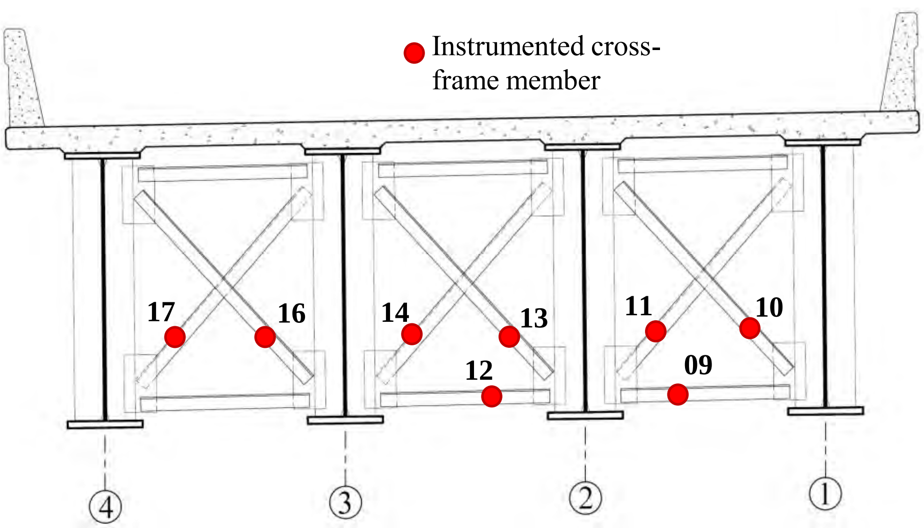

Figure E4-43: Instrumented cross-frame identification numbers at cross-frame line 10

As was outlined for the first two bridges, strain data for the influence line plots was collected as a time-history. The procedure used to transform time-history data to distance data is described in subsection E4.1.3.2.

Figure E4-44 through Figure E4-51 illustrate various measured influence line plots. Figure E4-44 and Figure E4-45 display the influence lines for bottom flange longitudinal stresses in the instrumented girders at cross-frame line 10 and 4, respectively. Figure E4-46 and Figure E4-47 display influence lines for lateral stresses in the instrumented bottom flanges at cross-frame lines 10 and 4, respectively. The sign convention for positive lateral bending stress was previously established in Section E4.1.3.2. Figure E4-48 through Figure E4-50 show the influence line plots for axial stresses in the instrumented cross-frame members.

Note that only three of the four-span unit are graphed on the x-axis for the girder-related plots and two spans for cross-frame-related plots. The influence of load application on the other spans is negligible for girders and cross-frames alike. For clarity, these portions of the respective influence line plots are not presented. Note that for all influence line plots, the results for Load Cases 0A through 0D are presented sequentially on the same figure such that trends can be more easily recognized.

Similar to the Bridge 1 and 2 results, commentary on the Bridge 3 results follows the same format introduced in Section E4.1.2. The three major concepts, with respect to the moving Load Case 0, are addressed by the observations from Figure E4-44 through Figure E4-47 for girders and Figure E4-48 through Figure E4-50 for cross-frame members. The bolded text represents the general categories investigated by the RT, and the commentary within that category are specific observations made for this data set.

- **Evaluate load distribution (transverse) and load influence (longitudinal) characteristics on girders.**
    - For Load Case 0A, which represents a truck traveling along the inner radius of the curve, girder 4 shows the largest bottom flange stresses. On the other hand, girder 1 sees the highest bottom flange stresses for Load Case 0D, which consists of a truck traveling along the outer radius of the curve. Comparatively, the maximum bottom flange stresses are considerably larger in girder 1 for Load Case 0D than in girder 4 for Load Case 0A. This phenomenon occurs due to the curved geometry of the bridge: the girder on the outer side of the curve develops higher bending stresses due to the torsional response of the deck, rotating about the chord of the curve, and the additional length of the outer-radius girder.
    - AASHTO LRFD distribution factors are not applicable for curved girders. Instead, older, approximate methods such as the V-load method and modern methods such as refined 3-D analysis are recommended to estimate live load forces in the girders. As such, the measured distribution is not compared to simple design factors, as was done for the Bridge 1 results.
    - The shape of the measured influence lines matches a simple 1-D qualitative influence line of a four-span continuous beam, which is similar to what is presented in Figure E4-7. Bottom flange stresses are most significant when the truck axles are centered over the longitudinal point of interest. For instance, longitudinal flange stresses at cross-frame line 4 are maximum when the truck is approximately over cross-frame line 4, and longitudinal flange stresses at cross-frame line 10 are maximum when the truck is over line 10.

      The influence of load on the span adjacent to the instrumented end span is more significant on girder stresses near line 4 than girder stress near line 10. At cross-frame line 10, maximum compressive stresses due to negative bending are generally on the order of one-third of the maximum tensile stresses due to positive bending. At cross-frame line 4, maximum compressive and tensile stresses are of the same magnitude. This observation makes sense given that stress ranges near dead load inflection points are usually subjected to nearly equal positive and negative bending moment from the live load effects.
- **Compare and evaluate measured girder stress (longitudinal and lateral) and deflections with established design metrics.**

  - Girder stresses at cross-frame line 10 are generally higher than girder stresses at cross-frame line 4. Per the preliminary FEA results, cross-frame line 10 is near the maximum positive moment region of the girders, and cross-frame line 4 is near the assumed inflection point from the uniform dead load condition. The measured data has good agreement with the FEA results.

    Additionally, the girder stresses measured on Bridge 3 are comparable to those measured on Bridge 1. This can be attributed to the fact that the span-to-depth ratio of the instrumented span at Bridge 3 is similar to the ratio of the span at Bridge 1; thus, the expected live load stresses should be of similar magnitude.

  - The measured bottom flange lateral bending stresses are generally small when compared to the corresponding longitudinal bending stresses, and a trend is less obvious. Given that the respective cross-frame (12′-3″) and girder (7.5′) spacings are small, it is intuitive that both the girder bottom flange longitudinal stresses and flange lateral bending stresses are small. An extended discussion on lateral bending stresses is provided in the static load case section later in this section.

- **Evaluate load distribution (transverse) and load influence (longitudinal) characteristics on cross-frames.**
  - Similar to the Bridge 1 and 2 results, cross-frame stress ranges were highly sensitive to the transverse position of the truck. Cross-frame members, especially diagonals, are prone to stress reversal as evidenced by the varied response to Load Cases 0A through 0D.
  - The shape of the influence lines suggests that cross-frame stresses are mostly sensitive to loading in close proximity to the cross-frame of interest. Only one stress cycle per truck passage was observed.

- **Compare and evaluate measured cross-frame stress with established design metrics.**
  - The cross-frame stress ranges along line 4 are higher when the truck is located approximately above girder 2 (Load Case 0C). In that position, the most significant differential deflections and torsional deformations appear to be between girder 1 and girder 2, as exhibited by forces in cross-frame elements 03 and 04 (diagonals).
  - The smallest overall measured stresses for this cross-frame line were observed for Load Case 0D, which suggests that the differential deflections and torsional deformations among the four girders are smaller for that load position.
  - Cross-frames at line 10, particularly for the diagonals located between girder 1 and girder 2, exhibit the largest stress ranges for the various Load Case 0 truck positions. This is logical given that the largest vertical deflections and torsional effects are expected on the outer-radius girder.
  - In all cases, the measured cross-frame stresses are significantly less than the constant-amplitude fatigue limit (CAFL) of 2.6 ksi for the Category E′ welded angle-to-gusset detail.
  - The maximum axial stresses for the instrumented cross-frame members are usually about one third of the maximum bottom flange girders stresses, for the same truck location and load case. This behavior is more comparable to the Bridge 1 data as opposed to the Bridge 2 data, where cross-frame stresses and girder stresses were of similar magnitude.

- **Understanding complex load paths based on unique characteristics of the measured data.**
  - As expected, the Load Case 0 data demonstrates that the curved geometry distributed a larger proportion of live loads to the outer radius girder.

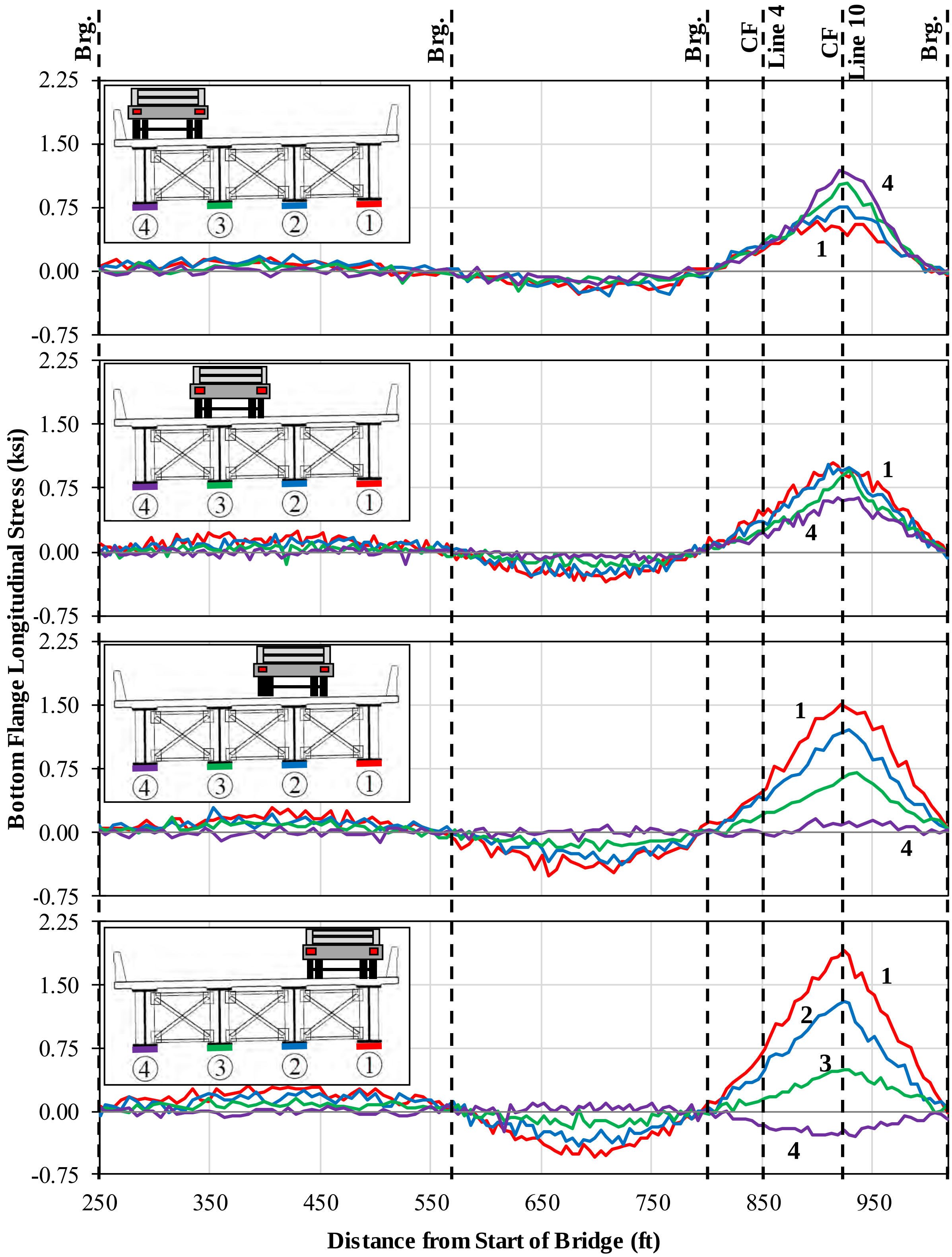

Figure E4-44: Influence line plots for bottom flange stresses at cross-frame line 10 (Load Case 0A through 0D)

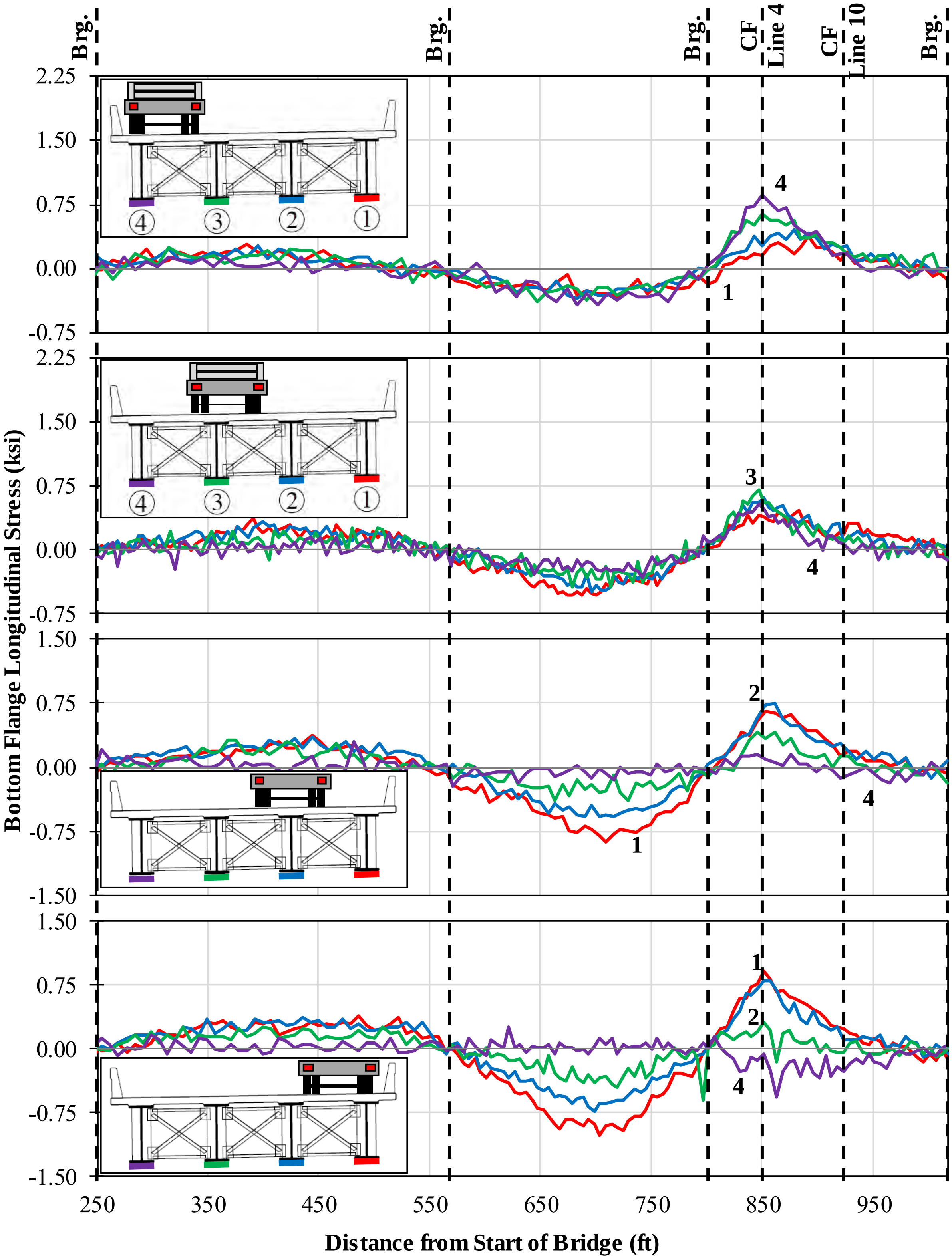

Figure E4-45: Influence line plots for bottom flange stresses at cross-frame line 4 (Load Case 0A through 0D)

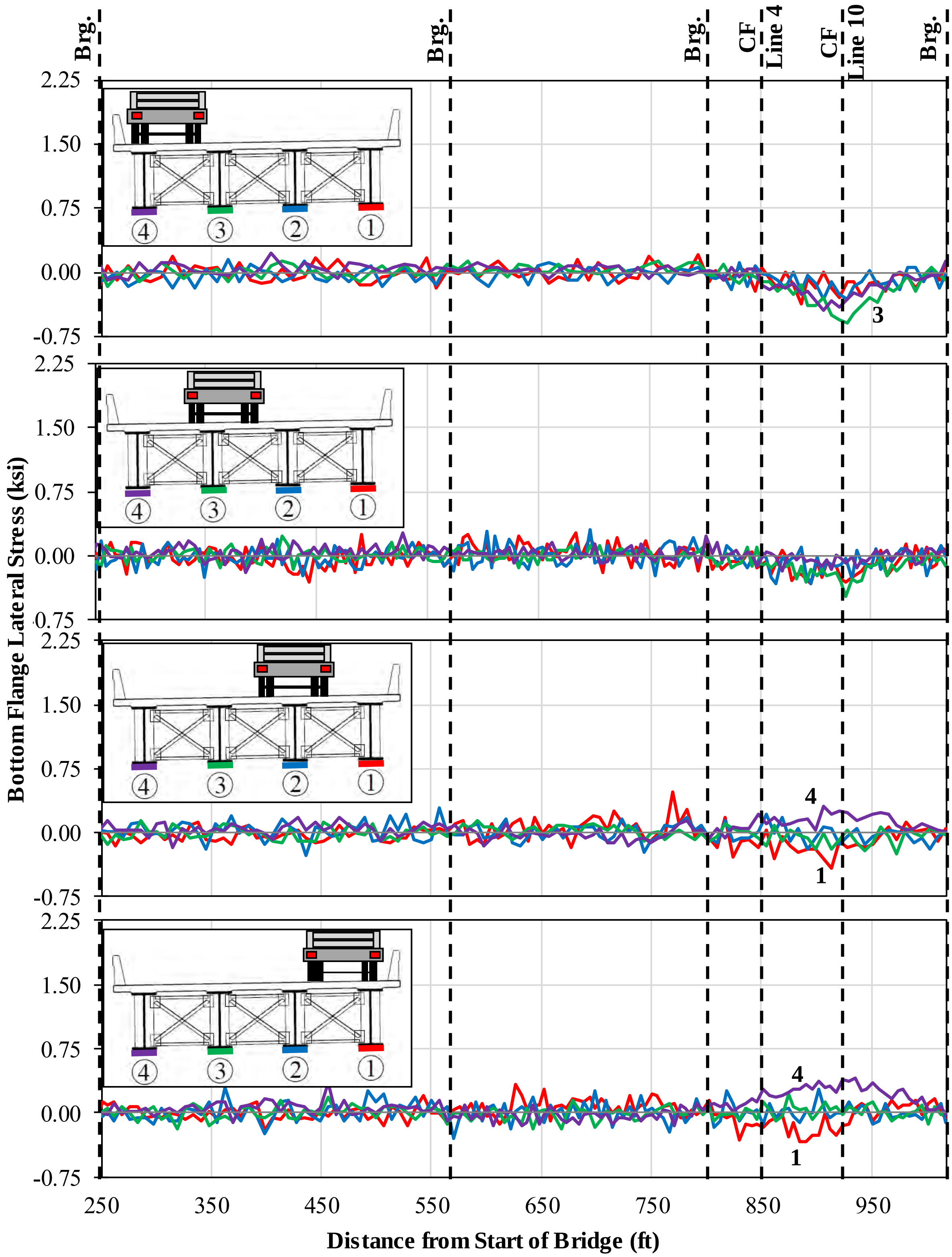

Figure E4-46: Influence line plots for bottom flange lateral stresses at cross-frame line 10 (Load Case 0A through 0D)

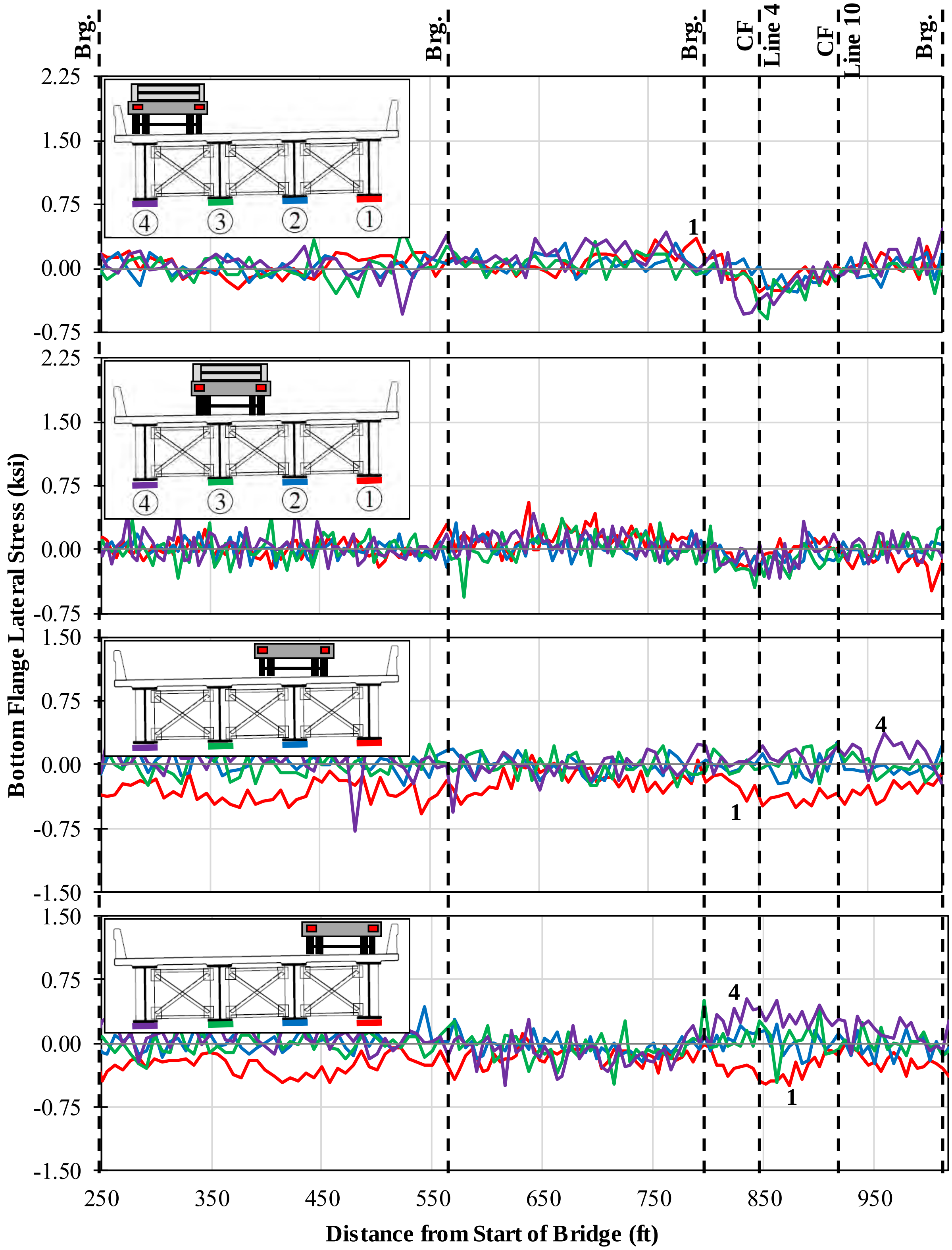

Figure E4-47: Influence line plots for bottom flange lateral stresses at cross-frame line 4 (Load Case 0A through 0D)

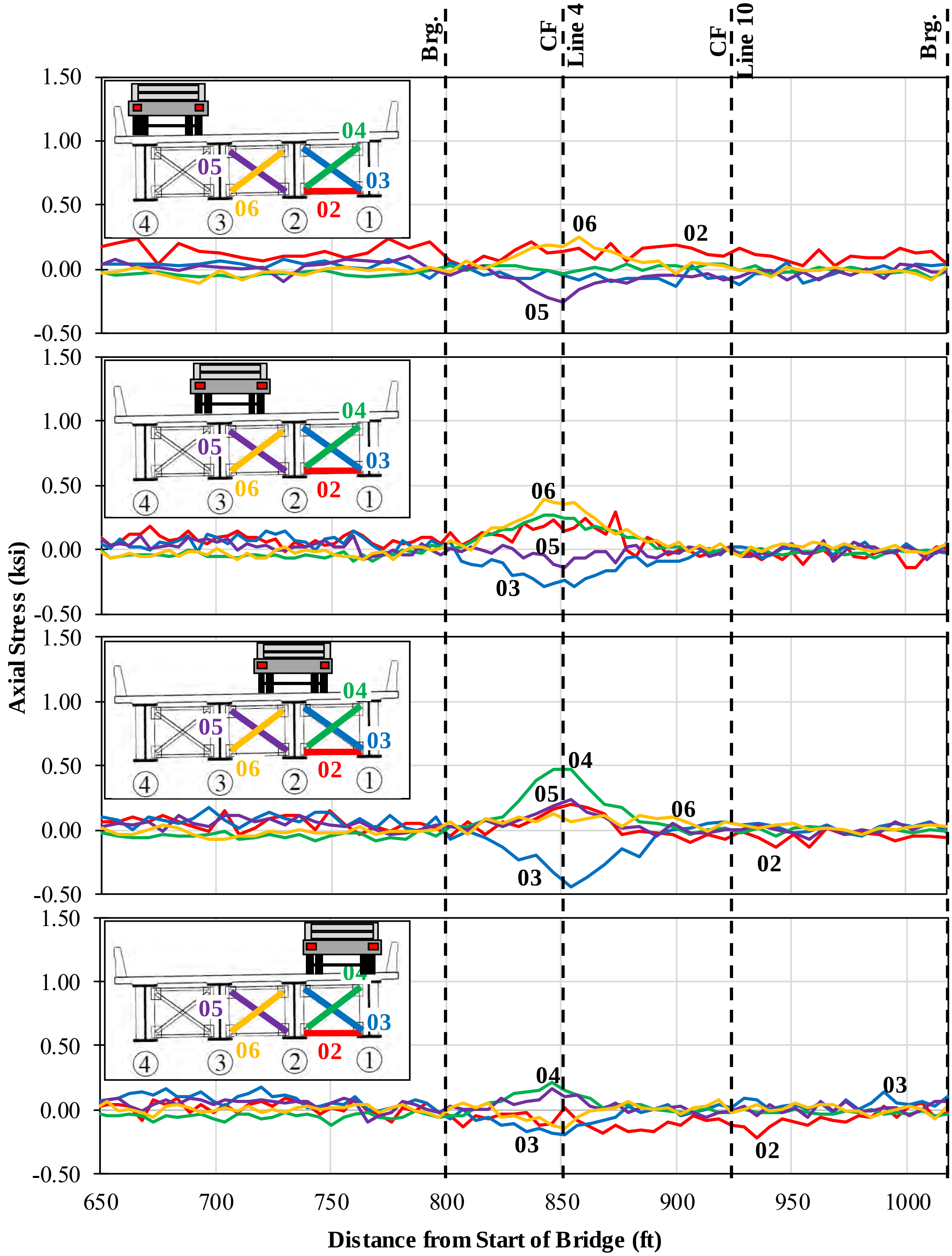

Figure E4-48: Influence line plots for cross-frame axial stresses at cross-frame line 4 between girders 1 and 3 (Load Cases 0A through 0D)

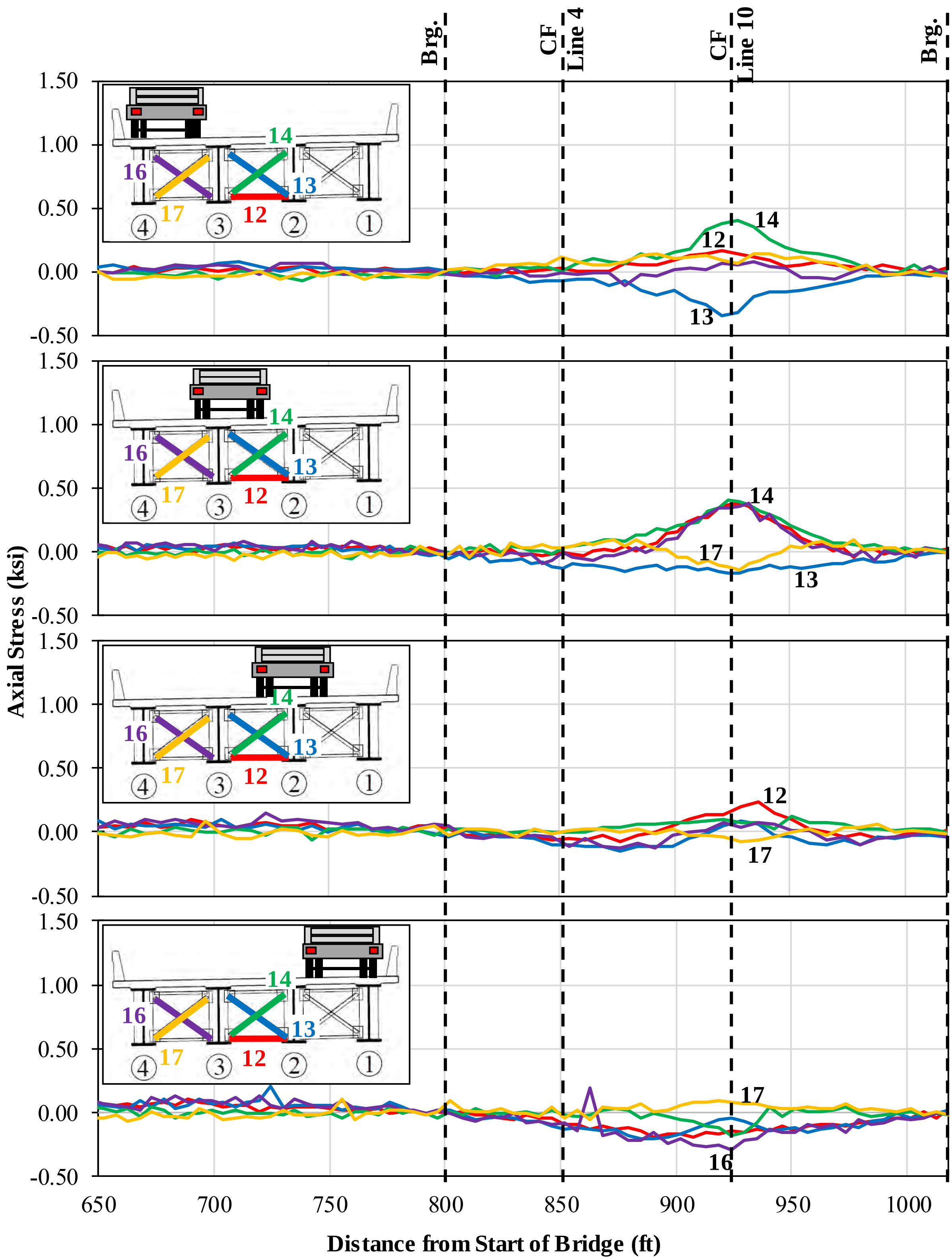

Figure E4-49: Influence line plots for cross-frame axial stresses at cross-frame line 10 between girders 2 and 4 (Load Cases 0A through 0D)

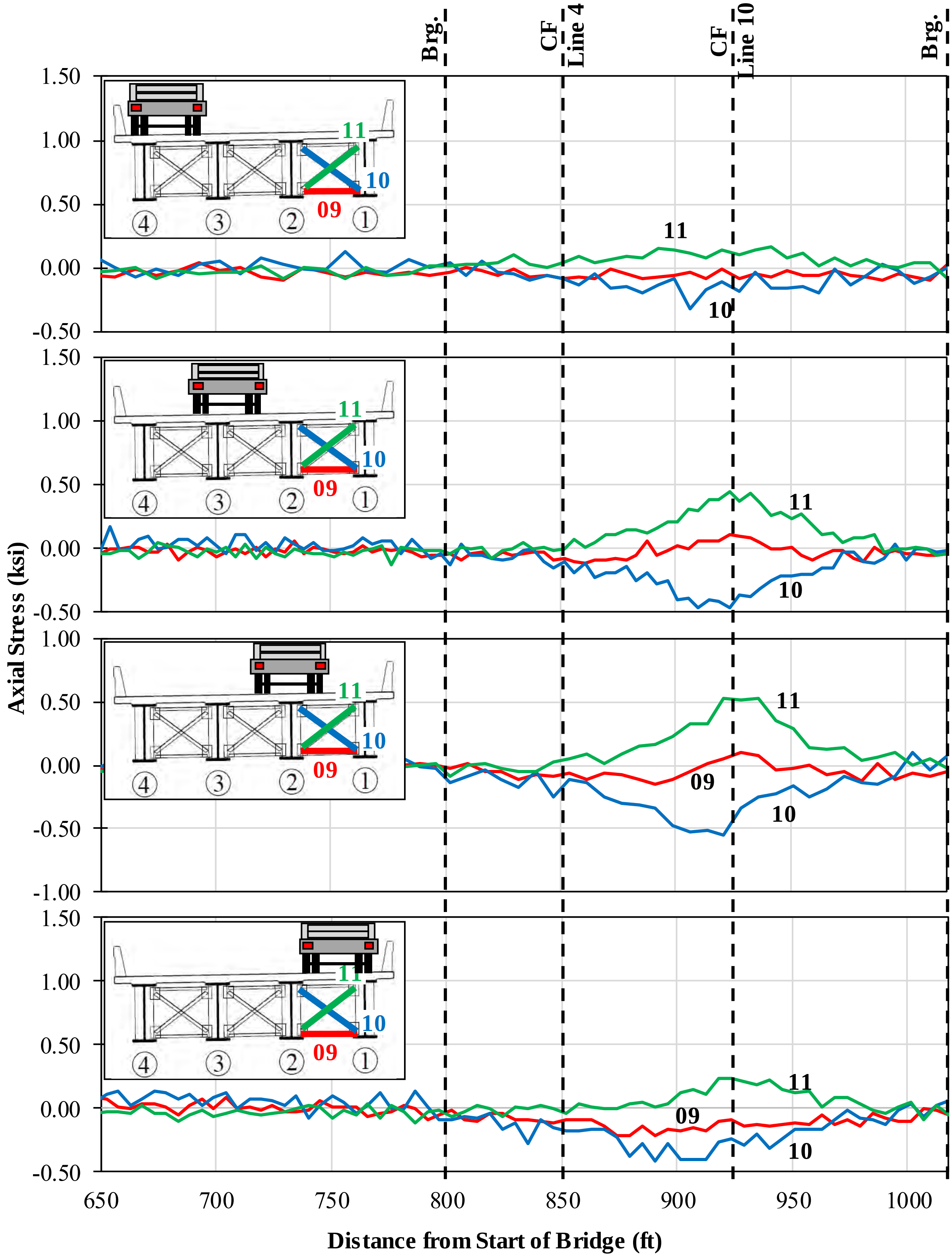

Figure E4-50: Influence line plots for cross-frame axial stresses at cross-frame line 10 between girders 1 and 2 (Load Cases 0A through 0D)

E4.1.5.3 Load Case 1-7 Strain Data for Bridge 3

Similar to the Bridge 1 and 2 live load tests, the primary purpose of Load Cases 1 through 7 is to measure strains in the instrumented members under static loading conditions. Each test truck in Load Cases 1 through 7 was driven and parked one at a time to the designated position, as the DAQ system recorded continuously and captured the stress state after each new truck loaded the bridge. The result is a stepped time-history response of increasing stress, as it was shown in subsection E4.1.3.3. The same procedure applied for Bridge 1 and Bridge 2 data was applied to Bridge 3 data in order to convert the time-history plots into a series of average, static stresses displayed in tabular form.

Table E4-13, Table E4-14, and Table E4-22 summarize results for bottom flange stresses in instrumented girders, lateral bending stresses in instrumented girders, and axial stresses in instrumented cross-frame members, respectively. These static stress tables, along with deflection measurements discussed in the subsequent section, serve as the metric by which the FEA model was validated. In Table E4-13 and Table E4-14, the columns are identified by G#, where # indicates the girder number, and CFL## where ## indicates the cross-frame line (either 4 or 10). Recall that the cross-frame member numbers in Table E4-22 were previously presented in Figure E4-42 and Figure E4-43. An example of cross-frame stresses for Load Case 3 is illustrated in Figure E4-51. This figure visually presents the Load Case 3 row of Table E4-22.

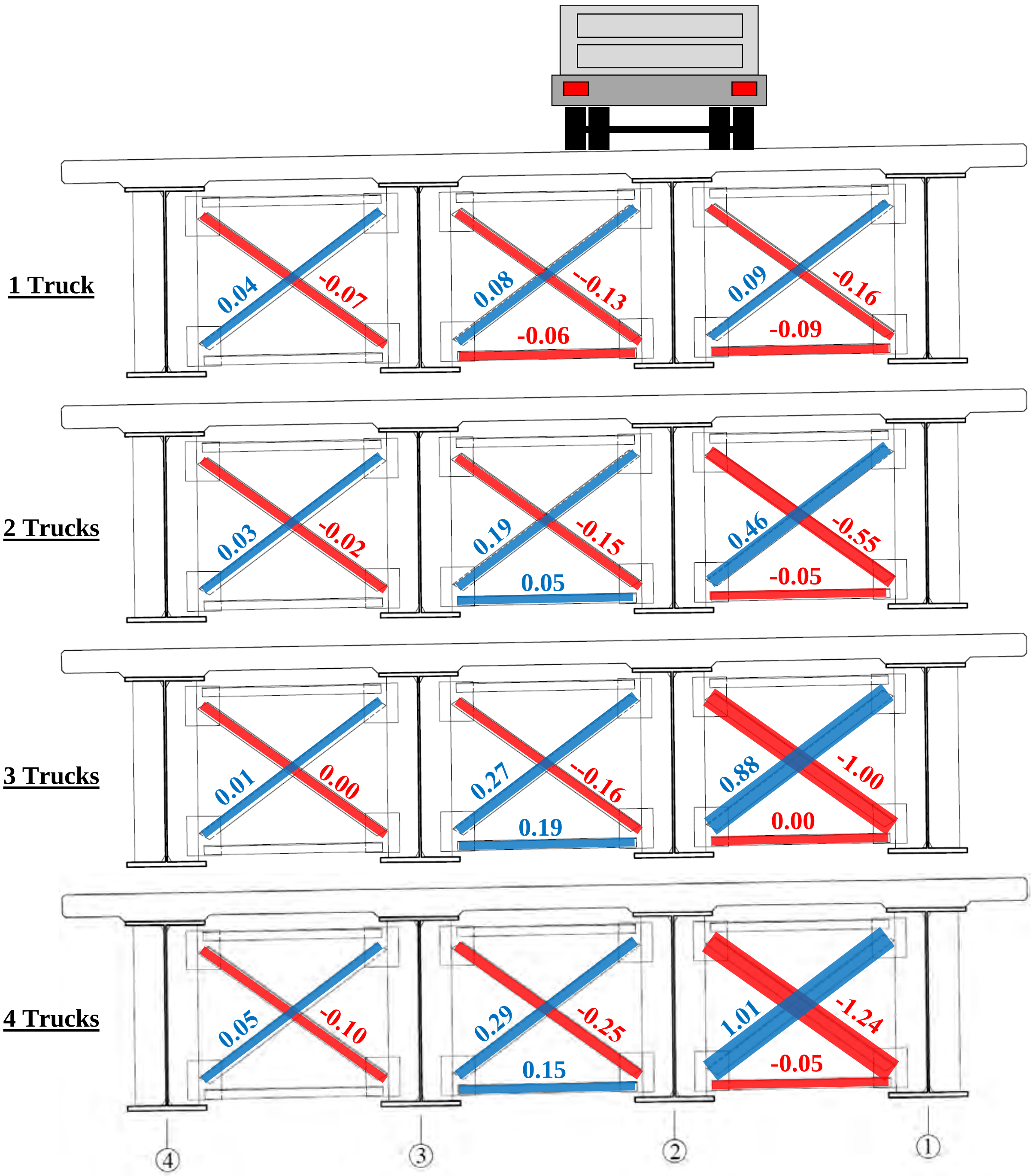

Figure E4-51: Cross-frame stress states at cross-frame line 10 during Load Case 3 (Units: ksi)

Table E4-13: Bottom flange longitudinal stresses in instrumented girders for Load Cases 1-7

Load Case	No. of Trucks	Bottom Flange Bending Stress (ksi)							
		G1 - CFL4	G2 - CFL4	G3 - CFL4	G4 - CFL4	G1 - CFL10	G2 - CFL10	G3 - CFL10	G4 - CFL10
1	1	0.12	0.11	0.06	0.02	0.32	0.45	0.57	0.70
	2	0.32	0.30	0.21	0.12	0.70	1.12	1.53	1.93
	3	0.55	0.56	0.44	0.39	1.15	1.86	2.52	3.13
	4	0.81	0.93	0.86	0.92	1.61	2.42	3.13	3.86
2	1	0.14	0.10	0.01	-0.05	0.62	0.54	0.45	0.41
	2	0.34	0.24	0.09	-0.03	1.41	1.38	1.24	1.09
	3	0.65	0.51	0.26	0.09	2.23	2.26	2.05	1.82
	4	1.04	0.88	0.56	0.41	2.91	2.88	2.56	2.27
3	1	0.10	0.06	-0.02	-0.18	1.00	0.63	0.34	0.10
	2	0.30	0.18	0.01	-0.27	2.29	1.61	0.90	0.23
	3	0.69	0.42	0.08	-0.36	3.71	2.68	1.50	0.33
	4	1.30	0.83	0.25	-0.39	4.62	3.42	1.89	0.35
4	1	0.10	0.02	-0.04	-0.10	1.28	0.67	0.27	-0.17
	2	0.32	0.13	-0.07	-0.24	2.96	1.76	0.71	-0.40
	3	0.74	0.38	-0.04	-0.39	4.67	2.91	1.19	-0.61
	4	1.42	0.80	0.06	-0.65	5.76	3.76	1.51	-0.87
5	1	0.21	0.30	0.35	0.41	0.39	0.57	0.67	0.78
	2	0.40	0.69	0.93	1.25	0.74	0.96	1.10	1.24
	3	0.54	1.06	1.47	1.99	0.97	1.18	1.32	1.46
	4	0.60	1.16	1.61	2.19	1.03	1.23	1.39	1.52
6	1	0.58	0.35	0.06	-0.21	1.23	0.86	-0.21	-0.21
	2	1.47	0.98	0.27	-0.36	2.06	1.42	-0.36	-0.36
	3	2.31	1.57	0.52	-0.49	2.55	1.73	-0.45	-0.45
	4	2.56	1.75	0.58	-0.58	2.67	1.77	-0.49	-0.49
7	1	0.19	0.18	0.11	0.13	0.42	0.69	0.96	1.21
	2	0.42	0.46	0.37	0.36	0.90	1.40	1.89	2.35
	3	0.65	0.58	0.36	0.21	2.64	2.59	2.37	2.14
	4	1.08	0.84	0.38	0.00	4.23	3.72	2.82	1.90

Table E4-14: Bottom flange lateral bending stresses in instrumented girders for Load Cases 1-7

Load Case	No. of Trucks	Bottom Flange Lateral Bending Stress (ksi)							
		G1 - CFL4	G2 - CFL4	G3 - CFL4	G4 - CFL4	G1 - CFL10	G2 - CFL10	G3 - CFL10	G4 - CFL10
1	1	-0.01	-0.01	-0.02	0.06	-0.08	-0.13	-0.31	-0.19
	2	0.00	-0.05	-0.06	0.02	-0.32	-0.37	-0.79	-0.54
	3	-0.06	-0.12	-0.16	-0.17	-0.49	-0.57	-1.25	-0.98
	4	-0.18	-0.27	-0.34	-0.49	-0.64	-0.71	-1.49	-1.24
2	1	0.01	-0.02	0.06	-0.01	-0.11	-0.10	-0.17	-0.14
	2	-0.01	-0.06	0.02	0.00	-0.27	-0.23	-0.48	-0.25
	3	-0.06	-0.11	-0.03	-0.10	-0.49	-0.38	-0.79	-0.48
	4	-0.14	-0.18	-0.14	-0.34	-0.65	-0.45	-0.96	-0.59
3	1	0.00	-0.03	0.00	-0.05	-0.10	0.03	-0.05	0.16
	2	-0.04	-0.06	0.02	-0.04	-0.20	0.03	-0.13	0.32
	3	-0.11	-0.09	0.07	0.05	-0.47	-0.03	-0.22	0.49
	4	-0.16	-0.11	0.07	0.17	-0.56	-0.04	-0.27	0.60
4	1	-0.05	0.00	0.02	0.12	0.10	0.00	0.04	0.21
	2	-0.07	0.01	0.12	0.26	0.13	0.11	0.10	0.56
	3	-0.09	-0.03	0.18	0.42	-0.15	0.08	0.13	0.86
	4	-0.21	-0.02	0.17	0.67	-0.61	0.11	0.20	1.14
5	1	-0.07	-0.09	-0.17	-0.28	-0.15	-0.13	-0.34	-0.30
	2	-0.19	-0.28	-0.52	-0.79	-0.26	-0.25	-0.50	-0.49
	3	-0.31	-0.42	-0.75	-1.21	-0.33	-0.30	-0.60	-0.53
	4	-0.37	-0.46	-0.80	-1.31	-0.36	-0.32	-0.65	-0.55
6	1	-0.06	0.02	0.03	0.26	-0.22	0.07	0.06	0.27
	2	-0.17	0.00	0.09	0.51	-0.34	0.09	0.08	0.46
	3	-0.30	0.05	0.22	0.67	-0.43	0.05	0.10	0.56
	4	-0.38	0.11	0.19	0.79	-0.46	0.13	0.12	0.58
7	1	-0.05	-0.01	0.00	-0.03	-0.30	-0.24	-0.50	-0.33
	2	-0.09	-0.11	-0.13	-0.19	-0.49	-0.46	-0.94	-0.78
	3	-0.14	-0.10	-0.09	-0.07	-0.59	-0.39	-0.85	-0.44
	4	-0.20	-0.11	-0.07	0.11	-0.78	-0.36	-0.82	-0.12

* Positive values indicate that the left side of the bottom flange sees more tension whereas negative values indicate that the right side of the bottom flange sees more tension.

Table E4-15: Axial stresses in instrumented cross-frame members for Load Cases 1-7

Load Case	No. of Trucks	Axial Stress (ksi)												
		CF 2	CF 3	CF 4	CF 5	CF 6	CF 9	CF 10	CF 11	CF 12	CF 13	CF 14	CF 16	CF 17
1	1	-0.01	-0.01	0.00	-0.03	-0.01	0.01	-0.09	0.06	0.03	-0.11	0.09	-0.07	0.15
	2	-0.02	-0.06	0.01	-0.05	0.00	-0.03	-0.17	0.08	0.07	-0.36	0.34	-0.14	0.38
	3	-0.01	-0.11	0.02	-0.11	0.02	-0.07	-0.29	0.17	0.17	-0.64	0.63	-0.14	0.55
	4	0.00	-0.18	0.05	-0.17	0.08	-0.08	-0.40	0.27	0.21	-0.78	0.78	-0.17	0.69
2	1	-0.03	-0.01	0.01	-0.02	0.01	-0.03	-0.15	0.08	0.00	-0.09	0.09	-0.05	0.09
	2	-0.06	-0.04	0.01	-0.04	0.02	0.04	-0.44	0.35	0.26	-0.30	0.45	0.22	0.07
	3	-0.07	-0.08	0.03	-0.08	0.05	0.09	-0.75	0.65	0.52	-0.50	0.81	0.46	0.04
	4	-0.06	-0.21	0.11	-0.11	0.14	0.06	-0.90	0.76	0.57	-0.62	0.94	0.46	0.11
3	1	-0.03	-0.02	0.01	-0.01	0.01	-0.09	-0.16	0.09	-0.06	-0.13	0.08	-0.07	0.04
	2	-0.09	-0.03	0.02	-0.02	0.03	-0.05	-0.55	0.46	0.05	-0.15	0.19	-0.02	0.03
	3	-0.17	-0.04	0.03	-0.05	0.05	0.00	-1.00	0.88	0.19	-0.16	0.27	0.00	0.01
	4	-0.23	-0.14	0.09	-0.07	0.11	-0.05	-1.24	1.01	0.15	-0.25	0.29	-0.10	0.05
4	1	0.00	-0.03	0.00	0.01	0.02	-0.08	-0.15	-0.03	-0.15	-0.15	0.03	-0.12	0.03
	2	-0.07	-0.02	0.01	0.00	0.04	-0.22	-0.47	0.13	-0.30	-0.25	-0.03	-0.35	0.09
	3	-0.20	0.04	0.01	-0.02	0.07	-0.31	-0.84	0.43	-0.39	-0.31	-0.11	-0.56	0.14
	4	-0.32	-0.02	0.02	-0.06	0.11	-0.42	-1.05	0.52	-0.52	-0.46	-0.14	-0.76	0.18
5	1	0.02	-0.06	0.01	-0.03	0.01	-0.11	-0.03	0.09	0.04	-0.13	0.15	-0.06	0.16
	2	0.00	-0.11	-0.01	-0.18	0.15	-0.03	-0.16	0.15	0.05	-0.21	0.23	-0.08	0.26
	3	-0.02	-0.14	-0.02	-0.34	0.31	-0.05	-0.18	0.18	0.05	-0.26	0.27	-0.11	0.31
	4	-0.04	-0.15	-0.01	-0.38	0.35	-0.05	-0.19	0.19	0.05	-0.27	0.28	-0.12	0.33
6	1	-0.13	-0.02	0.00	-0.05	0.05	-0.14	-0.19	0.04	-0.15	-0.17	0.00	-0.19	0.05
	2	-0.19	-0.18	0.12	-0.01	0.02	-0.22	-0.36	0.06	-0.24	-0.28	-0.01	-0.31	0.06
	3	-0.19	-0.36	0.25	0.09	-0.06	-0.27	-0.43	0.09	-0.30	-0.35	-0.02	-0.39	0.06
	4	-0.21	-0.40	0.29	0.11	-0.08	-0.28	-0.46	0.08	-0.32	-0.38	-0.02	-0.42	0.06
7	1	0.00	-0.03	-0.01	-0.04	0.00	-0.04	-0.09	0.02	0.04	-0.28	0.25	-0.08	0.23
	2	0.01	-0.09	0.00	-0.08	0.02	-0.08	-0.17	0.08	0.11	-0.54	0.53	-0.06	0.40
	3	-0.07	-0.08	0.02	-0.08	0.05	-0.17	-0.55	0.34	0.02	-0.61	0.47	-0.25	0.44
	4	-0.17	-0.11	0.03	-0.11	0.08	-0.25	-0.90	0.55	-0.10	-0.70	0.41	-0.45	0.49

Many of the same trends observed in the Load Case 0 data were also observed in the static Load Cases 1 through 7. Again, the same general format of the observations is followed. The bolded text represents the general categories investigated by the RT, and the commentary within that category are specific observations made for this data set.

- **Evaluate load distribution (transverse) and load influence (longitudinal) characteristics on girders.**
  - The transverse distribution of longitudinal girder stresses follows a nearly linear distribution with the outer radius girder 1 receiving a proportionally higher percentage of the load, given the torsional effects and added length of the outer girder. Figure E4-52 and Figure E4-53 demonstrate this phenomenon, which depicts the girder longitudinal and lateral bending stresses at cross-frame lines 10 and 4. For cross-frame line 10, Load Cases 1, 2, 3, 4 and 7 are shown whereas Load Cases 1, 3, 4, 5 and 6 are considered for cross-frame line 4. This figure shows how live loads were distributed through the deck and cross-frames into the girders. Load Cases 1, 2, 3, and 4 represent conditions in which a line of four trucks was centered about cross-frame line 10, positioned two feet from the left barrier, middle of the lane, six feet from the right barrier, and two feet from the right barrier, respectively. Load Cases 5 and 6 are analogous to Load Cases 1 and 4, respectively, but centered about cross-frame line 4. In Load Case 7, two rows of two trucks were located two feet from the left and right barriers, also centered about line 10. A visual depiction of these load cases is included in Table E3-5.

    Interestingly, the load distribution of Load Case 2 was nearly uniform. It is hypothesized that the transverse load application in this load case nearly coincided with the center of rotation of the curved girder system (about the chord of the span). Hence, the torsional effects were negligible, and the load is nearly concentric during this load case.

  - The lateral bending stress distribution in adjacent girders demonstrates that girder 4 along the inner radius of the curve experiences a large range of stress depending on the transverse location of the truck, and girder 1 along the outer radius maintained a nearly consistent stress level, independent of the truck position. This behavior is also presented in Figure E4-52 and Figure E4-53.

    The outer girder maintained a negative lateral flange stress (tension on the right tip), which indicates that the lateral force due to torsion acted outward for all transverse load positions. Lateral stresses on the inner girder switched signs depending on the load position. When the bottom flange of girder 1 was in tension (Load Case 1), the lateral stress was negative and was consistent with the outer girder; thus, the lateral force acted outward. However, when the bottom flange was in compression (Load Case 4), the lateral stress was positive, and the force acted inward of the curve. This behavior is consistent with fundamental concepts of curved beam analysis.

    Additionally, the fascia girders (girders 1 and 4) tended to experience higher lateral stress magnitudes than the interior girders. Note that cross-frames are continuous across interior girders but terminate at fascia girders. It is hypothesized that, at interior girders 2 and 3, there is a continuous load path with the cross-frames passing through the respective girders. At the fascia girders, that load path is disrupted; therefore, any lateral forces acting through the cross-frames must be transmitted to the bottom flange via lateral bending stresses.

- **Compare and evaluate measured girder stress (longitudinal and lateral) and deflections with established design metrics.**
  - The maximum girder stresses measured at cross-frame line 10 were higher than the maximum girder stresses measured at cross-frame line 4 for all load cases except for Load Case 5 and Load Case 6 where the trucks were centered longitudinally about line 4.
  - The maximum measured bottom flange lateral stresses were the highest of all three subject bridges, which was anticipated for a curved girder system. Curved girders develop torsional forces acting radially along the arc of the girder due to applied vertical loads, which is resisted by cross-frames and lateral bending the flanges. Those lateral flange stresses are greatly affected by the spacing of cross-frames and diaphragms.
- **Evaluate load distribution (transverse) and load influence (longitudinal) characteristics on cross-frames.**
  - Similar to the Load Case 0 results, cross-frame stresses were highly sensitive to the transverse position of the truck, as is demonstrated by the stress reversal in members from one load case to another.
  - Load influence effects are not applicable to Load Cases 1 through 7. Refer to Section E4.1.4.2 for more information regarding longitudinal load influence.
- **Compare and evaluate measured cross-frame stress with established design metrics.**
  - In all cross-frame members, measured axial stresses were less than the CAFL of 2.6 ksi
  - Maximum girder stresses were generally higher than the maximum axial stresses in the cross-frame members for equivalent load cases. This indicates that large cross-frame forces are not developed despite relatively large differential deflections and twist of the adjacent curved girders. A likely reason for this trend is the relatively close spacing of cross-frames used for Bridge 3 (approximately 12.75 feet along radial length).
- **Understanding complex load paths based on unique characteristics of the measured data.**
  - Torsional effects on the system are clearly observed in the data. Consequently, lateral warping stresses on the girder flanges are significant, and the distribution of live loads to the girders is disproportionate. These complex load path effects were studied further during the parametric study phase (Appendix F).

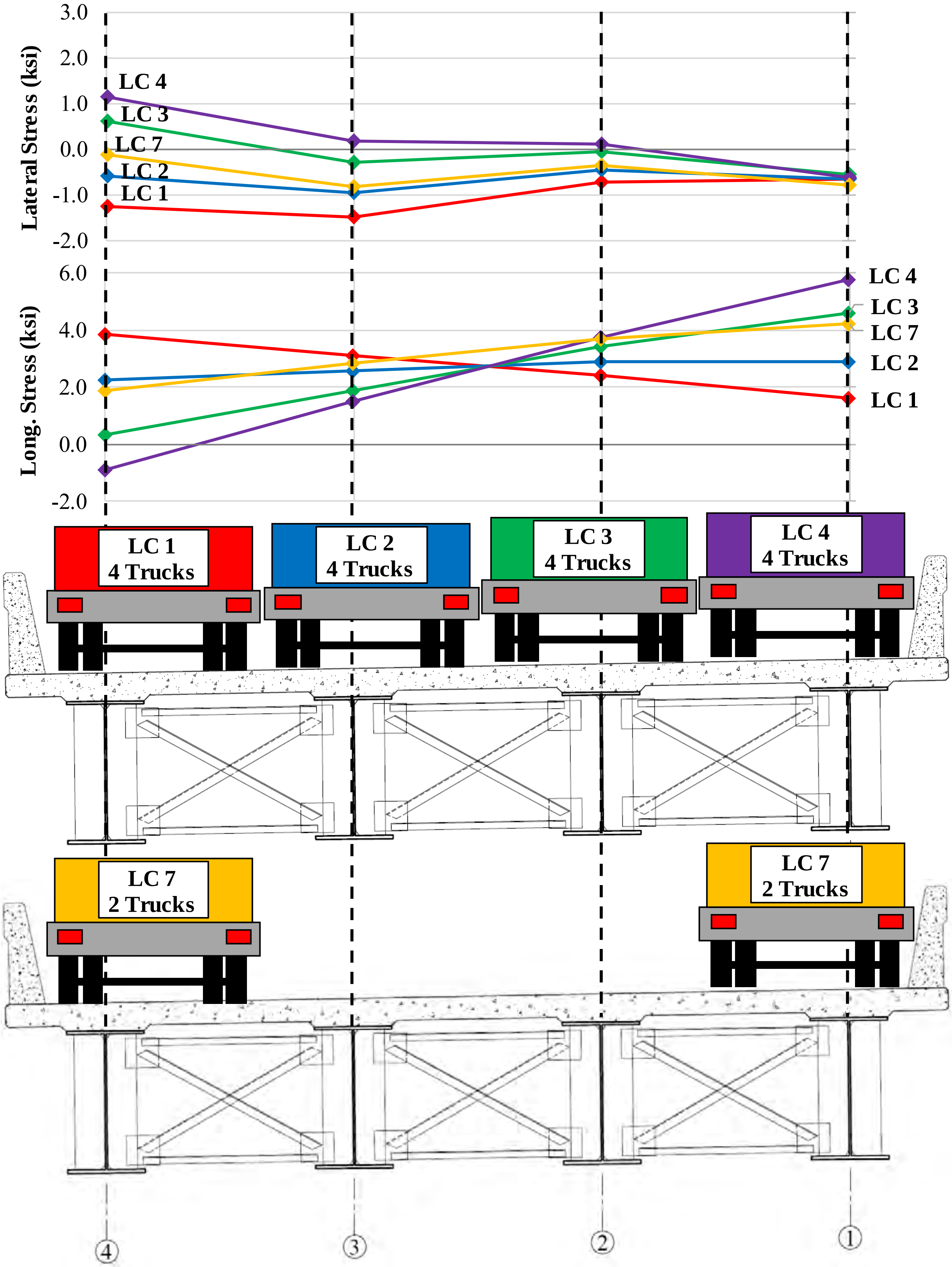

Figure E4-52: Distribution of girder bending stresses on instrumented girders along cross-frame line 10 for Load Cases 1, 2, 3, 4 and 7.

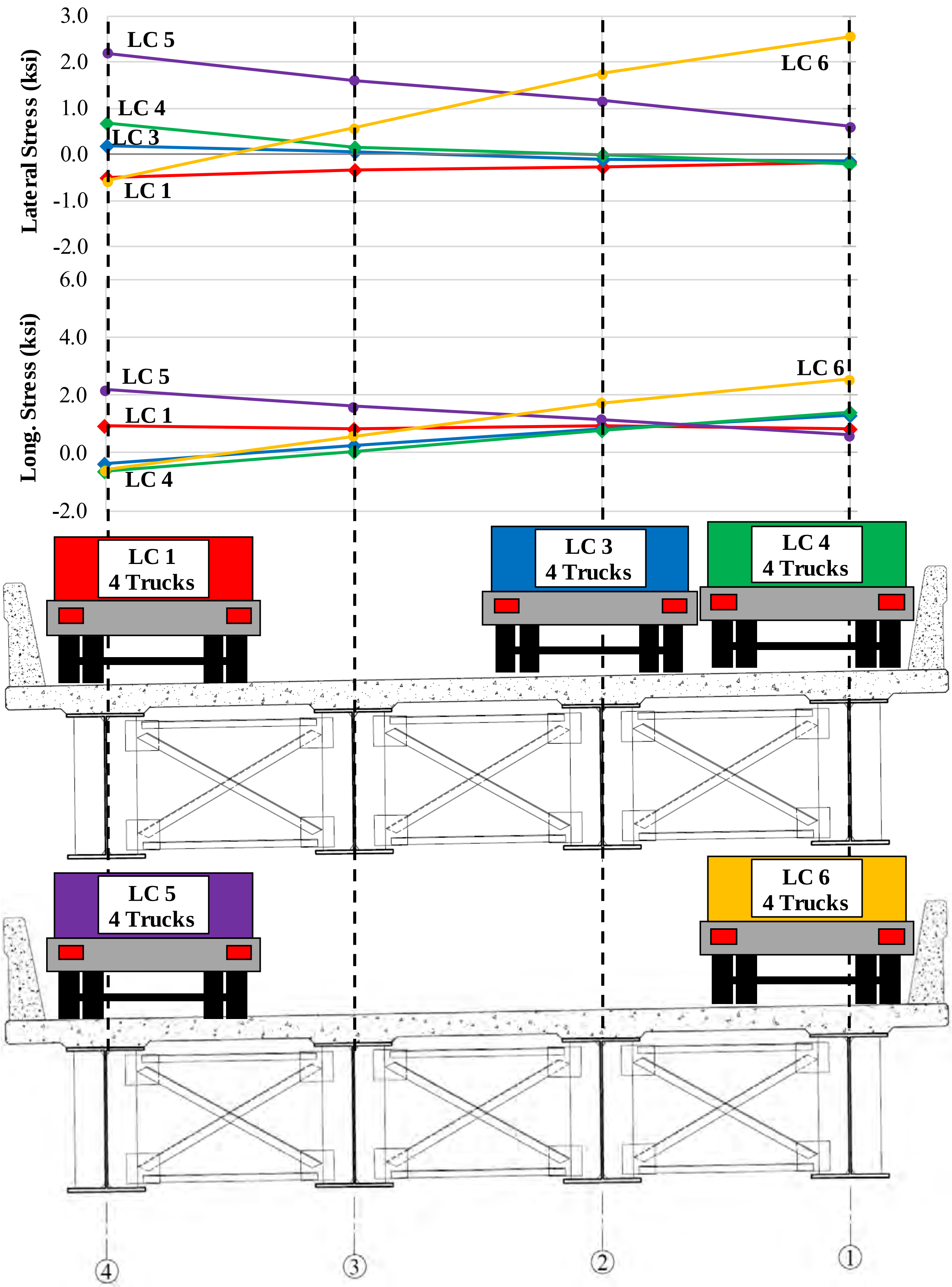

Figure E4-53: Distribution of girder bending stresses on instrumented girders along cross-frame line 4 for Load Cases 1, 3, 4, 5 and 6.

E4.1.5.4 Deflection Data for Bridge 3

Laser distance meter readings were taken after each truck was positioned on the bridge during each of the seven static load cases. As discussed previously, girder stresses were measured at cross-frame line 10; but due to ground accessibility beneath the bridge, deflections were measured at cross-frame line 11. The center of the bottom flange of all four girders were used as reference points. Table E4-16 summarizes those deflection measurements.

Table E4-16: Girder deflection measurements for Load Cases 1-7 at cross-frame line 11

Load Case	No. of Trucks	Vertical Deflections (in)			
		Girder 4	Girder 3	Girder 2	Girder 1
1	1	-0.22	-0.21	-0.08	-0.07
	2	-0.47	-0.31	-0.25	-0.18
	3	-0.68	-0.55	-0.34	-0.26
	4	-0.88	-0.71	-0.49	-0.35
2	1	-0.13	-0.16	-0.05	-0.21
	2	-0.29	-0.35	-0.33	-0.43
	3	-0.46	-0.56	-0.58	-0.66
	4	-0.62	-0.73	-0.79	-0.87
3	1	-0.04	-0.12	-0.25	-0.30
	2	-0.13	-0.34	-0.54	-0.70
	3	-0.24	-0.54	-0.87	-1.08
	4	-0.31	-0.72	-1.17	-1.50
4	1	-0.03	-0.14	-0.29	-0.39
	2	-0.08	-0.35	-0.63	-0.91
	3	-0.14	-0.55	-0.98	-1.44
	4	-0.20	-0.72	-1.36	-1.92
5	1	-0.18	-0.22	-0.10	-0.12
	2	-0.31	-0.33	-0.22	-0.17
	3	-0.38	-0.37	-0.26	-0.21
	4	-0.42	-0.39	-0.28	-0.22
6	1	-0.07	-0.21	-0.33	-0.50
	2	-0.09	-0.41	-0.60	-0.85
	3	-0.13	-0.50	-0.75	-1.10
	4	-0.13	-0.54	-0.83	-1.17
7	1	-0.21	-0.22	-0.10	-0.05
	2	-0.43	-0.39	-0.28	-0.17
	3	-0.50	-0.58	-0.64	-0.68
	4	-0.54	-0.77	-1.00	-1.23

Note that baseline deflection measurements of the bridge in an unloaded state were taken before each load case to account for temperature changes that might impact the vertical position of the girders. For Bridges 1 and 2, baseline measurements were taken only once at the start of the test. This procedure was modified for Bridge 3 because the test was conducted throughout the morning, instead of in the middle of the night. The temperature fluctuations between 8 am and 12 pm, when the test was performed, are typically significant, especially in July in Texas. As a means to zero out any thermal-related displacements, the RT measured baseline readings before Load Cases 1 through 7, which are summarized in Table E4-16. The measured deflections in the table reflect the different baseline readings that were taken for each load case.

Figure E4-54 and Figure E4-55 graphically show deflection measurements for Load Cases 1 through 7 as trucks were individually placed on the bridge. Four different measurements are plotted for each location, as each measurement corresponds to a new dump truck placed on the bridge. The specific loading increment is labeled on each plot as "#-##" where "#" indicates the Load Case and "##" refers to the number of trucks positioned on the deck.

From the results of the displacement study, several observations with regards to the curved bridge can be made. Again, the same general format of the observations is followed. The bolded text represents the general categories investigated by the RT, and the commentary within that category are specific observations made for this data set.

- **Evaluate load distribution (transverse) and load influence (longitudinal) characteristics on girders.**
    - The deck exhibits a nearly linear transverse behavior for deflections for all load cases, which is similar to the stress results outlined in Section E4.1.5.3 However, girder 1 deflected nearly twice as much during Load Case 4 (truck above girder 1) as girder 4 deflected during Load Case 1 (truck above girder 4). For a curved girder system, this is a logical trend. This behavior is similar to what was observed for the stress measurements. The torsional response of the curved system and the added length of the outer girder results in much larger displacements near the outer portion of the curve.
    - Second, the deflections are virtually the same for Load Case 2. In this case, the centroid of the load application was approximately the same as the line in which the curved system rotated. Hence, significant torsional response in the girder system did not occur for this load position. Differential deflections between adjacent girders are not significant, and thus cross-frame forces are relatively small.
    - Lastly, Load Case 6 shows significant deflections even though the load was applied over cross-frame line 4, almost 90 feet from the cross-frame line where deflections were measured.
    - Load influence effects are not applicable to deflection measurements. Refer to Section E4.1.3.2 for more information regarding longitudinal load influence.
- **Compare and evaluate measured girder stress (longitudinal and lateral) and deflections with established design metrics.**
    - Maximum deflections measured during this study correspond to a deflection-to-span ratio of nearly L/1350, which is comparable to what was measured at Bridge 1. This makes sense, given the span-to-depth ratios are similar for these two bridges.
- **Understanding complex load paths based on unique characteristics of the measured data.**
    - The deflection results from the static load cases are consistent with the girder stress results. The curved geometry of the bridge had a significant influence on the girder response to various transverse load positions.

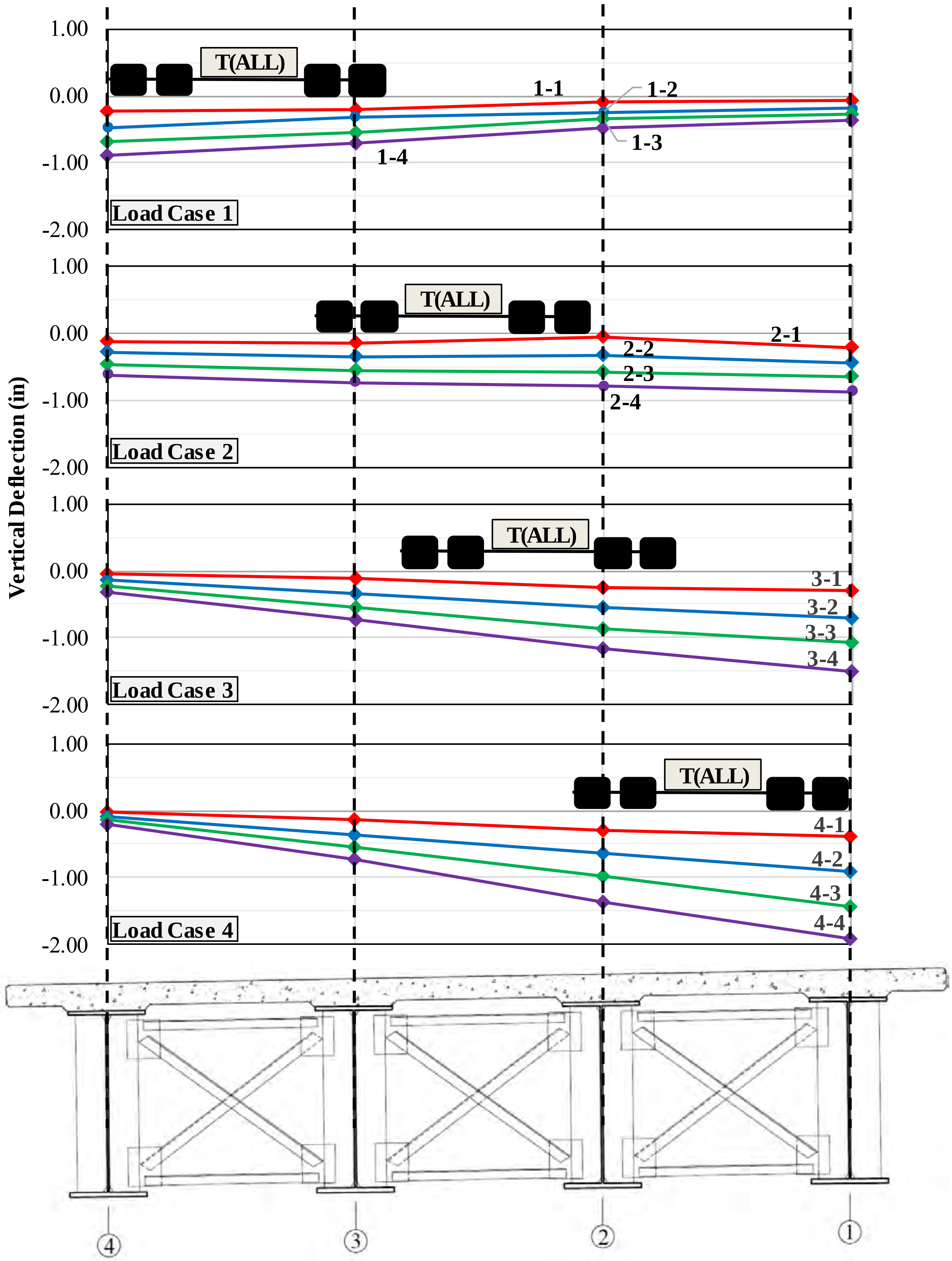

Figure E4-54: Girder deflection progression at cross-frame line 11 for Load Cases 1-4

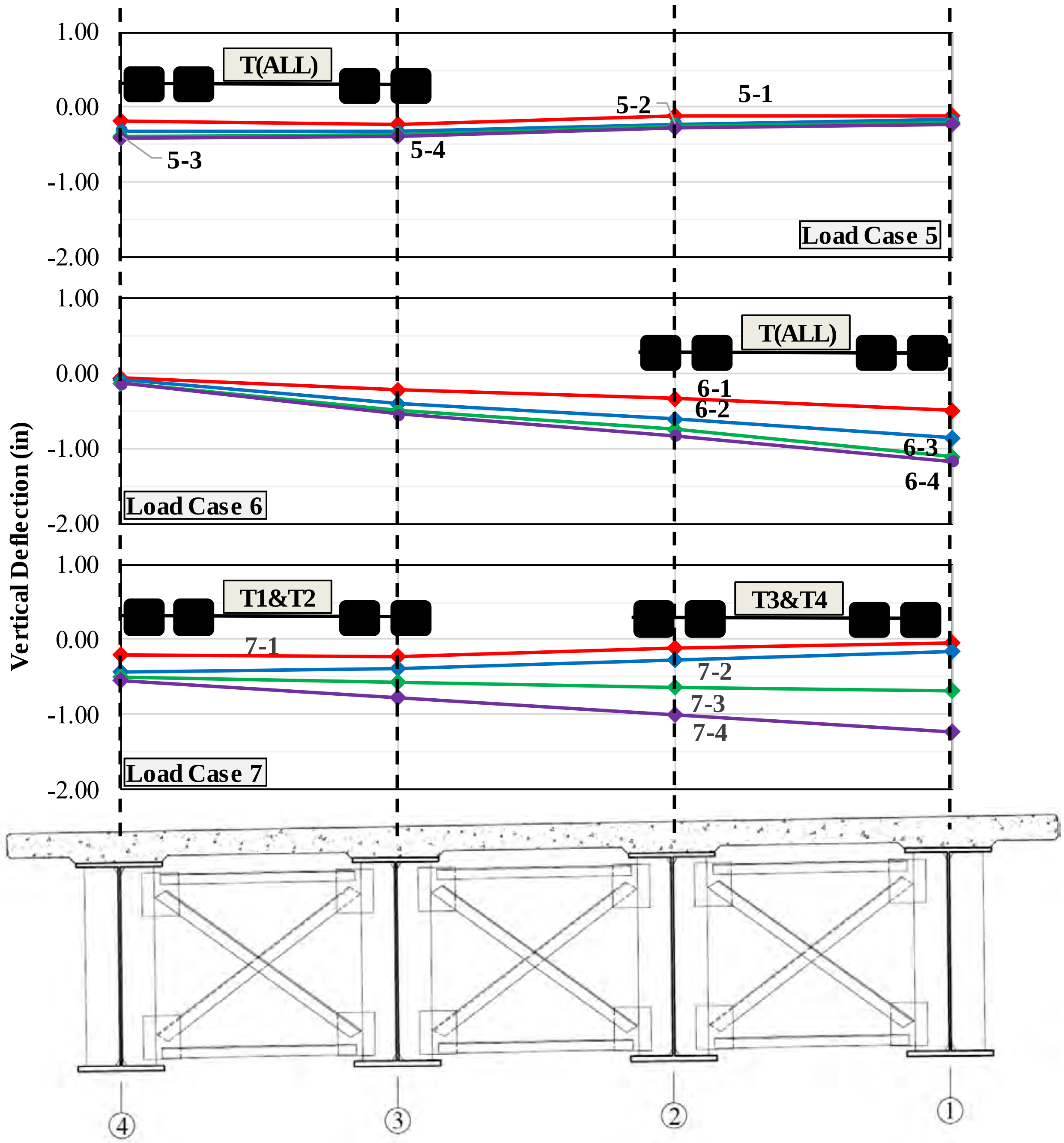

Figure E4-55: Girder deflection progression at cross-frame line 11 for Load Cases 5-7

E4.1.6 Comparison of Results

In this section, the results obtained during the live load test for each instrumented bridge are compared. Table E4-17 presents a summary of the stress and deflection measurements obtained for moving Load Case 0 and static Load Cases 1 through 7. Namely, the maximum and minimum stress ranges measured (longitudinal and lateral bending stress in instrumented girder flanges and axial stresses in instrumented cross-frames), maximum deflections, and important geometric properties of the instrumented span are tabulated.

As outlined above, the objective of the live load tests, aside from facilitating the validation of FEA models, is to make generalized observations about the response characteristics of cross-frames and girders in straight, skewed, and horizontally curved bridges based on the measured data. To organize the commentary on the results, the same outline introduced in Section E4.1.3.2 is used, which is represented by bolded text. The text below each bolded category lists the unique aspects and observations of each bridge.

Table E4-17: Comparison of live load test results

	Measurement (ksi, unless noted)	Bridge No.		
		1 (Straight)	2 (Skewed)	3 (Curved)
	Instrumented Span-to-Depth Ratio	32	25	27
LC 0	Longitudinal Flange Stress Range {min, max}	{-0.64, 2.43}	{-0.52, 0.94}	{-1.02, 1.91}
LC 0	Cross-Frame Stress Range {min, max}	{-0.84, 1.38}	{-0.41, 1.04}	{-0.53, 0.55}
LC 1-7	Longitudinal Flange Stress Range {min, max}	{-0.51, 5.67}	{-0.12, 1.32}	{-0.87, 5.76}
LC 1-7	Lateral Flange Stress Range {min, max}	{-0.89, 0.83}	{-0.51, 0.67}	{-1.49, 1.14}
LC 1-7	Cross-Frame Stress Range {min, max}	{-1.36, 2.68}	{-1.29, 1.93}	{-1.24, 1.01}
LC 1-7	Max Deflection (in)	1.48	0.29	1.92
LC 1-7	Max Deflection-to-Span Ratio	L/1573	L/5172	L/1350

- **Evaluate load distribution (transverse) and load influence (longitudinal) characteristics on girders.**
  - Although not explicitly addressed in Table E4-17, the lateral distribution of live loads to the girders was nearly linear for all three bridges. The measured data suggests that the composite deck and cross-frames generally provides ample stiffness in the transverse direction for these three bridges. In fact, AASHTO design criteria for distribution factors were consistently conservative when compared to the measured data.
  - As observed in Table E4-17, the highest negative bending moments (compressive bottom flange stresses) were measured at Bridge 3. The influence line plots for this curved bridge demonstrated that girder stresses in the instrumented span were influenced by loads two spans away. Bridges 1 and 2 showed significant load influence in the span closest to the instrumented span only.
- **Compare and evaluate measured girder stress (longitudinal and lateral) and deflections with established design metrics.**
  - The maximum longitudinal girder stresses measured in Bridges 1 and 3 far exceeded the maximum stresses in Bridge 2. Girder stresses are largely a function of the span-to-depth

ratio, and the girder depth at Bridge 2 is high relative to its span length. Plus, Bridge 2 is a highly redundant system with twelve girders supporting the deck, which offers more opportunity for transverse load distribution between the girders. The length of the instrumented span for Bridge 2 is also considerably lower than Bridges 1 and 3.

- The maximum bottom flange lateral stresses measured at Bridge 3 were nearly double of what was measured at the other two bridges. As discussed in Section E4.1.5.3, curved girders are prone to torsional forces acting radially on the bottom flanges. Therefore, it is not surprising to see the most significant lateral flange stresses at the Bridge 3. Bridge 2, on the other hand, experienced the least amount of lateral flange stress; the torsional stiffness of the full deck unit is comparatively high for the skewed bridge due to its 96-foot width.
- Maximum vertical deflections were measured at the outer girder of Bridge 3. Bridge 2, on the other hand, experienced the smallest vertical deflections under its static live load cases. Again, the trend is best explained by the span-to-depth ratios of the instrumented spans.

- **Evaluate load distribution (transverse) and load influence (longitudinal) characteristics on cross-frames.**
  - Although not explicitly addressed in Table E4-17, the transverse and longitudinal distribution of live loads to cross-frame elements was significantly localized when compared to load distribution to the girders. At all three bridges, the influence line plots for cross-frame members showed that only live loads in close proximity induced significant stresses in a given cross-frame member. In most cases, stress reversal was negligible when trucks maintained a consistent transverse position. Stress reversal, however, was significant when trucks were moved from one lane to another.
- **Compare and evaluate measured cross-frame stress with established design metrics.**
  - Cross-frame forces are induced when adjacent girders differentially deflect and/or twist when subjected to live loads. Thus, maximum cross-frame stresses are expected when girder deflections and twist are also maximized; traditionally, cross-frames in skewed and curved system are more prone to large load-induced stresses for these reasons. Based on the results summarized in Table E4-17, the largest cross-frame stresses measured during the live load tests were surprisingly at straight Bridge 1, and the smallest at curved Bridge 3. At first glance, this appears counterintuitive given that cross-frames are considered primary members in curved bridges. Bridge 2 cross-frame stresses are relatively small, but that is likely a function of the substantial bridge stiffness and shorter span. Given a comparable bridge span as the other bridges, the RT would expect the cross-frame forces to be the highest in a highly skewed bridge. These effects were studied in greater detail during Phase III of the project (Appendix F).
- **Understanding complex load paths based on unique characteristics of the measured data.**
  - Although helpful for validating the FEA models, the instrumentation performed at each bridge is still not an all-encompassing study. Strain gages and vertical deflections at discrete points only provide a snapshot of the bridge response. Many of the observations provided in this section were inferred by the RT based on engineering judgment and experience of processing measured data. This is especially true for more complex structures such as Bridge 2 and 3. Note that the parametric studies in Phase III provided better insight on how girders and cross-frames in straight, skewed, and curved bridges respond when subjected to live loads.

E4.2 In-Service Rainflow Data

E4.2.1 Overview of Collected Data

As previously mentioned in this appendix, in-service monitoring was performed at each bridge for approximately four weeks. Simplified rainflow counting techniques, developed by Downing and Socie (1982), were used to convert continuous strain history into a histogram of stress cycle counts. Stress histograms allow the RT to evaluate hours of time histories in a simple, condensed plot. This section of the appendix evaluates stress histograms for the instrumented components of the three subject bridges.

The histograms developed represent a spectrum of stress range measurements. These plots indicate (i) the number of truck events causing a significant stress cycle and (ii) the stress cycle magnitudes that a structural component typically experiences. The four-week monitoring period is sufficiently long to capture stabilized data as well as hourly, daily, and weekly trends that may deviate from normal or average conditions. Monitoring beyond four weeks has the possibility of improving the high tail of the stress spectrum, which are likely stress cycles due to overload or permit vehicles. However, these cycles are generally too infrequent to contribute significantly to the measured fatigue response (Connor and Fisher 2006).

In addition, three supplementary metrics derived from the histogram plots were used by the RT to compare data between the various instrumented components of the different bridges. These three metrics are:

- Effective stress range (S_{re}),
- Maximum stress range (S_{rm}), and
- Index stress range (S_{ri}).

Each of these three stress range metrics can be derived from simple post-processing of the histogram data. All three are effective tools for evaluating the fatigue performance of structural components and details. Effective and maximum stress ranges are defined in the current 9th Edition AASHTO LRFD Specifications (2020). Index stress range was a metric developed by Fasl (2013) and is not currently adopted by standard codes. The following subsections cover each of these metrics in a more detailed manner.

E4.2.1.1 Effective Stress Range Calculation

The effective stress range is a singular value that mathematically represents the response of a bridge component to the entire truck population. Fatigue damage to a bridge component, in reality, accumulates with many variable-amplitude cycles at non-uniform time intervals. The effective stress range relates the damage caused by those variable-amplitude stress cycles to a constant-amplitude stress cycle of equal cycle count. In terms of the measured histogram plots, the effective stress calculation essentially converts the full spectrum of stress bin counts to a singular bin of constant amplitude by relating accumulated damage (Figure E4-56).

It is commonly accepted that fatigue resistance above the CAFL, in terms of cycles, is inversely proportional to the cube of the stress range magnitude. This relationship is the basis of the stress-based, constant-amplitude approach for fatigue resistance (S-N curves) adopted by AASHTO LRFD and can be used to establish an equation for the effective stress range of a measured spectrum. This relationship is shown by the following expression:

$$N_f = \frac{A}{{S_r}^3} \qquad E4.1$$

where: N_f = number of cycles at constant-amplitude stress range, S_r, until failure; A = fatigue detail category constant per AASHTO LRFD (ksi^3); and S_r = constant-amplitude stress range magnitude (ksi).

Palmgren-Miner's rule (Miner 1945) is a cumulative damage theory used in AASHTO and is adopted by the RT for purposes of computing effective stress ranges of measured rainflow data. The following expression demonstrates that damage is the summation of all cycles of varying amplitude and that larger magnitudes produce proportionally higher damage than smaller magnitudes:

$$D = \sum_{j=1}^{k} \frac{n_j}{N_{f,j}} \qquad E4.2$$

where: D = damage accumulation index; n_j = number of cycles measured within j^{th} stress range, $S_{r,j}$ (stress range spectrum); and $N_{f,j}$ = number of cycles at j^{th} stress range, $S_{r,j}$, that would initiate failure.

In combining these expressions, the damage from the spectrum of variable-amplitude stress ranges (D_{var}) must be equal to the damage from a constant-amplitude cycle at the effective stress range (D_{con}). The effective stress range can be determined by setting these two entities equal. This relationship is demonstrated by the progression of the following expressions:

$$D_{var} = D_{con} \qquad E4.3$$

$$\sum_{j=1}^{k} \left[\frac{n_j}{\left(\frac{A}{S_{r,j}{}^3} \right)} \right] = \frac{N_m}{\left(\frac{A}{S_{re}{}^3} \right)} \qquad E4.4$$

$$S_{re} = \left(\sum_{j=1}^{k} \left(\frac{n_j}{N_m} \right) S_{r,j}{}^3 \right)^{1/3} \qquad E4.5$$

where: D_{var} = damage accumulation index related to variable-amplitude stress range spectrum, $S_{r,j}$; D_{con} = damage accumulation index related to constant-amplitude stress range at effective stress range, S_{re}; and N_m = total number of cycles measured

Figure E4-56 depicts this calculation graphically. A sample histogram of a cross-frame member at Bridge 2 presents the variable-amplitude stress range spectrum recorded at a cross-frame member for the entire monitoring period. This is presented on the left plot. The right plot depicts the histogram once all cycles are converted to a constant-amplitude cycle with its magnitude equivalent to the effective stress range. Note that the damage accumulated is equal for both the left and right sides of Figure E4-56. The stress range spectrum was truncated at 0.65 ksi. A detailed discussion of the truncating process and the bin size selection is provided in Section E4.2.2.1.

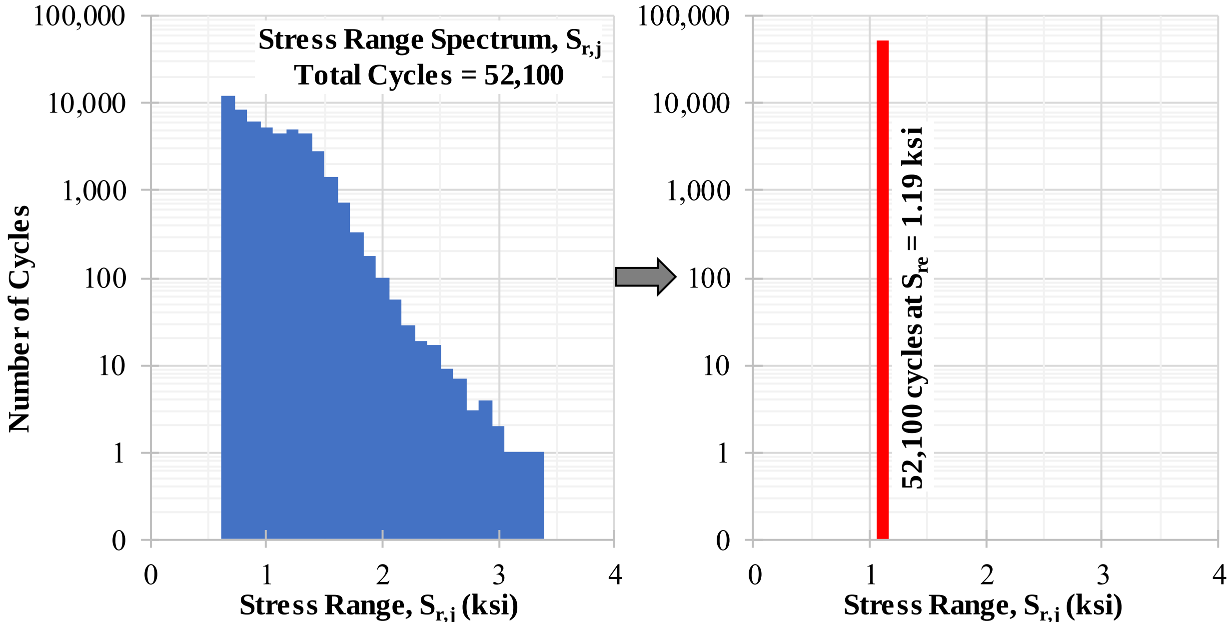

Figure E4-56: Graphical depiction of converting variable stress range spectrum to single effective stress range

E4.2.1.2 Maximum Stress Range Calculation

Similar to the effective stress range metric, the maximum stress range metric is rooted in AASHTO LRFD fatigue design criteria for both resistances and loads. In terms of fatigue resistance, a detail is considered to possess infinite life if less than 1-in-10,000 stress cycles exceed the CAFL of that fatigue detail. In other words, stress ranges with a probability of exceedance less than 1-in-10,000 (with respect to the CAFL) can be omitted when evaluating infinite life on a detail, given its infrequency.

Similarly, fatigue load factors for the infinite life (Fatigue I) and finite life (Fatigue II) limit states were recently calibrated based on a study of millions of weigh-in-motion (WIM) data points across the United States (Modjeski and Masters 2015). Through parametric studies on a simple line-girder model, the researchers determined appropriate load factors for the AASHTO HS-20 design truck to reflect the current state of the US truck population. Note that cross-frames were not considered in any way in the development of these load factors; these factors were calibrated strictly for bending moments in longitudinal girders.

In the development of analytical models, the respective low and high tails of the WIM data set were filtered as it was assumed that these occurrences are too infrequent to impact fatigue behavior. For the low tail, the data set excluded trucks with gross vehicles weights (GVW) less than 20 kips. For the high tail, truck effects in the upper 99.99th percentile were eliminated, which is similar to what was discussed above, except that the 0.01% probability of exceedance is independent of the CAFL stress.

In order to properly compare the AASHTO design criteria and the measured data, a consistent set of filtering assumptions was adopted. For purposes of evaluating AASHTO resistances, the RT assessed the maximum measured stress range with respect to the detail CAFL. For purposes of evaluating AASHTO loading criteria, the RT elected to evaluate the maximum stress range similar to the approach used to calibrate the fatigue load factors (the 99.99th percentile stress range). Approaching the problem this way allowed the RT to assess the frequency of overload or permit load cases. The measured data at each subject bridge provided several outliers for various instrumented cross-frame and girder flanges. These outlier stress cycles were likely a result of a heavy overload or permit vehicle, which would have been intentionally eliminated in the development of the AASHTO LRFD 9th Edition fatigue load factors. Note that the low tail of the stress range spectrum is addressed in Section E4.2.2.1.

The RT determined the 99.99th percentile maximum by first converting the stress histograms into an empirical cumulative density function (CDF) plot. The empirical CDF plot shows the percentage of counts for each stress bin compared to the total number of counts, summing to one. Stress cycles within bins that exceed 0.9999 of the empirical CDF were neglected from the spectrum. The 99.99th percentile maximum is then the threshold stress bin in which the empirical CDF exceeds 0.9999. Figure E4-57 shows a sample of this calculation for a different cross-frame member at Bridge 2. The top graph represents the full empirical CDF of the stress range spectrum. Note that most of the stress cycles occur at lower stress values; in this example, nearly 70% of the total recorded stress cycles were below 1.2 ksi in magnitude. The bottom plot zooms in on the upper tail of the CDF plot. The absolute maximum stress range recorded at this cross-frame member was 4.58 ksi. However, the empirical CDF plot exceeds 0.9999 at 3.77 ksi, meaning that any stress cycles above that threshold have less than a 1-in-10,000 chance of occurrence and are therefore truncated from the spectrum. For simplicity, the 99.99th percentile stress range is referred to as simply the maximum stress range for the remainder of the appendix. For the example above, the maximum stress range is 3.77 ksi.

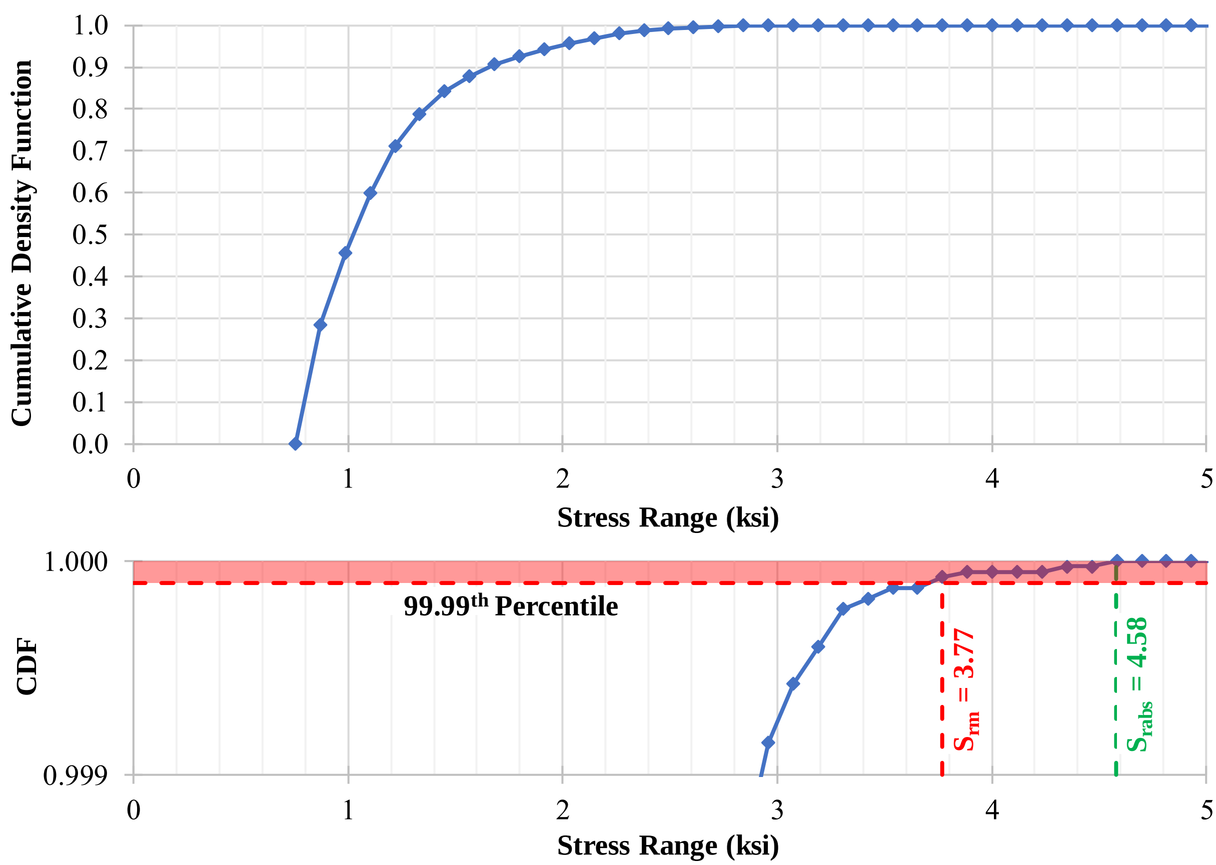

Figure E4-57: Sample cumulative density function depicting absolute maximum stress range and 99.99th percentile stress range

E4.2.1.3 Index Stress Range Calculation

Developed by Fasl (2013), the index stress range is an offset of the effective stress range. The effective stress range provides the engineer with a singular value to characterize a spectrum of measured stress cycles but lacks the inherent ability to characterize the frequency at which these stress cycles occur over time.

The index stress range facilitates comparisons between instrumentation locations, bridges, and even time-dependent trends by normalizing damage at each location of interest. The location of interest can be different components of the bridges such as girder flanges versus cross frame members.

A hypothetical example best demonstrates the differences in these metrics. This example focuses on two cross-frame members identified as members A and B. Cross-frame member A recorded 1,000 total cycles during a given monitoring period and yielded an effective stress range of 1.0 ksi based on the corresponding rainflow histogram. Cross-frame member B recorded 10,000 total cycles during the same monitoring period and had the same effective stress range of 1.0 ksi. In terms of the effective stress range metric, both of these members are considered equal. However, in terms of damage accumulation, cross-frame member B is a more severe case because it experienced ten times more stress cycles than member A. By normalizing the damage, the index stress range yields a relative sense of both the stress magnitudes and the frequency of occurrence. The index stress range allows a meaningful comparison to be made considering instrumentation locations, bridges, and even hourly and daily trends.

The measured stress range spectrum is normalized to the same index stress range, which is selected by the engineer. The mathematical procedure is similar to the steps performed in converting the stress range spectrum to an effective stress range in Eq. E4.5. The exception is that instead of solving directly for stress, the engineer establishes an index stress range and solves for the total number of cycles. This is demonstrated with the following expression, which is simply a rearranged form of Eq. E4.6:

$$N_i(S_{ri}) = \sum n_j \frac{{S_{r,j}}^3}{{S_{ri}}^3} \tag{E4.6}$$

where: $N_i(S_{ri})$ = number of equivalent cycles at index stress range, S_{ri}; and S_{ri} = index stress range. This formulation effectively equates the damage accumulated from the measured stress range spectrum to the constant-amplitude index stress range. The number of equivalent cycles at this index stress range provides a relative scale of damage accumulated based upon data from various sensors and bridges, given that the damage has been normalized.

As was recommended by Fasl (2013), the constant-amplitude fatigue limit (CAFL) established in AASHTO LRFD (2017) is a good index stress range to assume; although, any value can theoretically be used. For purposes of this research project, two different fatigue categories are of interest: Category E′ for cross-frames and Category C′ for built-up welded girders. Per Table E6.6.1.2.5-3 of AASHTO (2017), the CAFL for Category E′ and C′ is 2.6 and 12.0 ksi, respectively.

Although not cited in AASHTO, the E’ designation for single angle-to-gusset welded connections, was based upon fatigue tests on full-sized cross frames with single angle members conducted and discussed by Battistini et al. (2013) and McDonald and Frank (2009). In older versions of AASHTO LRFD Specifications, this same welded detail was classified as Category E, which corresponds to a CAFL of 4.5 ksi; it is important to note that each of the three subject bridges were designed in accordance to the older versions of the Specifications. This distinction is discussed further in subsequent sections of this chapter.

Alternatively, transverse stiffener-to-flange fillet welds are designated as Category C′, which often govern the fatigue design of bridge girders. For the sake of simplicity, the RT conservatively assumed that transverse stiffener weld occurs at the same depth from the natural axis as the location of the strain gages, which were positioned on the underside of the bottom flange. This assumption allowed the RT to make a direct comparison between the measured strain data and the design criteria for this critical welded detail.

E4.2.2 General Rainflow Counting Parameters

The major rainflow counting parameters, which were established based on data measured during the early troubleshooting phase of Stage I, included:

- Time window size,
- Number of bins and bin size,
- Threshold strain/stress, and
- Truncation strain/stress.

Time window size, number of bins and bin size, and threshold strain/stress were all parameters programmed onto the DAQ system. The truncation stress was implemented manually by the RT on the output files.

The time window size was held constant across all three subject bridges. The time window size indicates the frequency at which data was sent by the gateway, the centralized hub of the DAQ system. The RT selected 30-minute intervals based on previous experience with the WSN system. At the end of each 30-minute interval, data in the system was automatically tared to zero out any accumulated thermal effects.

In general, the bin size was limited by the capacity of the WSN DAQ system. Given the volume of strain gages and wireless nodes, the RT selected the bin size to maintain a reasonable number of bins per node, while also not adversely impacting the performance of the DAQ system and the rainflow algorithm. Using an excessive number of bins has the potential for overloading the WSN system in its attempt to communicate data files every 30 minutes. As a result, the RT settled on 50 total bins for its rainflow counting. Selecting the appropriate bin size balanced two different objectives: (i) the RT desired sufficiently small bin sizes as to refine the effective stress range calculations and (ii) given that the maximum stress bin is equal to the number of bins times the bin size, the RT wanted to ensure that no strain/stress cycles exceeded the maximum bin, for the strain gages on both the cross-frame members and girder flanges. This parameter was largely determined based on preliminary data observed during Stage I of the instrumentation process.

For Bridge 1, the RT elected to use 50 bins of 3 microstrain (0.087 ksi) size; for Bridge 2 and 3, the RT elected to use 50 bins of 4 microstrain (0.116 ksi) size to accommodate a perceived increase in girder stresses. Therefore, the maximum strain cycle was 150 microstrain (4.35 ksi stress cycle) and 200 microstrain (5.8 ksi stress cycle) for Bridges 1 and Bridges 2 and 3, respectively. Any cycles recorded above the maximum stress cycle values were placed in a separate bin; however, the bin above the maximum stress cycles did not indicate the actual magnitude of the cycle.

The threshold strain is the minimum cycle recorded by the WSN system. The threshold value was selected to eliminate electromechanical noise cycles from the rainflow histograms. The RT anticipated noise levels to be approximately ± 10 microstrain based on past experience and laboratory studies. As such, a 10-microstrain threshold value was used consistently across all three subject bridges. As is also common with field monitoring, data acquisition is sometimes prone to random, large noise spikes for various reasons. In this case, the random noise spikes would need to exceed 10 microstrain to register a cycle count on the histogram. In order to ensure all cycle counts recorded were reasonable (e.g. not a noise spike), the RT thoroughly reviewed the data set and eliminated any obvious outliers that were likely caused by noise and not live loads.

E4.2.2.1 Truncation Stress

As discussed in the subsequent Section E4.2.3, a major focus of this chapter is to compare measured stress ranges with factored design stresses in accordance with AASTHO Specifications. To make a comparison of measured and calculated design stresses, the truck population considered for each must also be similar.

The current AASHTO LRFD fatigue design loads and load factors were calibrated from millions of WIM data points from across the US, as mentioned in Section E4.2.1.2. Recall that the low tail of the spectrum was established as any truck with a GVW less than 20 kips; trucks weighing less than 20 kips were assumed to have negligible effect on damage accumulation. Note that a 20-kip truck is approximately equivalent to 40% of the truck used for the controlled live load test.

The RT sought to filter the measured data in a similar fashion to the design provisions, as to make reasonable comparisons. As was discussed in Section E4.2.1.2, the RT eliminated the high tail of the truck distribution with a similar filtering criterion (99.99th percentile of the data set). However, reproducing the same criteria for the low tail of the distribution is more challenging given that the rainflow data only shows stress cycle counts and does not indicate weight or position of the trucks. There is no methodology to definitively identify which measured stress cycles correspond to trucks with GVWs less than 20 kips.

Instead, the RT elected to adopt the approach recommended by Connor and Fisher (2006). All stress cycles below an established magnitude, defined as the truncation stress herein, were removed from the data set. In effect, the low tail of the data set was truncated. The truncation stress is similar to the threshold stress described above but serves a different purpose. Whereas the threshold stress/strain eliminates low-stress cycles to filter out electromechanical noise, the truncation stress filters out low-stress cycles that have little effect on the cumulative damage at a given fatigue detail.

Connor and Fisher (2006) also demonstrated that the selection of a truncation stress can significantly impact the effective stress range computed for the data set. Figure E4-58 illustrates an example of this trend for a girder flange at Bridge 1. In general terms, the calculated effective stress range increases as the truncation stress increases, and the number of cycles above that cutoff value drastically decreases as the truncation stress increases; note the log scale on the cycle count plot. Each variable is highly sensitive to the truncation stress selected by the engineer, which is crucial when attempting to compare effective stress ranges of measured data with the value predicted by the design code.

For example, if the data set was truncated at 1.0 ksi, meaning all stress cycle counts below 1.0 ksi were eliminated, the remaining data set includes 1,630 cycles at an effective stress range of 1.93 ksi. If the data set was truncated at 3.0 ksi, the remaining data set includes 134 cycles at an effective stress range of 3.53 ksi. Not only is there a distinct difference in the effective stress range between these two truncated data sets, but the damage accumulation index, defined on the right side of Eq. E4.4, is also different.

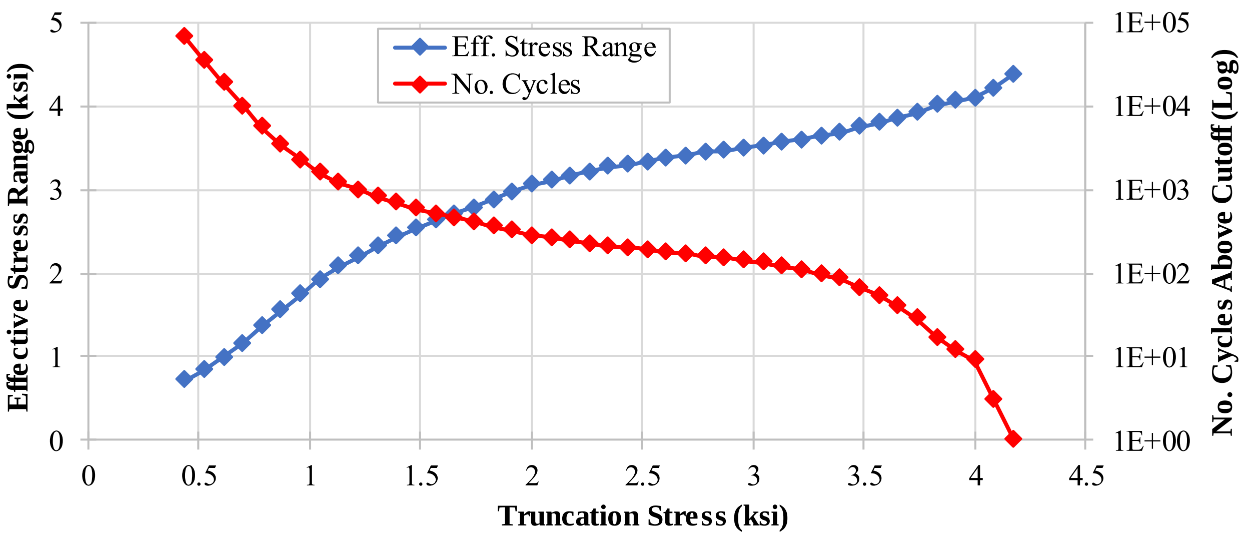

Figure E4-58: Sample of effective stress ranges and number of cycle counts using different truncation stress values

Despite only one example being presented here (Figure E4-58), it should be noted that similar trends were observed at every instrumented member on all three subject bridges.

Because the effective stress range calculation is sensitive to how the low-stress cycles are filtered from the data set, it was important for the RT to establish an appropriate truncation stress for data from both the cross-frames and girders. Connor and Fisher (2006) recommended that a truncation stress equal to one-fourth the CAFL is a reasonable value to use when processing rainflow data. Past research has shown that stress cycles below one-fourth the CAFL has little effect on the cumulative damage at a detail.

For the instrumented cross-frames, the one-fourth CAFL rule results in a truncation stress of 0.65 ksi, which is 25% of 2.6 ksi (CAFL for Category E′ detail). For the instrumented girder flanges, the one-fourth CAFL rule results in a truncation stress of 3.0 ksi, which is 25% of 12 ksi (CAFL for Category C′ detail). The RT initially evaluated all rainflow data under the one-fourth CAFL filtering criteria, but quickly realized that the majority of a typical measured stress range spectrum was below the truncation stress, especially for the girder flange data. In fact, there were a few instances in which the 3.0-ksi cutoff removed the entire data set for a girder flange. In other words, no stress cycles above 3.0 ksi were measured for the entire monitoring period; thus, removing all stress cycles below 3.0 ksi left a blank data set. Given that the simplified, one-fourth CAFL criteria is not appropriate for girder flange data, the RT refined its approach to computing the truncation stress.

It has been previously demonstrated that the cumulative damage provided by the effective stress range becomes asymptotic to the appropriate S-N curve as more low-stress cycles are considered (Connor and Fisher 2006). This behavior is demonstrated graphically in Figure E4-59 for girder flange data at Bridge 1. Note that these trends are consistent among all cross-frame and girder flange data sets despite only one representative example being presented in this appendix. The top plot in Figure E4-59 features several key items:

- The S-N curve for a Category C′ detail, as established by AASHTO LRFD Specifications, for reference,
- Data points representing the effective stress ranges and cycle counts of the data set under various levels of truncation (e.g. the first data point of 67,633 cycles at an effective stress range of 0.72 ksi corresponds to a truncation stress of 0.44 ksi; the second data point of 36,462 cycles at an effective stress range of 0.84 ksi corresponds to a truncation stress of 0.52 ksi, and so on), and
- The S-N curve with a log-log slope of -3 shifted to pass through the data point representing the smallest truncation stress (i.e. the data point with the highest cycle count and smallest effective stress range). This point is represented as “Point A” in Figure E4-59.

From the top plot, it is clear that the effective stress range and corresponding cycle count approaches the log-log slope of -3 as the truncation stress decreases. Conversely, the data points deviate rapidly from the log-log slope of -3 as higher stress levels are truncated from the data set. Another way of describing this trend is in terms of the damage accumulation. Damage is accumulated by cycles of all stress ranges and higher stress ranges cause proportionally higher damage relative to lower stress ranges. For low levels of truncation, the damage associated with the discarded stress cycles is insignificant, and therefore the data points are nearly on top of the shifted S-N curve. For higher levels of truncation, the damage associated with the discarded stress cycles becomes increasingly significant, such that the data points diverge from the shifted S-N curve.

The bottom plot isolates three important levels of truncation: (i) 0.44 ksi which represents the lowest value and the first data point on the plot, (ii) 1.0 ksi, and (iii) 3.0 ksi, which represents one-fourth of the CAFL. As stated above, the shifted S-N curve passes through the first data point (Point A), so no percentage of the accumulated damage is discarded at a truncation stress of 0.44 ksi. For a truncation stress of 3.0 ksi, approximately 23% of the accumulated damage is discarded from the data set, relative to the shifted S-N curve. The RT deemed this value too excessive. Instead, truncating the data set at 1.0 ksi only discards 10% of the accumulated damage, which has deemed acceptable for the RT. As such, a truncation stress of 1.0 ksi is considered more appropriate for this data set than one-fourth of the CAFL; this value provides a representative data set and yields reasonable effective stress estimates.

The procedure outlined in Figure E4-59 was conducted for all instrumented cross-frames and girder flanges. Rather than assigning a unique truncation stress for every instrumented member, the RT elected to assign a consistent truncation stress for each subject bridge based upon the collected data. The RT evaluated each data set individually, and an average truncation stress was determined for cross-frames and girder flanges at each bridge. The results of this study are presented in Table E4-18.

It should be noted that the one-fourth CAFL rule was appropriate for cross-frame data at all three subject bridges. However, the appropriate truncation stress for girder flanges was substantially less than one-fourth the CAFL at all three subject bridges. In other words, truncating girder rainflow data at 3.0 ksi would have resulted in artificially low cycle counts at high effective stress ranges. Truncating the data in accordance with Table E4-18 more accurately represented the stress range spectra at each bridge and the damage accumulated during the monitoring period.

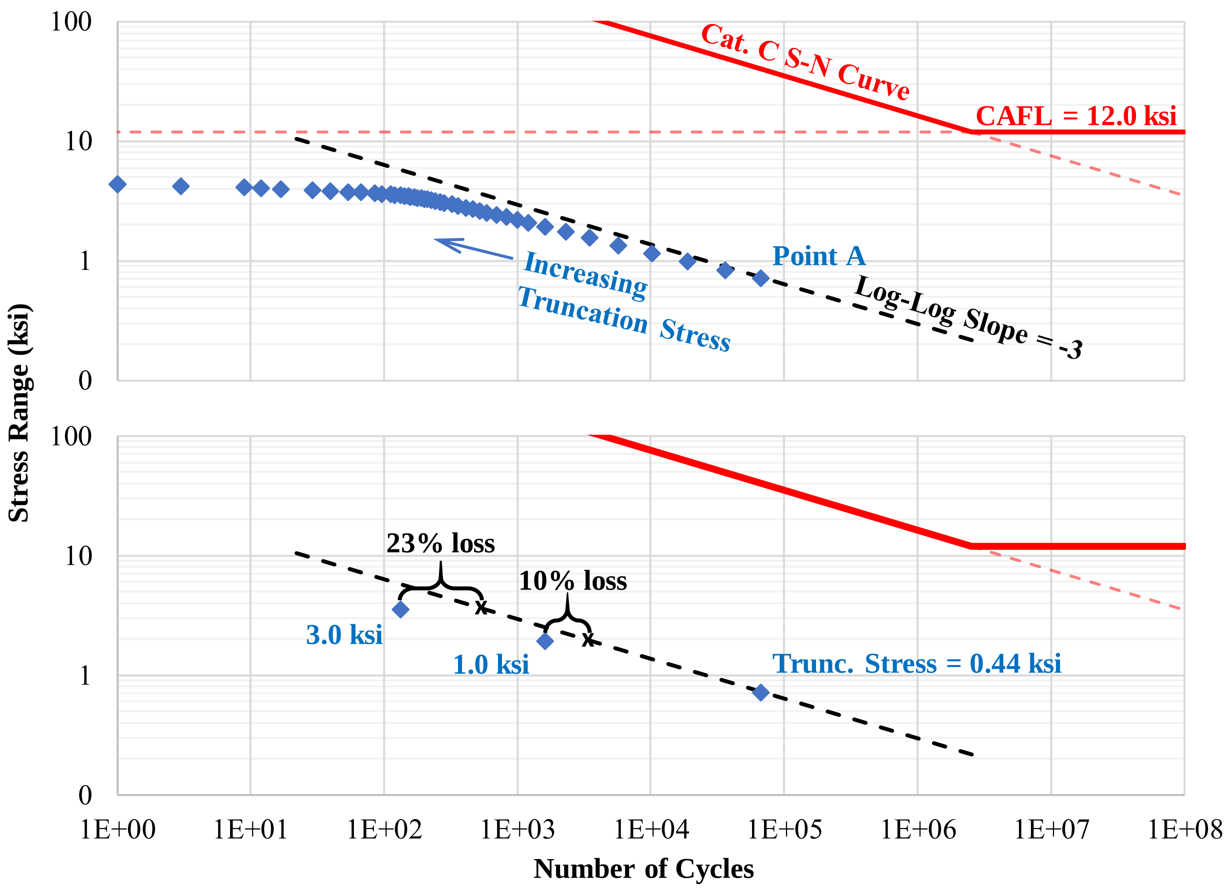

Figure E4-59: Sample plot demonstrating the effect of different levels of truncation on a data set

Table E4-18: Summary of truncation stresses assigned at each subject bridge

Bridge No.	Truncation Stress (ksi)	
	Cross-Frames	Girder Flanges
1	0.65	1.0
2	0.65	1.15
3	0.65	1.5

E4.2.3 Significance of Collected Data

In the subsequent sections of the appendix, several concepts related to the measured in-service data and AASHTO fatigue design are investigated.

First, the RT evaluated how the measured data compared to the AASHTO LRFD Specifications. Due to changes in the fatigue provisions since the bridges were designed, the team considered both the 8th Edition (2017) and 4^{th} Edition (2007), which was the code used to design the subject bridges. For the instrumented cross-frame members and girders, the RT performed a fatigue limit state design in accordance with both editions of the specifications. The factored design force effects and factored fatigue resistance were computed for each component of interest and compared to the corresponding measured response. The team elected to use a refined analysis to determine cross-frame and girder force effects per AASHTO LRFD Articles 3.6.1.4.3a and C6.6.1.2.1. Rather than using the validated Abaqus models outlined in Chapter E5, the commercial software introduced in Sections E3.2.1, E3.2.2, and E3.2.3, Software A, was utilized for the refined 3-D analysis. Acknowledging that different design engineers and software packages will provide different force effects, the RT sought to produce design results that reflect the common engineer and software program. Based upon this procedure, the RT can make observations on the accuracy of a common design approach.

The Software A model treats the composite deck and girders as shell elements and the cross-frame members are truss elements, modified by the stiffness reduction factor due to eccentric end connections discussed in Section E5.1. Additionally, the nominal fatigue resistance for each component was determined in accordance with AASHTO LRFD Articles 6.6.1.2.5. An example of the design procedures is presented for Bridge 1 in Section E4.2.4.

The benefits of comparing measured data to the design metrics of two editions of the Specifications are threefold:

1. The RT can evaluate how well a common 3-D refined analysis and the AASHTO fatigue loading criteria, that is calibrated for girders, predict cross-frame forces and to a lesser extent girder flange stresses.
2. The RT can evaluate how the instrumented bridge components performed with respect to the nominal fatigue resistance specified in AASHTO.
3. The RT can compare the past and present editions of the design specifications with respect to the measured rainflow data.

Also from this data, the RT evaluated daily and hourly trends at each bridge by comparing measured effective and index stresses ranges over shorter periods of time, instead of the full monitoring period. Studying these time-dependent effects emphasizes the importance of monitoring rainflow data for several weeks. The stress range spectra and effective stress calculations could be skewed if certain hours of the day or days of the week were neglected from the full data set. These trends are detailed for each bridge in the subsequent sections.

Lastly, the RT provide generalized comparisons between the fatigue characteristics of cross-frames in straight, skewed, and horizontally curved bridges. The significance of traffic patterns and overall bridge geometry with respect to the fatigue behavior are also discussed.

E4.2.4 Bridge 1 Results

The following subsections outline the in-service rainflow data for the instrumented cross-frames and girders of Bridge 1.

As detailed in Section E2.1, Bridge 1 has the largest instrumented span-to-depth ratio of the three subject bridges and serves as an off-ramp to northbound IH 45 traffic. The RT observed during several site visits that truck traffic on the bridge was sporadic. Relatively large cross-frame and girder stress cycles were expected given the greater flexibility of the superstructure despite the normal layout of cross-frames and pier supports. However, the larger stress cycles were expected to be infrequent, given the limited truck traffic.

Figure E4-4 and Figure E4-5 provide the cross-frame numbering scheme, which is used throughout this section. The girders are identified by the numbering scheme used on the design plan and the associated cross-frame line, which is provided graphically on Figure E3-12 through Figure E3-14.

E4.2.4.1 Cross-Frame Data for Bridge 1

As is shown in Table E3-1, in-service rainflow monitoring for Bridge 1 was conducted between March 10th and June 6th of 2018. In total, four weeks of in-service data was measured. The data presented in this section, however, is specifically from May 24th through June 6th, which represents a two-week period. As discussed in Section E3.1, the RT extended the instrumentation time of Bridge 1 to modify the programming on the DAQ system. Rainflow data before the modification only evaluated the response of each strain gage individually. Data after the modification evaluated both the individual response of a strain gage and the axial response of the full cross-frame member by a real-time linear regression algorithm. Consequently, the RT has elected to only present rainflow data of the axial response to match the design approach of this fatigue detail in AASHTO LRFD (2017).

Despite not being presented in this appendix, the data before the modification has been evaluated by the RT. By inspection, rainflow data of individual gages before the modification are comparable to rainflow data for individual gages during May 24th through June 6th. Given the similarities in the individual response, the RT is confident that the axial response of the initial monitoring period does not change the conclusions reached based upon the final two weeks of the monitoring period. The RT is also confident in this approach given that past research showed that one week is often adequate to obtain representative fatigue data (Fasl 2013).

For the two-week period between May 24th and June 6th, the axial stress rainflow counts for each cross-frame member were compiled and sorted into specific bins. A detailed discussion of the bin size and truncation stress parameters used for this data set is provided in Section E4.2.2. Figure E4-60 presents a sample histogram for cross-frame member 07, which includes rainflow counts summed over the entire monitoring period. Cross-frame member 07 is a diagonal between girders 2 and 3 near cross-frame line 4; this diagonal was one of the highest-stressed members during the controlled live load test. Also plotted on the figure are key benchmarks and the average number of occurrences in which those benchmarks were exceeded per day.

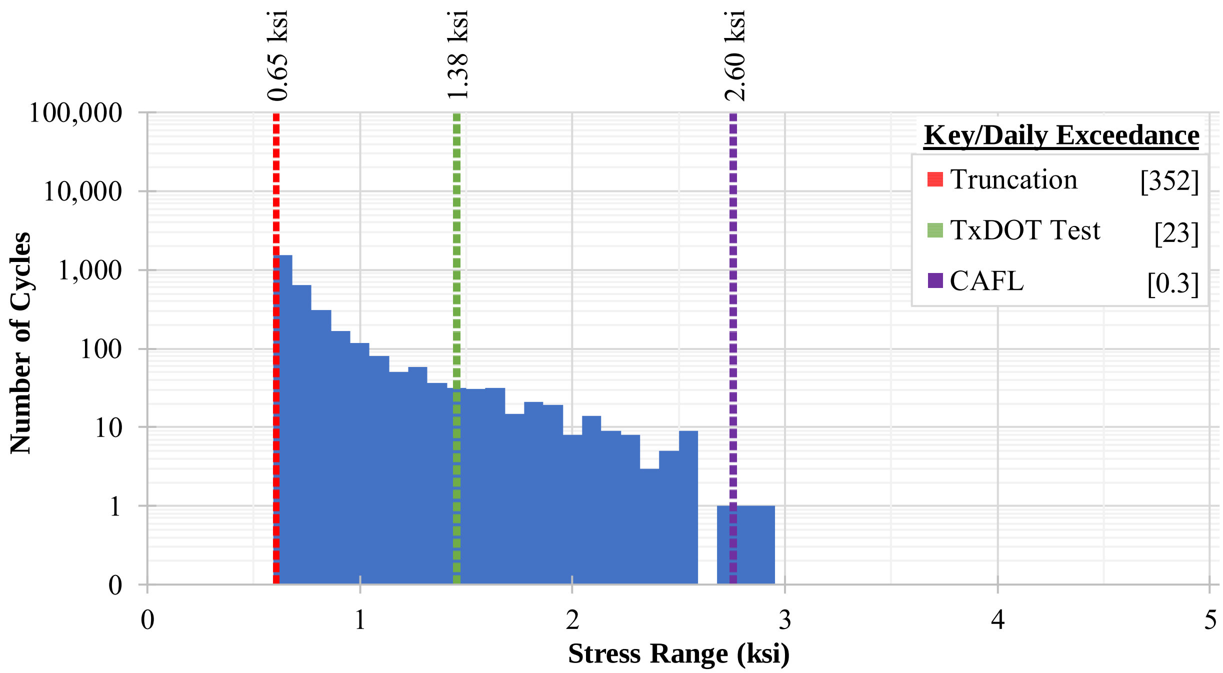

Figure E4-60: Sample rainflow histogram for cross-frame member 07 at Bridge 1

Figure E4-60 presents a few key concepts, many of which were introduced in Section E4.2.1 and E4.2.2. These concepts include:

- The truncation stress of 0.65 ksi, which corresponds to one-fourth of the CAFL, was implemented and is identified on the plot. All stress cycles measured below 0.65 ksi were eliminated from the data set as to not skew the effective stress range calculation.
- On average there were over 350 stress cycles per day that exceeded the truncation stress, and only 0.3 cycles per day that exceeded the Category E′ CAFL of 2.6 ksi. A detailed comparison of measured data and AASHTO design metrics are discussed later in this section.
- The "TxDOT Test" stress represents the maximum stress range recorded from the four, individual slow-speed truck passages of moving Load Case 0 (Section E4.1.3.2). The TxDOT trucks were comparable in weight to HS-16 (0.8*HS-20), the AASHTO fatigue truck representing the "effective truck," and approximately 2.5 times the GVW of the lower-bound truck considered in the development of the AASHTO fatigue load factors. This benchmark stress range gives a good reference point when evaluating the in-service fatigue data since the load test truck weights and positions are known, whereas the truck weights and positions for the in-service fatigue data are unknown. In this example, over 23 stress cycles per day exceeded this reference stress range.

Full data set histogram plots for the rest of the instrumented cross-frames are not presented in this appendix. Instead, a more convenient means for examining and comparing the data is to tabulate all key values, which include the measured effective, maximum, and index stress ranges. These measured values can then be compared to important AASHTO-related design metrics, as was outlined in Section E4.2.3. Table E4-19 presents the summarized comparison between measured values and AASHTO metrics. A key is provided below the table to describe what each major item represents and a reference within the appendix to find more information on that item.

To facilitate the understanding of Table E4-19, Figure E4-61 is a sample calculation showing how the factored design stresses and resistances were determined from the 4th Edition and 8th Edition of the

AASHTO LRFD Specifications. The sample calculation steps through the applicable AASHTO code provisions, states all assumptions made, and provides references to all AASHTO provisions, tables, and equations. Note that the 4^{th} Edition and 8^{th} Edition design forces are based on an analysis model that considers a stiffness reduction factor for all cross-frame members, despite this provision not being adopted into AASHTO LRFD until the 7^{th} Edition.

It should be emphasized that the factored force effects from the refined analysis, tabulated in Table E4-19 and explained in Figure E4-61, are intended to represent the likely methodology that most engineers approach fatigue design of cross-frame members. The RT acknowledges that the modeling technique and assumptions may play a significant role in the predicted design forces. However, by maintaining a common design and analysis approach, the RT can make observations pertaining to the accuracy of the AASHTO fatigue loads and typical modeling techniques.

Note that cross-frame member 13 was excluded from the Table E4-19. During the monitoring period from May 24^{th} through June 6^{th}, one of the four strain gages that were used to determine the axial stress in cross-frame member 13 experienced high noise levels and random stress peaks. The RT concluded that these stress peaks were not load-induced, but rather a product of electromechanical noise. The real-time linear regression algorithm is invalidated if one of the four gages at a cross-section are unreliable. Therefore, this cross-frame member is neglected from the study.

Also note that the infinite life (Fatigue I) design ratio related to the 8^{th} Edition of the AASHTO LRFD Specifications has been formatted with a strikethrough. As demonstrated in the sample calculation, Figure E4-61, the Fatigue II limit state governs fatigue design for this bridge given the low average daily truck traffic (ADTT). Fatigue I is consequently disregarded in the table.

Table E4-19: Comparison between measured rainflow cross-frame response and key AASHTO design metrics (Bridge 1)

	Measured Response			4th Edition				8th Edition | Fatigue II (Finite Life)				8th Edition | Fatigue I (Infinite Life)			
Cross-Frame No.	**Avg. Daily Equiv. Cycles @ 2.6 ksi**	**Measured Eff. Stress, S_{re} (ksi)**	**Measured 0.01% Stress, S_{rm} (ksi)**	**Design Stress, $\gamma\Delta f$ (ksi)**	**Nom. Resistance, ΔF_n (ksi)**	**% Error Analysis $\frac{(\gamma\Delta f - S_{re})}{S_{re}}$**	**Design Ratio $\frac{\Delta F_n}{S_{re}}$**	**Design Stress, $\gamma\Delta f$ (ksi)**	**Nom. Resistance, ΔF_n (ksi)**	**% Error Analysis $\frac{(\gamma\Delta f - S_{re})}{S_{re}}$**	**Design Ratio $\frac{\Delta F_n}{S_{re}}$**	**Design Stress, $\gamma\Delta f$ (ksi)**	**Nom. Resistance, ΔF_n (ksi)**	**% Error Analysis $\frac{(\gamma\Delta f - S_{rm})}{S_{rm}}$**	**Design Ratio $\frac{\Delta F_n}{S_{rm}}$**
02	12.1	0.76	1.87	1.11	2.25	47%	2.98	1.00	2.81	33%	3.72	2.20	2.60	17%	~~1.39~~
03	9.9	0.91	2.74	2.23	2.25	144%	2.47	1.86	2.81	104%	3.09	4.07	2.60	49%	~~0.95~~
04	4.7	0.98	3.00	2.12	2.25	116%	2.29	1.88	2.81	91%	2.86	4.11	2.60	37%	~~0.87~~
05	5.7	0.92	1.87	1.42	2.25	54%	2.44	1.29	2.81	40%	3.06	2.82	2.60	51%	~~1.39~~
06	1.9	0.70	1.35	1.01	2.25	44%	3.22	0.98	2.81	40%	4.03	2.14	2.60	59%	~~1.93~~
07	17.6	0.96	2.83	2.13	2.25	122%	2.35	1.94	2.81	103%	2.94	4.24	2.60	50%	~~0.92~~
08	11.2	0.83	3.35	2.14	2.25	158%	2.72	1.90	2.81	130%	3.40	4.16	2.60	24%	~~0.78~~
09	12.0	0.96	3.61	2.11	2.25	119%	2.33	1.93	2.81	100%	2.92	4.22	2.60	17%	~~0.72~~
10	2.9	0.86	1.52	1.44	2.25	68%	2.62	1.30	2.81	51%	3.28	2.83	2.60	86%	~~1.71~~
12	6.9	0.94	2.91	2.20	2.25	136%	2.41	1.84	2.81	97%	3.01	4.04	2.60	38%	~~0.89~~
16	18.7	0.85	3.61	2.05	2.25	142%	2.66	1.87	2.81	121%	3.32	4.10	2.60	14%	~~0.72~~
17	26.0	0.81	1.87	1.43	2.25	77%	2.79	1.28	2.81	59%	3.49	2.81	2.60	50%	~~1.39~~

Key:
Average Daily Equivalent Cycles = Average number of cycles per day at index stress (CAFL) that produces damage equivalent to that accumulated during monitoring period (Section E4.2.1.3)
Measured Effective Stress = Effective stress range computed on all histogram bins for entire monitoring period (Section E4.2.1.1)
Measured Maximum Stress = Minimum stress recorded in 99.99th percentile of histogram data (1-in-10,000 occurrence) (Section E4.2.1.2)
Design Stress = Factored design stress range based on refined 3D analysis and code-specified fatigue loading (Figure E4-61)
Nominal Resistance = Presumed fatigue resistance based on AASHTO 6.6.1.2.2 (Figure E4-61)
% Error in Analysis = Indicates how well code-specified fatigue loading and 3D model predicts the measured response (Figure E4-61)
Design Ratio = Indicates how the measured bridge response compares to the code-specified capacity for the appropriate limit state (Figure E4-61)

Note: The following calculations are based on the 4th Edition and 8th Edition of the AASHTO LRFD Design Specifications. Unless noted otherwise, the design procedures for these editions are the same. If the procedures do vary, the calculation will be broken out on each side of the page to clearly demonstrate the differences. References to AASHTO provisions and/or tables are the same for both editions, unless noted otherwise.

Inputs in yellow are unique to this bridge and this cross-frame member. Similar calculations were made for all instrumented components on the three subject bridges. Only the summary of those results is tabulated.

Section Properties

The following inputs describe the single angle section used for this cross-frame member, L4x4x3/8, and its connection to the gusset plate. These parameters are used to convert axial force to stress on the section. Note that the angle-to-gusset weld length is taken as 7" based on scaling the design plans; the measured distance in the field is closer to 6.7". Because these design metrics represent the common design practices, we will use 7" herein.

Gross area of angle: $A_g := 2.86\text{in}^2$

Distance to c.g.: $x_{bar} := 1.13\text{in}$

Length of angle-to-gusset weld: $L_{weld} := 7.0\text{in}$

In accordance with Table 6.6.1.2.3-1 Section 7.2 (no section number in 4th Ed.) the fatigue stress range of the single angle welded to the gusset shall be calculated on the effective net area of the cross-frame member. As such, the shear lag factor and effective net area are as follows:

Shear lag factor: $U := 1 - \dfrac{x_{bar}}{L_{weld}} = 0.84$

Effective net area: $A_e := U \cdot A_g = 2.4 \cdot \text{in}^2$

Traffic Patterns

The following inputs describe the traffic parameters of the bridge. These parameters are used to determine the average daily truck traffic (ADTT) used in the Fatigue II limit state design. Note that the class of highway is based on the classifications used in Table C3.6.1.4.2-1. This bridge is an off-ramp in an urban area; hence, "other urban" is selected. Also note that the ADT estimate used for the 4th Ed. design is based on the original design plans; the updated ADT amount is based on current TxDOT traffic maps and will be used for the 8th Ed. design. As expected, traffic counts have increased since the bridge was built in 2007.

No. of striped lanes: $N_{lanes} := 3$

Class of highway: Class := "Other Urban"

No. of traffic directions on bridge: $N_{dir} := 1$

4th Ed.	*8th Ed.*
Average daily traffic, ADT:	Average daily traffic, ADT:
$ADT_4 := 3300$	$ADT_8 := 4000$

The remaining parameters are also related to traffic patterns but are dependent on the inputs above. Unless specific traffic data is known, many of these parameters can be estimated based on AASHTO commentary. These estimates are the following: (1) the direction factor applies when a bridge carries

Figure E4-61: Sample calculation showing how AASHTO design metrics were determined

two directions of traffic, in which case C3.6.1.4.2 recommends assuming 55% of the total traffic flow in the critical direction, (2) the lane factor distributes the full traffic count into lanes based on recommended values [Table 3.6.1.4.2-1], (3) truck fraction factor assigns a percentage of the traffic as trucks, which are most important for fatigue evaluation [Table C3.6.1.4.2-1].

Direction factor:
$$f_{dir} := \begin{vmatrix} 1.0 & \text{if} & N_{dir} = 1 \\ 0.55 & \text{otherwise} & \end{vmatrix} = 1$$

Lane factor, p:
$$p := \begin{vmatrix} 1.0 & \text{if} & N_{lanes} = 1 \\ 0.85 & \text{if} & N_{lanes} = 2 \\ 0.80 & \text{otherwise} & \end{vmatrix} = 0.8$$

Truck fraction factor:
$$f_{truck} := \begin{vmatrix} 0.20 & \text{if} & Class = \text{"Rural Interstate"} \\ 0.15 & \text{if} & Class = \text{"Urban Interstate"} \\ 0.15 & \text{if} & Class = \text{"Other Rural"} \\ 0.10 & \text{if} & Class = \text{"Other Urban"} \end{vmatrix} = 0.1$$

Note that the average daily traffic, including all vehicles, is physically limited to 20,000 under normal conditions per C3.6.1.4.2.

4th Ed.

Average daily traffic in single-lane:

$$ADT_{sl.4} := \min\left(ADT_4 \cdot f_{dir} \cdot p\ ,\ 20000\right) = 2640$$

8th Ed.

Average daily traffic in single-lane:

$$ADT_{sl.8} := \min\left(ADT_8 \cdot f_{dir} \cdot p\ ,\ 20000\right) = 3200$$

The total traffic counts are then converted to the truck traffic counts.

4th Ed.

Average daily truck traffic in single-lane:

$$ADTT_{sl.4} := ADT_{sl.4} \cdot f_{truck} = 264$$

8th Ed.

Average daily truck traffic in single-lane:

$$ADTT_{sl.8} := ADT_{sl.8} \cdot f_{truck} = 320$$

Pertinent Loading Inputs

Per Table 3.4.1-1, Fatigue I and II limit states require that live load (LL), impact (IM), and centrifugal (CE) forces be considered in the load combination. LL force effects are determined by the calculations herein. IM effects are based on Table 3.6.2.1-1. Since there is no curvature to this bridge, CE effects are neglected.

Impact factor: $IM := 0.15$

Refined Analysis Overview

Per 3.6.1.4.3, refined analysis methods are permitted for determining the fatigue live load effects. The 3-D CSiBridge model was built in accordance to 4.6.3, to satisfy the requirements of 3.6.1.4.3a. The geometry of the bridge matches the design plans precisely. This model is representative of what most design engineers would develop for a comparable bridge structure. The model is built using shell elements for deck and girder elements and truss elements for cross-frame members. It is important to note that reduction in cross-frame stiffness due to end connection eccentricities of single-angle members was applied. Rather than applying the suggested uniform reduction factor of 0.65 (C4.6.3.3.4), the RT applied the full equations provided in Battistini et al (2012). And despite these reduction factors not being considered in the 4th Ed. specifications, R-factors were also applied to the model for 4th Ed. design

(Con't) Figure E4-61: Sample calculation showing how AASHTO design metrics were determined

force effects. The substructure elements with rigid foundation supports are also included in the model for completeness.

4th Ed.

To satisfy the fatigue live load requirements of 3.6.1.4.3 and C6.6.1.2.1, the maximum of two different conditions were considered: (1) a single fatigue design truck in accordance with 3.6.1.4.1 positioned transversely and longitudinally to maximize stress range at the cross-frame under consideration, and (2) 75% of a double fatigue truck case in which the trucks are positioned in different transverse positions and causing a stress reversal cycle. Both cases were considered by use of influence surface analysis.

8th Ed.

To satisfy the fatigue live load requirements of 3.6.1.4.3a and C6.6.1.2.1, a single fatigue design truck in accordance with 3.6.1.4.1 was assigned in the analysis model. The truck was positioned transversely and longitudinally to maximize stress range at the cross-frame under consideration by the use of influence surface analysis.

A minimum 1-foot load step is assigned both transversely and longitudinally to all influence surface analyses. It was determined that this increment sufficiently captures maximum force effects in critical cross-frame members. The influence surface method is recommended in C4.6.3.3.4 (section does not exist in 4th Ed.) for determining cross-frame force effects.

Note that influence surface analysis only provides enveloped maximum and minimum force effects due to moving the truck; it does not explicitly provide the location of the truck that caused the maximum effect. The enveloped values were used to obtain the code-specified loading conditions by the following methods:

4th Ed.

For case 1, the absolute maximum enveloped force (larger of max or min) minus zero stress was used for the design stress range. This assumes that there is no stress reversal when a moving truck maintains the same transverse position on the bridge, which is a reasonable assumption as evidenced by the live load test.

For case 2, 75% of the maximum stress minus the minimum stress was used for the stress range. This procedure conservatively acknowledges that the two fatigue trucks are in different transverse positions, despite not knowing the exact positions corresponding the max and min force effects.

8th Ed.

The absolute maximum enveloped force (larger of max or min) minus zero stress was used for the stress range. This assumes that there is no stress reversal when a moving truck maintains the same transverse position on the bridge, which is a reasonable assumption as evidenced by the live load test data.

Also note that the model was built assuming an 8-inch thick deck and a concrete stiffness based on 5.4.2.5. As is documented in Chapter 5 of this report, the validated model adjusted these parameters to better match the measured live load data. To reiterate, these design metrics are intended to represent the most common design practices, so the design parameters are used.

A screenshot of the 3-D model is presented below:

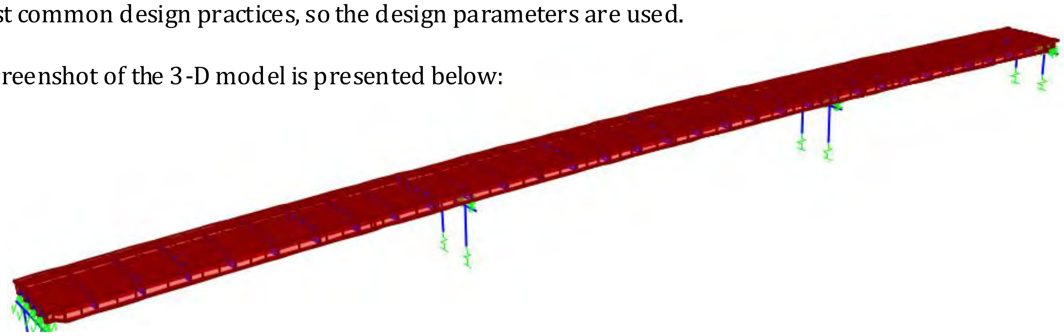

(Con't) Figure E4-61: Sample calculation showing how AASHTO design metrics were determined

Live Load Effects

The model was run based on the procedures outlined above. The following force effects are maximum and minimum enveloped axial forces from cross-frame member 07, based on the influence surface analysis of the AASHTO fatigue truck.

Maximum enveloped force: $P_{max} := 5.06kip$

Minimum enveloped force: $P_{min} := -2.84kip$

Fatigue evaluation is typically done in terms of stresses. Therefore, the force effects from the 3D model are converted to axial stress by dividing through the net effective area. Note that bending stresses in the single angle due to an eccentric end connection are implicitly considered in the fatigue category designation, and only the axial stresses are explicitly evaluated. This approach is consistent with Table 6.6.1.2.3-1, Section 7.2.

Maximum tensile stress: $f_t := \dfrac{P_{max}}{A_e} = 2.11 \cdot ksi$

Minimum compressive stress: $f_c := \dfrac{P_{min}}{A_e} = -1.18 \cdot ksi$

The design stress range was based on the assumptions made from the enveloped force effects above.

4th Ed.

Design stress range:

$\Delta_{f.4} := \max\left[f_t, -f_c, 0.75 \cdot \left(f_t - f_c\right)\right] = 2.47 \cdot ksi$

8th Ed.

Design stress range:

$\Delta_{f.8} := \max\left(f_t, -f_c\right) = 2.11 \cdot ksi$

Factored Force Effects

The factored force effect to be used in 6.6.1.2.2 includes the governing live load stress range, impact factor, and load factor. The different editions of the specifications vary in how they deal with load factors and fatigue limit states.

4th Ed.

One combined limit state is used for this edition. Infinite life and finite life are implicitly considered in the nominal fatigue resistance side of Eq. 6.6.1.2.2-1 and not the load side. As such, only one load factor is required.

Load factor: $\gamma_4 := 0.75$

8th Ed.

This edition differentiates between infinite life and finite life in Fatigue I and II, respectively. Two separate load factors are needed. Note that these load factors have been updated since the 7th Edition, as is discussed in this report.

Fatigue I load factor: $\gamma_{I.8} := 1.75$

Fatigue II load factor: $\gamma_{II.8} := 0.80$

Therefore, the factored design force effects for fatigue limit states are as follows:

4th Ed.

Factored force effect:

$\gamma\Delta_{f.4} := \gamma_4 \cdot \Delta_{f.4} \cdot (1 + IM) = 2.13 \cdot ksi$

8th Ed.

Factored Fatigue I force effect:

$\gamma\Delta_{f.I.8} := \gamma_{I.8} \cdot \Delta_{f.8} \cdot (1 + IM) = 4.25 \cdot ksi$

Factored Fatigue I force effect:

$\gamma\Delta_{f.II.8} := \gamma_{II.8} \cdot \Delta_{f.8} \cdot (1 + IM) = 1.94 \cdot ksi$

(Con't) Figure E4-61: Sample calculation showing how AASHTO design metrics were determined

Nominal Fatigue Resistance

The calculations up to this point have determined the factored design force effects, or the left side of Eq. 6.6.1.2.2-1. The remaining calculations focus on the nominal fatigue resistance, or the right side of the equation. The approach differs from 4th Ed. to 8th Ed. But before computing those resistances, several parameters are consistent across the different editions of the specifications. Note that the number of cycles per truck passage is largely based on Table 6.6.1.2.5-2 for transverse members with a spacing less than 20 feet. And despite the 4th Ed. design being based on double truck loading condition, C6.6.1.2.1 of the 4th Ed. acknowledges that "there is no allowance in this recommended practice for that fact that two trucks are required to cause the critical stress range." As such, two cycles per truck passage is considered for both editions.

No. of cycles per truck passage: $n := 2$

4th Ed.

Estimated no. of cycles in 75-yr life:

$$N_4 := 365 \cdot 75 \cdot ADTT_{sl.4} \cdot n = 1.45 \times 10^7$$

8th Ed.

Estimated no. of cycles in 75-yr life:

$$N_8 := 365 \cdot 75 \cdot ADTT_{sl.8} \cdot n = 1.75 \times 10^7$$

At the time of designing this bridge in 2007, single angles welded to gussets was still classified as Category E. It has since been modified as a Category E' detail. As such, the threshold stress used for infinite life design and the detail category constant, A, is different between the editions. The threshold values are based on Table 6.6.1.2.5-3 and the detail category constants are based on Table 6.6.1.2.5-1.

4th Ed.

Constant-amplitude threshold stress:

$$\Delta F_{th.4} := 4.5\text{ksi}$$

Detail category constant, A:

$$A_4 := 11.0 \cdot 10^8 \text{ksi}^3$$

8th Ed.

Constant-amplitude threshold stress:

$$\Delta F_{th.8} := 2.6\text{ksi}$$

Constant-amplitude threshold stress:

$$A_8 := 3.9 \cdot 10^8 \text{ksi}^3$$

From these parameters, the nominal fatigue resistance can be determined from 6.6.1.2.5. Remember that only one combined fatigue limit state existed in the 4th Ed. Also note that the resistance phi factor for fatigue is 1.0 per C6.6.1.2.2.

4th Ed.

Nominal fatigue resistance:

$$\Delta F_{n.4} := \min\left[\begin{vmatrix} \left(\dfrac{A_4}{N_4}\right)^{\frac{1}{3}} \\ \dfrac{1}{2} \cdot \Delta F_{th.4} \end{vmatrix}\right] = 2.25 \cdot \text{ksi}$$

8th Ed.

Nominal Fatigue I resistance:

$$\Delta F_{n.I.8} := \Delta F_{th.8} = 2.6 \cdot \text{ksi}$$

Nominal Fatigue II resistance:

$$\Delta F_{n.II.8} := \left(\frac{A_8}{N_8}\right)^{\frac{1}{3}} = 2.81 \cdot \text{ksi}$$

Per 6.6.1.2.3, the governing limit state is determined by comparing the single-lane average daily truck traffic with Table 6.6.1.2.3-2. The values in the table represent the truck traffic count in which infinite life and finite life resistances equate. Note that the values in Table 6.6.1.2.3-2

(Con't) Figure E4-61: Sample calculation showing how AASHTO design metrics were determined

were modified to consider n=2. For Category E', the equivalent number of cycles is equal to 4243.

Given the low $ADTT_{sl}$ for this bridge, Fatigue II governs the fatigue design.

$$\left| \begin{array}{ll} \text{"Fat. I"} & \text{if } ADTT_{sl.8} > 4243 \\ \text{"Fat. II"} & \text{otherwise} \end{array} \right. = \text{"Fat. II"}$$

Summary of Tabulated Data

The following values have been tabulated:

4th Ed.

Design stress: $\gamma\Delta_{f.4} = 2.13 \cdot ksi$

Nominal resistance: $\Delta F_{n.4} = 2.25 \cdot ksi$

8th Ed.

Fatigue I design stress: $\gamma\Delta_{f.I.8} = 4.25 \cdot ksi$

Fatigue I nominal resistance: $\Delta F_{n.I.8} = 2.6 \cdot ksi$

Fatigue II design stress: $\gamma\Delta_{f.II.8} = 1.94 \cdot ksi$

Fatigue II nominal resistance: $\Delta F_{n.II.8} = 2.81 \cdot ksi$

Comparing to Measured Data

The measured data for cross-frame member 07 includes the effective stress range and 0.01%-exceedance maximum stress range (based on axial stress) for the full data set. These values were computed in accordance with Sections 4.2.1.1 and 4.2.1.2 of the report.

Measured effective stress range: $S_{re} := 0.958ksi$

Measured 0.01% maximum stress range: $S_{rm} := 2.83ksi$

From these measured data and the design metrics, several observations can be made with regards to the fatigue behavior of this member, the accuracy of the commercial software, and how well the fatigue design loads represent the actual truck population. These comparisons are made with two ratios, presented in the summary table: analysis error percentage and design ratio.

Analysis error percentage quantifies how accurate the refined analysis model in conjunction with the AASHTO-defined fatigue loading predicted the cross-frame forces in member 07. Recall that the Fatigue II loading criteria in AASHTO reflects the "effective" truck in the load spectrum, so it can be compared directly to the measured effective stress range; Fatigue I reflects the 1-in-10,000 exceedance truck, so it can be compared directly to the measured maximum stress range. It is presented as a percent increase of the measured response. In other words, a positive 100% error means that the analysis model predicted an axial stress/force twice as high as the measured response.

The design ratio compares how the measured effective and maximum stress ranges compare to the corresponding AASHTO fatigue resistances. This ratio gives an indication of how well the fatigue detail is performing with respect to the design code.

4th Ed.

Analysis error percentage:

$$\%E_4 := \frac{\gamma\Delta_{f.4} - S_{re}}{S_{re}} = 122.42 \cdot \%$$

8th Ed.

Analysis error percentage (Fatigue I):

$$\%E_{I.8} := \frac{\gamma\Delta_{f.I.8} - S_{rm}}{S_{rm}} = 50.04 \cdot \%$$

(Con't) Figure E4-61: Sample calculation showing how AASHTO design metrics were determined

4th Ed.

Analysis error percentage:

$$\%E_4 := \frac{\gamma\Delta_{f.4} - S_{re}}{S_{re}} = 122.42\cdot\%$$

Design ratio:

$$DR_4 := \frac{\Delta F_{n.4}}{S_{re}} = 2.35$$

8th Ed.

Analysis error percentage (Fatigue I):

$$\%E_{I.8} := \frac{\gamma\Delta_{f.I.8} - S_{rm}}{S_{rm}} = 50.04\cdot\%$$

Analysis error percentage (Fatigue II):

$$\%E_{II.8} := \frac{\gamma\Delta_{f.II.8} - S_{re}}{S_{re}} = 102.61\cdot\%$$

Recall that Fatigue II governs for this design.

Design ratio:

$$DR_8 := \frac{\Delta F_{n.II.8}}{S_{re}} = 2.94$$

In terms of the analysis error, there are three major observations for this data set:

1. The refined analysis with the AASHTO design loads are always conservative, for both the effective and maximum cases (finite life and infinite life). At a minim um, the maximum stress range predicted by the code is 50% conservative from the measured maximum.
2. The 8th Ed. is more accurate than the 4th Ed. when it comes to effective stresses (122% conservative versus 103% conservative). This is largely a result of the SHRP 2 Project R19B, which recalibrated the fatigue limit state design parameters in AASHTO.
3. The design ratios for both editions are conservative and acceptable. Given the stress range spectrum measured at that cross-frame member, fatigue is currently not a concern.

(Con't) Figure E4-61: Sample calculation showing how AASHTO design metrics were determined

As stated in Section E4.2.3, anticipated goals of this in-service rainflow study were to (i) evaluate how well refined analyses and AASHTO fatigue loads predict cross-frame forces, (ii) evaluate how the instrumented members perform with respect to the nominal fatigue resistance, and (iii) compare past and present editions of the design specifications with respect to cross-frame fatigue. Those objectives are addressed by the observations from Table E4-19 below. Note that the bolded items provide a general discussion point that is used for each of the three bridges, and the text below the bolded category consists of observations unique to the instrumented cross-frame members at Bridge 1.

- **Comparing measured effective stress range (S_{re}) and measured equivalent cycle counts at the CAFL.** Higher effective stress ranges do not necessarily correspond to higher equivalent cycle counts. For example, member 17 has one of the lowest effective stress ranges measured (0.81 ksi), but it experienced the highest rate of equivalent 2.6-ksi cycles over the two-week monitoring period. The stress range spectrum has generally low magnitudes, but the frequency at which those cycles occur is greater than at any other member.
- **Comparing measured effective stress range (S_{re}) and measured maximum stress range (S_{rm}).** For the Bridge 1 cross-frames, higher effective stress ranges typically correspond to higher maximum stress ranges. An exception to the rule is cross-frame member 08. The low effective stress range (0.83 ksi) indicates that this member generally experienced smaller stress cycles; however, the (99.99th percentile) maximum stress is 3.35 ksi, which represents one of the highest cycles recorded of any instrumented member. The stress range spectrum of member 08 is generally

low, but it is prone to higher stress cycles presumably due to infrequent, heavy trucks in critical lanes.

- **Lane striping and traffic patterns affect the fatigue response of bridge components**. Cross-frame diagonals near the middle and right striped lanes (member 07, 09, 16, 17) have the highest rate of accumulated damage, as quantified by equivalent number of cycles at 2.6 ksi. Heavy trucks tend to drive in the lanes further to the right, so this trend makes sense. The top strut member (06) also has the least amount of damage accumulated, as expected.
- **Comparing measured maximum to effective stress ranges, S_{rm} to S_{re}, to the assumed 2.2 ratio (1.75/0.80) in AASHTO LRFD Specifications** (2017). Bridge 1 cross-frame data shows measured ratios ranging from 1.9 to 4.1 with the average at approximately at 2.8.
- **Comparing 4th Ed. factored design stresses ($\gamma\Delta f$) and 8th Ed. factored design stresses ($\gamma\Delta f$) for cross-frames and girders**. Design stresses based on the 4th Ed. criteria are between 2% and 20% more conservative than the design stresses based on the 8th Ed. criteria for cross-frames. This is because newer versions of AASHTO have eliminated the highly infrequent double-truck loading case for cross-frame fatigue design.
- **Comparing factored design stresses based on refined analysis and AASHTO fatigue loading criteria (4th Ed. and 8th Ed.) to measured effective and maximum stress ranges**. The 8th Ed. refined analysis overpredicts effective stress ranges between 33% and 130% and the maximum stress ranges between 14% and 86% compared to measured responses. In all cases for the Bridge 1 cross-frames, the AASHTO procedures resulted in a conservative prediction. Note that this inherent conservatism in the fatigue design criteria is extensively examined in Phase III (Appendix F) for a wider range of bridge geometries.
- **Comparing factored design stresses based on refined analysis ($\gamma\Delta f$) to the nominal fatigue resistance (ΔF_n)**. For the Bridge 1 cross-frames, all nominal resistances exceeded the design stresses, which implies a satisfactory design under both specifications. For example under 4th Ed. AASHTO, the factored design stress for member 03 is 2.23 ksi; the nominal resistance of the same member is 2.25 ksi. The capacity exceeds the demand.
- **Comparing the measured stress ranges (S_{re}, S_{rm}) to the nominal fatigue resistance (ΔF_n)**. For all Bridge 1 cross-frames, the nominal resistances exceeded all appropriate measured stress ranges, which implies all members are in a safe condition with respect to fatigue. For example, the lowest design ratio under the 8th Ed. criteria, listed in Table E4-19, is 2.86 for member 04. This ratio means that the nominal fatigue capacity of that member is nearly three times higher than the measured effective stresses.

Figure E4-62 shows these observations graphically on the same histogram plot presented in Figure E4-60, except that different benchmark stresses are overlaid. The benchmark stresses include measured effective stress range, AASHTO LRFD (8th Ed.) Fatigue II factored design stress, and AASHTO LRFD (8th Ed.) nominal resistance. These benchmarks illustrate the governing design check for cross-frame member 07 under the current specifications. From this histogram plot, it is clear that the measured effective stress range is less than the predicted, factored design stress, and the factored design stress is less than the nominal resistance. This relationship indicates a satisfactory design and safe fatigue detail.

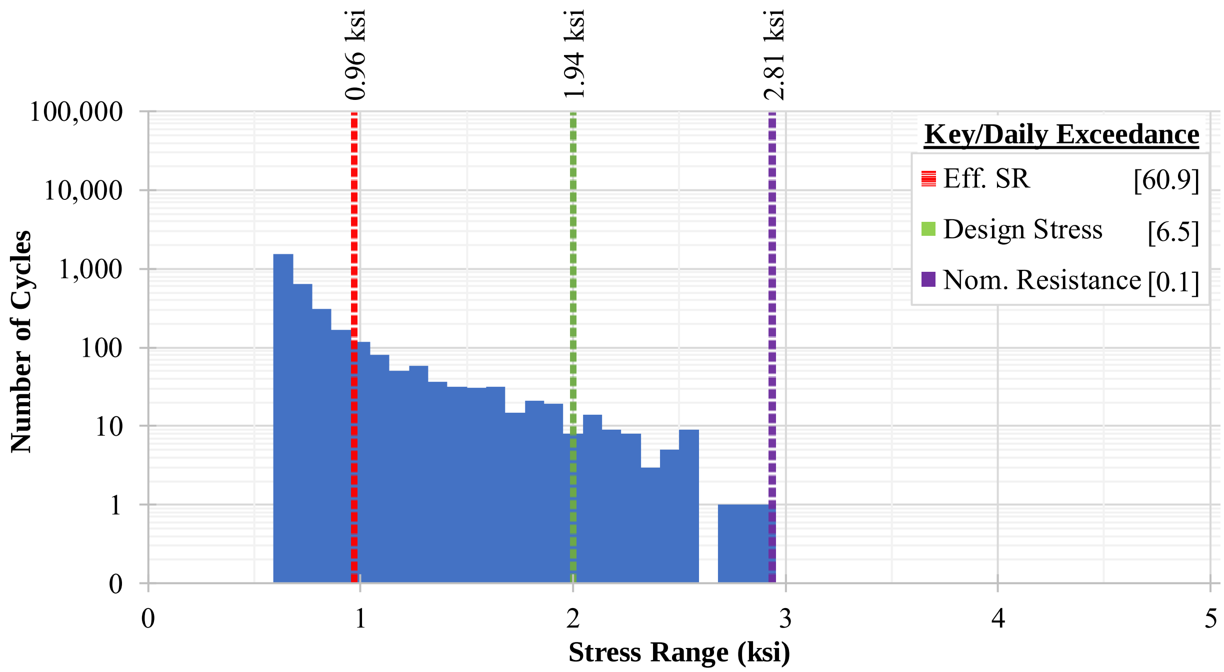

Figure E4-62: Sample rainflow histogram for cross-frame member 07 at Bridge 1 showing key Fatigue II design metrics

Another objective listed in Section E4.2.3 is to evaluate daily and hourly trends by comparing measured effective and index stresses ranges over different periods of time. The RT accomplished this by computing effective stress ranges and equivalent number of cycles at an index stress range (on a per hour basis), which was selected as 2.6 ksi, over various time windows of data. In Figure E4-63, those parameters were computed for each day of the monitoring period. In Figure E4-64, the parameters were computed for various three-hour windows. In both cases, two major benchmarks are included on the effective stress range axis for reference: the truncation stress (0.65 ksi) and the CAFL (2.6 ksi). These plots were developed for all instrumented cross-frame members, but only the results of cross-frame member 09 is presented. The trends are consistent for all members.

There are three major observations to note from the daily trend plot:

- Similar to the discussion in Section E4.2.1.3, normalizing damage as an equivalent number of cycles at an index stress range provides a much better indicator of stress range magnitude and frequency of major truck events. The trends are more obvious and pronounced for the equivalent number of cycles at 2.6 ksi than effective stress range.
- The effective stress range does deviate slightly throughout the week. This indicates that more heavy trucks make up the full truck spectrum during the week than during the weekend. This value, however, does not provide any insight on changes in truck traffic volume.
- Damage accumulation, as quantified by equivalent number of cycles at the index stress range (2.6 ksi), provides more insight on fluctuations in truck traffic volume. During weekends and holidays (5/28 is Memorial Day), damage accumulation is significantly less than during weekdays.

The observations for the hourly trend plot are similar to the daily trend plot, except that:

- Truck traffic volume and damage accumulation is greatest on average between 6 am and 12 pm. The same metrics are lowest between 9 pm and midnight. This indicates that heavy truck traffic is most prevalent on this bridge during the morning rush hour.

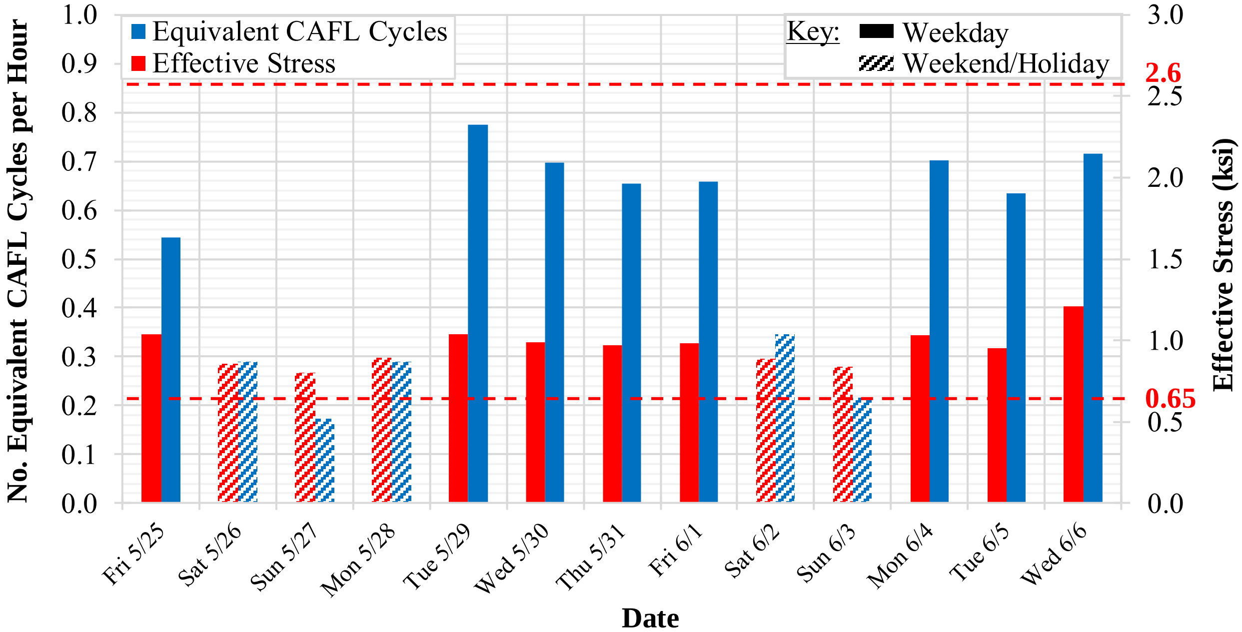

Figure E4-63: Daily stress range trends cross-frame member 09 at Bridge 1

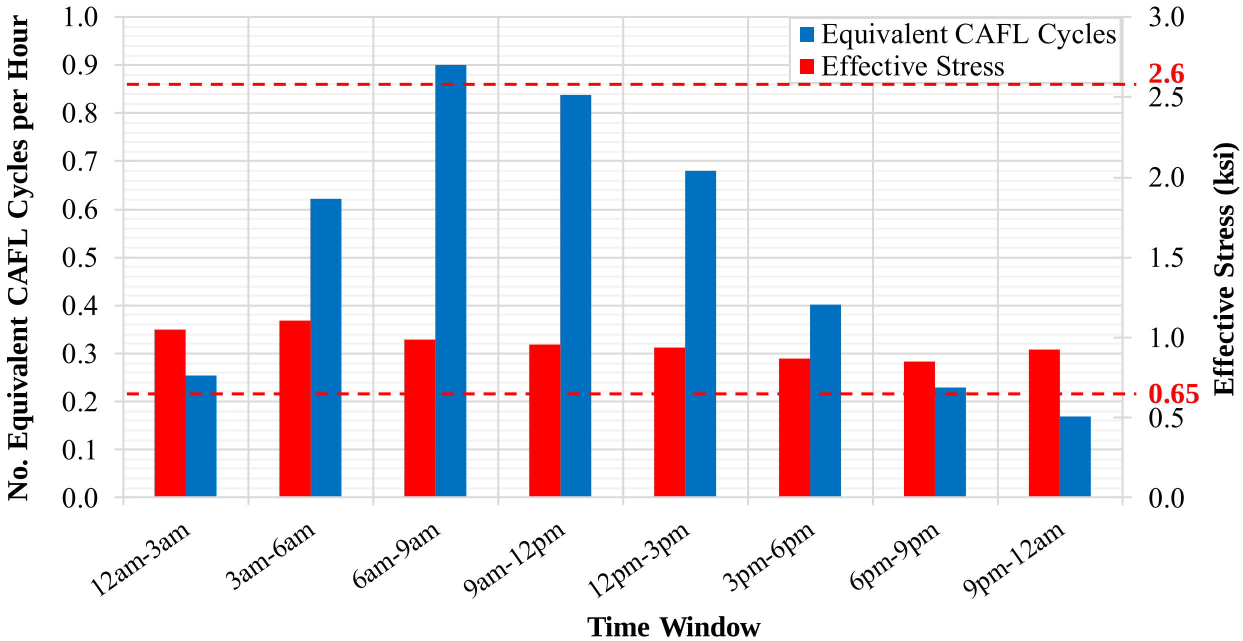

Figure E4-64: Hourly stress range trends cross-frame member 09 at Bridge 1

These time-dependent trends are interesting to note but are not critical in the overall scheme of fatigue evaluation, especially for the Fatigue II finite-life limit state. Effective trucks and effective stress ranges are intended to represent the full spectrum of applied loads over the life of the bridge. Time-dependent deviations are inherently considered in the design provisions. As such, the effective stress ranges of the measured data, computed in Table E4-19, are based on the full data set (i.e., the filtered data over the four-week monitoring period, where the tails of the spectra have been truncated); therefore, they inherently consider low and high periods of heavy truck traffic and effectively "average them out."

E4.2.4.2 Girder Data for Bridge 1

Similar to E4.2.4.1, rainflow data for select girder flanges was measured and processed by the RT. Many of the procedures outlined in the previous section were also replicated for the girder data. The same monitoring period (May 24th through June 6th) is presented in this section, and the same rainflow parameters including time window size, bin size, and threshold strain were implemented. The stress at which the bin counts were truncated for girder data, 1.0 ksi, is outlined in Section E4.2.2.

The major difference in how cross-frame and girder rainflow data was processed was the use of a real-time linear regression algorithm. As mentioned in Section E4.2.4.1, only the axial response of the cross-frames members was processed and presented in the appendix to match the design approach of the corresponding fatigue detail. The real-time linear regression algorithm isolated the axial component from bending stresses in the eccentrically loaded cross-frame members.

For the transverse stiffener-to-flange weld detail that is critical for girder flanges, the design approach is to evaluate both the load-induced longitudinal stresses and lateral stresses due to torsional deformation of the girder. The response of each flange tip is typically evaluated separately in the fatigue design checks, and the tip with the higher combined stresses governs. For bottom flanges in positive bending, the governing stress combination is typically the tensile stress range due to primary longitudinal bending and the tensile flange tip due to lateral flange bending. As outlined previously, the RT instrumented each girder bottom flange with two strain gages, each two inches from opposite tips (Figure E3-7). Each strain gage on a girder flange measured the combined effects of longitudinal and lateral bending components. To match the standard design approach, the response of each individual flange strain gage was processed, as opposed to a combined response. To simplify the post-processing, the RT assumed that the stresses at the extreme tips of the girder flange are equivalent to the stresses measured two inches inset from the tips. This assumption is reasonable given the wide flange widths of the three subject bridges.

Figure E4-65 presents a sample histogram for fascia girder 5 at cross-frame line 4 near the maximum positive moment region of the span. The right flange tip (right side relative to flow of northbound traffic) recorded more significant stress cycles than the left tip, likely due to the direction and magnitude of lateral bending stresses induced during truck events. As a result, only the critical right-tip histogram is presented. Note that rainflow counts were totaled over the entire monitoring period. Also plotted on the figure are key benchmarks and the average number of occurrences in which those benchmarks were exceeded per day. Note that the CAFL of 12 ksi is out of the plot range.

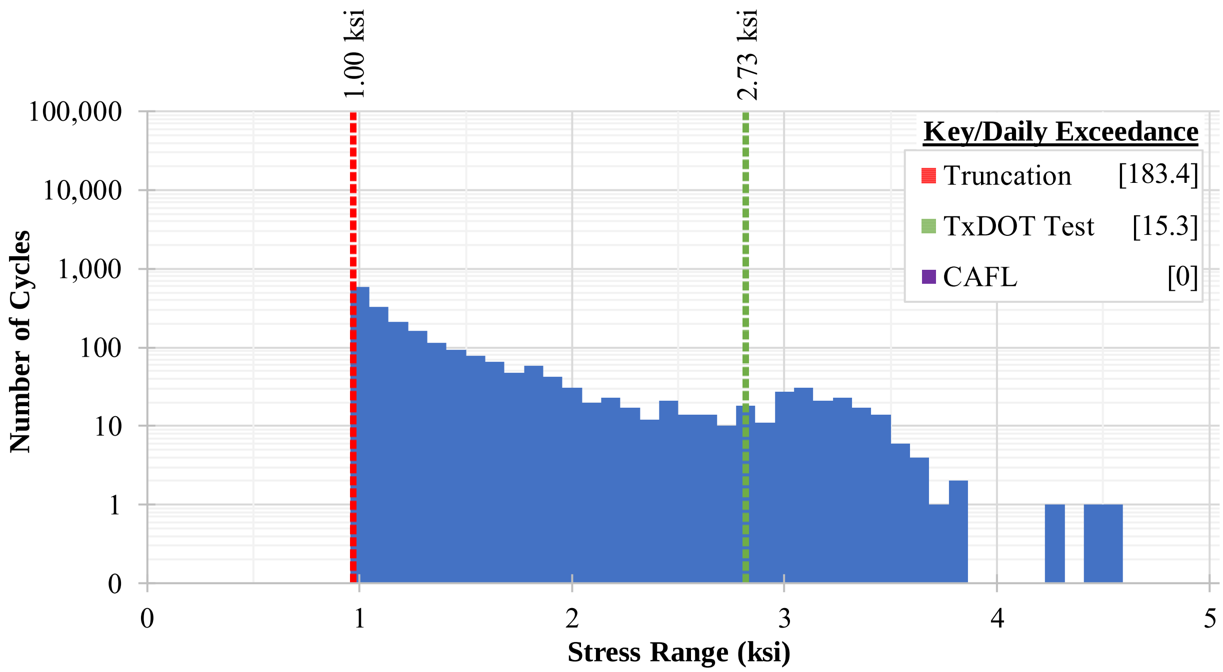

Figure E4-65: Sample rainflow histogram for the critical flange tips at girder 3 (near cross-frame line 4) at Bridge 1

Figure E4-65 presents a few key concepts, many of which were introduced in Section E4.2.1 and E4.2.2. These concepts include:

- The 1.0-ksi truncation stress outlined in Section E4.2.2.1 was implemented and is identified on the plot. All stress cycles measured below 1 ksi were eliminated from the data set as to not skew the effective stress range calculation. The stress range spectrum typically demonstrates higher stress cycles for girders than cross-frames, as shown in the comparison of Figure E4-60 and Figure E4-65.
- On average there were 180 stress cycles that exceeded the truncation stress per day, but none exceeded the Category C′ CAFL of 12 ksi. A detailed comparison of measured data and AASHTO design metrics is discussed later in this section.
- 15 stress cycles per day exceeded the "TxDOT Test" reference stress range, which is comparable in weight to the factored Fatigue II design truck.

Full data set histogram plots for the rest of the instrumented girder flanges are not presented in this appendix. Similar to the cross-frame data, a more convenient method to examine girder data is to tabulate all key values, which include the measured effective, maximum, and index stress ranges, and compare them to important AASHTO-related design metrics. Table E4-20 presents the summarized comparison between measured values and AASHTO metrics for girder flanges. The girders are identified by girder number, left or right tip, and cross-frame location (line 4 or 7).

A sample calculation showing how the factored design stresses and resistances for girder flanges were determined is not presented in this appendix. However, the procedure for girder flanges is similar to that shown in Figure E4-61 for cross-frame members. The same 3-D Software A model was used to perform an influence surface analysis of the AASHTO fatigue loads on the fully-composite bridge system. The deck and girders were modeled with shells elements, and the cross-frame members were modeled with truss elements, modified by the appropriate stiffness reduction factor due to end connection eccentricity. The major differences between the assumptions and approach made in Figure E4-61 and the calculations made for girder flanges are the following:

- Cross-frame stresses, modeled as truss elements, were determined outside of the analysis software by converting force to stress. Girder stresses are taken directly from the appropriate shell stresses in the model. Stresses were taken at the flange tips near the locations of the strain gages; but for a given girder, only the governing tip stress is presented in Table E4-20.
- Fatigue loading criteria for girders has remained consistent between the 4th and 8th Editions of the AASHTO LRFD Specifications, unlike the criteria for cross-frames which has eliminated the double-truck case. A single fatigue truck is to be positioned in various longitudinal and transverse positions, regardless of striped lanes, to maximize force effects in the girders. Since the influence surface analysis produces a stress envelope, certain assumptions were made with regards to the stress range. The stress range was conservatively taken as the difference between the maximum and minimum stresses. The RT acknowledges that the maximum and minimum stress could potentially correspond to different transverse truck positions, but major discrepancies in the stress range are not anticipated from this assumption.
- Several parameters are different for the Category C′ girder details, as opposed to the Category E′ cross-frame details. Those parameters include the fatigue category constant (A), constant-amplitude threshold stress (F_{TH}), and number of cycles per truck passage (n).

Note that both flange tips at girder 1 near cross-frame line 4 were excluded from Table E4-20. During the two-week monitoring period presented here, the rainflow data revealed a disproportionate percentage of high stress ranges, which the RT concluded to be a product of electromechanical noise. Since the rainflow results are not reliable, girder 1 data are neglected from the study.

Also note that the finite life (Fatigue II) design ratio related to the 8th Edition of the AASHTO LRFD Specifications has been formatted with a strikethrough. Unlike in Figure E4-61, the Fatigue I limit state governs fatigue design for this Category C′ detail despite the low average daily truck traffic (ADTT). As such, the design ratios for Fatigue II are not considered.

Table E4-20: Comparison between measured rainflow girder response and key AASHTO design metrics (Bridge 1)

Girder Flange ID	Measured Response			4th Edition				8th Edition | Fatigue II (Finite Life)				8th Edition | Fatigue I (Infinite Life)			
	Avg. Daily Equiv. Cycles @ 12 ksi	Measured Eff. Stress, S_{re} (ksi)	Measured 0.01% Stress, S_{rm} (ksi)	Design Stress, $\gamma\Delta f$ (ksi)	Nom. Resistance, ΔF_n (ksi)	% Error Analysis $\frac{(\gamma\Delta f - S_{re})}{S_{re}}$	Design Ratio $\frac{\Delta F_n}{S_{re}}$	Design Stress, $\gamma\Delta f$ (ksi)	Nom. Resistance, ΔF_n (ksi)	% Error Analysis $\frac{(\gamma\Delta f - S_{re})}{S_{re}}$	Design Ratio $\frac{\Delta F_n}{S_{re}}$	Design Stress, $\gamma\Delta f$ (ksi)	Nom. Resistance, ΔF_n (ksi)	% Error Analysis $\frac{(\gamma\Delta f - S_{rm})}{S_{rm}}$	Design Ratio $\frac{\Delta F_n}{S_{rm}}$
2R|4	0.94	1.40	3.70	2.65	6.00	89%	4.30	2.82	7.95	102%	~~5.69~~	6.17	12.00	67%	3.25
2L|4	1.82	1.54	4.39	2.65	6.00	72%	3.89	2.82	7.95	83%	~~5.15~~	6.17	12.00	41%	2.73
3R|4	0.93	1.40	3.70	1.90	6.00	35%	4.29	2.02	7.95	44%	~~5.68~~	4.42	12.00	20%	3.25
3L|4	1.70	1.47	4.22	1.90	6.00	29%	4.09	2.02	7.95	38%	~~5.42~~	4.42	12.00	5%	2.84
4R|4	1.28	1.43	3.78	2.97	6.00	108%	4.20	3.16	7.95	122%	~~5.57~~	6.92	12.00	83%	3.17
4L|4	1.21	1.39	4.13	2.97	6.00	113%	4.31	3.16	7.95	127%	~~5.71~~	6.92	12.00	67%	2.90
5R|4	0.58	1.93	4.39	4.22	6.00	119%	3.12	4.50	7.95	134%	~~4.13~~	9.85	12.00	124%	2.73
5L|4	0.51	1.88	4.39	4.22	6.00	124%	3.18	4.50	7.95	139%	~~4.22~~	9.85	12.00	124%	2.73
3R|7	1.38	1.39	2.83	1.85	6.00	34%	4.33	1.98	7.95	42%	~~5.73~~	4.32	12.00	53%	4.24
3L|7	1.11	1.35	2.57	1.85	6.00	37%	4.45	1.98	7.95	46%	~~5.89~~	4.32	12.00	68%	4.68
4R|7	1.91	1.47	4.13	2.77	6.00	89%	4.09	2.96	7.95	102%	~~5.41~~	6.47	12.00	57%	2.90
4L|7	1.26	1.38	3.18	2.77	6.00	101%	4.34	2.96	7.95	114%	~~5.75~~	6.47	12.00	104%	3.78

As stated in Section E4.2.3, the anticipated goals of this NCHRP project and specifically the in-service rainflow study largely focus on cross-frames. Previous research on cross-frames is less extensive than girders. In fact, the recent modifications to AASHTO fatigue load factors were based on line-girder parametric studies of weigh-in-motion data; three-dimensional effects and the contribution of cross-frames to distributing live loads were neglected (Modjeski and Masters 2015). Therefore, the results and observations outlined in Section E4.2.4.1 for cross-frames are perhaps more important to the project scope. However, studying the rainflow data for girders serves as a check on the current design standards for fatigue limit states, given that many of the provisions were calibrated specifically for girders.

The following observations from Table E4-20 are similar to the observations from Table E4-19. The same general format of the observations is followed. The bolded text represents the general categories investigated by the RT, and the commentary within that category are specific observations made for this data set.

- **Comparing measured effective stress range (S_{re}) and measured equivalent cycle counts at the CAFL.** Similar to the cross-frame response, higher effective stress ranges do not necessarily correspond to higher equivalent cycle counts at the index stress range, 12 ksi. For example, the left flange tip of girder 3 has one of the lower effective stress ranges measured (1.47 ksi) but experienced the one of the highest rate of equivalent 12.0-ksi cycles (1.70 cycles at 12 ksi per day). This behavior is consistent with Figure E4-19, which demonstrates that the middle girder experienced the lowest maximum stresses of the five-girder system. The middle girder experiences a high number of stress cycles relative to the other girders, but the magnitudes are not as large.
- **Comparing measured effective stress range (S_{re}) and measured maximum stress range (S_{rm}).** Similar to Bridge 1 cross-frames, girder flanges with higher effective stress ranges generally have higher maximum stress ranges.
- **Lane striping and traffic patterns affect the fatigue response of bridge components**. There is a clear distinction in girder response at each tip of a flange. For example, the right tip of the girder 2 flange accumulates damage at a rate of 0.94 cycles at 12 ksi per day, whereas the left tip accumulates damage at a rate of 1.82 cycles at 12 ksi per day. The differences in the effective stress ranges are also evident. Lateral flange stresses can contribute a significant amount, especially for girders that generally experience low bending.
- **Comparing measured maximum to effective stress ranges, S_{rm} to S_{re}, to the assumed 2.2 ratio (1.75/0.80) in AASHTO LRFD Specifications** (2017). Bridge 1 girder data shows measured ratios ranging from 1.9 to 3.0 with average at approximately 2.5.
- **Comparing 4th Ed. factored design stresses ($\gamma\Delta f$) and 8th Ed. factored design stresses ($\gamma\Delta f$) for cross-frames and girders**. Contrary to cross-frame criteria, factored design stresses in accordance with the 8th Ed. are consistently 7% more conservative than the factored design stresses in accordance with the 4th Ed. The load factors have increased from 0.75 to 0.8 for the "effective truck."
- **Comparing factored design stresses based on refined analysis and AASHTO fatigue loading criteria (4th Ed. and 8th Ed.) to measured effective and maximum stress ranges**. The 8th Ed. refined analysis overpredicts effective stress ranges between 38% and 139% and overpredicts maximum stress ranges between 5% and 124%. In general, the AASHTO procedures result in a conservative design.
- **Comparing factored design stresses based on refined analysis ($\gamma\Delta f$) to the nominal fatigue resistance (ΔF_n)**. For the Bridge 1 girders, all nominal resistance exceeded the design stresses, which implies a satisfactory design under both specifications. For example under 4th Ed. AASHTO, the governing, factored design stress for girder 5 is 4.22 ksi; the nominal resistance of the same flange is 6.0 ksi. The capacity exceeds the demand.

- **Comparing the measured stress ranges (S_{re}, S_{rm}) to the nominal fatigue resistance (ΔF_n).** For all Bridge 1 girders, the nominal resistances exceeded all appropriate measured stress ranges, which implies all members are in a safe condition with respect to fatigue. For example, the lowest design ratio under the 8th Ed. criteria is 2.73.

E4.2.5 Bridge 2 Results

The following subsections summarize the in-service rainflow data for the instrumented cross-frames and girders of Bridge 2.

As detailed in Section E2.2, Bridge 2 has the smallest instrumented span-to-depth ratio of the three subject bridges and carries five lanes of southbound IH 45 traffic. Truck traffic volume on this bridge is high, as observed by the RT during numerous site visits. Given the stiffness of the span, cross-frame and girder stress cycles are expected to be relatively low compared to other skewed bridges with comparable skew angles but longer span lengths. Major stress cycles are expected to be more frequent than what was observed at Bridge 1.

Refer to Figure E4-23 through Figure E4-25 for the cross-frame numbering scheme, which is used throughout this section. The girders are identified by the numbering scheme used on the design plan and the associated cross-frame line. This is provided graphically on Figure E3-19 through Figure E3-22.

E4.2.5.1 Cross-Frame Data for Bridge 2

Table E3-1 shows that in-service rainflow monitoring for Bridge 2 was conducted between June 12th through July 8th of 2018. In total, approximately four weeks of in-service data was measured. The instrumentation period as well as the removal was dictated by the schedule of the bridge owner. Note that there was no down period in the DAQ system to update the programming as with Bridge 1. The real-time linear regression algorithm was implemented from the first day of in-service monitoring through when the instrumentation was removed.

For the four-week period between June 12th and July 8th, the axial stress rainflow counts for each cross-frame member were compiled and sorted into specific bins. Bin size and truncation stress parameters used for this data set are provided in Section E4.2.2. Figure E4-66 presents a sample histogram for cross-frame member 08, which includes rainflow counts summed over the entire four-week monitoring period. Cross-frame member 08 is a diagonal between interior girders 21 and 22 near cross-frame line 5; this diagonal was one of the highest-stressed members during the controlled live load test. Also plotted on the figure are key benchmarks and the average number of occurrences in which those benchmarks were exceeded per day.

Many of the same observations can be made from Figure E4-66 as from Figure E4-60. The major difference between the sample histogram presented for Bridge 2 and Bridge 1 is the total number of counts above the truncation stress of 0.65 ksi. Cross-frame member 08 at Bridge 2 recorded nearly eight times the amount of cycles above the threshold stress per day than member 07 at Bridge 1. This demonstrates the difference in truck traffic volume between the two bridges.

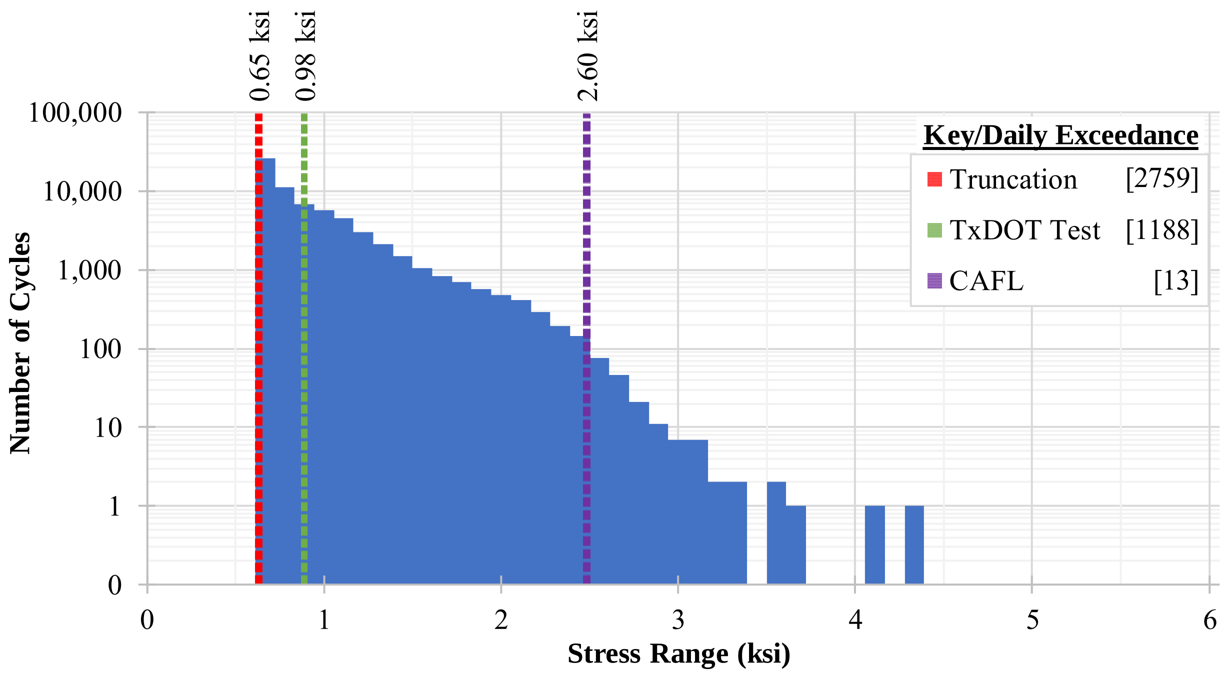

Figure E4-66: Sample rainflow histogram for cross-frame member 08 at Bridge 2

Full data set histogram plots for the rest of the instrumented cross-frames are not presented in this appendix; instead, the stress spectra are evaluated in terms for the three major metrics: effective stress range, maximum stress range, and index stress range. Similar to Table E4-19 for Bridge 1, Table E4-21 presents the comparison between measured data and AASHTO design metrics. The table summarizes all pertinent characteristics of the stress range spectra for each instrumented cross-frame member. Note that the infinite life (Fatigue I) design ratio related to the 8th Edition of the AASHTO LRFD Specifications has been formatted with a strikethrough. Similar to Bridge 1, the Fatigue II limit state governs fatigue design for Bridge 2 cross-frames.

Table E4-21: Comparison between measured rainflow cross-frame response and key AASHTO design metrics (Bridge 2)

Cross-Frame No.	Measured Response			4th Edition				8th Edition | Fatigue II (Finite Life)				8th Edition | Fatigue I (Infinite Life)			
	Avg. Daily Equiv. Cycles @ 2.6 ksi	Measured Eff. Stress, S_{re} (ksi)	Measured 0.01% Stress, S_{rm} (ksi)	Design Stress, $\gamma\Delta f$ (ksi)	Nom. Resistance, ΔF_n (ksi)	% Error Analysis $\frac{(\gamma\Delta f - S_{re})}{S_{re}}$	Design Ratio $\frac{\Delta F_n}{S_{re}}$	Design Stress, $\gamma\Delta f$ (ksi)	Nom. Resistance, ΔF_n (ksi)	% Error Analysis $\frac{(\gamma\Delta f - S_{re})}{S_{re}}$	Design Ratio $\frac{\Delta F_n}{S_{re}}$	Design Stress, $\gamma\Delta f$ (ksi)	Nom. Resistance, ΔF_n (ksi)	% Error Analysis $\frac{(\gamma\Delta f - S_{rm})}{S_{rm}}$	Design Ratio $\frac{\Delta F_n}{S_{rm}}$
01	4.1	0.83	1.68	1.63	1.71	96%	2.05	1.21	1.21	45%	1.45	2.64	2.60	57%	~~1.55~~
02	12.4	0.88	2.03	1.33	1.71	51%	1.94	1.05	1.21	19%	1.37	2.31	2.60	14%	~~1.28~~
03	6.1	0.82	1.45	1.28	1.71	56%	2.09	1.19	1.21	45%	1.48	2.61	2.60	80%	~~1.79~~
04	29.3	0.93	2.15	1.86	1.71	100%	1.84	1.48	1.21	59%	1.30	3.23	2.60	51%	~~1.21~~
05	2.7	0.79	1.10	0.84	1.71	5%	2.16	0.78	1.21	-2%	1.53	1.70	2.60	54%	~~2.36~~
07	502.0	0.97	2.73	1.47	1.71	53%	1.77	1.53	1.21	59%	1.26	3.35	2.60	23%	~~0.95~~
08	245.0	1.16	3.77	1.94	1.71	68%	1.48	1.83	1.21	58%	1.05	4.00	2.60	6%	~~0.69~~
09	123.7	1.12	3.54	2.28	1.71	104%	1.53	1.99	1.21	78%	1.08	4.36	2.60	23%	~~0.73~~
10	41.2	1.15	3.31	1.80	1.71	56%	1.49	1.82	1.21	58%	1.05	3.98	2.60	20%	~~0.79~~
11	206.0	1.19	3.19	1.84	1.71	55%	1.44	1.83	1.21	54%	1.02	3.99	2.60	25%	~~0.82~~
13	15.3	0.83	1.80	1.59	1.71	92%	2.07	1.25	1.21	51%	1.46	2.74	2.60	52%	~~1.45~~
15	48.6	0.87	1.91	1.06	1.71	21%	1.96	0.80	1.21	-9%	1.39	1.75	2.60	-9%	~~1.36~~
16	0.4	0.78	0.99	1.45	1.71	87%	2.21	1.23	1.21	59%	1.56	2.70	2.60	174%	~~2.64~~
17	45.6	0.87	1.80	2.15	1.71	148%	1.98	1.93	1.21	123%	1.40	4.22	2.60	135%	~~1.45~~

A sample calculation, similar to Figure E4-61, is not presented for Bridge 2. The procedure for Bridge 2 is similar to that shown in Figure E4-61; the same modeling techniques and assumptions outlined for the Bridge 1 model were also used for the Bridge 2 model. The major differences between the approach used for Bridge 1 and Bridge 2 are related to traffic-pattern inputs. For Bridge 2, the number of lanes and ADTT are much higher than for Bridge 1. These variables affect the Fatigue II nominal resistance calculation.

The observations from Table E4-21 (Bridge 2) are similar to the observations from Table E4-19 (Bridge 1). The bolded text represents the general discussion points that were introduced in Section E4.2.4, and the commentary within the bolded category describes unique aspects of the cross-frame data at Bridge 2. Note that the comparisons between Bridge 1 and 2 are presented in Section E4.2.7.

- **Comparing measured effective stress range (S_{re}) and measured equivalent cycle counts at the CAFL.** Similar to the Bridge 1 cross-frame data, higher effective stress ranges do not necessarily correspond to higher equivalent cycle counts at 2.6 ksi. For example, cross-frame member 07 has the fifth highest effective stress ranges measured (0.97 ksi) but experienced the highest rate of equivalent 2.6-ksi cycles (502 cycles at 2.6 ksi per day).
- **Comparing measured effective stress range (S_{re}) and measured maximum stress range (S_{rm}).** Similar to the Bridge 1 data, higher measured effective stress ranges typically relate to higher measured maximum stress ranges.
- **Lane striping and traffic patterns affect the fatigue response of bridge components**. Cross-frame diagonals along cross-frame line 5 near midspan (member 07, 08, 09, 10, and 11) have the highest rate of accumulated damage. Cross-frame members near the supports experience less fatigue damage despite the close proximity to a support. This behavior demonstrates that maximum differential deflections and torsional deformations of the girders occurred near midspan.
- **Comparing measured maximum to effective stress ranges, S_{rm} to S_{re}, to the assumed 2.2 ratio (1.75/0.80) in AASHTO LRFD Specifications** (2017). Bridge 2 cross-frame data shows measured ratios ranging from 1.3 to 3.3 with the average at approximately 2.3.
- **Comparing 4th Ed. factored design stresses ($\gamma\Delta f$) and 8th Ed. factored design stresses ($\gamma\Delta f$) for cross-frames and girders**. Similar to the Bridge 1 data, factored 4th Ed. design stresses are typically more conservative than the 8th Ed. factored design stresses, despite the increase in load factors. The exceptions are cross-frame members 07 and 10, in which the 8th Ed. loading conditions and load factors produced slightly higher design stresses than the 4th Ed. provisions.
- **Comparing factored design stresses based on refined analysis and AASHTO fatigue loading criteria (4th Ed. and 8th Ed.) to measured effective and maximum stress ranges**. Similar to the Bridge 1 data, refined analysis generally results in a conservative prediction of force for both maximum and effective stress ranges when compared to the measured data. The exceptions are member 05 (effective stress) and 15 (effective and maximum), in which the refined analysis underpredicted force effects between 2% and 9%. However, the underpredicted cross-frame members had very small measured and predicted stresses, compared to the other instrumented cross-frame members of interest.
- **Comparing factored design stresses based on refined analysis ($\gamma\Delta f$) to the nominal fatigue resistance (ΔF_n)**. For the Bridge 2 cross-frames, most members exhibited a satisfactory design. However, there were a few instances in which the factored design stress exceeded the nominal resistance, which would indicate an inadequate design. For example, cross-frame member 09 exhibited an overstress of 25% with respect to 4th Ed. code criteria. These observed "deficiencies" are likely due to different modeling techniques and design assumptions used by the original design engineer. Similar observations can be made when using the 8th Ed. as the standard, where Fatigue II is the governing limit state.
- **Comparing the measured stress ranges (S_{re}, S_{rm}) to the nominal fatigue resistance (ΔF_n)**. For all the Bridge 2 cross-frames, the nominal resistances exceeded all appropriate measured stress

ranges, which implies all members are safe with respect to fatigue. For example, the lowest design ratio under the 8th Ed. criteria is 1.02 for member 1.

Figure E4-67 shows these observations graphically on the same histogram plot presented in Figure E4-66 with different benchmark stresses overlaid: measured effective stress range, AASHTO LRFD (8th Ed.) Fatigue II factored design stress, and AASHTO LRFD (8th Ed.) nominal resistance. These benchmarks illustrate the governing design check for cross-frame member 08 under the current specifications. From this histogram plot, it is evident that the measured effective stress range is less than the factored design stress and the nominal resistance. During the four-week period, over 660 stress cycles per day exceeded the nominal Fatigue II resistance, but the cumulative effect of the entire truck population did not exceed the estimated design capacity. However, the design stress does exceed the nominal resistance, which would indicate a poor original design. As previously mentioned, this discrepancy is likely a result of different design assumptions made between the original designer and the RT, which only emphasizes the potential variability with refined analysis results.

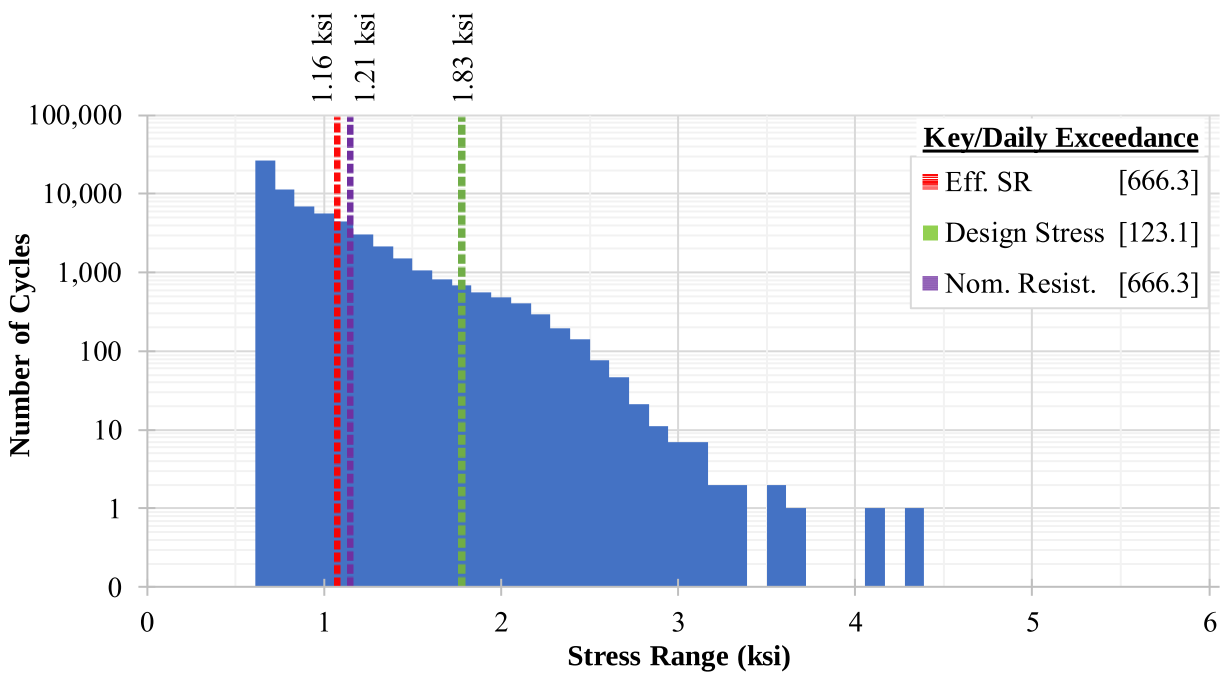

Figure E4-67: Sample rainflow histogram for cross-frame member 08 at Bridge 2 showing key Fatigue II design metrics

Similar to Section E4.2.4.1 for Bridge 1, the RT also evaluated the daily and hourly trends of the Bridge 2 data. The procedures used to infer time-dependent trends for Bridge 1 data were replicated for the Bridge 2 data; refer to Section E4.2.4.1 for more information. Figure E4-68 presents the daily trends of the rainflow data for cross-frame member 08 of Bridge 2, and Figure E4-69 presents the hourly trends. From these plots, similar conclusions can be made about the Bridge 2 data and the Bridge 1 data. Damage accumulation, as quantified by equivalent number of cycles at 2.6 ksi, is highest during the weekdays and lowest during the weekends and holidays (July 4th). Additionally, truck traffic volume and damage accumulation are greatest on average between 6 am and noon, which is similar to Bridge 1, and least between 9 pm and midnight.

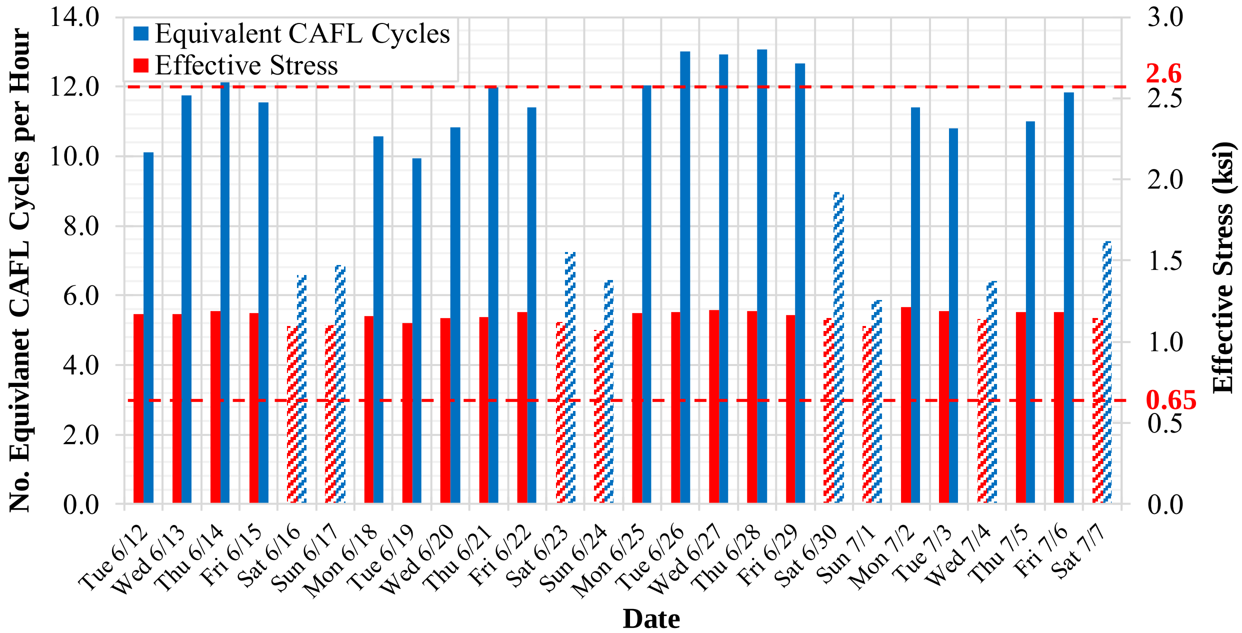

Figure E4-68: Daily stress range trends cross-frame member 08 at Bridge 2

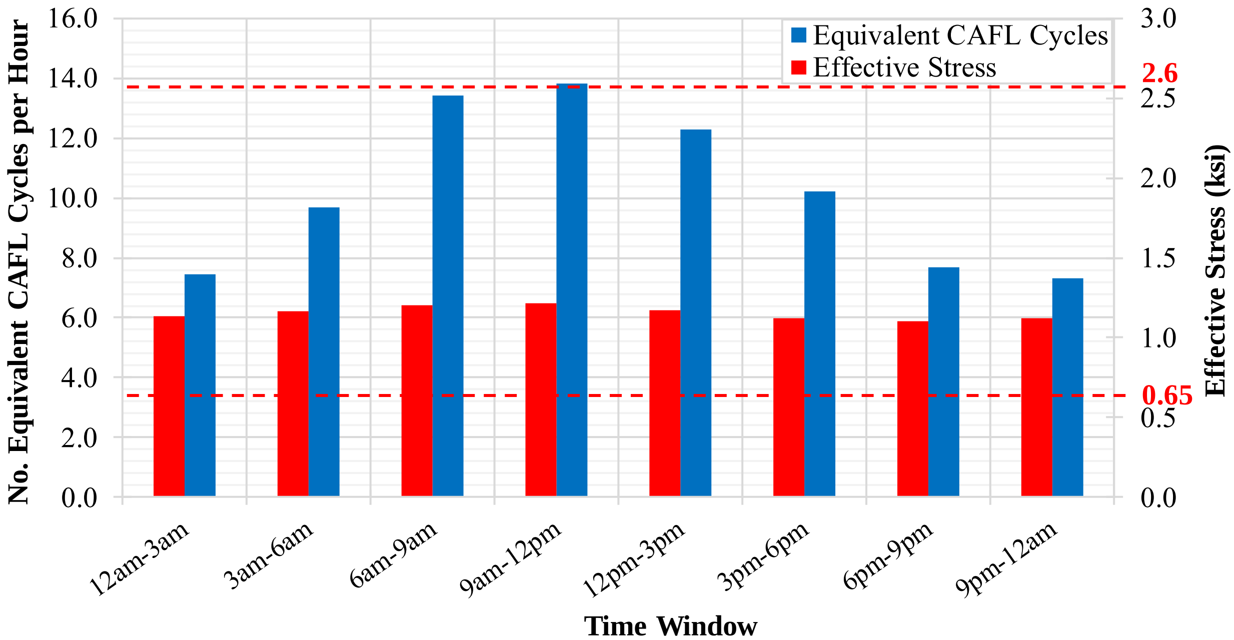

Figure E4-69: Hourly stress range trends cross-frame member 08 at Bridge 2

As discussed in Section E4.2.4.1, these time-dependent trends are not critical in the overall scheme of the fatigue evaluation. The effective stress range of the entire four-week data set, tabulated in Table E4-21, captures the peaks and valleys of the full truck spectrum and quantify its cumulative effect.

E4.2.5.2 Girder Data for Bridge 2

Similar to E4.2.5.1, rainflow data for selected girder flanges was measured and processed by the RT for Bridge 2. Many of the procedures outlined in the previous section were replicated for the girder data. The same monitoring period (June 12th through July 8th) are presented in this section, and the same rainflow parameters including time window size, bin size, and truncation stress were implemented. Similar to the Bridge 1 girder data, the response of each individual flange strain gage was processed to match the design approach of the critical Category C′ detail, as opposed to a combined response like the cross-frame data. The truncation stress was selected as 1.15 ksi, as outlined in Section E4.2.2.1.

Figure E4-70 presents a sample histogram for girder 19 at cross-frame line 8. Girder 19 at line 8 is near the assumed uniform dead load inflection point in the three-span continuous girder, so stress cycles are expected to include significant stress reversal. The right flange tip (right side relative to flow of southbound traffic) recorded more significant stress cycles than the left tip, likely due to the direction and magnitude of lateral bending stresses induced during truck events. As a result, only the critical right-tip histogram is presented. Note that rainflow counts are the totaled values over the entire four-week monitoring period. Also plotted on the figure are key benchmarks and the average number of occurrences in which those benchmarks were exceeded per day.

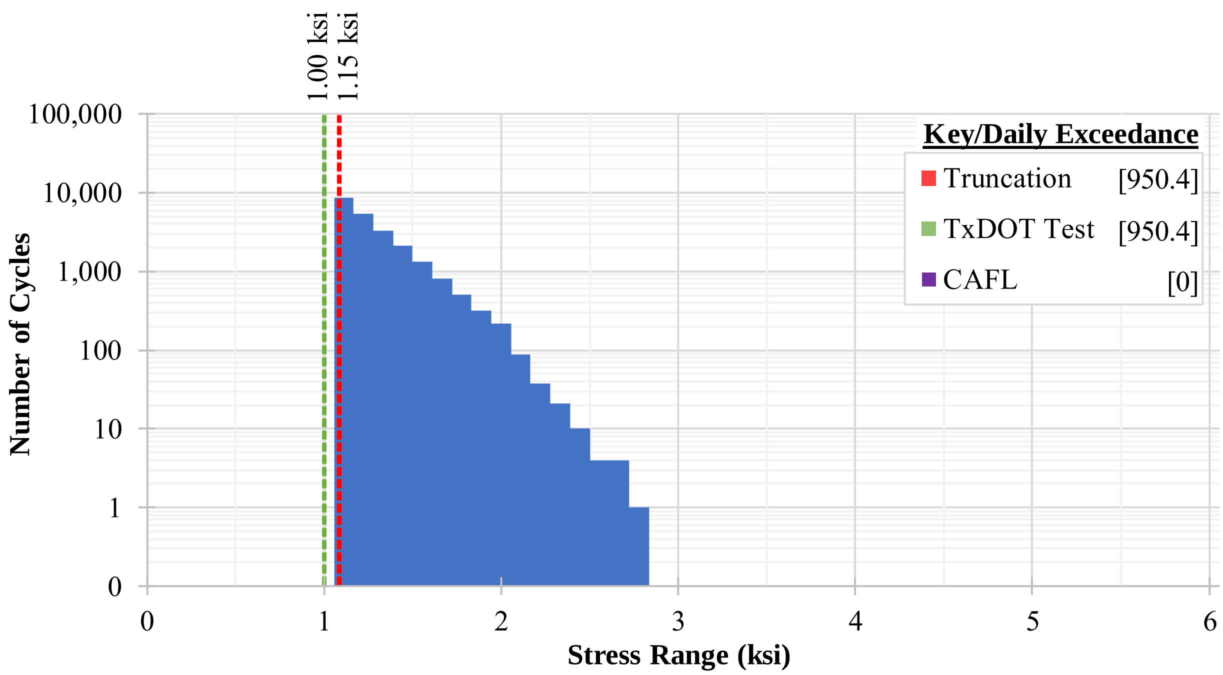

Figure E4-70: Sample rainflow histogram for the critical flange tips at Girder 19 (near cross-frame line 8) at Bridge 2

Many of the same observations can be made from Figure E4-70 as from Figure E4-65. The 1.15-ksi threshold was exceeded about 950 times per day, which is still less than the estimated ADTT for this bridge. This indicates that many of those estimated truck events result in very low stress ranges, below 1.15 ksi. The relatively short span length and redundancy of the system are both contributors to the low stresses.

Similar to the cross-frame data, Table E4-22 presents the comparison between measured data and AASHTO design metrics. The table summarizes all pertinent characteristics of the stress range spectra for each instrumented girder flange tip. The girders are identified by girder number, left or right tip, and cross-frame location (line 5 or 8).

A sample calculation similar to Figure E4-61 is not provided in this appendix for Bridge 2 girders. But it should be noted that many of these same means and methods were used, including modeling technique and design assumptions. The major differences between the approach used for the Bridge 2 cross-frames and girders are similar to what was discussed in Section E4.2.4.2 for Bridge 1. Recall that several design parameters including the fatigue detail category (A) differ from cross-frames and girders.

Note that both flange tips at girders 21 and 22 near cross-frame line 5 were excluded from the summary table due to a disproportionate percentage of high stress ranges, which the RT concluded to be a product of electromechanical noise. Also note that the finite life (Fatigue II) design ratio related to the 8th Edition of the AASHTO LRFD Specifications has been formatted with a strikethrough. The Fatigue I limit state governs fatigue design for this Category C′ detail.

The following observations from Table E4-22 are similar to the observations from Table E4-21, unless specified herein:

- **Comparing measured effective stress range (S_{re}) and measured equivalent cycle counts at the CAFL.** Similar to the Bridge 2 cross-frame response, higher effective stress ranges for the girders do not necessarily correspond to higher equivalent cycle counts at 12 ksi.
- **Comparing measured effective stress range (S_{re}) and measured maximum stress range (S_{rm}).** Similar to the Bridge 2 cross-frames, girder flanges with higher effective stress ranges generally have higher maximum stress ranges.
- **Lane striping and traffic patterns affect the fatigue response of bridge components**. Similar to the Bridge 1 girders, there is a clear distinction in girder response at each tip of a flange. For example, the left tip of the girder 20 flange accumulates damage at a rate of 0.77 cycles at 12 ksi per day, whereas the right tip accumulates damage at a rate of 0.44 cycles at 12 ksi per day. Lateral flange stresses can contribute a significant amount, especially for girders that generally experience low bending stresses.
- **Comparing measured maximum to effective stress ranges, S_{rm} to S_{re}, to the assumed 2.2 ratio (1.75/0.80) in AASHTO LRFD Specifications** (2017). The Bridge 2 girder data shows measured ratios ranging from 1.8 to 2.5, with the average at approximately 2.0.
- **Comparing 4th Ed. factored design stresses ($\gamma\Delta f$) and 8th Ed. factored design stresses ($\gamma\Delta f$) for cross-frames and girders**. Similar to Bridge 1 girders, factored design stresses in accordance with the 8th Ed. are consistently 7% more conservative than the factored design stresses in accordance with the 4th Ed.
- **Comparing factored design stresses based on refined analysis and AASHTO fatigue loading criteria (4th Ed. and 8th Ed.) to measured effective and maximum stress ranges**. Refined analysis with 8th Ed. loading criteria generally underpredicts the effective stress ranges by as low as 22%. The maximum stress ranges are consistently underpredicted for girder 19. Note that the girders with underpredicted force effects all had very low stress ranges; in some cases, the predicted stress range was less than the truncation stress.
- **Comparing factored design stresses based on refined analysis ($\gamma\Delta f$) to the nominal fatigue resistance** (ΔF_n). For the Bridge 2 girders, all nominal resistance exceeded the design stresses, which implies a satisfactory design under both specifications.
- **Comparing the measured stress ranges (S_{re}, S_{rm}) to the nominal fatigue resistance** (ΔF_n). For all Bridge 2 girders, the nominal resistances exceeded all appropriate measured stress ranges, which implies all members are in a safe condition with respect to fatigue. For example, the lowest design ratio under 8th Ed. criteria is 3.51.

Table E4-22: Comparison between measured rainflow girder response and key AASHTO design metrics (Bridge 2)

Girder Flange ID	Measured Response			4th Edition				8th Edition | Fatigue II (Finite Life)				8th Edition | Fatigue I (Infinite Life)			
	Avg. Daily Equiv. Cycles @ 12 ksi	Measured Eff. Stress, S_{re} (ksi)	Measured 0.01% Stress, S_{rm} (ksi)	Design Stress, $\gamma\Delta f$ (ksi)	Nom. Resistance, ΔF_n (ksi)	% Error Analysis $\frac{(\gamma\Delta f - S_{re})}{S_{re}}$	Design Ratio $\frac{\Delta F_n}{S_{re}}$	Design Stress, $\gamma\Delta f$ (ksi)	Nom. Resistance, ΔF_n (ksi)	% Error Analysis $\frac{(\gamma\Delta f - S_{re})}{S_{re}}$	Design Ratio $\frac{\Delta F_n}{S_{re}}$	Design Stress, $\gamma\Delta f$ (ksi)	Nom. Resistance, ΔF_n (ksi)	% Error Analysis $\frac{(\gamma\Delta f - S_{rm})}{S_{rm}}$	Design Ratio $\frac{\Delta F_n}{S_{rm}}$
20R|5	0.44	1.37	2.84	1.52	3.43	10%	2.49	1.62	3.43	18%	~~2.49~~	3.54	12.00	25%	4.22
20L|5	0.77	1.39	3.42	1.52	3.43	9%	2.46	1.62	3.43	16%	~~2.46~~	3.54	12.00	3%	3.51
19R|8	1.65	1.44	2.84	1.05	3.43	-27%	2.38	1.12	3.43	-22%	~~2.38~~	2.46	12.00	-14%	4.22
19L|8	1.12	1.42	2.84	1.05	3.43	-26%	2.42	1.12	3.43	-21%	~~2.42~~	2.46	12.00	-14%	4.22
18R|8	1.15	1.41	2.73	1.23	3.43	-13%	2.42	1.31	3.43	-7%	~~2.42~~	2.87	12.00	5%	4.40
18L|8	0.92	1.41	2.49	1.23	3.43	-12%	2.44	1.31	3.43	-7%	~~2.44~~	2.87	12.00	15%	4.81

E4.2.6 Bridge 3 Results

The following subsections outline the in-service rainflow data for the instrumented cross-frames and girders of Bridge 3.

As detailed in Section E2.3, Bridge 3 has the second largest instrumented span-to-depth ratio of the three subject bridges and has a single striped line of traffic. The bridge serves as a link from SH 146 to the nearby port. As observed by the RT during several site visits, truck traffic on this bridge is heavy, so major stress cycles are expected to be frequent. Given the curvature and relative flexibility of the span, girder stress cycles are expected to be high compared to Bridges 1 and 2.

Refer to Figure E4-42 and Figure E4-43 for the cross-frame numbering scheme, which will be used throughout this section. The girders will be identified by the numbering scheme used on the design plan and the associated cross-frame line. This is provided graphically on Figure E3-27 through Figure E3-29.

E4.2.6.1 Cross-Frame Data for Bridge 3

As is shown in Table E3-1, in-service rainflow monitoring for Bridge 3 was conducted between July 14th through August 10th of 2018. In total, just under four weeks of in-service data was measured. The installation and removal of the instrumentation was dictated by the schedule of the bridge owner. Note that there was no down period in the DAQ system to update the programming as with Bridge 1. The real-time linear regression algorithm was implemented from the first day of in-service monitoring until the instrumentation was removed.

For the four-week period, the axial stress rainflow counts for each cross-frame member were compiled and sorted into specific bins. Bin size and truncation stress parameters used for this data set are provided in Section E4.2.2. Figure E4-71 presents a sample histogram for cross-frame member 10, which includes rainflow counts summed over the entire four-week monitoring period. Cross-frame member 10 is a diagonal between interior girders 1 and 2 near cross-frame line 10, and this diagonal was one of the highest-stressed members during the controlled live load test. Also plotted on the figure are key benchmarks and the average number of occurrences in which those benchmarks were exceeded per day.

Many of the same observations can be made from Figure E4-71 as from Figure E4-60 and Figure E4-66. Note that the total number of counts above the threshold stress of 0.65 ksi is large compared to Bridge 1 and comparable to Bridge 2. This demonstrates the differences in truck traffic volume between the three subject bridges.

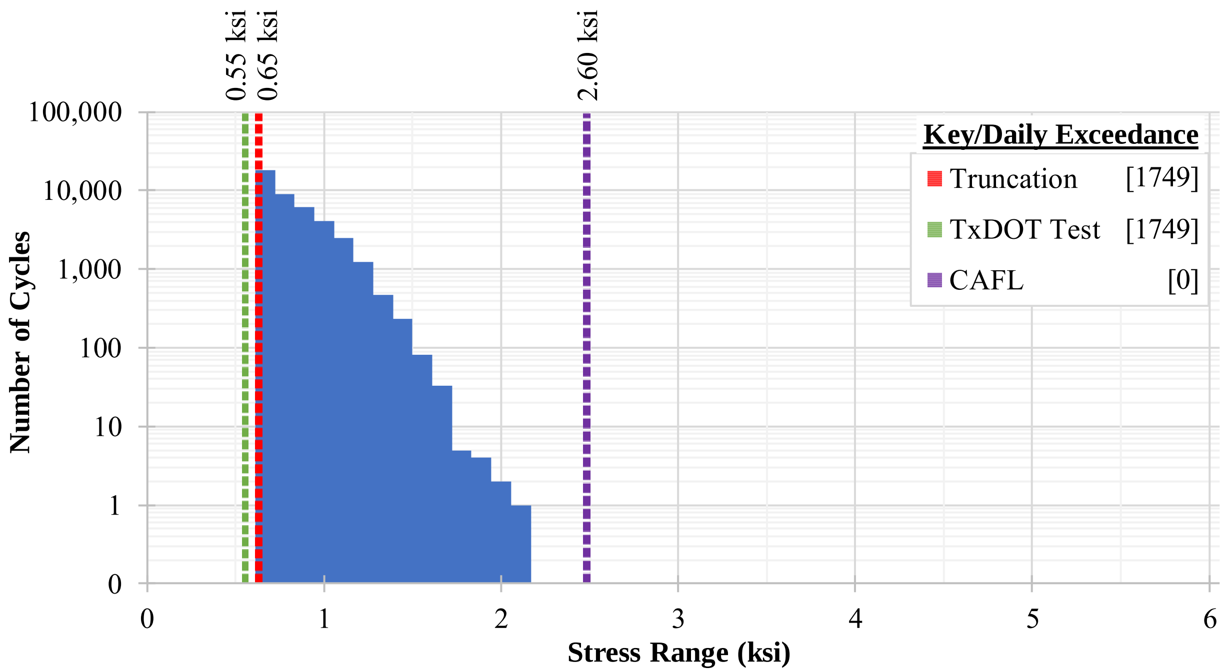

Figure E4-71: Sample rainflow histogram for cross-frame member 10 at Bridge 3

Similar to Table E4-19 for Bridge 1 and Table E4-21 for Bridge 2, Table E4-23 presents the comparison between measured data and the AASHTO design metrics. The table summarizes all pertinent characteristics of the stress range spectra for each instrumented cross-frame member. Note that the finite life (Fatigue II) design ratio related to the 8th Edition of the AASHTO LRFD Specifications has been formatted with a strikethrough. The Fatigue I limit state governs fatigue design for Bridge 3 cross-frames, given the high ADTT of this bridge.

Table E4-23: Comparison between measured rainflow cross-frame response and key AASHTO design metrics (Bridge 3)

	Measured Response			4th Edition				8th Edition | Fatigue II (Finite Life)				8th Edition | Fatigue I (Infinite Life)			
Cross-Frame No.	**Avg. Daily Equiv. Cycles @ 2.6 ksi**	**Measured Eff. Stress, S_{re} (ksi)**	**Measured 0.01% Stress, S_{rm} (ksi)**	**Design Stress, $\gamma\Delta f$ (ksi)**	**Nom. Resistance, ΔF_n (ksi)**	**% Error Analysis $\frac{(\gamma\Delta f - S_{re})}{S_{re}}$**	**Design Ratio $\frac{\Delta F_n}{S_{re}}$**	**Design Stress, $\gamma\Delta f$ (ksi)**	**Nom. Resistance, ΔF_n (ksi)**	**% Error Analysis $\frac{(\gamma\Delta f - S_{re})}{S_{re}}$**	**Design Ratio $\frac{\Delta F_n}{S_{re}}$**	**Design Stress, $\gamma\Delta f$ (ksi)**	**Nom. Resistance, ΔF_n (ksi)**	**% Error Analysis $\frac{(\gamma\Delta f - S_{rm})}{S_{rm}}$**	**Design Ratio $\frac{\Delta F_n}{S_{rm}}$**
02	1.6	0.77	1.10	0.52	1.36	-34%	1.75	0.44	0.96	-43%	~~1.24~~	0.97	2.60	-12%	2.36
03	16.8	0.87	2.84	0.67	1.36	-23%	1.57	0.70	0.96	-19%	~~1.11~~	1.54	2.60	-46%	0.91
04	3.2	0.81	1.45	0.87	1.36	7%	1.69	0.71	0.96	-11%	~~1.19~~	1.56	2.60	8%	1.79
05	2.5	0.78	1.10	0.55	1.36	-29%	1.74	0.51	0.96	-35%	~~1.23~~	1.12	2.60	1%	2.36
06	3.8	0.80	1.10	0.61	1.36	-23%	1.71	0.59	0.96	-26%	~~1.21~~	1.29	2.60	17%	2.36
09	0.5	0.77	0.99	0.61	1.36	-20%	1.77	0.65	0.96	-15%	~~1.26~~	1.43	2.60	45%	2.64
10	84.2	0.95	2.14	0.84	1.36	-11%	1.44	0.89	0.96	-5%	~~1.02~~	1.96	2.60	-9%	1.21
11	16.4	0.86	1.91	0.90	1.36	5%	1.58	0.79	0.96	-8%	~~1.12~~	1.74	2.60	-9%	1.36
12	2.7	0.81	1.33	0.95	1.36	18%	1.68	0.85	0.96	5%	~~1.19~~	1.86	2.60	39%	1.95
13	1.1	0.79	0.99	0.66	1.36	-16%	1.72	0.71	0.96	-11%	~~1.22~~	1.54	2.60	56%	2.64
14	10.2	0.83	1.33	0.68	1.36	-18%	1.63	0.73	0.96	-12%	~~1.16~~	1.59	2.60	19%	1.95
16	6.2	0.84	2.15	0.80	1.36	-5%	1.62	0.75	0.96	-11%	~~1.15~~	1.63	2.60	-24%	1.21
17	1.1	0.78	1.10	0.51	1.36	-34%	1.74	0.47	0.96	-40%	~~1.23~~	1.03	2.60	-7%	2.36

A sample calculation, similar to Figure E4-61, is not presented for Bridge 3. The same modeling techniques and assumptions outlined in Figure E4-61 for the Bridge 1 model were also used for the Bridge 3 model. The major differences between the approach used for Bridge 1 and Bridge 3 are related to traffic-pattern inputs. For Bridge 3, the number of lanes is less, but the ADTT is much higher than for Bridge 1. These variables affect the Fatigue II nominal resistance calculation.

The observations from Table E4-23 (Bridge 3) are similar to the observations from Table E4-19 (Bridge 1). The bolded text serves as general discussion points that are consistent between each bridge. The commentary below each bolded category summarizes the unique aspects of the cross-frame data at Bridge 3. Note that comparisons between the three subject bridges are made in Section E4.2.7.

- **Comparing measured effective stress range ($\boldsymbol{S_{re}}$) and measured equivalent cycle counts at the CAFL.** For Bridge 3, the members with higher effective stress ranges generally correspond to higher equivalent cycle counts at 2.6 ksi.
- **Comparing measured effective stress range ($\boldsymbol{S_{re}}$) and measured maximum stress range ($\boldsymbol{S_{rm}}$).** Similar to the Bridge 1 data, higher measured effective stress ranges typically relate to higher measured maximum stress ranges.
- **Lane striping and traffic patterns affect the fatigue response of bridge components**. Cross-frame diagonals in the bay between girders 1 and 2, regardless of cross-frame line (member 03, 10, and 11) have the highest rate of accumulated damage. Girder 1, the fascia girder with the longest arc length, deflects the most under live loads. Thus, it makes sense that the largest differential deflections and highest measured cross-frame stress ranges were typically in this bay.
- **Comparing measured maximum to effective stress ranges, $\boldsymbol{S_{rm}}$ to $\boldsymbol{S_{re}}$, to the assumed 2.2 ratio (1.75/0.80) in AASHTO LRFD Specifications** (2017). The Bridge 3 cross-frame data shows measured ratios ranging from 1.3 to 3.3 with the average at approximately 1.8.
- **Comparing 4th Ed. factored design stresses ($\boldsymbol{\gamma \Delta f}$) and 8th Ed. factored design stresses ($\boldsymbol{\gamma \Delta f}$) for cross-frames and girders**. Similar to the Bridge 1 data, factored 4th Ed. design stresses are typically more conservative than the factored 8th Ed. design stresses. Exceptions are cross-frame members 03, 09, 10, 13, and 14, in which the 8th Ed. loading conditions and load factors produced higher design stresses than the 4th Ed. provisions.
- **Comparing factored design stresses based on refined analysis and AASHTO fatigue loading criteria (4th Ed. and 8th Ed.) to measured effective and maximum stress ranges**. For Bridge 3 cross-frames, refined analysis consistently underpredicts effective stress ranges when compared to the measured data by as much as 34%, and underpredicts maximum stress ranges for six of the thirteen instrumented cross-frame members. The design stresses, in many cases, were close to or below the truncation stress.
- **Comparing factored design stresses based on refined analysis ($\boldsymbol{\gamma \Delta f}$) to the nominal fatigue resistance ($\boldsymbol{\Delta F_n}$)**. For the Bridge 3 cross-frames, all members exhibited a satisfactory design under both set of editions of design criteria.
- **Comparing the measured stress ranges ($\boldsymbol{S_{re}, S_{rm}}$) to the nominal fatigue resistance ($\boldsymbol{\Delta F_n}$)**. For all Bridge 3 cross-frames, the nominal resistances exceeded all appropriate measured stress ranges, except for an 8th Ed. Fatigue I check of member 03. The design ratio in this case is 0.91, which means that maximum measured stress range exceeded the capacity; but more specifically, the rate at which the nominal Fatigue I resistance was exceeded was more than 1-in-10,000 occurrences. Under 4th Ed. provisions where this detail category was considered E instead of E′, this same member is acceptable.

Figure E4-72 shows these observations graphically on the same histogram plot presented in Figure E4-71 with different benchmark stresses overlaid: measured maximum stress range, AASHTO LRFD (8th Ed.) Fatigue I factored design stress, and AASHTO LRFD (8th Ed.) nominal resistance. These benchmarks illustrate the governing design check for cross-frame member 10 under the current specifications. From this histogram plot, it is evident that the measured effective stress range is less than the nominal resistance, but greater than the factored design stress. This indicates that the refined model and AASHTO fatigue loading criteria underpredicted the maximum stress range; despite that, the measured maximum stress range is still well below the Fatigue I nominal resistance, the CAFL.

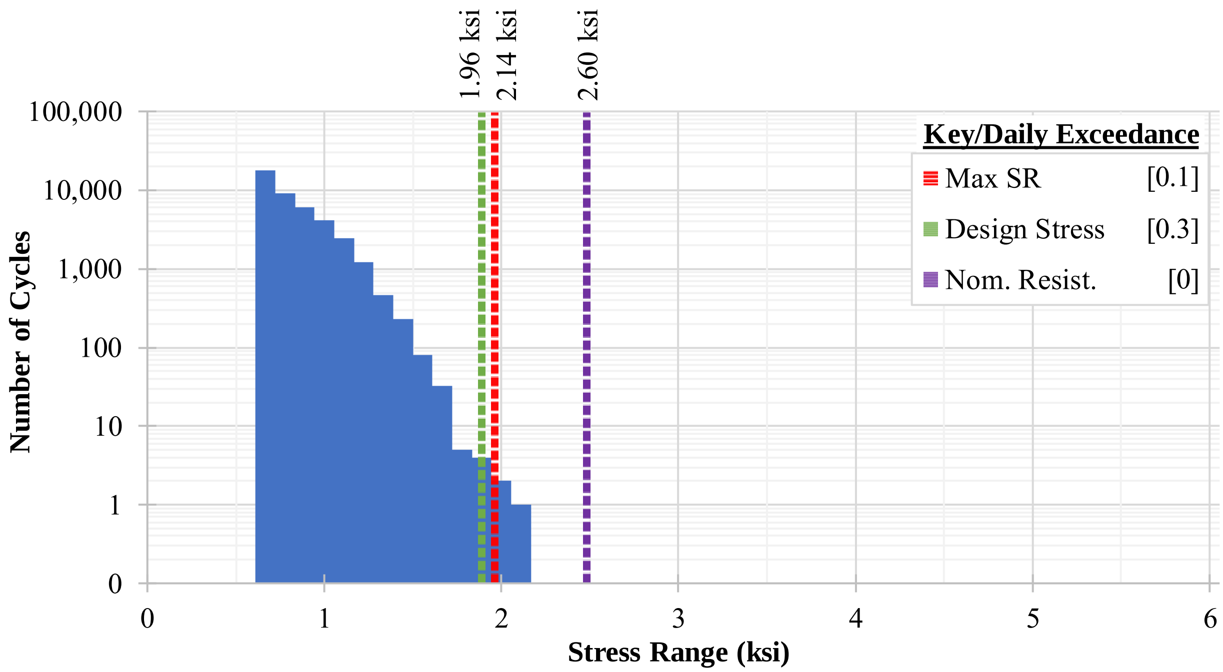

Figure E4-72: Sample rainflow histogram for cross-frame member 10 at Bridge 3 showing key Fatigue II design metrics

Similar to Section E4.2.4.1 for Bridge 1, the RT also evaluated the daily and hourly trends of the Bridge 3 data. The procedures used to infer time-dependent trends for Bridge 1 data were replicated for Bridge 3 data; refer to Section E4.2.4.1 for more information. Figure E4-73 presents the daily trends of the rainflow data for cross-frame member 10 of Bridge 3, and Figure E4-74 presents the hourly trends. From these plots, similar conclusions can be made about the Bridge 3 data and the Bridge 1 and 2 data. Damage accumulation, as quantified by equivalent number of cycles at 2.6 ksi, is highest during the weekdays and lowest during the weekends. Note that July 28th and 29th are left blank due to the load test conducted during that weekend. Additionally, truck traffic volume and damage accumulation are greatest on average between 9 am and 3 pm and are least between 6 pm and 6 am.

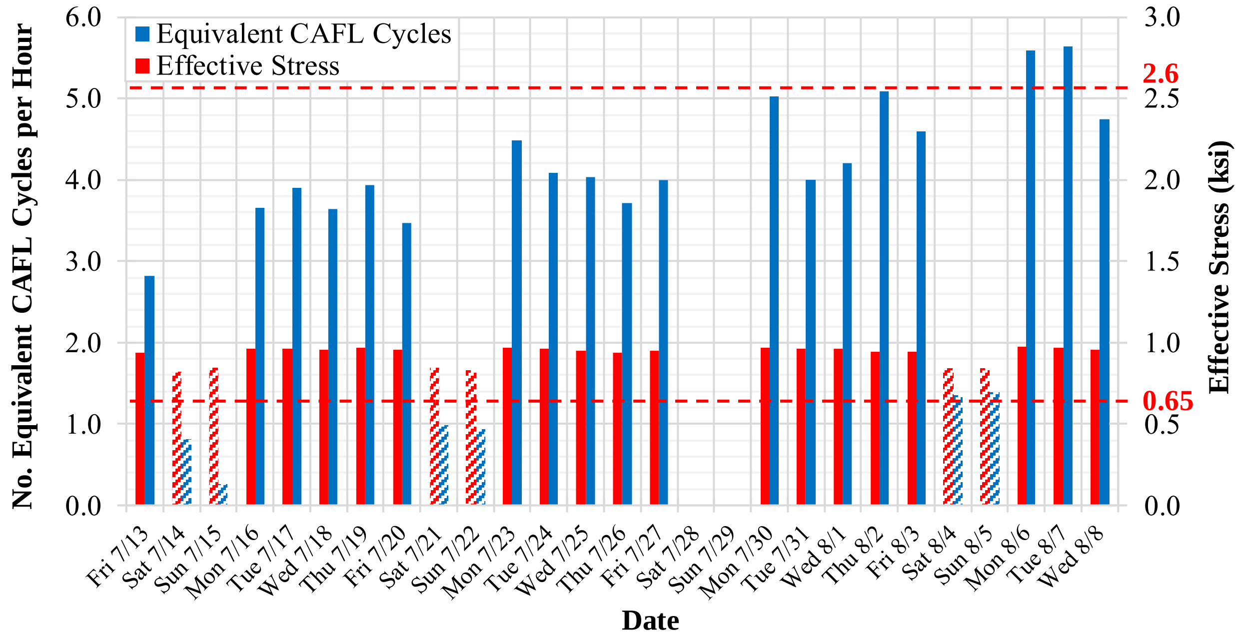

Figure E4-73: Daily stress range trends cross-frame member 10 at Bridge 3

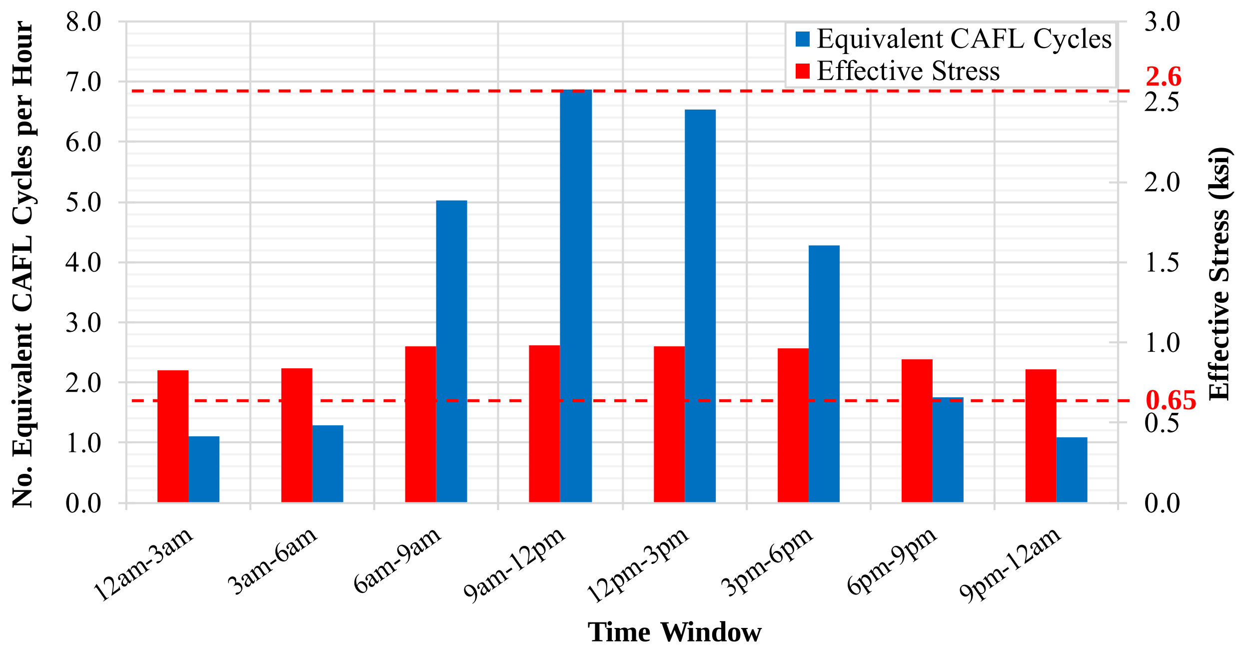

Figure E4-74: Hourly stress range trends cross-frame member 10 at Bridge 3

As discussed in Section E4.2.4.1, these time-dependent trends are not critical in the overall scheme of the fatigue evaluation. The effective stress range of the entire four-week data set, tabulated in Table E4-23, captures the peaks and valleys of the full truck spectrum and quantify its cumulative effect.

E4.2.6.2 Girder Data for Bridge 3

Similar to Section E4.2.6.1, rainflow data for select girder flanges was measured and processed by the RT for Bridge 3. Many of the procedures outlined in the previous section were replicated for the girder data. The same monitoring period (July 4th through August 10th) are presented in this section, and the same rainflow parameters including time window size, bin size, and threshold strain were implemented. Similar to the Bridge 1 and Bridge 2 girder data, the response of each individual flange strain gage was processed to match the design approach of the critical Category C′ detail, as opposed to a combined response like the cross-frame data. The truncation stress was selected as 1.5 ksi, as outlined in Section E4.2.2.1.

Figure E4-75 presents a sample histogram for fascia girder 1 at cross-frame line 10, near the maximum positive moment region of the span. The right flange tip (right side relative to flow of traffic) recorded more significant stress cycles than the left tip, likely due to the direction and magnitude of lateral bending stresses induced during truck events. As a result, only the critical right-tip histogram is presented. Note that rainflow counts are the totaled values over the entire four-week monitoring period. Also plotted on the figure are key benchmarks and the average number of occurrences in which those benchmarks were exceeded per day.

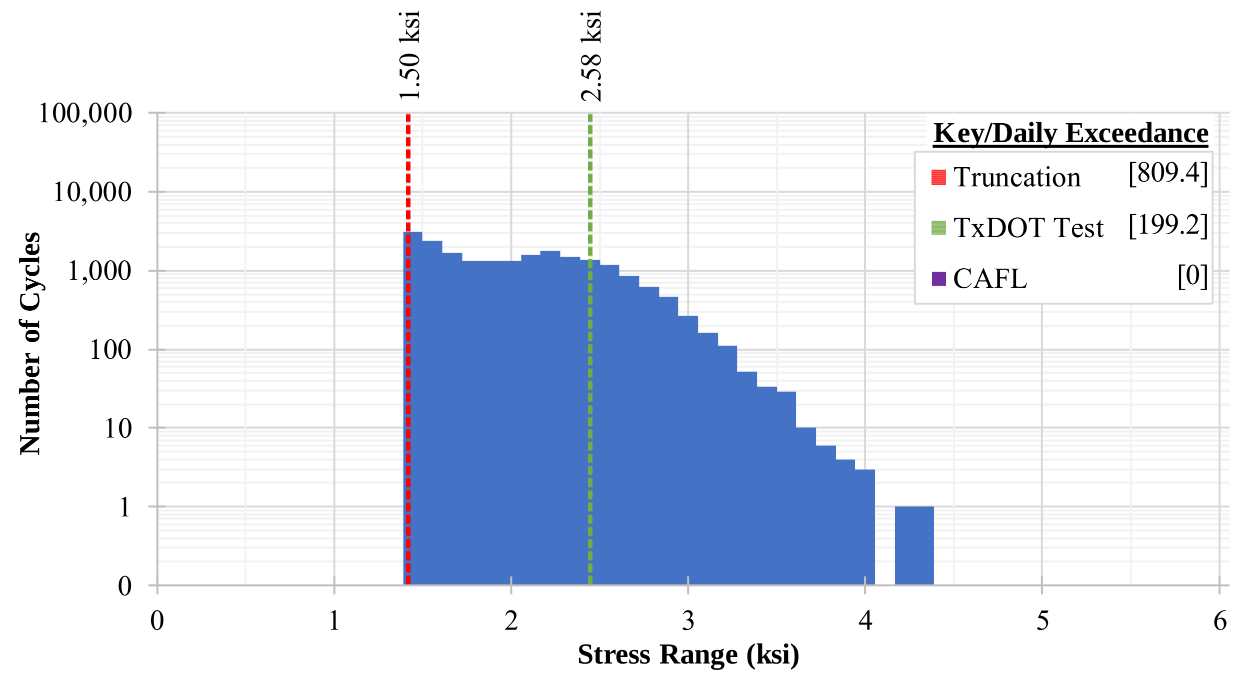

Figure E4-75: Sample rainflow histogram for the critical flange tips at Girder 1 (near cross-frame line 10) at Bridge 3

Many of the same observations can be made from Figure E4-75 as from Figure E4-65 and Figure E4-70. The 1.50-ksi threshold was exceeded about 810 times per day on average. The cycle count about that 1.50-ksi cutoff is substantially higher than any girders on Bridges 1 and 2. This indicates that the high truck traffic volume induces larger bending stresses on girder 1 at Bridge 3 than any other girders instrumented, likely due to the long span length and curvature.

Similar to the cross-frame data, Table E4-24 presents the comparison between measured data and AASHTO metrics. The table summarizes all pertinent characteristics of the stress range spectra for each instrumented girder flange tip. The girders are identified by girder number, left or right tip, and cross-frame location (line 4 or 10).

A sample calculation similar to Figure E4-61 is not provided in this appendix for the Bridge 3 girders. The same means and methods were used on Bridge 3, including modeling technique and design assumptions. The major differences between the approach used for Bridge 3 cross-frames and girders are similar to what was previously discussed in Section E4.2.4.2 for Bridge 1. Recall that several design parameters including the fatigue detail category (A) differ from cross-frames and girders.

Note that the finite life (Fatigue II) design ratio related to the 8th Edition of the AASHTO LRFD Specifications has been formatted with a strikethrough. The Fatigue I limit state governs fatigue design for this Category C′ detail.

The following observations from Table E4-24 are similar to the observations from Table E4-23, unless specified herein:

- **Comparing measured effective stress range (S_{re}) and measured equivalent cycle counts at the CAFL.** Similar to the Bridge 3 cross-frame response, higher effective stress ranges for girders generally correspond to higher equivalent cycle counts at 12 ksi.
- **Comparing measured effective stress range (S_{re}) and measured maximum stress range (S_{rm}).** Similar to the Bridge 3 cross-frames, girder flanges with higher effective stress ranges generally have higher maximum stress ranges.
- **Lane striping and traffic patterns affect the fatigue response of bridge components**. Similar to Bridge 1 girders, there is a clear distinction in girder response at each tip of a flange. For example, the right tip of the girder 1 flange at line 10 accumulates damage at a rate of 5.66 cycles at 12 ksi per day, whereas the left tip accumulates damage at a rate of cycles at 3.76 ksi per day. Lateral flange stresses can contribute a significant amount for curved bridges.
- **Comparing measured maximum to effective stress ranges, S_{rm} to S_{re}, to the assumed 2.2 ratio (1.75/0.80) in AASHTO LRFD Specifications** (2017). The Bridge 3 girder data shows measured ratios ranging from 1.6 to 2.1 with the average at approximately 1.8.
- **Comparing 4th Ed. factored design stresses ($\gamma\Delta f$) and 8th Ed. factored design stresses ($\gamma\Delta f$) for cross-frames and girders**. Similar to the Bridge 1 girders, factored design stresses in accordance with the 8th Ed. are consistently 7% more conservative than the factored design stresses in accordance with the 4th Ed.
- **Comparing factored design stresses based on refined analysis and AASHTO fatigue loading criteria (4th Ed. and 8th Ed.) to measured effective and maximum stress ranges**. Refined analysis with 8th Ed. loading generally overpredicts the effective stress ranges with a few exceptions. The maximum stress ranges are consistently overpredicted. For the girders in which the model underpredicts the force effects, the flange stresses are generally very low when compared to the other girder flanges of interest.
- **Comparing factored design stresses based on refined analysis ($\gamma\Delta f$) to the nominal fatigue resistance (ΔF_n)**. For the Bridge 3 girders, there were a few instances in which the design stress exceeded the corresponding nominal resistance under 4th Ed. criteria. This implies that the original design of the fascia girder was inadequate. This is likely a result of differing analysis methods and design assumptions between the original designer and the RT.
- **Comparing the measured stress ranges (S_{re}, S_{rm}) to the nominal fatigue resistance (ΔF_n)**. For all Bridge 3 girders, the nominal resistances exceeded all appropriate measured stress ranges, which implies all members are in a safe condition with respect to fatigue. For example, the lowest design ratio under 8th Ed. criteria is 2.76.

Table E4-24: Comparison between measured rainflow girder response and key AASHTO design metrics (Bridge 3)

Girder Flange ID	Measured Response			4th Edition				8th Edition | Fatigue II (Finite Life)				8th Edition | Fatigue I (Infinite Life)			
	Avg. Daily Equiv. Cycles @ 12 ksi	Measured Eff. Stress, S_{re} (ksi)	Measured 0.01% Stress, S_{rm} (ksi)	Design Stress, $\gamma\Delta f$ (ksi)	Nom. Resistance, ΔF_n (ksi)	% Error Analysis $\frac{(\gamma\Delta f - S_{re})}{S_{re}}$	Design Ratio $\frac{\Delta F_n}{S_{re}}$	Design Stress, $\gamma\Delta f$ (ksi)	Nom. Resistance, ΔF_n (ksi)	% Error Analysis $\frac{(\gamma\Delta f - S_{re})}{S_{re}}$	Design Ratio $\frac{\Delta F_n}{S_{re}}$	Design Stress, $\gamma\Delta f$ (ksi)	Nom. Resistance, ΔF_n (ksi)	% Error Analysis $\frac{(\gamma\Delta f - S_{rm})}{S_{rm}}$	Design Ratio $\frac{\Delta F_n}{S_{rm}}$
1R|4	2.61	1.96	3.89	3.70	2.72	89%	1.39	3.95	2.72	102%	~~1.39~~	8.64	12.00	122%	3.09
1L|4	1.66	1.85	3.42	3.70	2.72	100%	1.47	3.95	2.72	114%	~~1.47~~	8.64	12.00	152%	3.51
2R|4	2.40	1.91	3.65	2.49	2.72	30%	1.42	2.66	2.72	39%	~~1.42~~	5.82	12.00	59%	3.28
2L|4	1.73	1.84	3.42	2.49	2.72	36%	1.48	2.66	2.72	45%	~~1.48~~	5.82	12.00	70%	3.51
3R|4	2.02	1.85	3.19	1.58	2.72	-15%	1.47	1.68	2.72	-9%	~~1.47~~	3.68	12.00	15%	3.76
3L|4	0.74	1.75	2.73	1.58	2.72	-10%	1.55	1.68	2.72	-4%	~~1.55~~	3.68	12.00	35%	4.40
4R|4	1.30	1.83	3.07	2.02	2.72	11%	1.49	2.16	2.72	18%	~~1.49~~	4.72	12.00	54%	3.90
4L|4	0.38	1.73	2.84	2.02	2.72	17%	1.57	2.16	2.72	25%	~~1.57~~	4.72	12.00	66%	4.22
1R|10	5.66	2.30	4.47	4.72	2.72	106%	1.18	5.04	2.72	120%	~~1.18~~	11.02	12.00	147%	2.69
1L|10	3.76	2.12	4.12	4.72	2.72	123%	1.28	5.04	2.72	138%	~~1.28~~	11.02	12.00	168%	2.91
2R|10	3.70	2.16	3.77	3.17	2.72	47%	1.26	3.38	2.72	57%	~~1.26~~	7.39	12.00	96%	3.18
2L|10	3.47	2.06	4.35	3.17	2.72	54%	1.32	3.38	2.72	64%	~~1.32~~	7.39	12.00	70%	2.76
3R|10	2.59	2.01	3.54	1.81	2.72	-10%	1.35	1.93	2.72	-4%	~~1.35~~	4.21	12.00	19%	3.39
3L|10	1.21	1.83	3.65	1.81	2.72	-1%	1.48	1.93	2.72	5%	~~1.48~~	4.21	12.00	15%	3.28
4R|10	1.45	1.91	3.54	3.10	2.72	62%	1.42	3.31	2.72	73%	~~1.42~~	7.24	12.00	105%	3.39
4L|10	0.62	1.80	3.07	3.10	2.72	72%	1.51	3.31	2.72	84%	~~1.51~~	7.24	12.00	136%	3.90

E4.2.7 Comparison of Results

The final objective listed in Section E4.2.3 is to compare fatigue characteristics of cross-frames and girders in straight, skewed, and horizontally curved bridges and discuss the significance of traffic patterns and overall bridge geometry with respect to fatigue response. This topic is addressed in two different ways. First, the general observations carried out through Sections E4.2.4, E4.2.5, and E4.2.6 are reexamined in this section, but with a broader scope. These observations evaluate how the AASHTO LRFD Design Specifications performed with respect to the measured data for three different types of bridges. Second, the measured stress range spectra for cross-frames and girders at each bridge are compared. From this, generalized conclusions are made about how geometry (span-to-depth ratio, bridge width and redundancy, skew, curvature, etc.) impacts fatigue response for cross-frames and girders alike.

As noted earlier, the bolded observations represent the general discussion points identified for each bridge. The commentary below each bolded category summarizes the trends and comparisons between different bridges as well as between cross-frames and girders.

- **Comparing measured effective stress range (S_{re}) and measured equivalent cycle counts at the CAFL.** Cross-frames and girders with higher effective stress ranges generally had higher equivalent cycle counts, but not always. The major takeaway from this finding is that the equivalent cycle count metric better represents stress range magnitudes and frequency of truck events than effective stress ranges.
- **Comparing measured effective stress range (S_{re}) and measured maximum stress range (S_{rm}).** Cross-frames and girders with higher effective stress ranges also generally had higher maximum stress ranges. It is intuitive that stress range spectra with frequent high-stress cycles also have higher effective stress ranges since the metrics are related.
- **Lane striping and traffic patterns affect the fatigue response of bridge components**. The response to this observation is divided between cross-frames and girders: (a) It was observed in load test data (Section E4.1) that cross-frame force effects are highly sensitive to transverse position of truck. Similarly, it was inferred from the rainflow data that truck traffic frequency per lane impacts the damage accumulation of cross-frame members. Additionally, areas of maximum girder deflection and twist (typically near maximum positive moment region) resulted in the highest damage rates for cross-frames, especially for diagonal members. With this in mind, cross-frame members that accumulated the most damage during the monitoring period were generally near the maximum positive moment region and near the heavily trafficked lanes for heavy trucks (right lane). This trend was consistent across all three subject bridges. (b) Load distribution for girder stress has proven to be more even, as evidenced by the live load test data and the rainflow data. Fascia girders tended to accumulate more damage than adjacent interior girders due to less load distribution near the deck edge and the frequency of trucks in the rightmost lane. Also note that lateral bending stresses are also critical to understand fatigue response of girder flanges, especially for curved systems.
- **Comparing measured maximum to effective stress ranges, S_{rm} to S_{re}, to the assumed 2.2 ratio (1.75/0.80) in AASHTO LRFD Specifications** (2017). The measured ratios were well scattered but generally close to 2.2. The sensitive nature of the effective stress range calculation to the truncation stress selected caused any significant deviations in this ratio.
- **Comparing 4th Ed. factored design stresses ($\gamma\Delta f$) and 8th Ed. factored design stresses ($\gamma\Delta f$) for cross-frames and girders**. The response to this observation is divided between cross-frames and girders: (a) For cross-frames, the 4th Ed. loading criteria generally resulted in higher force predictions than the 8th Ed. criteria despite the lower load factor, minus a few exceptions. Recent updates to the AASTHO Specification (2017) increased the load factors but eliminated the double-truck fatigue load case. Recent AASHTO LRFD Specifications also eliminated excess conservatism from its fatigue loading criteria of cross-frames. In general, the fatigue loading model

is examined in great depth in Phase III of the project for a wide range of bridge geometries (Appendix F) (b) For girders, the loading criteria has not changed between the code updates, but the load factors have. Consequently, the 8th Ed. consistently results in stress predictions 7% higher than the 4th Ed.

- **Comparing factored design stresses based on refined analysis and AASHTO fatigue loading criteria (4th Ed. and 8th Ed.) to measured effective and maximum stress ranges**. The response to this observation is divided between effective stress ranges and maximum stress ranges: (a) Refined analysis generally provides a conservative estimate of effective stress ranges for cross-frame members and girder flanges. Notable exceptions though were the Bridge 3 cross-frames. In the cases where refined analysis underpredicted force effects when compared to measured data, the stress ranges were very small and, at times, less than the truncation stress selected. In these select instances, the fatigue limit state is not a concern for these members given the low stress range spectra such that an underpredicted stress has no impact on the adequacy of the design. (b) For maximum stress ranges, the same general trends apply. Force predictions of the Bridge 3 girders proved to be the most underestimated. Underpredicting the design force effect would only be a major concern if the refined analysis predicted a maximum stress range below the CAFL, but the actual, measured maximum stress range exceeded it. This scenario occurred only for one instrumented member: cross-frame member 03 at Bridge 3. However, it should be noted that this cross-frame detail was originally designed as Category E (CAFL of 4.5 ksi) and has since changed to E′ (2.6 ksi) after the bridge was constructed.
- **Comparing factored design stresses based on refined analysis ($\boldsymbol{\gamma\Delta f}$) to the nominal fatigue resistance ($\boldsymbol{\Delta F_n}$)**. In general, the original fatigue designs of instrumented cross-frame and girder flange elements, as best replicated by the RT, were satisfactory. There were a few instances in which this statement was not true, namely for select Bridge 2 cross-frames and Bridge 3 girders. Any implied "design deficiencies" are likely due to differences in the analysis approach of the original designer and the RT and not an oversight by the designer. Note that Bridges 2 and 3 have complex geometries, and analysis models with complex geometries tend to be more sensitive to modeling assumptions and techniques than simple geometries like Bridge 1, where no "design deficiencies" were observed.
- **Comparing the measured stress ranges ($\boldsymbol{S_{re}, S_{rm}}$) to the nominal fatigue resistance ($\boldsymbol{\Delta F_n}$)**. Except for one case, the measured stress range spectra for instrumented cross-frames and girders were well within the limits established by current and past AASHTO LRFD Specifications. The maximum stress range measured at a cross-frame diagonal in Bridge 3 exceeded the nominal fatigue resistance under current provisions; although, the same member is considered safe under 4th Ed. provisions. Recall that fatigue detail category has changed since Bridge 3 was designed, which best explains why an "unsafe condition" exists.

The equivalent number of cycles at the CAFL stress (damage accumulation metric), effective stress ranges, and maximum stress ranges at each bridge can also be compared to get a relative sense of how each bridge responded to normal truck traffic. Table E4-25 and Table E4-26 present the results for the instrumented cross-frames and girder flanges at each bridge, respectively. The table specifically presents the range, maximum and minimum, of those measured values at each bridge; for example, the maximum effective stress range for Bridge 1 cross-frames corresponds to member 04 and the minimum corresponds to member 06. It is acknowledged that the maximum and minimum values could potentially vary had other members on the bridge been instrumented. With that said, the RT believes that the instrumented members are generally representative of all cross-frame or girder flanges on the instrumented spans.

Table E4-25: Ranges of all equivalent cycles, effective stress ranges, and maximum stress ranges measured for cross-frames at each subject bridge

Bridge No.	Measured Range {Min, Max}		
	Avg. Daily Equiv. Cycles @ 2.6 ksi	Effective Stress, S_{re} (ksi)	Maximum Stress, S_{rm} (ksi)
1	{1.9 – 26.0}	{0.70 – 0.98}	{1.35 – 3.61}
2	{0.4 – 502.0}	{0.78 – 1.19}	{0.99 – 3.77}
3	{0.5 – 84.2}	{0.77 – 0.95}	{0.99 – 2.84}

Table E4-26: Ranges of all equivalent cycles, effective stress ranges, and maximum stress ranges measured for girders at each subject bridge

Bridge No.	Measured Range {Min, Max}		
	Avg. Daily Equiv. Cycles @ 12 ksi	Effective Stress, S_{re} (ksi)	Maximum Stress, S_{rm} (ksi)
1	{0.5 – 1.9}	{1.35 – 1.93}	{2.57 – 4.39}
2	{0.4 – 1.7}	{1.37 – 1.44}	{2.49 – 3.42}
3	{0.6 – 5.7}	{1.73 – 2.16}	{2.73 – 4.47}

From Table E4-25, it is obvious that critical cross-frames at Bridge 2 (skewed) saw higher rates of damage accumulation, effective stress ranges, and maximum stress ranges in comparison to critical cross-frames at the other two bridges. As mentioned previously, the damage accumulation rate at a consistent index stress range quantifies not only the stress range magnitudes, but also the frequency of significant cycles. By Bridge 2 having the highest damage accumulation rates, it implies that the cross-frames in this skewed system see slightly higher stress ranges than the normal and curved systems and that the truck traffic on Bridge 2 is high. Bridge 1 (normal) and Bridge 3 (curved) have comparable effective stress ranges, but the damage accumulation rate at Bridge 3 is generally much higher because the ADTT is much higher.

The trends in girder stresses are quite different in Table E4-26. Critical girder flanges on curved Bridge 3 saw the highest damage accumulation rates, effective stress ranges, and maximum stress ranges. The ranges at Bridge 2 were generally the least of the three bridges. Recall that the respective span-to-depth ratio of the instrumented spans at Bridges 1, 2, and 3 are 32, 25, and 27. Also recall from Section E4.1 that the measured vertical deflections were the smallest at Bridge 2 during the controlled live load tests. Therefore, it is intuitive that the stiffer Bridge 2 span sees the smallest girder stress range spectra. Bridge 3 girders recorded higher stress ranges than Bridge 1 largely due to the added component of significant girder twist and lateral bending stresses induced in the flanges.

When comparing cross-frame and girder ranges, it appears that cross-frames accumulate damage at a faster rate than girders at first glance. However, it must be emphasized that the equivalent cycle counts in Table E4-25 and Table E4-26 are based on different index stresses. Recall that the damage accumulation index is proportional to the cube of the index stress range. Had the same index stress be applied to both tables, it would be apparent that girders accumulate more damage than cross-frames do, given that the stress range spectra are typically of higher magnitude for girder flanges than cross-frame members.

It is important to note that these observations and trends are based on three unique bridge geometries and traffic patterns. These concepts may vary depending on different geometries (different span lengths, number of girders, skew index, flexibility, etc.) and different traffic patterns (different truck population in another part of the US). The effects of varying bridge geometries were studied in depth during the parametric study phase (Phase III) of the project. Refer to Appendix F for those results. With that in mind, the following items summarize big-picture concepts learned from the in-service monitoring study (which are reexamined in Phase III):

- Fatigue damage is directly correlated to truck traffic patterns. High ADTT rates at Bridges 2 and 3 generally in more significant damage accumulation.
- Cross-frames in skewed systems generally result in the highest stress range spectra, relative to the girder stresses in the same unit. Critical cross-frames at Bridge 2 have higher effective stress ranges, despite the overall system being very stiff and the girders having low stress ranges. Additionally, cross-frames in Bridge 2 are placed in contiguous lines, which typically result in larger cross-frame force demands.
- With span-to-depth ratios equal, girders in curved systems generally have the largest girder stress ranges, combining longitudinal effects due to in-plane bending and lateral bending effects due to torsional deformation of the section. Note that Bridge 3 has a tight girder spacing and radius of curvature, which can potentially influence these results.

CHAPTER E5

Part 1 of Analytical Program

The field data outlined in the last chapter, particularly from the controlled live load tests, were vital in validating the FEA models that were used in the parametric studies. Results from the preliminary FEA models, introduced in Section E3.2, provided a good starting point for the comparison with the measured strain and vertical deflection readings from the load tests, and appropriate modifications to the model were made. In this chapter, the modifications required to obtain good agreement with the measured data are discussed in detail.

The chapter is organized into four subsections. In the first subsection, various modeling parameters that were studied during the validation process are outlined. The parameters were generally consistent across all three bridge models. The three subsequent sections present three key items for each subject bridge: (i) the preliminary results prior to validation, (ii) the relative impact of each modeling parameter on the model, and (iii) the final validated results. By presenting both the preliminary and validated results, importance of acquiring field data is emphasized.

The preliminary models were based on assumed as-designed conditions of the bridge, which was the most appropriate starting point with no field data available at the time. The validated models, on the other hand, are based on measured dimensions and measured data of instrumented structural components. Collecting data allowed the RT to fine-tune the parameters of the model as to more closely match the current conditions of the bridge system. Note that the validated models outlined here were used to conduct parametric studies in Phase III of the NCHRP project.

E5.1 Modeling Parameters and Assumptions

As introduced previously, two different preliminary models were developed by the RT for each bridge: one modeling cross-frames with full shell elements and another modeling cross-frames as truss members with stiffness reduction factors due to eccentric end connections. For the validation studies conducted and presented here, only the full shell models are considered. For all three bridges, the models consisted solely of shell elements except for the bearing pads, for which the stiffness is addressed later in this section as a key modeling parameter. Note that the truss-element modeling approach of cross-frames, which is traditionally done in 3D commercial software programs, is addressed extensively in the Phase III summary (Appendix F).

Prior to validating the models, the RT compiled a list of modeling parameters that are most likely to affect the predicted girder and cross-frame responses to live loads. In the process of validating the models, the sensitivity of the model to each parameter was evaluated. Preliminary sensitivity studies indicated which parameters are the most critical. Once the most critical parameters were identified, the RT reviewed literature and used engineering judgement to establish reasonable bounds for those parameters. In general terms, a user can manipulate a model in many ways to achieve the target solution; however, those changes may not be a good representation of the actual structural system. The RT was interested in achieving good agreement between measurements and FEA predictions but not at the expense of using unreasonable assumptions. Based on the literature review and many model configurations, the RT was able to select a consistent set of parameters and assumptions that not only improved the accuracy of the results compared to the measured data, but also are defensible based on common engineering practice.

The following subsections address each key modeling parameter separately. As noted earlier, these parameters were considered in each bridge model, and the RT ultimately elected to apply these parameters consistently across the three bridge models given the geographical proximity and the similar construction dates. These key modeling parameters are as follows:

- Boundary conditions,
- Contribution of concrete rails,
- Elastic concrete modulus,
- Dimensioning of important structural components,
- Loading conditions, and
- Constraints and FEA mesh density.

Subsequently presented sections E5.2, E5.3, and E5.4 discuss unique aspects of the bridge models with respect to these key parameters, as well as how these modifications affected the final results.

E5.1.1 Boundary Conditions

All three subject bridges were constructed with elastomeric bearings in accordance with TxDOT standard details. Each bridge consisted of some combination of expansion, fixed, or expansion sliding bearings. To match the nomenclature used in the TxDOT standards, these three bearing types will be abbreviated as “E”, “F”, and “ES” bearings herein. For all three bearing types, an elastomeric pad is sandwiched between a sole plate welded to the bottom flange of the girder and a concrete pedestal on the bent or abutment seat. Note that base plates between the bottom of the bearing pad and the concrete pedestal are not typically used in Texas. A front elevation of an E-type and F-type elastomeric bearing detail is provided in Figure E5-1. A threaded anchor rod through the sole plate anchors the girder to the substructure to restrain excessive lateral movements. The difference between E-type and F-type bearings is the slotted holes that are utilized in E-type bearings to accommodate longitudinal movement of the bridge, largely due to thermal effects. A close-up view of an ES-type bearing detail is provided in Figure E5-2. Note that a thin PTFE sheet and stainless steel plate is added to the detail. These bearing types permit longitudinal movement through two mechanisms: shear and rotational deformation of the elastomeric pad and sliding of the PTFE sheet over the stainless steel plate.

Figure E5-3 shows an E-type elastomeric bearing photographed on abutment 1 of Bridge 2. This photo was taken in July. The bridge had likely expanded due to the high temperatures, which explains why the elastomeric bearing is deformed in the direction of the abutment back wall.

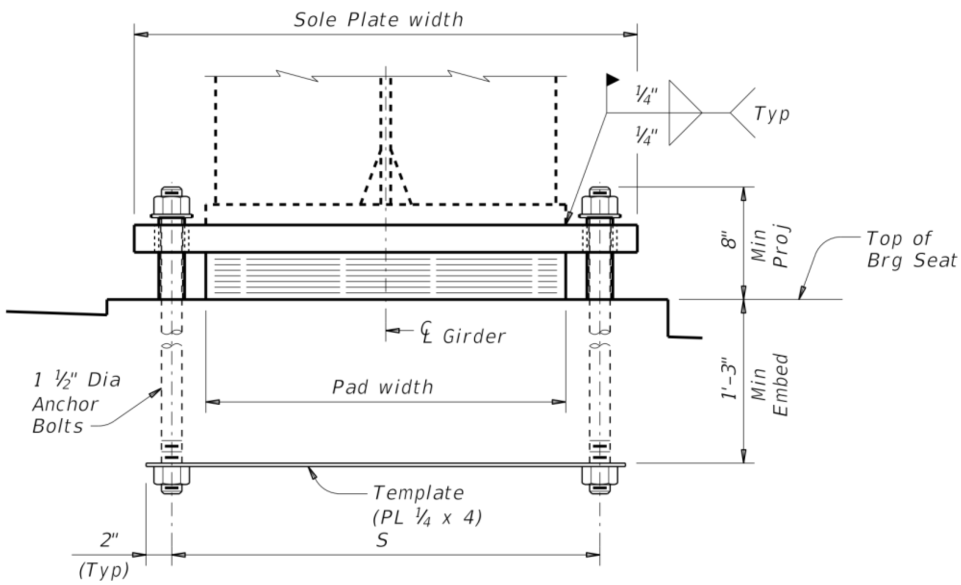

Figure E5-1: Front elevation of standard elastomeric bearing detail for E- and F-type bearings (from TxDOT standard drawing SGEB)

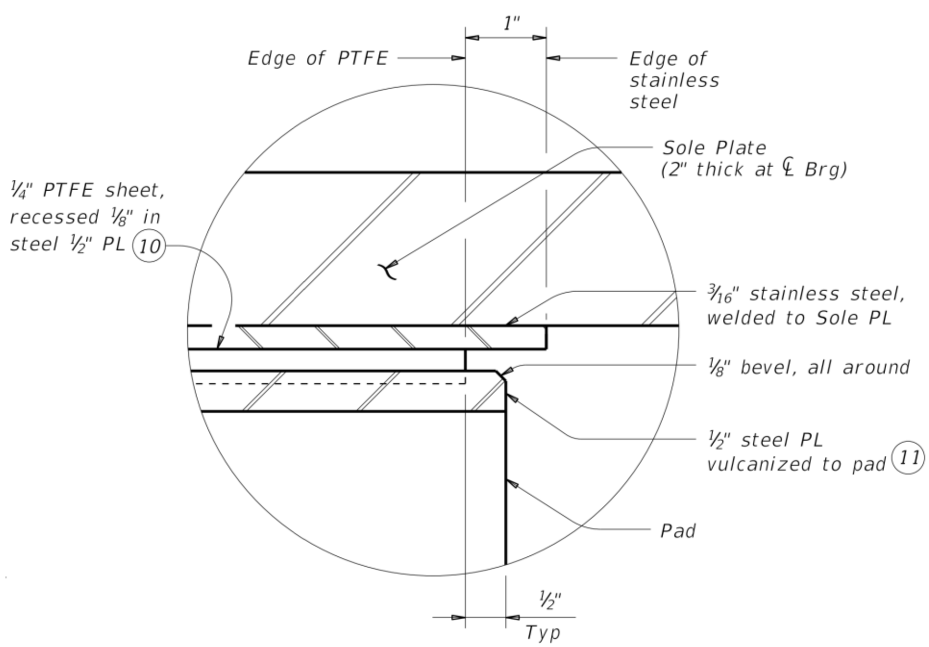

Figure E5-2: Close-up of standard elastomeric bearing detail for ES-type bearing (from TxDOT standard drawing SGEB)

Figure E5-3: Expansion bearing photographed at Bridge 2

Variations in the estimated stiffness of the bearing supports can affect the global response of a bridge unit to live loads. This is particularly true for curved bridges, where live loads not only induce vertical reactions on bearing elements but also lateral reactions due to the resulting thrust of the system from its curved shape. Based upon the results of initial sensitivity studies, it was apparent to the RT that selecting an appropriate stiffness for the bearing elements would be important to validating the models.

As mentioned in the introductory section of this chapter, these 3D FEA models were comprised entirely of shell elements except for the bearings. In the preliminary models, expansion bearings were modeled as vertical point supports only that permitted free lateral movement; fixed bearings restrained all three translation degrees of freedom. Based on the preliminary results, it was obvious that this first-guess approach produced conservative deflection results. The stiffness of the bearing is a function of the elastomeric pad, friction (for ES bearings only), and the anchor bolts, if engaged by contacting the inside of the slotted hole that guides the expansion/contraction of the bridge. Given that the elastomeric and friction terms act in series and the anchor bolts are not engaged for this magnitude of loading, the much more flexible elastomeric term controls the overall effective stiffness. As such, slip was not explicitly considered in the bearing elements, which is a reasonable assumption given the service-level type loads applied during the live load tests.

In the final validated model, the RT assigned longitudinal and transverse stiffness to the E- and ES-type bearings through springs. Although the shear stiffness of the elastomeric pad is small, the RT found that the stiffness should not be neglected. It was also assumed that the stiffness of ES-type bearings is similar to that of E-type bearings. Given that the expected deformations due to live loads are small, the RT also assumed the anchor rods would not be engaged; thus, both the stiffness in the longitudinal and transverse directions were equivalent to the shear stiffness of the elastomeric pad. Note that in the vertical direction, it was assumed that ample stiffness is provided such that a pinned condition is reasonable; the substructure and foundation elements were assumed rigid.

The shear stiffness of the elastomeric pads was estimated based on the guidance provided in 8th Edition AASHTO LRFD Specifications. A stiffness equation was adapted from Equation 14.6.3.1-2 in AASHTO and is shown below:

$$k_{bearing} = \frac{GA}{h_{rt}} \quad E5.1$$

where: G = shear modulus of the elastomer material, A = bearing area of the pad; and h_{rt} = height of the pad. The hardness of the elastomer pad was not provided in the design plans available, so the RT elected to conservatively assume a hardness of 50. Per AASHTO LRFD Table 14.7.6.2-1, a hardness of 50 corresponds to a temperature-dependent shear modulus in the range of 0.095 ksi and 0.120 ksi. The RT performed sensitivity studies and ultimately decided to assign 0.10 ksi as the shear modulus at all three bridges. This value represents a likely average condition for the bearings.

Given that the bearings used at these three bridges are standard details, the area and height of each pad are provided in standard TxDOT drawings. Table E5-1 summarizes the computed lateral stiffness of the expansion bearings given the assumed shear modulus and documented dimensions of the pad. Note that the number attached to each E- or ES-type is related to TxDOT standard sizes. Also note the “EE” bearings are simply E-type bearings at the end of the span.

Table E5-1: Assumed lateral stiffness of expansion bearings in FEA models

Bearing Type	Used at Bridges	Stiffness Assigned (kips/in)
E6	1, 3	9.4
E7	2	10.4
E9	2	11.7
EE4	2	6.2
ES6	1, 3	10.2

As illustrated in Table E5-1, the spring stiffness of the expansion bearings assigned in the three models ranged from 6 to 12 kips per inch. The coordinate system of these springs followed the orientation of the bearing pad, which typically was aligned with the axis of the supported girder, not the pier cap or bearing seat. As an example, Figure E5-4 demonstrates how lateral bearing springs were assigned to the FEA model of curved Bridge 3.

The relative impact of this modification to each respective bridge model is discussed in the subsequent sections.

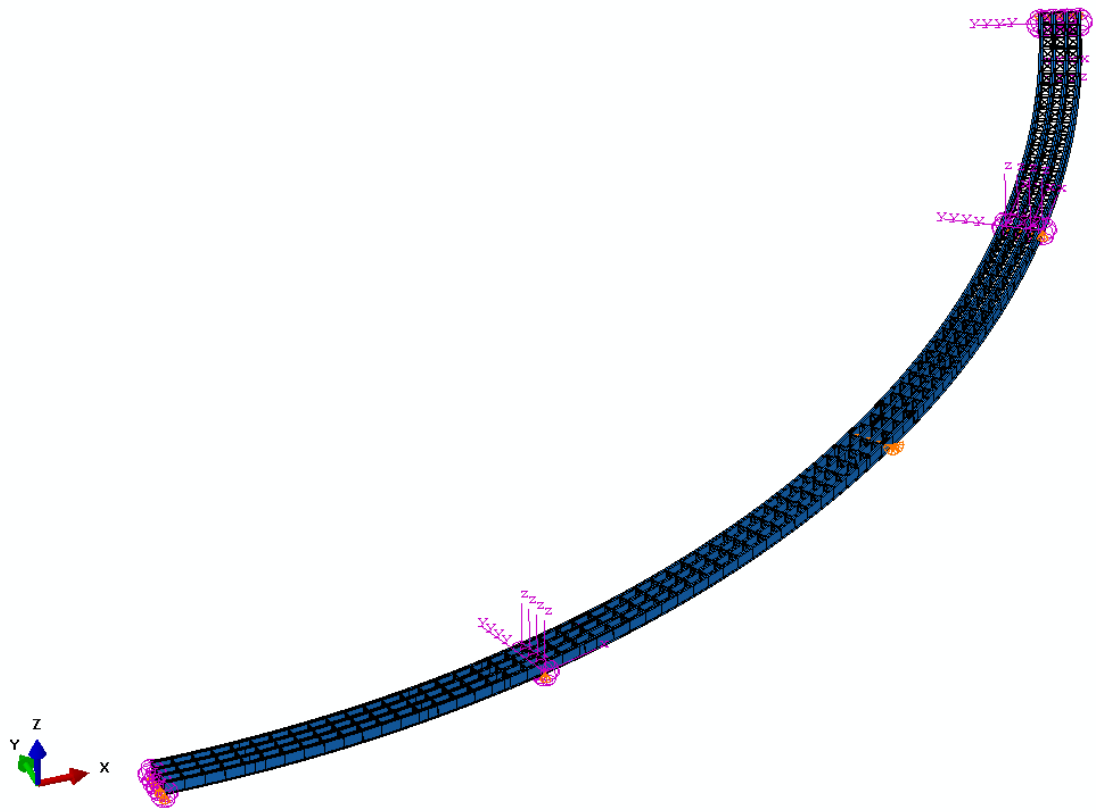

Figure E5-4: Screenshot of Bridge 3 model demonstrating boundary conditions assignments

E5.1.2 Contribution of Concrete Rails

At all three bridges, a standard TxDOT concrete bridge rail is fixed to each edge of the deck. TxDOT refers to this rail as type SSTR; the design height of SSTR rails are three feet measured from the top of the deck. They have a tapered shape with 6 inches in thickness at the top of the rail and 13 inches at the base. Figure E5-5 shows the SSTR rail used at Bridge 3. In the preliminary FEA models, the concrete rails were neglected, as is traditionally done in design for all three bridges. This assumption overestimated girder deflections when compared to the measured deflections from the live load tests.

Note that there are scuppers and intermediate joints in the barrier in Figure E5-5, such that it is not a continuous structural element. Although not continuous, the RT observed through running several model iterations that the stiffness of the discontinuous rail still contributes to the stiffness of the superstructure. Consequently, the RT added a discontinuous shell element to represent its stiffness contribution. Gaps of 1.2" were assigned at every 25 feet to simulate the discontinuity of the rails. The rail was also partitioned four times along its height. At each segment, the shell thickness was incrementally increased as to effectively represent the tapered shape of the section. Figure E5-6 illustrates an extruded view of the rail in Abaqus, modeled as shell elements with intermediate joints.

Figure E5-5: SSTR-type concrete rail used at Bridge 3 (adapted from Google Maps)

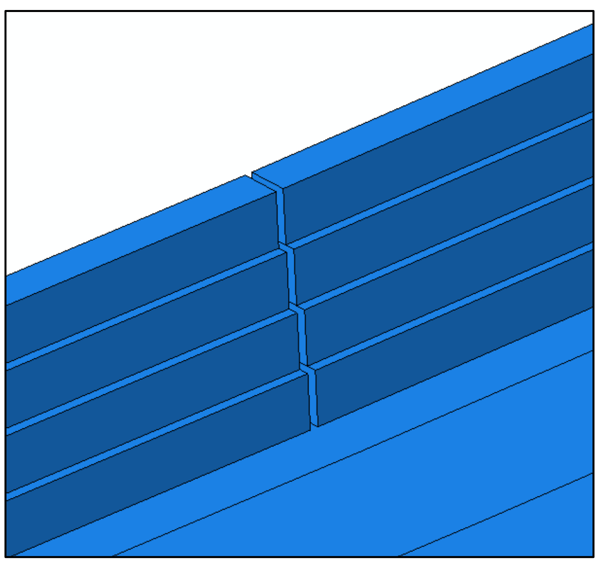

Figure E5-6: Representative concrete rail element in the validated FEA models

The stiffness of the concrete rails with respect to its modulus of elasticity is discussed in the next section.

E5.1.3 Elastic Concrete Stiffness

The assumed stiffness of the concrete deck and rails was also proven to significantly affect girder stresses and deflections in the FEA models. Consequently, the RT investigated the appropriate concrete stiffness to assume for each bridge model. In preliminary models, ACI design values for concrete modulus of elasticity (E_c) based on the specified concrete compressive strength were used ($57\sqrt{f'_c}$), but the RT recognized that design codes inherently provide lower-bound estimates. In order to validate the model and represent the actual conditions of the bridge, higher values of E_c were warranted. Given that coring the deck and rails was not feasible and the mix designs were not available, the RT sought to select a reasonable and defensible value for E_c that was representative of an average value for Texas and was larger than the lower-bound value used in design.

Equation 5.4.2.4-1 in the 8th Edition of AASHTO LRFD Specifications shows that the modulus of elasticity of concrete is a function of the following variables: specified concrete compressive strength (f'_c), unit weight of the concrete (w_c), and a correction factor for source of aggregate (K_1). The equation is shown below:

$$E_C = 120{,}000 K_1 {w_c}^{2.0} {f'_c}^{0.33} \qquad \text{E5.2}$$

where: w_c is in units of kcf, and f'_c is in units of ksi. Equation 5.4.2.4-1 was based on the research findings documented in NCHRP Report 595 (Rizkalla, et al. 2007). Note that the equation was slightly modified between the release of the report and the implementation into the AASHTO LRFD Specifications. The equation is a curve fit of the predicted modulus with values measured from many cylinder tests. The curve is fit through the middle of the data set, so it represents a mean value. Given that an average value was desired, the RT adopted the AASHTO equation as the basis for its assumption. The RT then investigated each of the individual variables to see if a higher value of E_c was justified.

In many cases, the actual compressive strength of a concrete mix is larger than the specified strength. The strength specified on the Bridge 1 and 2 design plans was 4 ksi, and the specified strength for Bridge 3 was 4.5 ksi. The rails at all three bridges are specified as Class C concrete. In review of the TxDOT Standard Specifications (2014), Class C concrete for bridge rails is specified as 3.6 ksi minimum compressive strength.

A typical mean-to-specified compressive strength ratio is around 1.2 to 1.25 for specified strengths of 3.6, 4, and 4.5 ksi (Nowak and Szerszen 2003). Therefore, it is likely that the actual compressive strength of the concrete decks and rails on the three subject bridges is higher than the specified value. But considering the E_c equation was derived for the specified f'_c and not a mean f'_c, utilizing a higher, mean compressive strength into the equation would effectively double-count the effects of an increased strength. Consequently, the RT used the specified strength when computing the concrete modulus to use in the FEA models.

Similarly, the unit weight of concrete can vary but 0.150 kcf is an average value for normal-weight concrete. As such, the RT simply used that value in computing E_c.

The aggregate factor (K_1) is to be taken as 1.0 in design unless physical tests have been performed. NCHRP Report 496 (Tadros, et al. 2003) documented research about prestress losses in concrete bridge girders. As part of the experimental program, researchers tested concrete mixes from several states and determined that Texas aggregates were stiffer relative to the other states. So much so, that a K_1 factor of 1.321 was proposed as an average value for Texas. Additionally, researchers at Ferguson Laboratory routinely measure E_c values from central Texas ready-mix plans that are consistent with the published K_1 factor. As such, the RT elected to assign an aggregate factor of 1.30.

With these assumptions in mind, the concrete deck modulus for the validated FEA models of Bridges 1 and 2 was taken as 5,500 ksi, while the modulus of Bridge 3 was taken as 5,800 ksi. Note that the preliminary models assumed 3,604 ksi and 3,830 ksi, respectively. Similarly, the modulus of the concrete rail was consistently taken as 5,300 ksi in the validated model; again, concrete rails were neglected in the preliminary model. The updated values represent a likely, average condition for the concrete used at the subject bridges, whereas the preliminary values represent a lower-bound estimate. As is documented in the subsequent sections, stiffening the concrete deck and rails in the FEA model resulted in much more accurate predictions of girder stresses and deflections.

E5.1.4 Important Dimensions

The RT also recognized that dimensions on design plans may not match the as-constructed conditions of the bridges. Prior to any site visits or load tests, the preliminary FEA models were based on the design plans, which was the best information available at the time. During the site visits, the RT collected measurements of all pertinent structural elements, including girder flanges, connection and gusset plate dimensions, cross-frame dimensions, concrete deck thickness, and haunch dimensions, which was briefly outlined in Chapter E3. Dimensions such as girder flanges and cross-frame dimensions were trivial; those field measurements served largely as checks to the design plans. Other dimensions such as deck thickness and haunch dimensions are generally more variable than steel plate thicknesses.

The RT acknowledged that the thickness of the deck is likely more (or less) than the 8-inch dimension specified on the design plans. Additionally, stay-in-place corrugated metal deck forms were used to construct the decks at all three bridges. The depth of the ribs, which run transversely from girder to girder, was measured as 2 inches at all three bridges; this extra concrete has the potential to add stiffness to the deck.

The dimensions of the haunch, particularly the thickness, can significantly deviate from what is shown on the design plans in order to achieve the desired deck elevations and slope. The RT measured the haunch thickness at discrete locations along the width and length of the instrumented spans, as documented in Chapter E3. Both the deck and haunch thickness could potentially affect the location of the elastic neutral axis, which in turns affects the stiffness of the composite girder system.

Through sensitivity studies, the RT learned that adjusting the deck thickness by an inch or increasing the haunch dimension by an inch had a negligible effect on girder stresses and deflections when compared to the modulus of the concrete deck. This trend was observed for all three bridge models. As such, this studied modeling parameter was not implemented into the final validated model. The as-designed dimensions were used in the final model. Figure E5-7 presents an extruded cross-sectional view of the Bridge 3 model. The deck and haunch thicknesses are based on the specified value in the design plans.

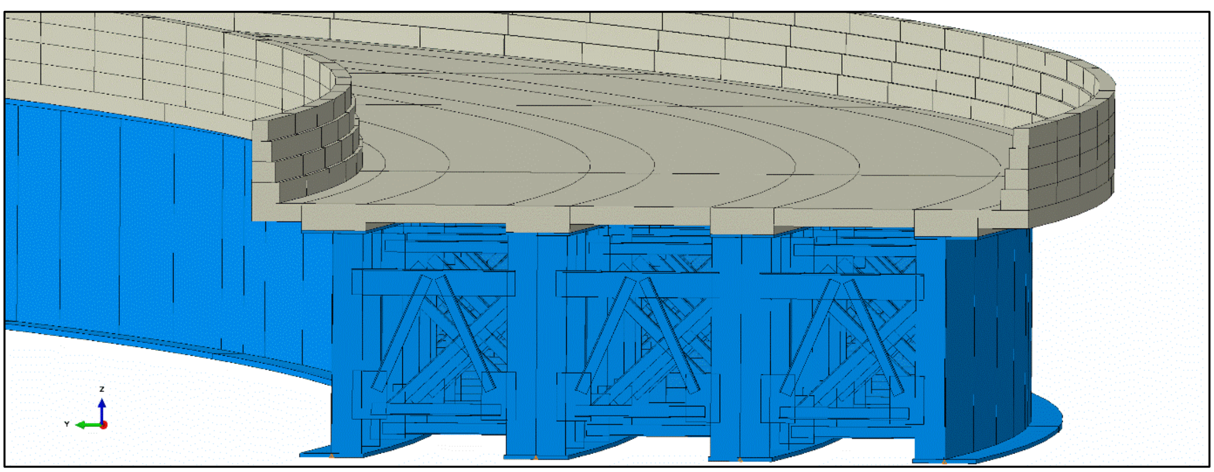

Figure E5-7: Cross-section of validated Bridge 3 model showing deck and haunch thickness

E5.1.5 Loading Conditions

As previously discussed, the seven static load cases from the controlled live load tests served as the basis for which the FEA models were validated. Applying a static load of known weight and known location can be easily replicated in the Abaqus software. Each of the three-axle trucks of known weight were modeled in Abaqus as a series of six point loads. The exact positioning of the trucks for each static load case was also considered in the models based on the measurements taken during each load case.

In order to accomplish this in the FEA software, the deck shells were partitioned based on the position of each truck for each load case. Static point loads corresponding to the wheel loads were then applied directly to nodes on the shell elements representing the deck. This procedure is demonstrated in Figure E5-8 for Bridge 3.

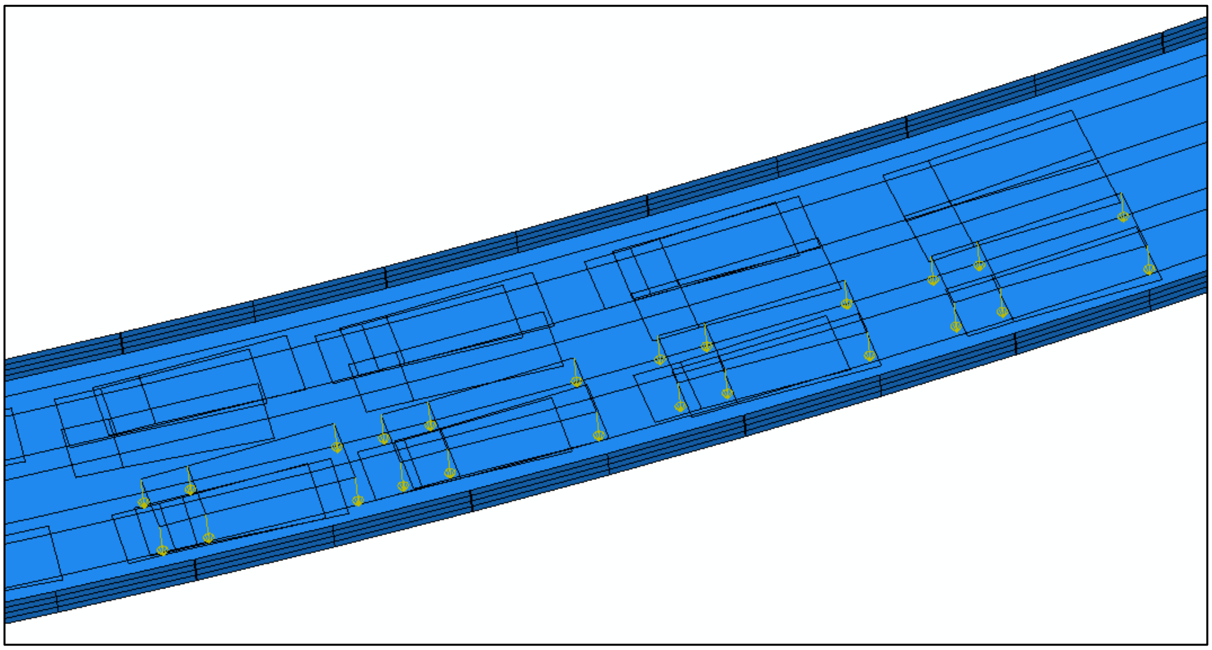

Figure E5-8: Partitioned deck shells for the application of truck loads

The procedure for applying live loads was consistent for the preliminary model and the validated model. The results in the subsequent sections reflect the same load cases and same modeling approach.

E5.1.6 Constraints and Meshing

Similar to the loading conditions, the procedures used to constrain and mesh shell elements were consistent across the preliminary and validated models. However, it is important to outline the modeling approach used. In general, elements such as webs, flanges, and stiffeners are physically connected by welds in reality; therefore, the elements in the FEA models representing these components are comprised of nodes that merged together at connected edges to simulate the welded connection. Besides the fabricated girders, other structural connections existed between elements such as cross-frame gusset plates to connection plates on the girders, and these connections in the FEA model are referred to as "parallel shells" in this discussion. Parallel shells, which are physically connected by welds in reality but are not physically connected in Abaqus, were connected with tie constraints. This example is illustrated in Figure E5-9. Lastly, top flanges of girders were constrained to the deck shell to simulate full composition action of the system.

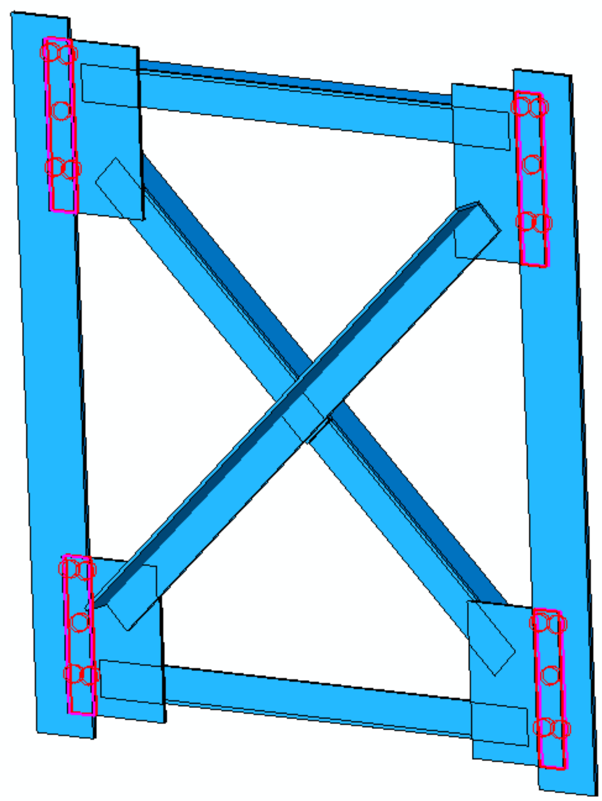

Figure E5-9: Cross-frame detail showing tie constraints between connection plates and gusset plates

Additionally, different shell components were assigned different mesh sizes depending on the geometry. The concrete deck and rails were assigned with a 10-inch mesh, the girders and stiffeners with a 6-inch mesh, and the cross-frame angles and connection plates with a 2-inch mesh. The bottom flanges of the girders were assigned a 2-inch mesh at locations in which strain gages were installed; this allowed the RT to output girder stresses from the same location as the field-measured data. The minimum integration points used through the thickness of a shell was taken as five. These mesh sizes proved to adequately balance analysis run time and accuracy of results.

E5.1.7 Summary of Modeling Parameters

As outlined in the previous subsections, the RT investigated a number of parameters that impacted the analytical results to varying degrees. Sensitivity studies were performed to gauge the relative impact of each parameter. Some parameters, including refining boundary conditions, increasing concrete stiffness, and including the concrete rail improved the analytical results. Other parameters such as deck and haunch thickness proved to have negligible effects.

Ultimately, the RT adopted a consistent set of assumptions for the three models. These assumptions are summarized in Table E5-2 below. In the subsequent sections, the RT documents key analytical results based on the preliminary set of assumptions and the validated set of assumptions in Table E5-2. The relative impact of each parameter specific to a bridge is also discussed.

Table E5-2: Summary of the key modeling parameters modified

Modeling Parameter	Pertinent Characteristic	
	Preliminary Model	Validated Model
Expansion bearing boundary conditions	Pinned vertically; free to translate	Pinned vertically; assigned elastic springs laterally
Concrete modulus	Deck: 3,600 ksi (3,800 ksi for Bridge 3)	Deck: 5,500 ksi (5,800 ksi for Bridge 3) Rail: 5,300 ksi
Presence of rail	No	Yes

E5.2 Bridge 1 Validation

In this section, the results of both the preliminary and validated models for Bridge 1 are compared to the measured data. Hence, this section is divided into two major subsections: preliminary model results and validated model results. Commentary on trends and observations with respect to the key modeling parameters outlined in Section E5.1 is also provided for both models.

In particular, analytical results of girder deflections, girder flange stresses, and cross-frame forces from the seven static load cases performed are assessed. The longitudinal bending component of the girder flange stresses and the axial force in the cross-frames were primarily used to validate the models. Figure E5-10 presents a screenshot of the FEA model for Bridge 1 as a reference; note that only the steel framing is shown for clarity.

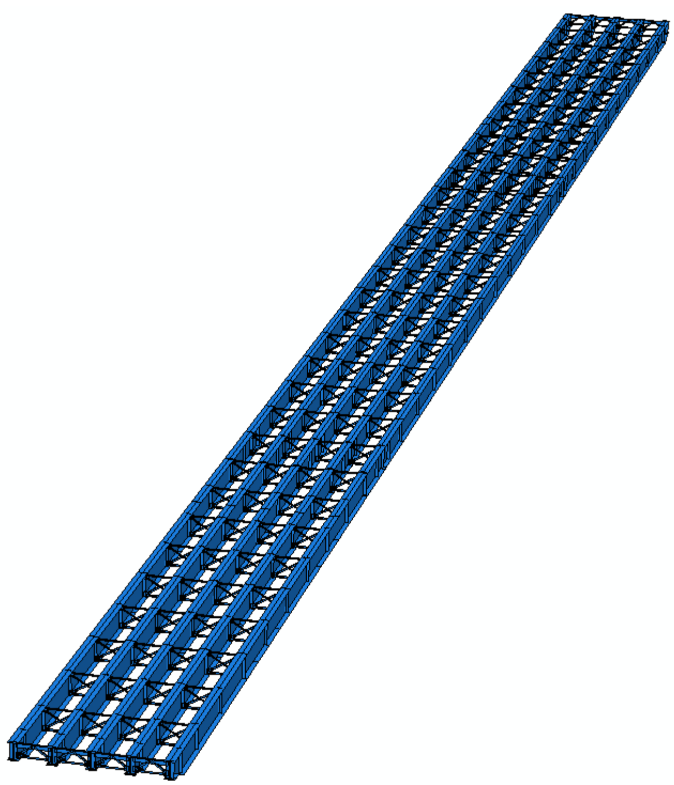

Figure E5-10: Isometric view of the Bridge 1 FEA model (steel framing only)

E5.2.1 Preliminary Model Results

Initially, the RT developed the Bridge 1 FEA model based largely on the design plans and conservative design code approaches. The seven static load cases performed during the controlled live load test were simulated in the model, and the RT obtained analytical results for girder deflections, girder flange stresses, and cross-frame forces. Data from the FEA models were noted at the same location as the field-measured data such that an accurate comparison between the values could be made.

In the interest of brevity, the RT focuses only on the most pertinent data to validating the model. Although all the measured data was recorded and reviewed, the most pertinent data was often selected as the loading that caused the largest deflections, girder stresses, or cross frame forces.

First, Table E5-3 presents the full results for girder deflections. The model validation often began by investigating the girder deflections. If there is significant error in deflection estimates, then the model is likely in need of refinement. Once reasonable agreement was obtained with the girder deflections, the RT then focused on the girder stresses and cross-frame forces. Table E5-3 presents the field-measured deflections, the analytical results from Abaqus, and the percent error between these two values. Note that the measured data presented in the table represent the final step of each load case in which all four dump trucks loaded the bridge. The specific intermediate cases are not discussed in this appendix but were used by the RT in the validation process. A positive error indicates that the analytical results exceeded the measured data, and a negative error indicates the opposite.

Recall from Section E4.1.3.4 that deflection measurements were obtained from all five girders across the width of the bridge at cross-frame line 4 in Span 11 during each load case. Also note that the field-measured data presented in Table E5-3 was previously presented in Table E4-6.

Table E5-3: Preliminary analytical versus measured girder deflections at cross-frame line 4 for Load Cases 1-7 (Bridge 1)

Load Case	Data Type	Vertical Deflections (in)				
		Girder 1	Girder 2	Girder 3	Girder 4	Girder 5
1	Measured	1.48	1.12	0.71	0.38	-0.09
	Analytical	1.92	1.37	0.81	0.27	0.25
	Error	30%	22%	14%	-29%	-4%
2	Measured	1.44	1.06	0.70	0.43	-0.04
	Analytical	1.78	1.32	0.83	0.36	-0.1
	Error	23%	24%	20%	-17%	152%
3	Measured	0.68	0.67	0.70	0.79	0.70
	Analytical	0.75	0.81	0.85	0.85	0.82
	Error	10%	21%	23%	7%	18%
4	Measured	-0.07	0.29	0.64	1.17	1.44
	Analytical	-0.20	0.30	0.81	1.35	1.87
	Error	208%	3%	26%	15%	30%
5	Measured	0.77	0.77	0.77	0.93	0.88
	Analytical	0.90	0.94	0.97	1.02	1.06
	Error	17%	22%	25%	9%	20%
6	Measured	0.01	0.30	0.58	1.05	1.29
	Analytical	-0.11	0.31	0.73	1.17	1.60
	Error	-961%	1%	27%	12%	24%
7	Measured	0.81	0.71	0.62	0.66	0.46
	Analytical	0.9	0.84	0.77	0.65	0.54
	Error	11%	19%	24%	0%	18%

From Table E5-3, it is apparent that the percent error is highly sensitive to the magnitude of deflection. Although some of the error is undoubtedly due to modeling assumptions, some of the error is also due to resolution of the field measurements. Attempting to accurately model very small deflections in the field is not practical nor warranted. Deflections near zero tend to have higher errors associated with them given that field-measured result is in the denominator of the equation. More critical values to compare are deflections of higher magnitude. For instance, the deflection of girder 1 during load case 1 (1.48 inches) was the maximum value recorded during the load test. For this particular case, the preliminary analysis predicted a deflection of 1.92 inches. Similarly, the deflection of girder 5 during load case 4 was also a significant value. The percent error associated with this load case is +30%. It is apparent that the FEA model underestimated the stiffness of the bridge and therefore overestimated the deflections.

As a means to simplify Table E5-3 and present only the most pertinent information, Table E5-4 displays the results of the ten highest deflection magnitudes. Those maximum magnitudes typically happened during load cases 1, 2, 4, 5, and 6. In terms of validating a model, reaching good agreement with critical measurements was deemed more important than improving error on a small magnitude deflection. This top-ten approach is replicated for all subsequent analytical results presented herein. For reference, full analytical and measured results are presented in Chapter E6.

Table E5-4: Preliminary analytical versus measured girder deflections at cross-frame line 4 for pertinent load cases (Bridge 1)

Load Case	Girder No.	Vertical Deflections (in)		Percent Error
		Measured	Analytical	
1	G1	1.48	1.92	30%
1	G2	1.12	1.37	22%
2	G1	1.44	1.78	23%
2	G2	1.06	1.32	24%
4	G4	1.17	1.35	15%
4	G5	1.44	1.87	30%
5	G4	0.93	1.02	9%
5	G5	0.88	1.06	20%
6	G4	1.05	1.17	12%
6	G5	1.29	1.60	24%

It is observed from Table E5-4 that the preliminary model for Bridge 1 underestimated the composite stiffness of the bridge unit. The preliminary model overestimated deflections by about 10 to 30%. A similar trend was observed when comparing analytical and measured bottom flange girder stresses. Table E5-5 summarizes those results. Critical bottom flange stresses were overestimated by the preliminary model around 20 to 30% when compared to the measured data. Note the flanges are identified by G#, where # indicates the girder number, and CFL##, where ## indicates the cross-frame line (either 4 or 7).

Table E5-5: Preliminary analytical versus measured girder bottom flange stresses for pertinent load cases (Bridge 1)

Load Case	Girder No.	Average Bottom Flange Stress (ksi)		Percent Error
		Measured	Analytical	
1	G1-CFL4	5.59	7.25	30%
1	G2-CFL4	4.14	5.07	23%
2	G1-CFL4	5.32	6.68	26%
2	G2-CFL4	3.96	4.91	24%
4	G4-CFL4	4.00	4.98	24%
4	G5-CFL4	5.67	7.06	24%
5	G3-CFL4	3.22	3.82	19%
5	G4-CFL4	3.32	4.09	23%
6	G5-CFL4	3.57	4.27	19%
6	G5-CFL4	4.42	5.46	24%

Lastly, critical cross-frame forces from the preliminary model are summarized in Table E5-6. Similar to the girder deflections and stresses, the FEA model generally overestimated the critical cross-frame forces by as much as 70%. Underestimating the stiffness of the bridge unit increased differential deflections and cross-frame forces. Recall that the cross-frame numbers in Table E5-6 were previously established in Figure E4-4 and Figure E4-5 of the appendix; additionally, a positive cross-frame force represents tension.

Table E5-6: Preliminary analytical versus measured cross-frame axial forces for pertinent load cases (Bridge 1)

Load Case	Cross-Frame No.	Axial Force (kips)		Percent Error
		Measured	Analytical	
3	CF-3	5.03	5.92	18%
3	CF-4	5.68	9.67	70%
3	CF-7	7.67	9.77	27%
3	CF-8	6.41	10.24	60%
3	CF-9	7.45	9.07	22%
3	CF-12	5.37	6.66	24%
7	CF-4	4.37	7.20	65%
7	CF-7	4.58	5.64	23%
7	CF-9	5.09	6.63	30%
7	CF-16	6.74	6.08	-10%

Based on the results summarized in Table E5-4, Table E5-5, and Table E5-6, the RT performed sensitivity studies on the three major modeling parameters listed in Table E5-2 to identify which parameters improved the accuracy of the FEA. As previously discussed, the preliminary model results suggested that the composite stiffness of the girders was underestimated. Therefore, it is not surprising that the addition of the concrete rails and the modification of the concrete stiffness to the final validated model was found to improve the analytical results. Assigning lateral springs to the bearings also had significant effects on the analytical results. The subsequent section presents the improved results of the validated model, which implemented the modifications summarized in Table E5-2.

E5.2.2 Validated Model Results

Table E5-7, Table E5-8, and Table E5-9 present the summarized results of the validated model once the key modeling parameters discussed previously were modified. Table E5-7, Table E5-8, and Table E5-9 compare the validated analytical results with the measured data for critical girder deflections, girder stress, and cross-frame force effects, respectively. For reference, the percent error associated with the validated model and the preliminary model are both presented in the tables.

It is apparent that increasing the stiffness of the concrete deck and including a discontinuous concrete rail stiffened the bridge and consistently improved the analytical results. Critical girder deflections, which were once uniformly overestimated, improved to smaller errors of -11 to +5%. The RT deemed deflection errors within 10 to 15% acceptable given the complexity of the bridge and potential uncertainty in the measured data. Critical girder stresses also consistently improved; validated model errors were on the order of 10-15%, which is also considered acceptable by the RT.

Stiffening the concrete deck also relieved some force in the critical cross-frame members. Table E5-9demonstrates that the accuracy of the model with respect to cross-frame forces has improved. It is important to note that the error associated with cross-frame forces is noticeably higher than what is observed for girder stresses or deflections, which was expected by the RT. Load paths and flexural behavior of girders is a better understood problem for structural engineers, so validating girder measurements was expected to be a more straightforward task. Cross-frames, on the other hand, have much more complex and less-understood load paths. Even when the most sophisticated full-shell, 3-D FEA model with precise measurements is developed for a bridge, the errors associated with the critical cross-frame forces still ranged from -12 to +60%. It is also acknowledged that correlation between the analytical and measured results is also potentially impacted by the resolution and accuracy of the strain gages, but that source of uncertainty is difficult to quantify. The RT further investigated the larger errors in cross-frame forces in the Phase III summary, Appendix F.

Table E5-7: Validated analytical versus measured girder deflections at cross-frame line 4 for pertinent load cases (Bridge 1)

Load Case	Girder No.	Vertical Deflections (in)		Percent Error	
		Measured	Analytical	Validated	Preliminary
1	G1	1.48	1.48	0%	30%
1	G2	1.12	1.09	-2%	22%
2	G1	1.44	1.38	-5%	23%
2	G2	1.06	1.06	0%	24%
4	G4	1.17	1.08	-7%	15%
4	G5	1.44	1.45	0%	30%
5	G4	0.93	0.88	-5%	9%
5	G5	0.88	0.91	4%	20%
6	G4	1.05	0.93	-11%	12%
6	G5	1.29	1.21	-6%	24%

Table E5-8: Validated analytical versus measured girder bottom flange stresses for pertinent load cases (Bridge 1)

Load Case	Girder No.	Avg. Bottom Flange Stress (ksi)		Percent Error	
		Measured	Analytical	Validated	Preliminary
1	G1-CFL4	5.59	6.46	16%	30%
1	G2-CFL4	4.14	4.53	9%	23%
2	G1-CFL4	5.32	6.00	13%	26%
2	G2-CFL4	3.96	4.42	11%	24%
4	G4-CFL4	4.00	4.45	11%	24%
4	G5-CFL4	5.67	6.30	11%	24%
5	G3-CFL4	3.22	3.66	14%	19%
5	G4-CFL4	3.32	3.88	17%	23%
6	G5-CFL4	3.57	4.12	15%	19%
6	G5-CFL4	4.42	4.75	8%	24%

Table E5-9: Validated analytical versus measured cross-frame axial forces for pertinent load cases (Bridge 1)

Load Case	Cross-Frame No.	Axial Force (kips)		Percent Error	
		Measured	Analytical	Validated	Preliminary
3	CF-3	5.03	5.53	10%	18%
3	CF-4	5.68	8.99	58%	70%
3	CF-7	7.67	8.77	14%	27%
3	CF-8	6.41	9.50	48%	60%
3	CF-9	7.45	8.14	9%	22%
3	CF-12	5.37	6.19	15%	24%
7	CF-4	4.37	6.65	52%	65%
7	CF-7	4.58	5.13	12%	23%
7	CF-9	5.09	5.97	17%	30%
7	CF-16	6.74	5.49	-19%	-10%

Specific cases from Table E5-7, Table E5-8, and Table E5-9 are presented graphically in Figure E5-11, Figure E5-12, and Figure E5-13. These figures are intended to provide a visual context for the results that have been presented in tabular format up to this point. Figure E5-11 shows the measured girder deflections compared to the corresponding analytical results (both preliminary and validated models) for load cases 1 and 4. It is evident that the validated model results exhibit good agreement with the measured results. Similar observations were made for the other load cases not shown.

Figure E5-12 shows the maximum flange stress in each girder across the bridge width under load case 2 and 4 loads. The measured response is compared to the analytical results of the preliminary model and the validated model. Again, the validated model results have better agreement with the measured data than the preliminary model results for both sample load cases. Similar observations were made for the other load cases not presented.

Lastly, Figure E5-13 displays the cross-frame forces at line 4 under load case 3 loading; the measured data and the analytical results from both the preliminary and validated models are plotted sequentially. Again, it is evident that the validated model shows improved accuracy on cross-frame forces for this case. The same statement can be said for the remaining load cases not presented in this figure. It should also be noted that validating cross-frame forces proved to be considerably more difficult than girder deflections or stresses. This inherently speaks to the level of understanding with respect to cross-frame analysis and load-induced behavior.

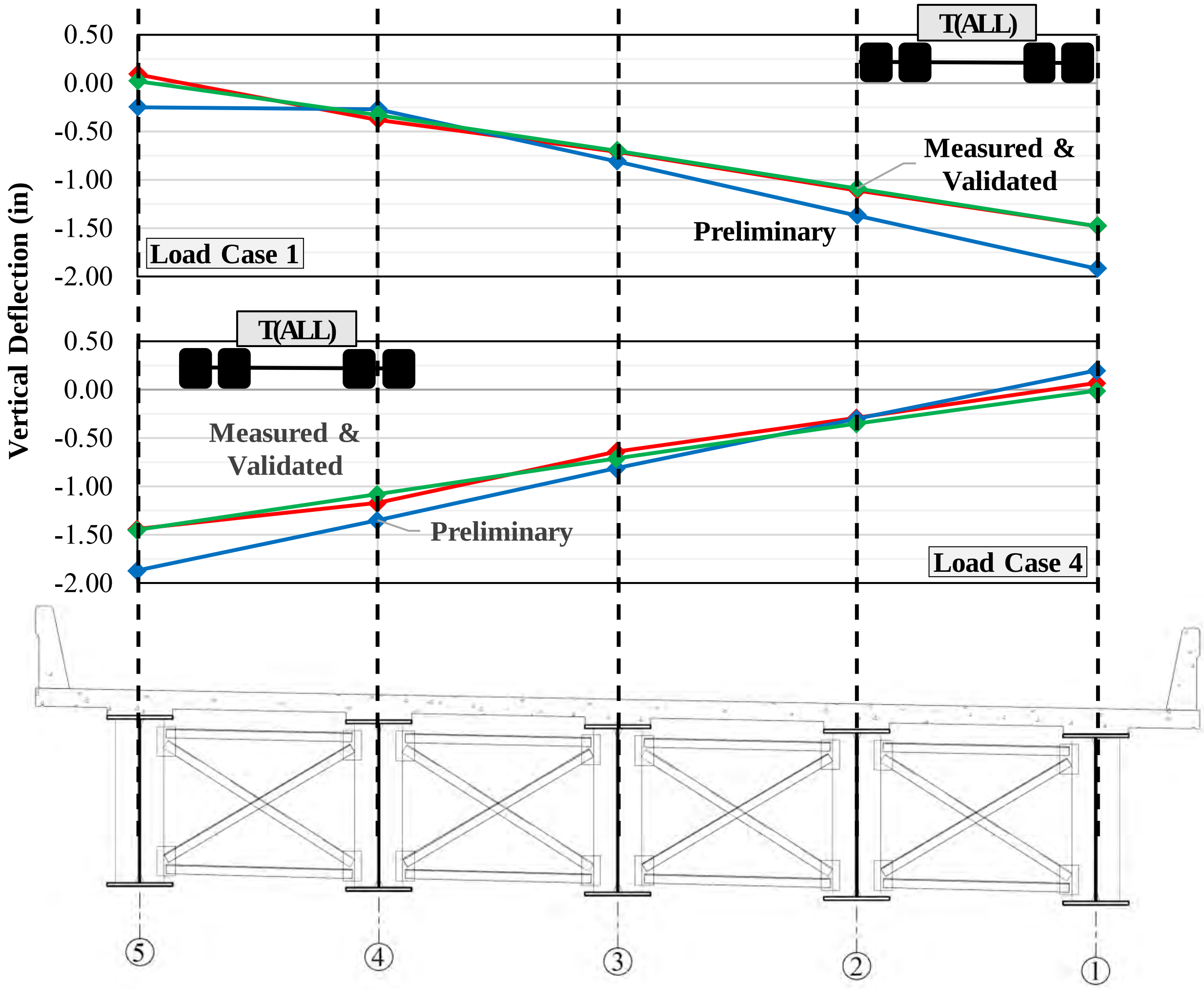

Figure E5-11: Comparing measured data, preliminary model results, and validated model results for load case 1 and 4 girder deflections

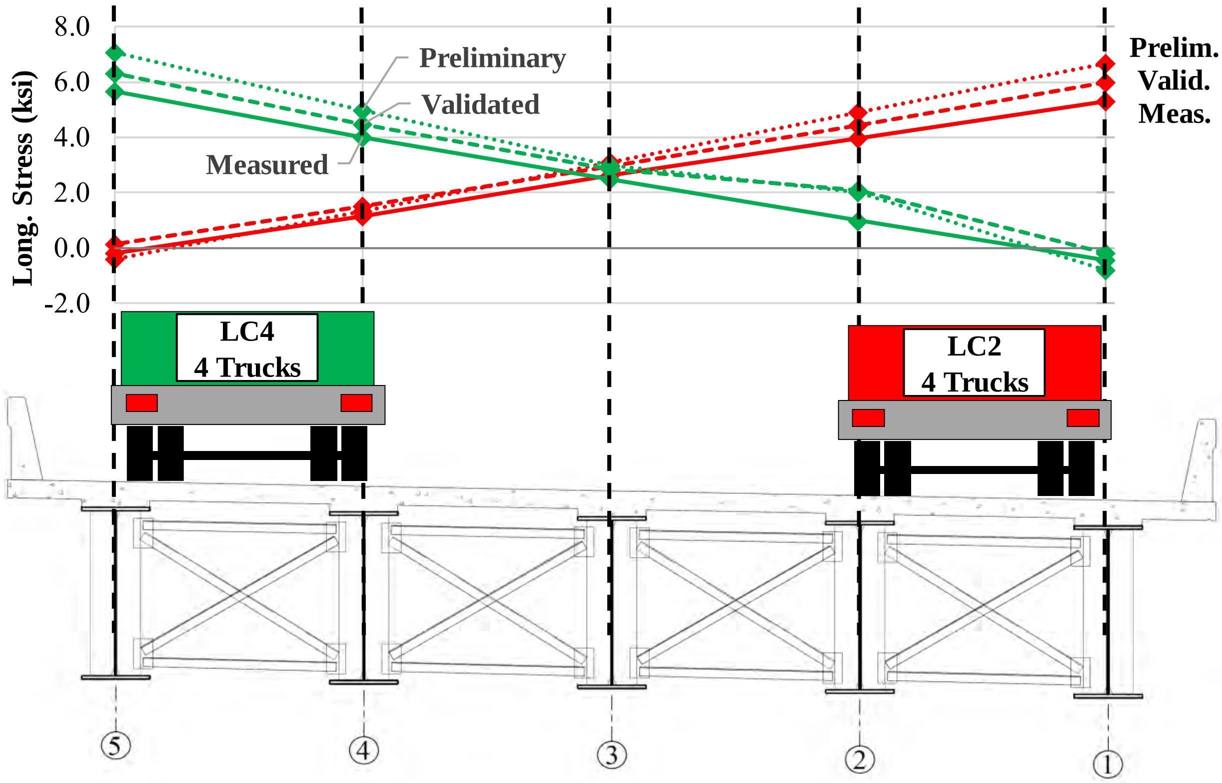

Figure E5-12: Comparing measured data, preliminary model results, and validated model results for load case 2 and 4 girder flange stresses

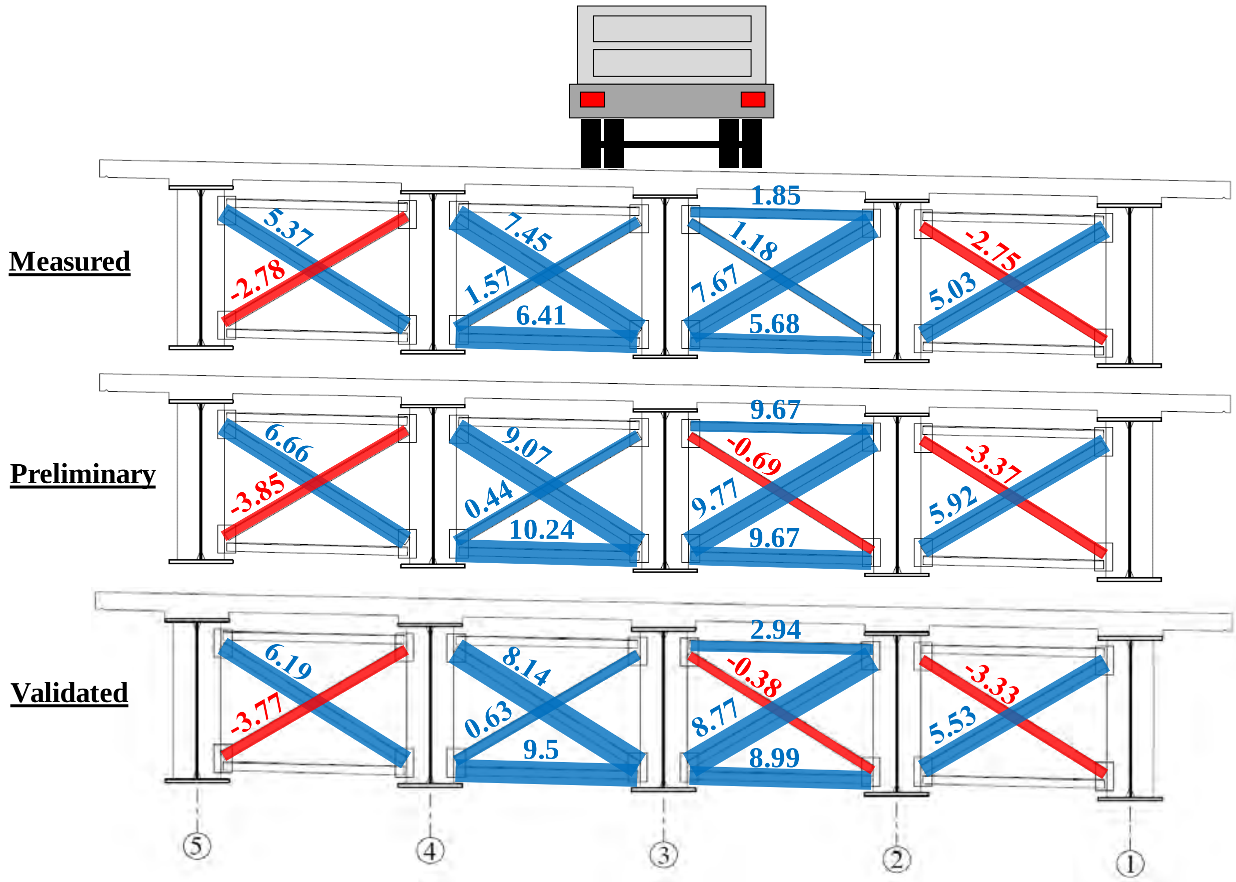

Figure E5-13: Comparing measured data, preliminary model results, and validated model results for load case 3 cross-frame forces at line 4 (Units: kips)

Based on these results, the RT was confident that parametric studies could be successfully conducted on straight bridges with normal supports and similar properties in Phase III of the project.

E5.3 Bridge 2 Validation

In this section, the results of both the preliminary and validated models for Bridge 2 are compared to the measured data in the same way as Bridge 1 model validation. Commentary on trends and observations with respect to the key modeling parameters is provided for both models. Figure E5-14 presents a screenshot of the FEA model for Bridge 2 as a reference; note that only the steel framing is shown for clarity.

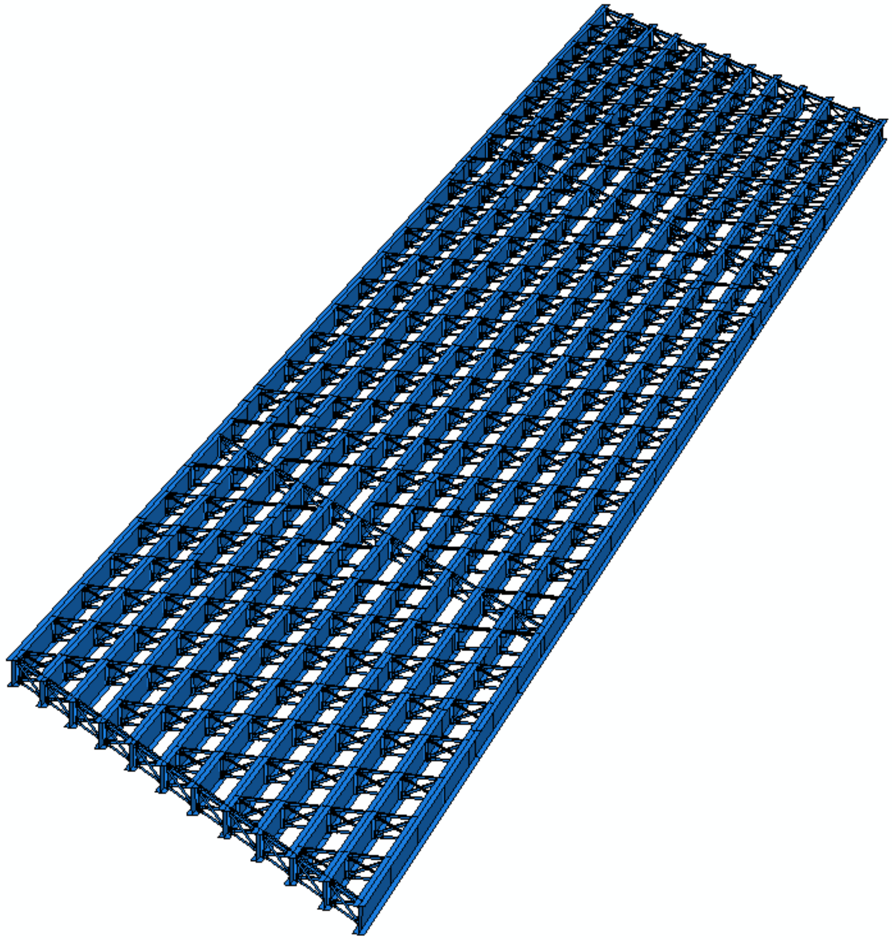

Figure E5-14: Isometric view of the Bridge 2 FEA model (steel framing only)

E5.3.1 Preliminary Model Results

Similar to the preliminary model of Bridge 1, the Bridge 2 preliminary model was based on the design plans and conservative design code approaches. From this model, the RT obtained analytical results for girder deflections, girder flange stresses, and cross-frame forces for seven static load cases. Again, only the ten most critical cases are presented in this appendix; full analytical results are provided in Chapter E6. Table E5-10 presents the results of the ten highest deflection magnitudes and compares those preliminary analytical results with the measured data.

Table E5-10: Preliminary analytical versus measured girder deflections for pertinent load cases (Bridge 2)

Load Case	Girder No.	Vertical Deflections (in)		Percent Error
		Measured	Analytical	
1	G23-CFL4	0.28	0.32	14%
1	G24-CFL6	0.14	0.15	8%
2	G23-CFL4	0.31	0.41	32%
2	G24-CFL6	0.15	0.19	23%
2	G21-CFL6	0.14	0.17	23%
3	G18-CFL6	0.18	0.18	1%
4	G23-CFL4	0.23	0.27	20%
4	G21-CFL6	0.18	0.17	-2%
6	G18-CFL6	0.20	0.24	16%
7	G14-CFL8	0.24	0.43	77%

It is observed from Table E5-10 that the preliminary model for Bridge 2 generally underestimated the composite stiffness of the bridge unit The error was typically on the order of +10 to +30% with a few exceptions.

The RT hypothesizes that the 77% error associated with load case 7 is due to the presence of the parallel northbound IH-35 bridge. The instrumented southbound and adjacent northbound bridges are identical in geometry and are connected by an intermediate concrete barrier. Although traffic was stopped on the SB side of IH-45 during the testing, the NB traffic continued as normal and likely impacted some of the results. Figure E5-15 and Figure E5-16 present the full cross-section of the parallel bridges and the connection detail of the barrier, respectively. Despite a longitudinal joint between the bridges, the concrete rail is anchored to each deck and provides continuity and an alternate load path. The RT neglected this connection and the parallel NB bridge for both the preliminary and validated models for simplicity. As a result, the predicted deflection in the FEA model for load case 7 is expected to be higher than the measured values.

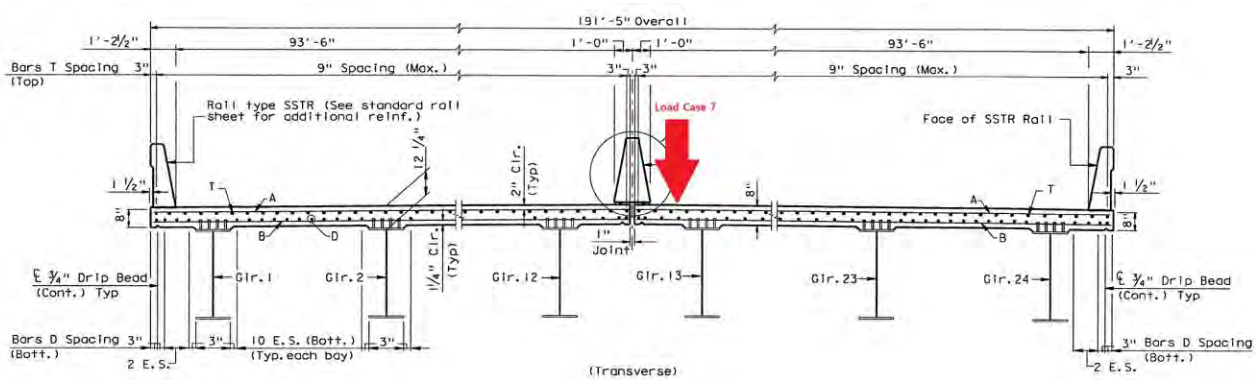

Figure E5-15: Transverse section of Bridge 2 (from contract plans provided by TxDOT)

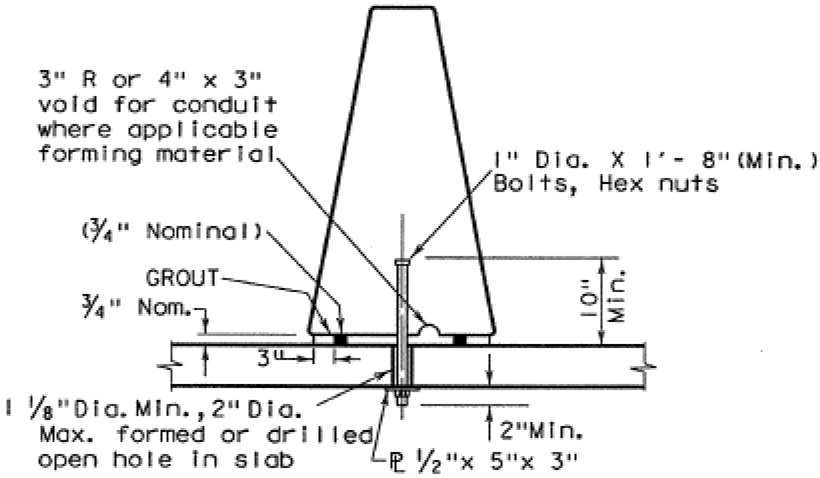

Figure E5-16: Connection detail for the interior concrete rail at Bridge 2 (from contract plans provided by TxDOT)

Table E5-11 summarizes and compares critical results of analytical and measured bottom flange girder stresses. The table presents the ten highest bottom flange stress magnitudes. Those maximum magnitudes typically happened during load cases 1 through 5. Unlike the Bridge 1 results, girder deflections and girder stresses were measured at different locations, so the load cases presented in Table E5-10 and Table E5-11 are also different. A similar trend for the girder deflections is also observed for bottom flange stresses. Critical bottom flange stresses were overestimated by the preliminary model around 10-30% when compared to the measured data.

Table E5-11: Preliminary analytical versus measured girder bottom flange stresses for pertinent load cases (Bridge 2)

Load Case	Girder No.	Average Bottom Flange Stress (ksi)		Percent Error
		Measured	Analytical	
1	G22-CFL5	1.07	1.37	28%
2	G22-CFL5	1.08	1.42	31%
2	G21-CFL5	1.11	1.43	29%
2	G20-CFL5	0.96	1.19	23%
3	G21-CFL5	1.07	1.27	19%
3	G20-CFL5	1.29	1.51	17%
4	G22-CFL5	1.32	1.63	23%
4	G21-CFL5	1.27	1.52	19%
4	G20-CFL5	1.05	1.29	22%
5	G21-CFL5	1.09	1.20	11%

Lastly, critical cross-frame forces from the preliminary model are summarized in Table E5-12. Those maximum magnitudes typically happened during load cases 2, 3, 4, and 5. Similar to the girder deflections and stresses, the FEA model generally overestimated the critical cross-frame forces by as much as 52%.

Similar to Bridge 1, underestimating the stiffness of the bridge unit lead to increased differential deflections and cross-frame forces.

Table E5-12: Preliminary analytical versus measured cross-frame axial forces for pertinent load cases (Bridge 2)

Load Case	Cross-Frame No.	Axial Force (kips)		Percent Error
		Measured	Analytical	
2	CF-2	-6.18	-8.30	34%
2	CF-3	-4.33	-6.58	52%
2	CF-4	6.12	8.70	42%
3	CF-9	6.45	7.35	14%
3	CF-11	9.25	10.09	9%
4	CF-7	8.73	11.04	26%
4	CF-10	6.93	7.60	10%
5	CF-8	5.77	5.99	4%
5	CF-9	6.33	7.46	18%
5	CF-10	5.87	6.15	5%

Based on the result summarized in Table E5-10, Table E5-11, and Table E5-12, it is observed that the preliminary model is more flexible than the real bridge. Therefore, concrete rails were added, the concrete modulus was modified, and lateral springs were assigned to the bearings to better capture the actual stiffness of the system based upon field measurements. The subsequent section summarizes the improved results of the validated model.

E5.3.2 Validated Model Results

Table E5-13, Table E5-14, and Table E5-15 summarize and compare results of the validated analytical results with the measured data for critical girder deflections, girder stress, and cross-frame forces, respectively. From the tables, it is observed that increasing the stiffness of the concrete deck and including a discontinuous concrete rail stiffened the bridge; consequently, the critical deflections improved to smaller errors of -15 to 15%, excluding the special load case 7 deflection discussed previously. The critical bottom flange stresses also improved consistently with errors of +5 to 18%, which were previously +11 to 31%. In comparison to the other two FEA models, the addition of the concrete rails had the least impact on the skewed Bridge 2. Given the high redundancy and width of this bridge, the effect of barriers is proportionally less significant.

The errors associated with the critical cross-frame forces also improved for the validated model. Errors ranged from -2 to +20%, which was deemed acceptable by the RT.

Table E5-13: Validated analytical versus measured girder deflections for pertinent load cases (Bridge 2)

Load Case	Girder No.	Vertical Deflections (in)		Percent Error	
		Measured	Analytical	Validated	Preliminary
1	G23-CFL4	0.28	0.27	-3%	14%
1	G24-CFL6	0.14	0.12	-10%	8%
2	G23-CFL4	0.31	0.34	12%	32%
2	G24-CFL6	0.15	0.15	3%	23%
2	G21-CFL6	0.14	0.14	4%	23%
3	G18-CFL6	0.18	0.16	-8%	1%
4	G23-CFL4	0.23	0.23	2%	20%
4	G21-CFL6	0.18	0.15	-15%	-2%
6	G18-CFL6	0.20	0.22	6%	16%
7	G14-CFL8	0.24	0.36	50%	77%

Table E5-14: Validated analytical versus measured girder bottom flange stresses for pertinent load cases (Bridge 2)

Load Case	Girder No.	Avg. Bottom Flange Stress (ksi)		Percent Error	
		Measured	Analytical	Validated	Preliminary
1	G22-CFL5	1.07	1.24	16%	28%
2	G22-CFL5	1.08	1.28	18%	31%
2	G21-CFL5	1.11	1.30	17%	29%
2	G20-CFL5	0.96	1.08	12%	23%
3	G21-CFL5	1.07	1.22	15%	19%
3	G20-CFL5	1.29	1.46	13%	17%
4	G22-CFL5	1.32	1.52	15%	23%
4	G21-CFL5	1.27	1.42	12%	19%
4	G20-CFL5	1.05	1.21	15%	22%
5	G21-CFL5	1.09	1.14	5%	11%

Table E5-15: Validated analytical versus measured cross-frame axial forces for pertinent load cases (Bridge 2)

Load Case	Cross-Frame No.	Axial Force (kips)		Percent Error	
		Measured	Analytical	Validated	Preliminary
2	CF-2	-6.18	-7.29	18%	34%
2	CF-3	-4.33	-5.47	26%	52%
2	CF-4	6.12	-7.24	18%	42%
3	CF-9	6.45	6.87	7%	14%
3	CF-11	9.25	10.11	9%	9%
4	CF-7	8.73	10.20	17%	26%
4	CF-10	6.93	7.26	5%	10%
5	CF-8	5.77	5.63	-2%	4%
5	CF-9	6.33	6.99	10%	18%
5	CF-10	5.87	5.77	-2%	5%

Specific cases from Table E5-13, Table E5-14, and Table E5-15 are presented graphically in Figure E5-17, Figure E5-18, and Figure E5-19. Figure E5-17 shows the measured girder deflections compared to the corresponding analytical results (both preliminary and validated models) for load case 2. Figure E5-18 compares the analytical and measured bottom flange stress in girder 20, 21 and 22 under load case 2. Lastly, Figure E5-19 displays the cross-frame forces at line 5 under load case 5 loading; the measured data and the analytical results from both the preliminary and validated models are plotted sequentially. In all three figures, the validated model provides more accurate predictions than the preliminary model.

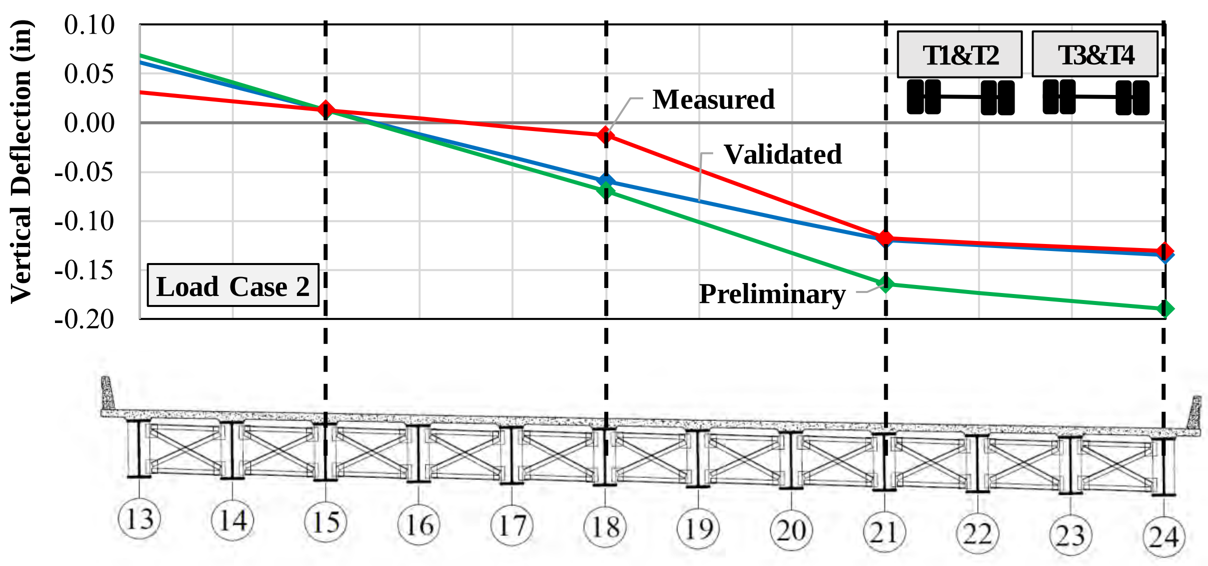

Figure E5-17: Comparing measured data, preliminary model results, and validated model results for load case 2 girder deflections

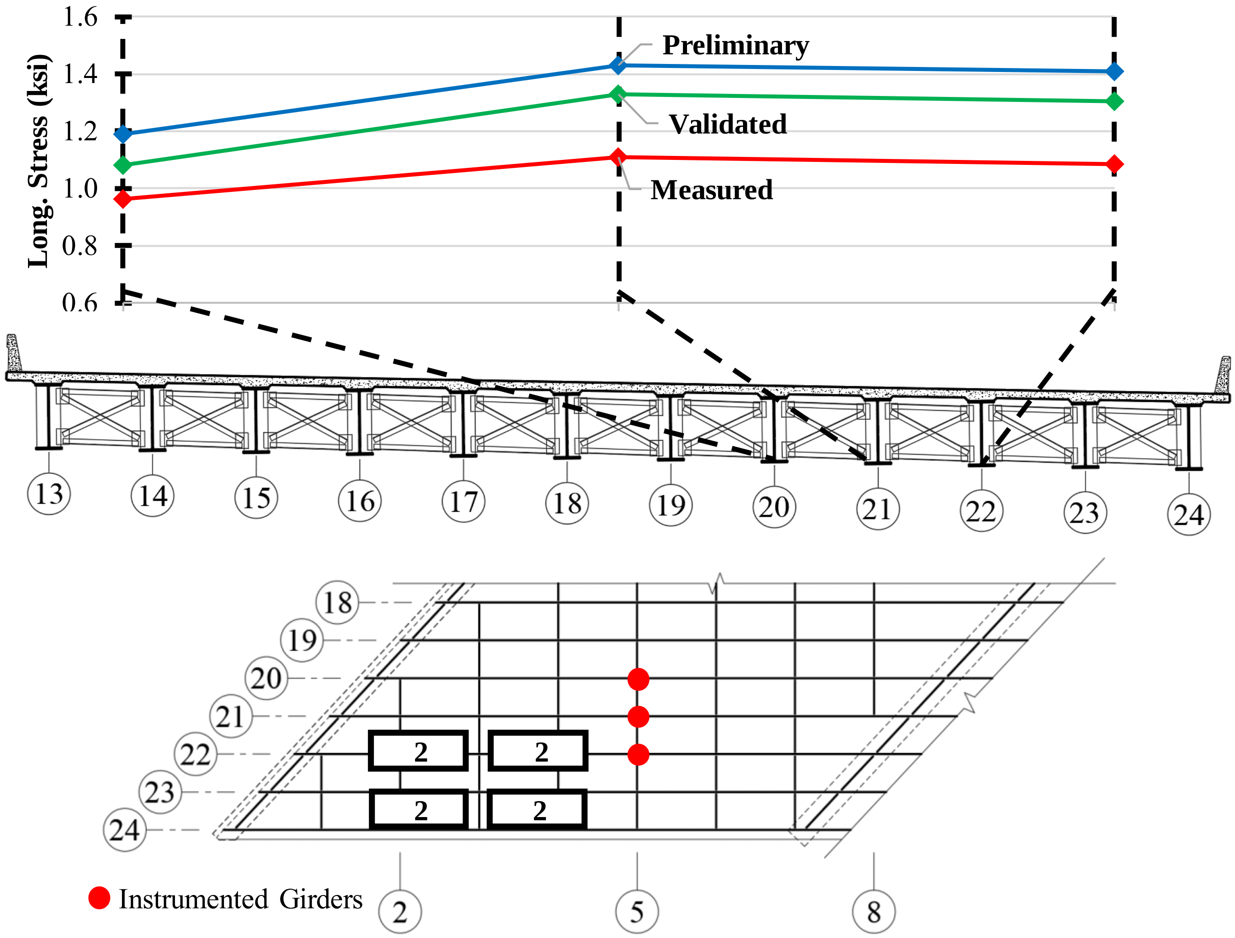

Figure E5-18: Comparing measured data, preliminary model results, and validated model results for load case 2 girder flange stresses of line 5

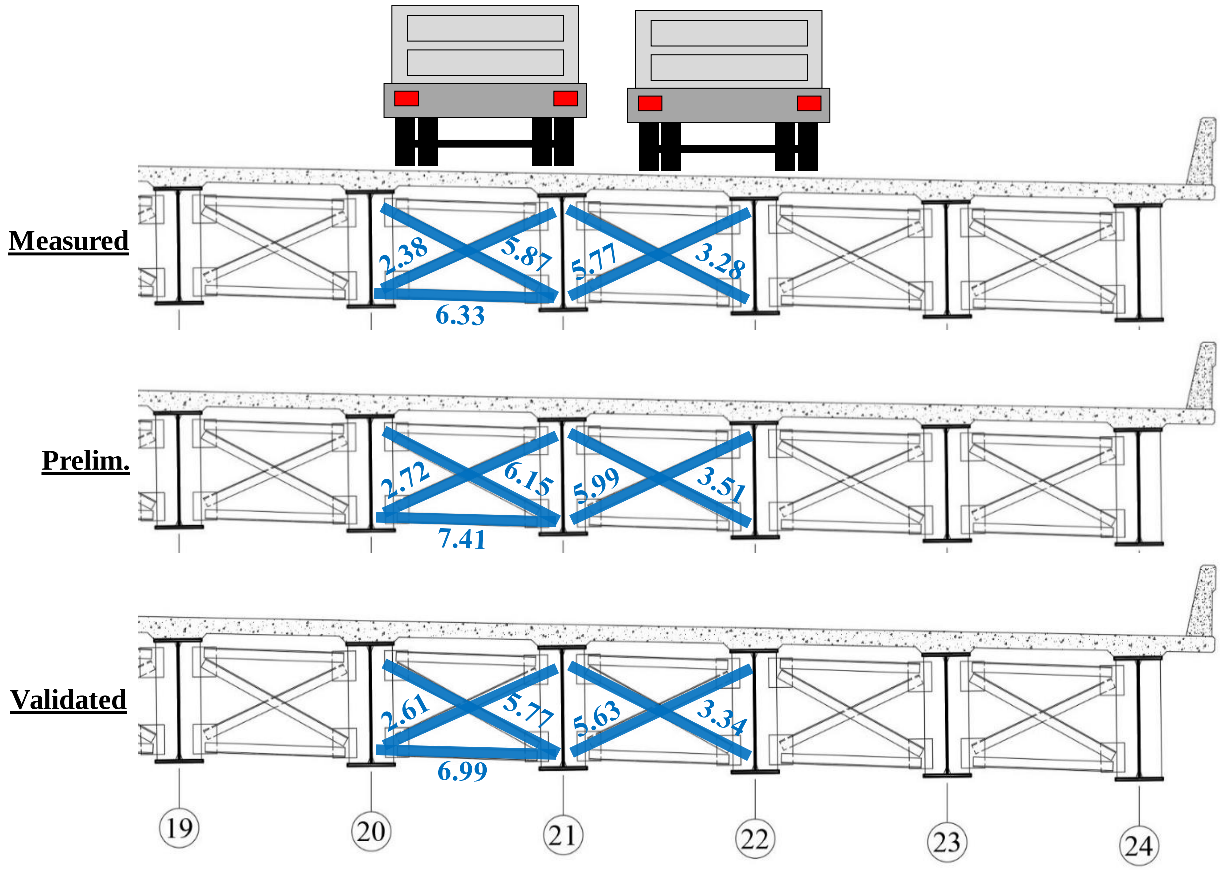

Figure E5-19: Comparing measured data, preliminary model results, and validated model results for load case 5 cross-frame forces at line 5 (Units: kips)

Based on these results, the RT was confident that parametric studies could be successfully conducted on straight bridges with skewed supports and similar properties in Phase III of the project.

E5.4 Bridge 3 Validation

The results of the preliminary and validated models for Bridge 3 are compared to the measured data in this section. Commentary on trends and observations with respect to the key modeling parameters is also provided for both models. Figure E5-20 presents a screenshot of the FEA model for Bridge 3 as a reference; note that only the steel framing is shown for clarity

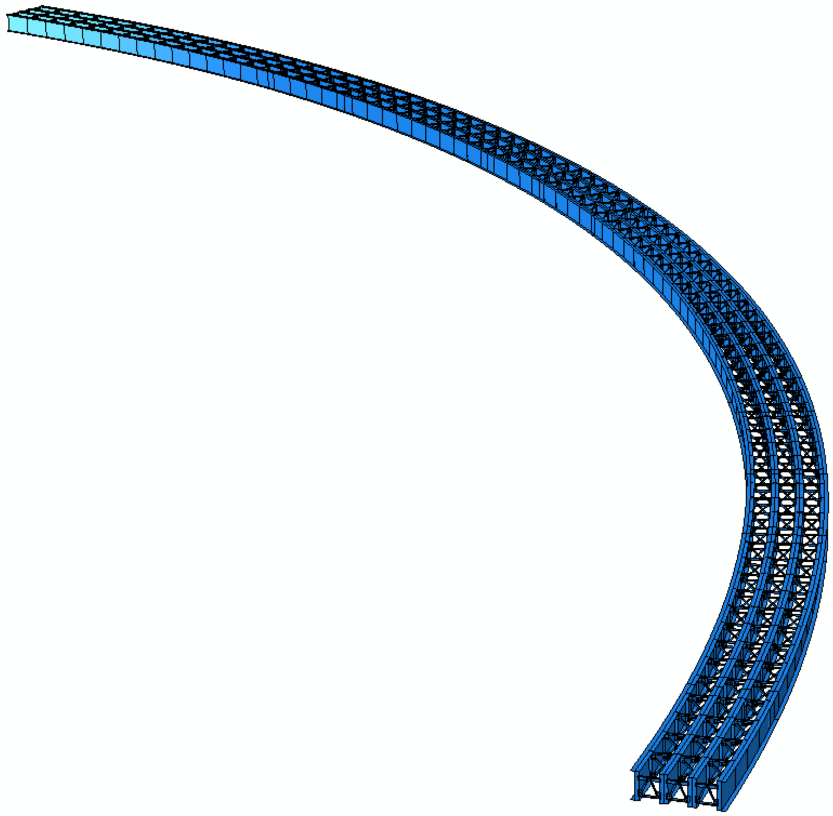

Figure E5-20: Isometric view of the Bridge 3 FEA model (steel framing only)

E5.4.1 Preliminary Model Results

The Bridge 3 FEA model was also developed based on the design plans and conservative design code approaches. The RT obtained analytical results for girder deflections, girder flange stresses, and cross-frame forces for seven static load cases. To simplify the comparisons, only the top most critical measurements are presented herein.

First, Table E5-16 presents the results of the ten highest deflection magnitudes. Measured deflections are compared to the preliminary analytical results for these ten critical cases.

Table E5-16: Preliminary analytical versus measured girder deflections at cross-frame line 11 for pertinent load cases (Bridge 3)

Load Case	Girder No.	Vertical Deflections (in)		Percent Error
		Measured	Analytical	
1	G4	0.88	1.04	18%
2	G1	0.87	1.11	28%
3	G1	1.50	2.12	42%
3	G2	1.17	1.54	32%
4	G1	1.92	2.71	42%
4	G2	1.36	1.85	35%
6	G1	1.17	1.61	38%
6	G2	0.83	1.10	34%
7	G1	1.23	1.70	38%
7	G2	1.00	1.35	35%

It is observed from Table E5-16 that the preliminary model for Bridge 3 consistently underestimated the composite stiffness of the bridge unit. Errors in the results ranged from +18 to 42%.

Table E5-17 summarizes the results of preliminary analytical and measured bottom flange girder stresses. Similar to the girder deflections, the bottom flange stress results also indicate that the stiffness of the composite system is underestimated, as the analytical girder stresses consistently exceeded the measured values by +13 to 29%.

Table E5-17: Preliminary analytical versus measured girder bottom flange stresses at cross-frame line 10 for pertinent load cases (Bridge 3)

Load Case	Girder No.	Average Bottom Flange Stress (ksi)		Percent Error
		Measured	Analytical	
1	G3	3.13	3.72	19%
1	G4	3.86	4.37	13%
2	G1	2.91	3.54	22%
2	G2	2.88	3.40	18%
3	G1	4.62	5.97	29%
3	G2	3.42	4.18	22%
4	G1	5.76	7.34	27%
4	G2	3.76	4.63	23%
7	G1	4.23	5.32	26%
7	G2	3.72	4.43	19%

Lastly, critical cross-frame forces from the preliminary model are summarized in Table E5-18. It is observed that model generally overestimated the critical cross-frame forces by as much as 27%. This is consistent with what was observed from the preliminary models of Bridge 1 and 2.

Table E5-18: Preliminary analytical versus measured cross-frame axial forces at cross-frame line 10 for pertinent load cases (Bridge 3)

Load Case	Cross-Frame No.	Axial Force (kips)		Percent Error
		Measured	Analytical	
1	CF-13	-3.75	-4.05	8%
1	CF-14	3.74	4.50	20%
2	CF-10	-4.30	-5.14	20%
2	CF-11	3.66	4.49	22%
2	CF-14	4.50	5.35	19%
3	CF-10	-5.93	-7.31	23%
3	CF-11	4.84	6.15	27%
4	CF-10	-5.03	-5.69	13%
4	CF-16	-3.66	-4.13	13%
7	CF-10	-4.29	-4.85	13%

Based on the result summarized in Table E5-16, Table E5-17, and Table E5-18, it was apparent that the preliminary model was more flexible than the real bridge. Consequently, the RT elected to modify the model in accordance with modeling parameters in Table E5-2. The subsequent section presents the improved results of the validated model.

E5.4.2 Validated Model Results

Table E5-19, Table E5-20, and Table E5-21 summarize and compare the results of the validated analytical results with the measured data for critical girder deflections, girder stress, and cross-frame forces, respectively. From these tables, it is observed that increasing the stiffness of the concrete deck and including a discontinuous concrete rail stiffened the superstructure, and consequently the error in critical deflections improved to +1 to 12%. Similarly, the analytical results for critical bottom flange stresses also improved with the errors ranging from +3 to 14%.

The RT found that the addition of the discontinuous concrete rail had the proportionally highest effect on the curved bridge FEA model in comparison to the other two models. The additional stiffness from the rails increased the global torsional stiffness of the unit, which subsequently lowered the predicted girder deflections and stresses.

By stiffening the concrete deck in the FEA model, the RT expected to subsequently decrease the predicted cross-frame forces. But despite the marked improvements in the predicted girder responses, the errors associated with the critical cross-frame forces increased after the modifications to the model were made. As demonstrated by Table E5-21, the error associated with a cross-frame members 10 and 11 (diagonals between girders 1 and 2) for select load cases have increased. The RT investigated this behavior further in the Phase III of the project as to reduce error in critical cross-frame forces.

Table E5-19: Validated analytical versus measured girder deflections at cross-frame line 11 for pertinent load cases (Bridge 3)

Load Case	Girder No.	Vertical Deflections (in)		Percent Error	
		Measured	Analytical	Validated	Preliminary
1	G4	0.88	0.89	1%	18%
2	G1	0.87	0.91	5%	28%
3	G1	1.50	1.68	12%	42%
3	G2	1.17	1.24	6%	32%
4	G1	1.92	2.14	12%	42%
4	G2	1.36	1.48	8%	35%
6	G1	1.17	1.26	8%	38%
6	G2	0.83	0.87	6%	34%
7	G1	1.23	1.37	11%	38%
7	G2	1.00	1.10	11%	35%

Table E5-20: Validated analytical versus measured girder bottom flange stresses at cross-frame line 10 for pertinent load cases (Bridge 3)

Load Case	Girder No.	Avg. Bottom Flange Stress (ksi)		Percent Error	
		Measured	Analytical	Validated	Preliminary
1	G3	3.13	3.50	12%	19%
1	G4	3.86	3.98	3%	13%
2	G1	2.91	3.21	10%	22%
2	G2	2.88	3.20	11%	18%
3	G1	4.62	5.27	14%	29%
3	G2	3.42	3.87	13%	22%
4	G1	5.76	6.43	12%	27%
4	G2	3.76	4.26	13%	23%
7	G1	4.23	4.76	13%	26%
7	G2	3.72	4.15	12%	19%

Table E5-21: Validated analytical versus measured cross-frame axial forces at cross-frame line 10 for pertinent load cases (Bridge 3)

Load Case	Cross-Frame No.	Axial Force (kips)		Percent Error	
		Measured	Analytical	Validated	Preliminary
1	CF-13	-3.75	-3.91	4%	8%
1	CF-14	3.74	4.35	16%	20%
2	CF-10	-4.30	-5.38	25%	20%
2	CF-11	3.66	5.35	46%	22%
2	CF-14	4.50	4.99	11%	19%
3	CF-10	-5.93	-7.55	27%	23%
3	CF-11	4.84	7.49	55%	27%
4	CF-10	-5.03	-6.14	22%	13%
4	CF-16	-3.66	-4.32	18%	13%
7	CF-10	-4.29	-5.30	24%	13%

Specific cases from Table E5-19, Table E5-20, and Table E5-21 are presented graphically in Figure E5-21, Figure E5-22, and Figure E5-23. Figure E5-21 and Figure E5-22 show the measured girder deflections and stresses compared to the corresponding analytical results (both preliminary and validated models) for load case 4, respectively. Note that girder deflections are taken at cross-frame line 11 and stresses at line 10. Figure E5-23 presented the cross-frame forces in line 10 under load case 4 loading. The measured data and the analytical results are plotted sequentially. From these figures, it is apparent that the validated model improved the accuracy with respect to girder deflections and stresses, but the error in cross-frame force predictions increased for select cross-frame members.

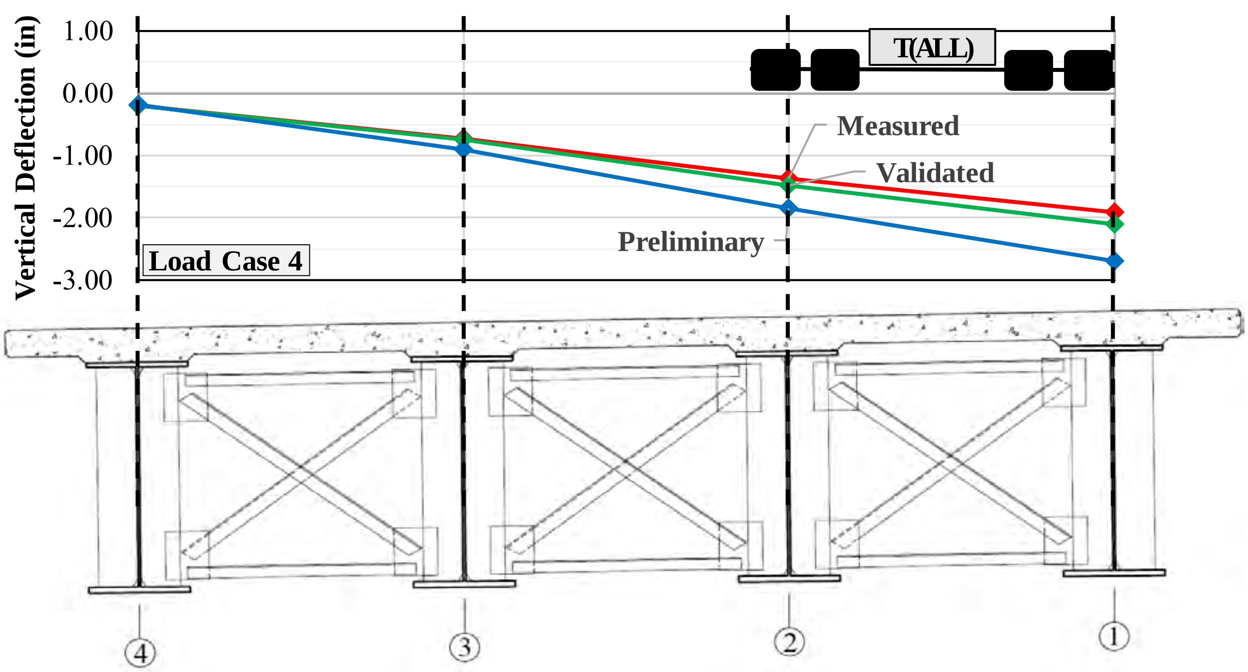

Figure E5-21: Comparing measured data, preliminary model results, and validated model results for load case 4 girder deflections

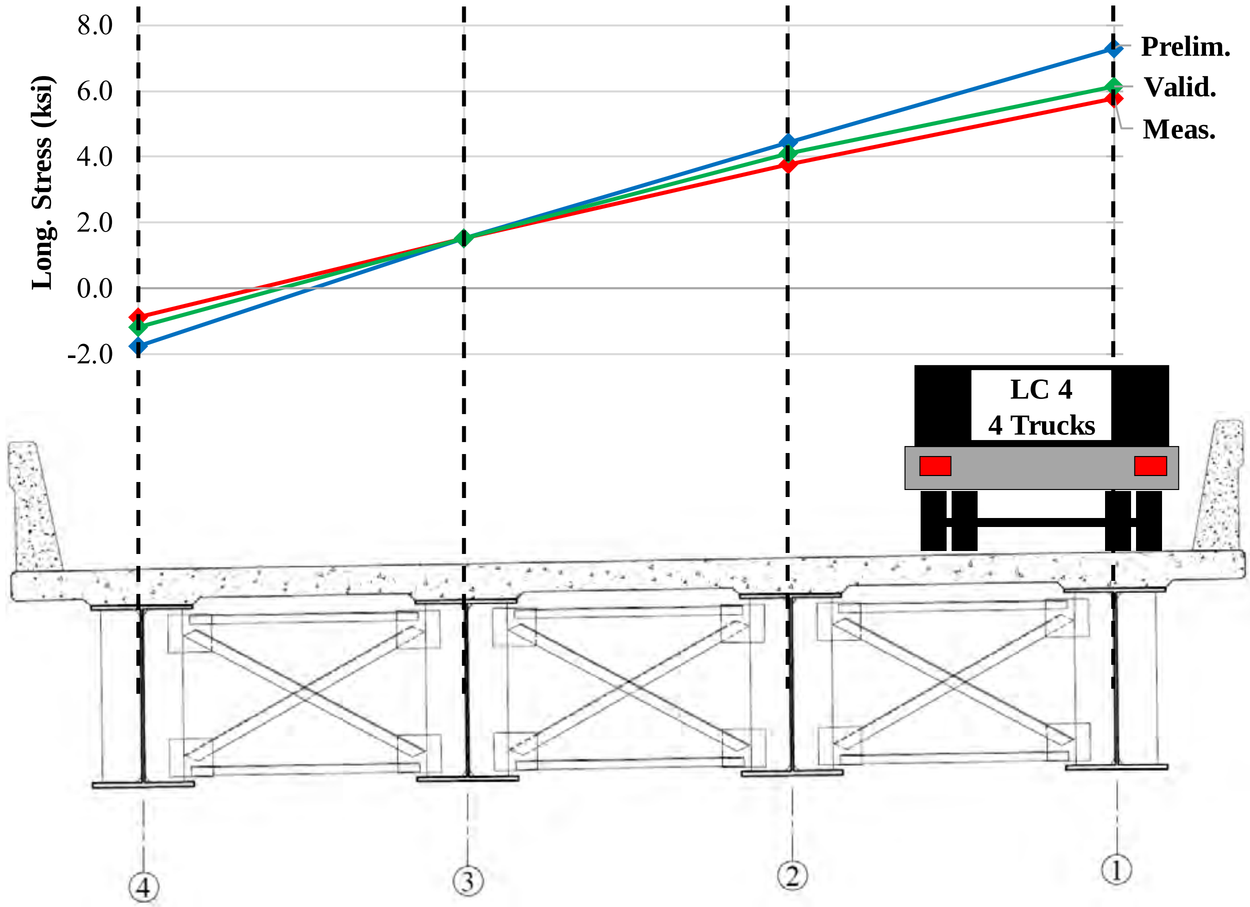

Figure E5-22: Comparing measured data, preliminary model results, and validated model results for load case 4 girder flange stresses

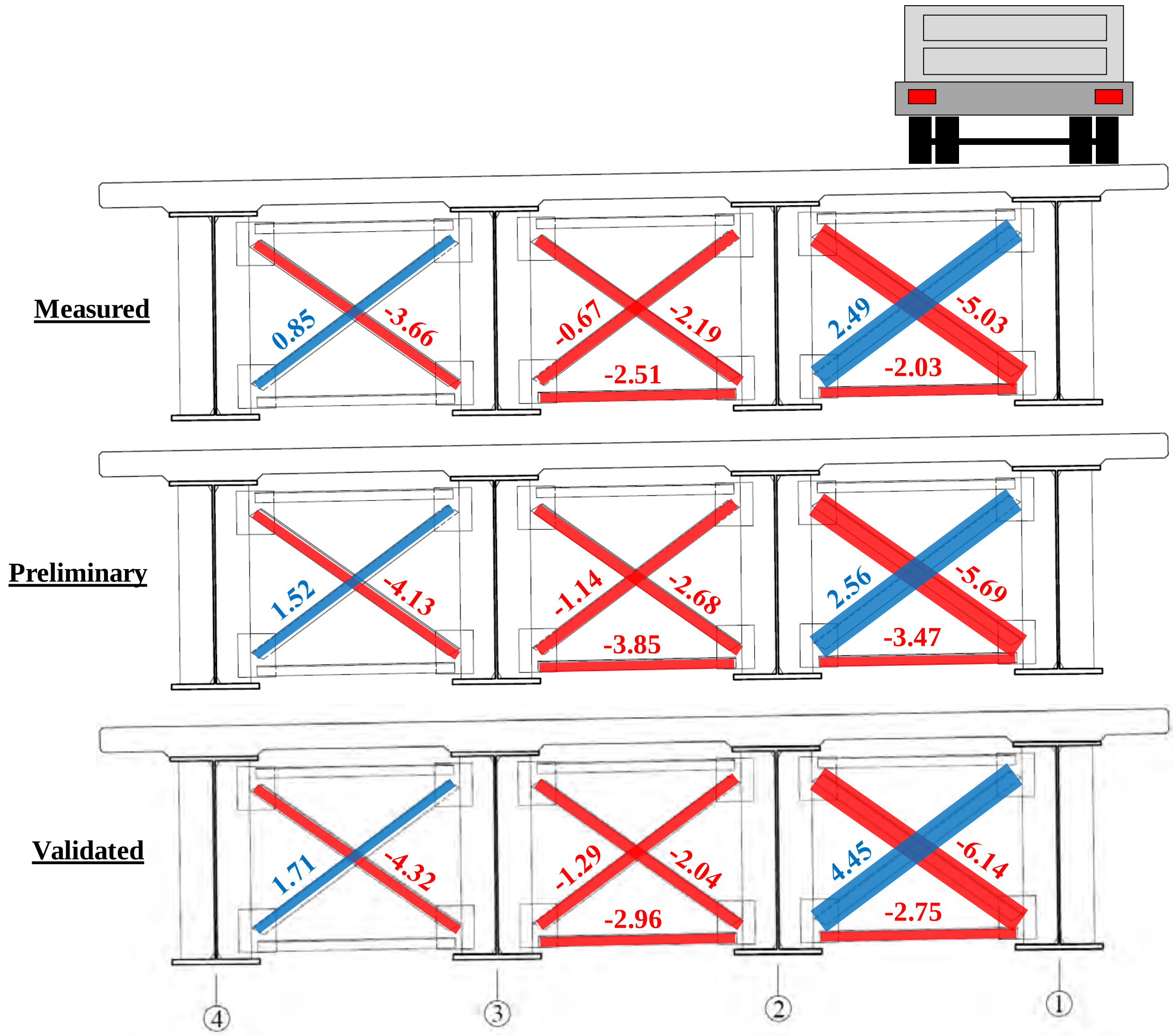

Figure E5-23: Comparing measured data, preliminary model results, and validated model results for load case 4 cross-frame forces at line 10 (Units: kips)

References

American Association of State Highway and Transportation Officials. 2017. *LRFD Bridge Design Specifications.* 8th Ed. Washington, D.C.

—. 2020. *LRFD Bridge Design Specifications.* 9th. Washington, D.C.

Battistini, A., Wang, W., Donahue, S., Helwig, T., Engelhardt, M., and Frank, K. 2013. *Improved Cross Frame Details for Steel Bridges.* Report No. 0-6564-1, Austin, TX: Center for Transportation Research.

Connor, R., and J. Fisher. 2006. "Identifying Effective and Ineffective Retrofits for Distortion Fatigue Cracking in Steel Bridges Using Field Instrumentation." *Journal of Bridge Engineering* (American Society of Civil Engineers) 11 (6): 745-752.

Downing, S., and D. Socie. 1982. "Simple Rainflow Counting Algorithms." *International Journal of Fatigue* (Butterworth & Co) 31-40.

Fasl, J. 2013. *Estimating the Remaining Fatigue Life of Steel Bridges Using Field Measurements.* PhD Dissertation, Austin, TX: The University of Texas at Austin.

Helwig, T., and Z. Fan. 2000. *Field and Computational Studies of Steel Trapezoidal Box Girder Bridges.* TxDOT Research Report 1395-3, Houston, Texas: The University of Houston.

McDonald, G., and K. Frank. 2009. *The Fatigue Performance of Angle Cross-Frame Members in Bridges.* MS Thesis, Austin, Texas: The University of Texas at Austin.

Micro-Measurements. 2018. *Weldable Strain Gages.* http://www.vishaypg.com/docs/11519/standard-weldable.pdf.

Miner, M. 1945. "Cumulative Damage in Fatigue." *Journal of Applied Mechanics* 12: 159-164.

Modjeski and Masters. 2015. *Bridges for Service Life Beyond 100 Years: Service Limit State Design.* SHRP 2 Report S2-R19B-RW-1, Washington, D.C.: Transportation Research Board.

Nowak, A., and M. Szerszen. 2003. "Calibration of Design Code for Buildings (ACI 318): Part 1—Statistical Models for Resistance." *ACI Structural Journal* (American Concrete Institute) 100: 383-389.

Rizkalla, S., A. Mirmiran, P. Zia, H. Russell, and R. Mast. 2007. *Applications of the LRFD Bridge Design Specifications to High-Strength Structural Concrete: Flexural and Compression Provisions.* NCHRP Report 595, Washington, D.C.: Transportation Research Board.

Tadros, M., N. Al-Omaishi, S. Seguirant, and J. Gallt. 2003. *Prestress Losses in Pretensioned High-Strength Concrete Bridge Girders.* NCHRP Report 496, Washington, D.C.: Transportation Research Board.

Texas Department of Transportation. 2014. "Standard Specifications for Construction and Maintenance of Highways, Streets, and Bridges."

CHAPTER E6

Model Validation Results

For reference, this chapter provides the full set of model validation results that were summarized previously in Chapter E5. Several tables are included that examine the preliminary and final analytical results in terms of girder deflections, girder flange stresses, and cross-frame stresses.

Table E6-1: Preliminary analytical versus measured girder deflections at cross-frame line 4 for Load Cases 1-7 of Bridge 1

Load Case	Data Type	Vertical Deflections (in)				
		Girder 1	Girder 2	Girder 3	Girder 4	Girder 5
1	Measured	1.48	1.12	0.71	0.38	-0.09
	Analytical	1.92	1.37	0.81	0.27	0.25
	Error	30%	22%	14%	-29%	-4%
2	Measured	1.44	1.06	0.70	0.43	-0.04
	Analytical	1.78	1.32	0.83	0.36	-0.1
	Error	23%	24%	20%	-17%	152%
3	Measured	0.68	0.67	0.70	0.79	0.70
	Analytical	0.75	0.81	0.85	0.85	0.82
	Error	10%	21%	23%	7%	18%
4	Measured	-0.07	0.29	0.64	1.17	1.44
	Analytical	-0.20	0.30	0.81	1.35	1.87
	Error	208%	3%	26%	15%	30%
5	Measured	0.77	0.77	0.77	0.93	0.88
	Analytical	0.90	0.94	0.97	1.02	1.06
	Error	17%	22%	25%	9%	20%
6	Measured	0.01	0.30	0.58	1.05	1.29
	Analytical	-0.11	0.31	0.73	1.17	1.60
	Error	-961%	1%	27%	12%	24%
7	Measured	0.81	0.71	0.62	0.66	0.46
	Analytical	0.9	0.84	0.77	0.65	0.54
	Error	11%	19%	24%	0%	18%

Table E6-2: Preliminary analytical versus measured girder bottom flange stresses for Load Cases 1-7 of Bridge 1

Load Case	Data Type	Average Bottom Flange Stress (ksi)						
		G1-CFL4	G2-CFL4	G3-CFL4	G4-CFL4	G5-CFL4	G3-CFL7	G4-CFL7
1	Measured	5.59	4.14	2.50	0.89	-0.51	0.74	0.45
	Analytical	7.25	5.07	2.97	0.96	-0.96	1.24	0.48
	Error	30%	23%	19%	8%	87%	69%	6%
2	Measured	5.32	3.96	2.62	1.14	-0.19	0.75	0.53
	Analytical	6.68	4.91	3.10	1.32	-0.40	1.26	0.62
	Error	26%	24%	18%	15%	105%	68%	17%
3	Measured	2.27	2.49	2.77	2.53	2.48	0.59	0.91
	Analytical	2.77	3.04	3.25	3.19	3.03	1.05	1.19
	Error	22%	22%	17%	26%	22%	78%	31%
4	Measured	-0.46	0.98	2.49	4.00	5.67	0.75	1.54
	Analytical	-0.79	2.02	2.98	4.98	7.06	1.27	1.87
	Error	71%	106%	20%	24%	24%	70%	22%
5	Measured	2.99	3.13	3.22	3.32	3.57	0.72	1.01
	Analytical	3.65	3.79	3.82	4.09	4.27	1.25	1.23
	Error	22%	21%	19%	23%	19%	74%	22%
6	Measured	-0.24	0.91	2.00	3.21	4.42	1.11	2.58
	Analytical	-0.38	1.02	2.46	4.05	5.46	1.93	3.04
	Error	63%	12%	23%	26%	24%	74%	18%
7	Measured	2.42	2.4	2.28	1.77	1.54	1.28	1.42
	Analytical	3.04	2.93	2.72	2.23	1.84	2.09	1.78
	Error	26%	22%	19%	26%	19%	63%	25%

Table E6-3: Preliminary analytical versus measured cross-frame axial stresses for Load Cases 1-7 of Bridge 1

Load Case	Data Type	Axial Force (kips)												
		CF-2	**CF-3**	**CF-4**	**CF-5**	**CF-6**	**CF-7**	**CF-8**	**CF-9**	**CF-10**	**CF-12**	**CF-13**	**CF-15**	**CF-17**
1	Measured	0.67	-0.59	-1.38	1.18	-0.68	-3.89	-2.69	-2.23	-2.12	-3.31	1.12	-1.07	0.00
	Analytical	1.05	0.16	-2.60	2.16	-1.15	-5.08	-4.57	-2.70	-1.36	-3.76	1.70	-0.63	-0.07
	Error	56%	-127%	88%	83%	69%	31%	70%	21%	-36%	13%	51%	-41%	-
2	Measured	-0.75	2.51	0.93	3.20	-0.06	-2.37	-1.03	-0.18	-1.82	-1.96	0.59	-0.14	-0.43
	Analytical	-0.87	4.32	1.46	4.69	0.16	-3.59	-1.94	0.04	-1.95	-2.38	0.99	0.26	-0.26
	Error	16%	72%	58%	46%	-361%	51%	89%	-123%	7%	21%	67%	-290%	-38%
3	Measured	-2.75	5.03	5.68	1.18	1.85	7.67	6.41	7.45	1.47	5.37	-2.78	2.26	0.58
	Analytical	-3.37	5.92	9.67	-0.69	9.67	9.77	10.24	9.07	0.44	6.66	-3.85	2.09	-0.15
	Error	22%	18%	70%	-159%	423%	27%	60%	22%	-70%	24%	39%	-7%	-127%
4	Measured	1.05	-2.45	-2.15	-1.81	-0.36	-1.67	-1.13	-3.11	1.12	-0.11	0.24	-1.16	0.09
	Analytical	1.56	-3.40	-3.95	-1.33	-0.57	-2.14	-1.82	-4.59	2.63	1.01	0.81	-1.14	0.72
	Error	49%	39%	84%	-27%	61%	28%	61%	48%	136%	-985%	241%	-2%	731%
5	Measured	-0.12	0.69	-0.39	1.28	-0.09	-1.97	-0.58	-2.10	0.67	0.13	-0.08	-0.34	-0.17
	Analytical	0.02	1.90	-0.45	2.82	-0.23	-3.38	-0.83	-3.05	2.03	1.21	0.46	-0.10	0.00
	Error	-117%	177%	15%	120%	166%	72%	44%	45%	202%	817%	-674%	-72%	-98%
6	Measured	0.59	-1.46	-1.20	-1.29	-0.26	-0.52	-0.06	-2.11	1.78	1.13	-0.29	-2.68	2.27
	Analytical	0.87	-1.92	-1.96	-1.12	-0.23	-0.57	0.23	-3.03	3.10	2.51	0.05	-2.80	2.52
	Error	48%	32%	64%	-13%	-11%	10%	-455%	44%	74%	122%	-117%	5%	11%
7	Measured	-2.49	4.25	4.37	2.10	1.45	4.58	3.75	5.09	-0.30	2.36	-1.41	6.74	-0.40
	Analytical	-3.25	5.48	7.20	1.64	3.13	5.64	5.94	6.63	-1.58	2.92	-1.74	6.08	-1.81
	Error	31%	29%	65%	-22%	115%	23%	58%	30%	430%	24%	24%	-10%	355%

Table E6-4: Validated analytical versus measured girder deflections at cross-frame line 4 for Load Cases 1-7 of Bridge 1

Load Case	Data Type	Vertical Deflections (in)				
		Girder 1	Girder 2	Girder 3	Girder 4	Girder 5
1	Measured	1.48	1.12	0.71	0.38	-0.09
	Analytical	1.48	1.09	0.70	0.33	-0.02
	Error	0%	-2%	-1%	-12%	-76%
2	Measured	1.44	1.06	0.70	0.43	-0.04
	Analytical	1.38	1.06	0.73	0.40	0.08
	Error	-5%	0%	5%	-8%	-315%
3	Measured	0.68	0.67	0.70	0.79	0.70
	Analytical	0.66	0.71	0.75	0.74	0.71
	Error	-4%	6%	8%	-6%	2%
4	Measured	-0.07	0.29	0.64	1.17	1.44
	Analytical	0.01	0.35	0.71	1.08	1.45
	Error	-118%	23%	10%	-7%	0%
5	Measured	0.77	0.77	0.77	0.93	0.88
	Analytical	0.80	0.83	0.85	0.88	0.91
	Error	3%	7%	9%	-5%	4%
6	Measured	0.01	0.30	0.58	1.05	1.29
	Analytical	0.09	0.36	0.64	0.93	1.21
	Error	567%	19%	11%	-11%	-6%
7	Measured	0.81	0.71	0.62	0.66	0.46
	Analytical	0.74	0.72	0.67	0.59	0.51
	Error	-9%	1%	9%	-10%	11%

Table E6-5: Validated analytical versus measured girder bottom flange stresses for Load Cases 1-7 of Bridge 1

Load Case	Data Type	Average Bottom Flange Stress (ksi)						
		G1-CFL4	G2-CFL4	G3-CFL4	G4-CFL4	G5-CFL4	G3-CFL7	G4-CFL7
1	Measured	5.59	4.14	2.50	0.89	-0.51	0.74	0.45
	Analytical	6.46	4.53	2.83	1.22	-0.33	1.17	0.88
	Error	16%	9%	13%	38%	-35%	59%	95%
2	Measured	5.32	3.96	2.62	1.14	-0.19	0.75	0.53
	Analytical	6.00	4.42	2.95	1.52	0.13	1.19	0.96
	Error	13%	11%	13%	33%	-169%	58%	80%
3	Measured	2.27	2.49	2.77	2.53	2.48	0.59	0.91
	Analytical	2.73	2.91	3.10	3.02	2.94	1.00	1.11
	Error	20%	17%	12%	20%	18%	69%	22%
4	Measured	-0.46	0.98	2.49	4.00	5.67	0.75	1.54
	Analytical	-0.19	2.07	2.84	4.45	6.30	1.19	1.37
	Error	-58%	112%	14%	11%	11%	60%	-11%
5	Measured	2.99	3.13	3.22	3.32	3.57	0.72	1.01
	Analytical	3.60	3.64	3.66	3.88	4.12	1.17	1.14
	Error	21%	16%	14%	17%	15%	63%	13%
6	Measured	-0.24	0.91	2.00	3.21	4.42	1.11	2.58
	Analytical	0.19	1.25	2.35	3.58	4.75	1.84	2.43
	Error	-179%	38%	18%	11%	8%	65%	-6%
7	Measured	2.42	2.40	2.28	1.77	1.54	1.28	1.42
	Analytical	2.84	2.73	2.59	2.19	1.91	1.99	1.59
	Error	17%	13%	14%	24%	24%	55%	12%

Table E6-6: Validated analytical versus measured cross-frame axial stresses for Load Cases 1-7 of Bridge 1

Load Case	Data Type	Axial Force (kips)												
		CF-2	**CF-3**	**CF-4**	**CF-5**	**CF-6**	**CF-7**	**CF-8**	**CF-9**	**CF-10**	**CF-12**	**CF-13**	**CF-15**	**CF-17**
1	Measured	0.67	-0.59	-1.38	1.18	-0.68	-3.89	-2.69	-2.23	-2.12	-3.31	1.12	-1.07	0.00
	Analytical	0.47	-0.29	-2.37	1.72	-0.97	-4.38	-4.13	-2.32	-1.48	-3.51	1.62	-0.53	-0.08
	Error	-30%	-50%	72%	45%	43%	13%	53%	4%	-30%	6%	44%	-50%	-
2	Measured	-0.75	2.51	0.93	3.20	-0.06	-2.37	-1.03	-0.18	-1.82	-1.96	0.59	-0.14	-0.43
	Analytical	-1.22	3.48	1.33	3.90	0.21	-2.91	-1.64	0.20	-1.95	-2.20	0.90	0.30	-0.25
	Error	63%	38%	44%	22%	-452%	23%	60%	-212%	7%	12%	52%	-320%	-43%
3	Measured	-2.75	5.03	5.68	1.18	1.85	7.67	6.41	7.45	1.47	5.37	-2.78	2.26	0.58
	Analytical	-3.33	5.53	8.99	-0.38	2.94	8.77	9.50	8.14	0.63	6.19	-3.77	1.92	-0.06
	Error	21%	10%	58%	-132%	59%	14%	48%	9%	-57%	15%	35%	-15%	-111%
4	Measured	1.05	-2.45	-2.15	-1.81	-0.36	-1.67	-1.13	-3.11	1.12	-0.11	0.24	-1.16	0.09
	Analytical	1.44	-3.17	-3.48	-1.44	-0.64	-1.79	-1.56	-3.92	2.19	0.57	0.19	-0.93	0.57
	Error	37%	29%	62%	-21%	79%	7%	38%	26%	96%	-598%	-19%	-20%	555%
5	Measured	-0.12	0.69	-0.39	1.28	-0.09	-1.97	-0.58	-2.10	0.67	0.13	-0.08	-0.34	-0.17
	Analytical	-0.25	1.40	-0.29	2.15	-0.21	-2.65	-0.59	-2.39	1.52	0.81	0.06	-0.04	-0.02
	Error	106%	104%	-27%	68%	145%	35%	2%	14%	125%	518%	-179%	-89%	-87%
6	Measured	0.59	-1.46	-1.20	-1.29	-0.26	-0.52	-0.06	-2.11	1.78	1.13	-0.29	-2.68	2.27
	Analytical	0.78	-1.82	-1.69	-1.17	-0.29	-0.42	0.27	-2.56	2.63	2.02	-0.40	-2.25	2.05
	Error	32%	24%	42%	-9%	11%	-19%	-517%	22%	48%	78%	40%	-16%	-10%
7	Measured	-2.49	4.25	4.37	2.10	1.45	4.58	3.75	5.09	-0.30	2.36	-1.41	6.74	-0.40
	Analytical	-3.11	5.00	6.65	1.49	2.79	5.13	5.55	5.97	-1.25	2.76	-1.80	5.49	-1.43
	Error	25%	18%	52%	-29%	92%	12%	48%	17%	319%	17%	28%	-19%	259%

Table E6-7: Preliminary analytical versus measured girder deflections at cross-frame line 4 for Load Cases 1-7 of Bridge 2

Load Case	Data Type	Vertical Deflections (in)					
		G23-CF4	G24-CF6	G21-CF6	G18-CF6	G15-CF6	G14-CF8
1	Measured	0.28	0.14	0.12	0.05	0.03	0.02
	Analytical	0.32	0.15	0.15	0.08	0.02	0.00
	Error	14%	8%	22%	71%	-38%	-75%
2	Measured	0.31	0.15	0.14	0.03	0.01	0.05
	Analytical	0.41	0.19	0.17	0.07	0.01	0.00
	Error	32%	23%	23%	127%	-10%	-102%
3	Measured	0.06	0.01	0.14	0.18	0.07	0.05
	Analytical	0.10	0.04	0.14	0.18	0.07	0.05
	Error	70%	559%	-2%	1%	2%	19%
4	Measured	0.23	0.10	0.18	0.07	0.01	0.05
	Analytical	0.27	0.13	0.17	0.08	0.02	0.01
	Error	20%	31%	-2%	13%	29%	-88%
5	Measured	0.11	0.06	0.18	0.06	0.03	0.03
	Analytical	0.14	0.07	0.16	0.09	0.02	0.02
	Error	27%	26%	-11%	51%	-8%	-54%
6	Measured	0.02	0.01	0.09	0.20	0.17	0.16
	Analytical	0.05	0.20	0.09	0.24	0.20	0.20
	Error	171%	3012%	3%	16%	19%	24%
7	Measured	0.01	-0.03	0.05	0.03	0.12	0.24
	Analytical	-0.01	0.02	0.01	0.08	0.22	0.43
	Error	-267%	-149%	-77%	146%	85%	77%

Table E6-8: Preliminary analytical versus measured girder bottom flange stresses for Load Cases 1-7 of Bridge 2

Load Case	Data Type	Average Bottom Flange Stress (ksi)				
		G22-CFL5	G21-CFL5	G20-CFL5	G19-CFL8	G18-CFL8
1	Measured	1.07	0.95	0.84	0.04	0.09
	Analytical	1.37	1.25	1.10	0.29	0.29
	Error	28%	32%	30%	575%	221%
2	Measured	1.08	1.11	0.96	0.12	0.14
	Analytical	1.42	1.43	1.19	0.44	0.38
	Error	31%	29%	23%	275%	171%
3	Measured	0.79	1.07	1.29	0.17	0.20
	Analytical	0.96	1.27	1.51	0.06	0.27
	Error	22%	19%	17%	-66%	36%
4	Measured	1.32	1.27	1.05	0.07	0.14
	Analytical	1.63	1.52	1.29	0.34	0.34
	Error	23%	19%	22%	398%	137%
5	Measured	0.9	1.09	0.85	0.18	0.18
	Analytical	1.17	1.2	1.03	0.31	0.33
	Error	30%	11%	21%	76%	87%
6	Measured	0.42	0.65	0.81	0.60	0.83
	Analytical	1.17	1.2	1.03	0.31	0.33
	Error	182%	87%	28%	-48%	-60%
7	Measured	0.01	0.08	0.10	0.03	0.18
	Analytical	0.02	0.08	0.17	0.17	0.42
	Error	22%	4%	80%	412%	129%

Table E6-9: Preliminary analytical versus measured cross-frame axial stresses for Load Cases 1-7 of Bridge 2

Load Case	Data Type	Axial Force (kips)													
		CF-1	**CF-2**	**CF-3**	**CF-4**	**CF-5**	**CF-7**	**CF-8**	**CF-9**	**CF-10**	**CF-11**	**CF-13**	**CF-15**	**CF-16**	**CF-17**
1	Measured	-3.94	-0.71	-1.76	-2.13	-0.62	0.59	1.50	1.26	1.79	-0.11	1.32	1.11	0.57	0.79
	Analytical	-6.15	-0.83	-2.93	-3.24	0.39	0.92	2.32	2.23	2.54	0.24	5.19	2.86	2.06	1.55
	Error	56%	18%	66%	52%	-	56%	55%	76%	42%	-	294%	158%	262%	97%
2	Measured	0.35	-6.18	-4.33	-6.12	-1.05	2.81	-1.12	-1.39	1.51	-3.02	1.41	1.04	0.61	0.07
	Analytical	-0.56	-8.30	-6.58	-8.70	0.52	4.08	1.10	-1.03	2.23	-3.60	6.07	3.15	2.50	1.44
	Error	-	34%	52%	42%	-	45%	-	-26%	48%	19%	331%	204%	311%	2079
3	Measured	1.43	2.26	1.96	3.40	-0.08	-1.43	4.06	6.45	-1.08	9.25	3.42	3.60	1.65	2.47
	Analytical	1.44	2.46	2.45	3.19	-0.15	-1.56	4.27	7.35	-1.54	10.09	7.20	5.20	3.56	3.63
	Error	1%	9%	25%	-6%	102%	9%	5%	14%	43%	9%	110%	45%	116%	47%
4	Measured	4.40	-1.70	-0.29	0.98	-1.72	8.73	2.70	3.72	6.93	-1.90	1.48	1.21	0.70	0.81
	Analytical	4.99	-2.79	-0.73	0.06	-1.64	11.04	1.69	4.54	7.60	-2.86	5.46	2.90	2.21	1.43
	Error	13%	64%	150%	-94%	-5%	26%	-38%	22%	10%	51%	269%	139%	218%	77%
5	Measured	0.85	0.53	0.45	1.13	-0.45	3.28	5.77	6.33	5.87	2.38	2.28	1.75	1.10	1.11
	Analytical	0.51	0.29	0.33	0.63	-0.30	3.51	5.99	7.46	6.15	2.72	6.23	2.93	2.74	0.67
	Error	-41%	-45%	-27%	-45%	-33%	7%	4%	18%	5%	14%	173%	67%	148%	-39%
6	Measured	0.85	1.53	1.25	2.15	-0.02	-1.33	-0.51	-0.18	-1.67	1.64	-1.44	2.15	-2.04	2.87
	Analytical	0.92	1.64	1.57	2.17	-0.18	-1.35	-0.54	-0.50	-1.83	1.86	-6.09	0.60	-6.88	8.78
	Error	7%	7%	26%	1%	711%	1%	5%	179%	9%	14%	322%	-72%	238%	206%
7	Measured	0.08	0.20	0.19	0.31	0.03	-0.23	-0.67	-0.78	-0.49	-0.54	-1.96	-2.68	-0.36	-2.29
	Analytical	0.47	0.78	0.76	1.03	-0.07	-0.43	-0.87	-1.22	-0.66	-0.66	-8.88	-7.17	-1.05	-8.86
	Error	453%	287%	296%	230%	-	90%	29%	57%	35%	22%	352%	168%	195%	287%

Table E6-10: Validated analytical versus measured girder deflections at cross-frame line 4 for Load Cases 1-7 of Bridge 2

Load Case	Data Type	Vertical Deflections (in)					
		G23-CF4	G24-CF6	G21-CF6	G18-CF6	G15-CF6	G14-CF8
1	Measured	0.28	0.14	0.12	0.05	0.03	0.02
	Analytical	0.27	0.12	0.13	0.07	0.02	0.01
	Error	-3%	-10%	4%	52%	-35%	-49%
2	Measured	0.31	0.15	0.14	0.03	0.01	0.05
	Analytical	0.34	0.15	0.14	0.07	0.01	0.01
	Error	12%	3%	4%	100%	4%	-87%
3	Measured	0.06	0.01	0.14	0.18	0.07	0.05
	Analytical	0.09	0.04	0.12	0.16	0.06	0.05
	Error	47%	450%	-12%	-8%	-7%	11%
4	Measured	0.23	0.10	0.18	0.07	0.01	0.05
	Analytical	0.23	0.11	0.15	0.07	0.02	0.01
	Error	2%	8%	-15%	1%	36%	-75%
5	Measured	0.11	0.06	0.18	0.06	0.03	0.03
	Analytical	0.12	0.06	0.14	0.08	0.02	0.02
	Error	8%	3%	-22%	37%	-9%	-44%
6	Measured	0.02	0.01	0.09	0.20	0.17	0.16
	Analytical	0.05	0.02	0.08	0.22	0.18	0.18
	Error	152%	206%	-5%	6%	7%	9%
7	Measured	0.01	-0.03	0.05	0.03	0.12	0.24
	Analytical	0.00	-0.01	0.02	0.07	0.19	0.36
	Error	-120%	-78%	-67%	117%	57%	50%

Table E6-11: Validated analytical versus measured girder bottom flange stresses for Load Cases 1-7 of Bridge 2

Load Case	Data Type	Average Bottom Flange Stress (ksi)				
		G22-CFL5	G21-CFL5	G20-CFL5	G19-CFL8	G18-CFL8
1	Measured	1.07	0.95	0.84	0.04	0.09
	Analytical	1.24	1.14	1.01	0.25	0.28
	Error	16%	21%	20%	482%	204%
2	Measured	1.08	1.11	0.96	0.12	0.14
	Analytical	1.28	1.30	1.08	0.39	0.36
	Error	18%	17%	12%	232%	158%
3	Measured	0.79	1.07	1.29	0.17	0.20
	Analytical	0.92	1.22	1.46	0.04	0.26
	Error	17%	15%	13%	-78%	31%
4	Measured	1.32	1.27	1.05	0.07	0.14
	Analytical	1.52	1.42	1.21	0.30	0.32
	Error	15%	12%	15%	341%	128%
5	Measured	0.90	1.09	0.85	0.18	0.18
	Analytical	1.11	1.14	0.98	0.30	0.32
	Error	23%	5%	16%	69%	83%
6	Measured	0.42	0.65	0.81	0.60	0.83
	Analytical	0.54	0.70	0.92	0.48	0.88
	Error	30%	9%	14%	-21%	6%
7	Measured	0.01	0.08	0.10	0.03	0.18
	Analytical	0.06	0.12	0.19	0.21	0.41
	Error	367%	47%	100%	520%	123%

Table E6-12: Validated analytical versus measured cross-frame axial stresses for Load Cases 1-7 of Bridge 2

Load Case	Data Type	Axial Force (kips)													
		CF-1	**CF-2**	**CF-3**	**CF-4**	**CF-5**	**CF-7**	**CF-8**	**CF-9**	**CF-10**	**CF-11**	**CF-13**	**CF-15**	**CF-16**	**CF-17**
	Measured	-3.94	-0.71	-1.76	-2.13	-0.62	0.59	1.50	1.26	1.79	-0.11	1.32	1.11	0.57	0.79
1	Analytical	-4.88	-0.71	-2.31	-2.46	0.13	1.03	2.24	2.28	2.45	0.42	4.36	2.43	1.73	1.35
	Error	24%	0%	31%	15%	-	74%	49%	81%	37%	-	232%	120%	204%	72%
	Measured	0.35	-6.18	-4.33	-6.12	-1.05	2.81	-1.12	-1.39	1.51	-3.02	1.41	1.04	0.61	0.07
2	Analytical	0.22	-7.29	-5.47	-7.24	0.17	3.85	-0.74	-0.59	2.20	-3.06	5.09	2.65	2.11	1.20
	Error	-37%	18%	26%	18%	-	37%	-34%	-57%	46%	1%	262%	156%	247%	1726
	Measured	1.43	2.26	1.96	3.40	-0.08	-1.43	4.06	6.45	-1.08	9.25	3.42	3.60	1.65	2.47
3	Analytical	1.49	2.41	2.34	3.21	-0.21	-1.60	3.96	6.87	-1.40	10.11	6.40	4.76	3.07	3.61
	Error	5%	6%	20%	-6%	180%	11%	-2%	7%	30%	9%	87%	32%	86%	46%
	Measured	4.40	-1.70	-0.29	0.98	-1.72	8.73	2.70	3.72	6.93	-1.90	1.48	1.21	0.70	0.81
4	Analytical	4.85	-2.21	-0.35	0.48	-1.72	10.20	1.99	4.54	7.26	-2.49	4.66	2.48	1.90	1.23
	Error	10%	30%	21%	-51%	0%	17%	-26%	22%	5%	31%	215%	105%	173%	52%
	Measured	0.85	0.53	0.45	1.13	-0.45	3.28	5.77	6.33	5.87	2.38	2.28	1.75	1.10	1.11
5	Analytical	0.64	0.37	0.42	0.79	-0.36	3.34	5.63	6.99	5.77	2.61	5.54	2.59	2.50	0.51
	Error	-25%	-30%	-8%	-30%	-21%	2%	-2%	10%	-2%	9%	143%	48%	126%	-54%
	Measured	0.85	1.53	1.25	2.15	-0.02	-1.33	-0.51	-0.18	-1.67	1.64	-1.44	2.15	-2.04	2.87
6	Analytical	0.92	1.55	1.46	2.09	-0.19	-1.32	-0.63	-0.54	-1.81	1.62	-5.81	0.61	-6.56	8.35
	Error	8%	1%	17%	-3%	772%	-1%	23%	198%	8%	-1%	303%	-72%	222%	191%
	Measured	0.08	0.20	0.19	0.31	0.03	-0.23	-0.67	-0.78	-0.49	-0.54	-1.96	-2.68	-0.36	-2.29
7	Analytical	0.40	0.64	0.62	0.85	-0.04	-0.31	-0.74	-1.04	-0.53	-0.65	-7.62	-6.18	-0.88	-7.64
	Error	370%	220%	223%	172%	-	36%	10%	33%	7%	20%	288%	131%	146%	233%

Table E6-13: Preliminary analytical versus measured girder deflections at cross-frame line 4 for Load Cases 1-7 of Bridge 3

Load Case	Data Type	Vertical Deflections (in)			
		Girder 1	Girder 2	Girder 3	Girder 4
1	Measured	0.35	0.49	0.71	0.88
	Analytical	0.38	0.60	0.82	1.04
	Error	7%	23%	16%	18%
2	Measured	0.87	0.79	0.73	0.62
	Analytical	1.11	0.99	0.87	0.74
	Error	28%	26%	19%	20%
3	Measured	1.50	1.17	0.72	0.31
	Analytical	2.12	1.54	0.95	0.36
	Error	42%	32%	32%	14%
4	Measured	1.92	1.36	0.72	0.20
	Analytical	2.71	1.85	0.98	0.12
	Error	42%	35%	36%	-37%
5	Measured	0.22	0.28	0.39	0.42
	Analytical	0.27	0.36	0.46	0.55
	Error	22%	32%	16%	30%
6	Measured	1.17	0.83	0.54	0.13
	Analytical	1.61	1.10	0.60	0.10
	Error	38%	34%	11%	-27%
7	Measured	1.23	1.00	0.77	0.54
	Analytical	1.70	1.35	0.99	0.64
	Error	38%	35%	28%	19%

Table E6-14: Preliminary analytical versus measured girder bottom flange stresses for Load Cases 1-7 of Bridge 3

Load Case	Data Type	Average Bottom Flange Stress (ksi)							
		G1-CFL4	G2-CFL4	G3-CFL4	G4-CFL4	G1-CFL10	G2-CFL10	G3-CFL10	G4-CFL10
1	Measured	0.81	0.93	0.86	0.92	1.61	2.42	3.13	3.86
	Analytical	0.95	0.96	0.84	0.76	1.78	2.83	3.72	4.37
	Error	17%	2%	-2%	-17%	11%	17%	19%	13%
2	Measured	1.04	0.88	0.56	0.41	2.91	2.88	2.56	2.27
	Analytical	1.11	0.84	0.53	0.32	3.54	3.40	2.95	2.42
	Error	7%	-4%	-6%	-22%	22%	18%	16%	7%
3	Measured	1.30	0.83	0.25	-0.39	4.62	3.42	1.89	0.35
	Analytical	1.32	0.66	0.12	-0.45	5.97	4.18	2.07	-0.14
	Error	2%	-21%	-53%	16%	29%	22%	9%	-139%
4	Measured	1.42	0.80	0.06	-0.65	5.76	3.76	1.51	-0.87
	Analytical	1.43	0.31	-0.07	-0.86	7.34	4.63	1.46	-1.70
	Error	1%	-62%	-209%	33%	27%	23%	-3%	95%
5	Measured	0.60	1.16	1.61	2.19	1.03	1.23	1.39	1.52
	Analytical	0.71	1.26	1.74	2.17	1.16	1.45	1.63	1.73
	Error	18%	9%	8%	-1%	12%	18%	17%	14%
6	Measured	2.56	1.75	0.58	-0.58	2.67	1.77	-0.49	-0.49
	Analytical	3.05	1.84	0.57	-0.77	3.54	2.17	0.61	-0.94
	Error	19%	6%	-1%	33%	33%	23%	-224%	91%
7	Measured	1.08	0.84	0.38	0.00	4.23	3.72	2.82	1.90
	Analytical	1.19	0.75	0.31	-0.15	5.32	4.43	3.17	1.77
	Error	10%	-11%	-16%	-4914%	26%	19%	12%	-7%

Table E6-15: Preliminary analytical versus measured cross-frame axial stresses for Load Cases 1-7 of Bridge 3

Load Case	Data Type	Axial Force (kips)												
		CF 2	**CF 3**	**CF 4**	**CF 5**	**CF 6**	**CF 9**	**CF 10**	**CF 11**	**CF 12**	**CF 13**	**CF 14**	**CF 16**	**CF 17**
1	Measured	-0.02	-0.88	0.23	-0.82	0.37	-0.39	-1.91	1.29	1.00	-3.75	3.74	-0.79	3.29
	Analytical	-0.22	-1.03	0.18	-1.31	0.90	-0.28	-2.03	1.51	1.39	-4.05	4.50	-1.44	2.81
	Error	1135%	17%	-19%	61%	142%	-28%	6%	18%	39%	8%	20%	81%	-14%
2	Measured	-0.28	-1.00	0.54	-0.54	0.66	0.30	-4.30	3.66	2.71	-2.98	4.50	2.20	0.51
	Analytical	-0.60	-0.74	0.57	-0.81	1.03	0.30	-5.14	4.49	3.29	-3.29	5.35	2.19	-0.13
	Error	119%	-26%	6%	50%	57%	0%	20%	22%	21%	10%	19%	-1%	-126%
3	Measured	-1.08	-0.67	0.44	-0.32	0.54	-0.24	-5.93	4.84	0.73	-1.20	1.39	-0.49	0.24
	Analytical	-1.36	-0.13	0.71	-0.14	0.80	-0.69	-7.31	6.15	0.77	-1.00	1.03	-0.73	0.10
	Error	26%	-81%	63%	-55%	49%	185%	23%	27%	6%	-17%	-25%	48%	-59%
4	Measured	-1.52	-0.11	0.10	-0.27	0.54	-2.03	-5.03	2.49	-2.51	-2.19	-0.67	-3.66	0.85
	Analytical	-1.82	0.44	0.75	0.26	0.78	-3.47	-5.69	2.56	-3.85	-2.68	-1.14	-4.13	1.52
	Error	20%	-494%	650%	-196%	43%	71%	13%	3%	53%	22%	70%	13%	79%
5	Measured	-0.17	-0.73	-0.06	-1.80	1.66	-0.24	-0.90	0.92	0.25	-1.30	1.35	-0.56	1.59
	Analytical	-0.02	-0.89	0.24	-2.41	2.60	-0.27	-1.21	1.08	0.23	-1.33	1.59	-0.97	1.47
	Error	-87%	23%	-474%	34%	57%	10%	34%	18%	-8%	3%	17%	72%	-8%
6	Measured	-0.99	-1.90	1.40	0.51	-0.37	-1.35	-2.20	0.39	-1.52	-1.81	-0.11	-2.03	0.27
	Analytical	-1.71	-2.09	2.48	-0.13	-0.13	-1.90	-2.48	0.29	-2.04	-2.19	-0.17	-1.93	0.44
	Error	73%	10%	77%	-125%	-64%	40%	12%	-26%	35%	21%	61%	-5%	67%
7	Measured	-0.81	-0.51	0.16	-0.50	0.36	-1.22	-4.29	2.65	-0.48	-3.35	1.94	-2.17	2.32
	Analytical	-1.08	-0.25	0.43	-0.47	0.77	-1.94	-4.85	3.11	-0.92	-3.72	1.97	-3.00	2.55
	Error	33%	-52%	165%	-7%	113%	59%	13%	18%	93%	11%	2%	38%	10%

Table E6-16: Validated analytical versus measured girder deflections at cross-frame line 4 for Load Cases 1-7 of Bridge 3

Load Case	Data Type	Vertical Deflections (in)			
		Girder 1	Girder 2	Girder 3	Girder 4
1	Measured	0.35	0.49	0.71	0.88
	Analytical	0.35	0.53	0.71	0.89
	Error	-2%	8%	0%	1%
2	Measured	0.87	0.79	0.73	0.62
	Analytical	0.91	0.83	0.74	0.65
	Error	5%	5%	1%	5%
3	Measured	1.50	1.17	0.72	0.31
	Analytical	1.68	1.24	0.79	0.35
	Error	12%	6%	10%	10%
4	Measured	1.92	1.36	0.72	0.20
	Analytical	2.14	1.48	0.81	0.16
	Error	12%	8%	13%	-20%
5	Measured	0.22	0.28	0.39	0.42
	Analytical	0.24	0.32	0.39	0.47
	Error	9%	15%	0%	11%
6	Measured	1.17	0.83	0.54	0.13
	Analytical	1.26	0.87	0.49	0.11
	Error	8%	6%	-9%	-15%
7	Measured	1.23	1.00	0.77	0.54
	Analytical	1.37	1.10	0.84	0.58
	Error	11%	11%	8%	7%

Table E6-17: Validated analytical versus measured girder bottom flange stresses for Load Cases 1-7 of Bridge 3

Load Case	Data Type	Average Bottom Flange Stress (ksi)							
		G1-CFL4	G2-CFL4	G3-CFL4	G4-CFL4	G1-CFL10	G2-CFL10	G3-CFL10	G4-CFL10
1	Measured	0.81	0.93	0.86	0.92	1.61	2.42	3.13	3.86
	Analytical	0.86	0.88	0.77	0.70	1.71	2.71	3.50	3.98
	Error	5%	-6%	-10%	-24%	6%	12%	12%	3%
2	Measured	1.04	0.88	0.56	0.41	2.91	2.88	2.56	2.27
	Analytical	0.96	0.76	0.49	0.33	3.21	3.20	2.82	2.30
	Error	-7%	-13%	-12%	-19%	10%	11%	10%	1%
3	Measured	1.30	0.83	0.25	-0.39	4.62	3.42	1.89	0.35
	Analytical	1.09	0.57	0.13	-0.32	5.27	3.87	2.04	0.10
	Error	-16%	-32%	-50%	-18%	14%	13%	8%	-71%
4	Measured	1.42	0.80	0.06	-0.65	5.76	3.76	1.51	-0.87
	Analytical	1.16	0.27	-0.03	-0.66	6.43	4.26	1.49	-1.24
	Error	-18%	-66%	-154%	2%	12%	13%	-1%	43%
5	Measured	0.60	1.16	1.61	2.19	1.03	1.23	1.39	1.52
	Analytical	0.67	1.20	1.63	2.01	1.09	1.38	1.53	1.59
	Error	11%	4%	1%	-8%	6%	12%	10%	5%
6	Measured	2.56	1.75	0.58	-0.58	2.67	1.77	-0.49	-0.49
	Analytical	2.63	1.68	0.57	-0.58	3.07	1.98	0.63	-0.68
	Error	3%	-4%	-1%	-1%	15%	12%	-229%	40%
7	Measured	1.08	0.84	0.38	0.00	4.23	3.72	2.82	1.90
	Analytical	1.00	0.66	0.30	-0.07	4.76	4.15	3.06	1.77
	Error	-8%	-21%	-19%	-2412%	13%	12%	8%	-7%

Table E6-18: Validated analytical versus measured cross-frame axial stresses for Load Cases 1-7 of Bridge 3

Load Case	Data Type	Axial Force (kips)												
		CF 2	**CF 3**	**CF 4**	**CF 5**	**CF 6**	**CF 9**	**CF 10**	**CF 11**	**CF 12**	**CF 13**	**CF 14**	**CF 16**	**CF 17**
1	Measured	-0.02	-0.88	0.23	-0.82	0.37	-0.39	-1.91	1.29	1.00	-3.75	3.74	-0.79	3.29
	Analytical	-0.16	-1.05	0.48	-1.15	0.83	-0.10	-2.28	1.96	1.79	-3.91	4.35	-0.26	2.22
	Error	793%	19%	111%	41%	125%	-73%	19%	53%	79%	4%	16%	-68%	-32%
2	Measured	-0.28	-1.00	0.54	-0.54	0.66	0.30	-4.30	3.66	2.71	-2.98	4.50	2.20	0.51
	Analytical	-0.42	-0.84	0.80	-0.71	0.92	0.57	-5.38	5.35	3.67	-2.40	4.99	2.64	-0.31
	Error	54%	-16%	48%	32%	40%	94%	25%	46%	36%	-20%	11%	20%	-160%
3	Measured	-1.08	-0.67	0.44	-0.32	0.54	-0.24	-5.93	4.84	0.73	-1.20	1.39	-0.49	0.24
	Analytical	-1.03	-0.25	0.81	-0.14	0.64	-0.25	-7.55	7.49	1.41	-0.60	0.90	-0.64	0.17
	Error	-5%	-62%	85%	-56%	17%	2%	27%	55%	93%	-50%	-35%	31%	-32%
4	Measured	-1.52	-0.11	0.10	-0.27	0.54	-2.03	-5.03	2.49	-2.51	-2.19	-0.67	-3.66	0.85
	Analytical	-1.40	0.21	0.76	0.17	0.57	-2.75	-6.14	4.45	-2.96	-2.04	-1.29	-4.32	1.71
	Error	-8%	-286%	666%	-162%	5%	36%	22%	79%	18%	-7%	93%	18%	101%
5	Measured	-0.17	-0.73	-0.06	-1.80	1.66	-0.24	-0.90	0.92	0.25	-1.30	1.35	-0.56	1.59
	Analytical	0.06	-0.99	0.51	-2.28	2.46	-0.18	-1.32	1.30	0.40	-1.29	1.47	-0.59	1.25
	Error	-135%	37%	-890%	27%	48%	-26%	46%	42%	58%	0%	8%	5%	-22%
6	Measured	-0.99	-1.90	1.40	0.51	-0.37	-1.35	-2.20	0.39	-1.52	-1.81	-0.11	-2.03	0.27
	Analytical	-1.17	-2.43	3.16	0.18	-0.16	-1.57	-2.60	1.18	-1.67	-1.81	-0.26	-2.06	0.62
	Error	18%	28%	126%	-65%	-56%	16%	18%	200%	10%	0%	143%	1%	133%
7	Measured	-0.81	-0.51	0.16	-0.50	0.36	-1.22	-4.29	2.65	-0.48	-3.35	1.94	-2.17	2.32
	Analytical	-0.82	-0.37	0.57	-0.44	0.63	-1.38	-5.30	4.49	0.13	-3.24	1.85	-2.29	2.23
	Error	2%	-29%	249%	-12%	75%	13%	24%	70%	-126%	-3%	-4%	6%	-4%